Corinna Klapproth

Adaptive Numerical Integration of Dynamical Contact Problems

Cuvillier Verlag Göttingen
Internationaler wissenschaftlicher Fachverlag

Adaptive Numerical Integration of Dynamical Contact Problems

Dissertation
zur Erlangung des akademischen Grades
des Doktors der Naturwissenschaften
am Fachbereich Mathematik und Informatik
der Freien Universität Berlin

Corinna Klapproth

Dezember 2010

Bibliografische Information der Deutschen Nationalbibliothek
Die Deutsche Nationalbibliothek verzeichnet diese Publikation in der Deutschen Nationalbibliographie; detaillierte bibliographische Daten sind im Internet über http://dnb.d-nb.de abrufbar.
1. Aufl. - Göttingen: Cuvillier, 2011
Zugl.: (FU) Berlin, Univ., Diss., 2010

978-3-86955-769-4

Betreuer/Erstgutachter: Prof. Dr. Dr. h.c. Peter Deuflhard
Freie Universität Berlin und Zuse-Institut Berlin (ZIB)

Zweitgutachter: Prof. Dr. Dr. h.c. Ernst Hairer
Universität Genf

Datum der Disputation: 18. März 2011

© CUVILLIER VERLAG, Göttingen 2011
Nonnenstieg 8, 37075 Göttingen
Telefon: 0551-54724-0
Telefax: 0551-54724-21
www.cuvillier.de

Alle Rechte vorbehalten. Ohne ausdrückliche Genehmigung des Verlages ist es nicht gestattet, das Buch oder Teile daraus auf fotomechanischem Weg (Fotokopie, Mikrokopie) zu vervielfältigen.
1. Auflage 2011
Gedruckt auf säurefreiem Papier.

978-3-86955-769-4

Contents

Introduction 1

1. The Motion of the Human Knee as a Dynamical Contact Problem 5
- 1.1. The Human Knee . . . 5
- 1.2. Basics of the Mathematical Model . . . 6
- 1.3. Strong and Variational Problem . . . 11
- 1.4. Conservation Properties and Persistency Condition . . . 16

2. Newmark Methods 23
- 2.1. Classical Newmark Method . . . 25
- 2.2. Contact–Implicit Newmark Method . . . 28
- 2.3. Contact–Stabilized Newmark Method . . . 29
- 2.4. Improved Contact–Stabilized Newmark Method . . . 32
- 2.5. Numerical Comparison . . . 36

3. A Perturbation Result – Viscosity and Physical Energy Norm 45
- 3.1. Elasticity . . . 46
- 3.2. Viscoelasticity . . . 48
- 3.3. Interpretation of the Stability Condition . . . 53
- 3.4. Approximations of the Signorini Condition . . . 57

4. Consistency – Bounded Variation 59
- 4.1. Newmark Methods in Function Space . . . 59
- 4.2. Consistency Error in Physical Energy Norm . . . 66
- 4.3. Consistency Error in a Discrete Displacement Norm . . . 78
- 4.4. Consistency Error for Permanent Active Contact . . . 82

5. Convergence Theory 91
- 5.1. Discrete Perturbation Results . . . 91
  - 5.1.1. A Discrete Perturbation Result in Discrete Displacement Norm . . . 92
  - 5.1.2. Discrete Stability Condition . . . 94
  - 5.1.3. A Discrete Perturbation Result in Physical Energy Norm . . . 99
- 5.2. Convergence . . . 103
  - 5.2.1. Convergence in Physical Energy Norm . . . 106

5.2.2. Convergence in Discrete Displacement Norm 108

6. Adaptive Timestep Control **111**
6.1. Towards an Asymptotic Error Expansion 111
6.1.1. Conical Derivative 112
6.1.2. Extension of Extrapolation Techniques 114
6.1.3. Construction of a Higher-Order Scheme 116
6.1.4. Discussion of Consistency Order 124
6.2. Timestep Control 127
6.2.1. Error Estimator in the Absence of Contact 128
6.2.2. Error Estimator in the Presence of Contact 129
6.2.3. Combined Timestep Strategy 131
6.3. Global Discretization Error 134

7. Numerical Results **137**
7.1. Hertzian Contact Problem 137
7.2. Motion of the Human Knee 142

Conclusion **149**

A. Inequalities **151**

B. Interpretation of Contact Stresses **153**
B.1. An Abstract Trace Theorem 153
B.2. Localization on Active Contact Boundaries 154
B.3. Localization on Critical Contact Boundaries 156
B.4. Interpretation of Discrete Contact Stresses 158

List of Symbols **i**

Bibliography **xii**

Danksagung **xiii**

Zusammenfassung **xv**

Introduction

The present thesis deals with the efficient adaptive numerical integration of dynamical contact problems. This is the core problem in the fast and robust simulation of stresses arising in a real patient's knee joint for different kinds of loading situations. The topic is of high interest in the field of *computer-assisted therapy planning*, which aims at the generation of a "virtual patient" [17]. This tool allows the design of effective treatment options and precise surgery strategies within a clinical environment. Potential tasks of patient-specific techniques in orthopedics are osteotomic interventions and the construction and selection of implants or fixation devices.

For realistic predictions of therapeutical manipulations, numerical simulation and optimization are applied on a detailed three-dimensional geometry of the individual patient's knee (obtained from anatomical CT or MRT image data). In view of a reasonable clinical application, the necessary computations have to be performed on local workstations in clinics within short time frames. Moreover, the solutions have to be resilient enough to serve as a basis for responsible medical decisions. With regard to these conditions, highest level requirements have to be set on the efficiency and accuracy of the applied numerical techniques.

The appropriate approach to cope with this mathematical challenge is the construction of an adaptive numerical integrator for the dynamical contact problem. For this purpose, dynamical contact problems have to be analyzed precisely from both the analytical and the numerical point of view.

Dynamical Contact Problems. In 1933, Antonio Signorini introduced the frictionless static contact problem of a linearly elastic body with a rigid foundation [85], which today is called Signorini problem. Since then, the modeling of contact phenomena classically employs Signorini's contact conditions in displacements, which are based on a linearization of the physically meaningful non-penetrability of masses.

Following the same approach in the time-dependent case leads to highly nonlinear second-order variational problems, where the actual zone of contact is a priori unknown. When the phase of contact changes, shocks are caused, which identify the hyperbolic structure of the problem. This inhibits general regularity of an evolution, even if the rest of the data are smooth. Partial regularity results and some discussion on the subject have been published in [13, 23, 68].

For dynamical contact problems between a linearly elastic body and a rigid foundation that are formulated via Signorini's contact conditions, the first existence and

uniqueness results were obtained by Duvaut and Lions [23]. They studied problems with prescribed time-constant normal stresses where the contact surface is known in advance. However, up to date, existence results have only been provided for special cases such as some simple geometric settings and one-dimensional problems [68, 83]. A general existence or even uniqueness theory in conjunction with pure linear elasticity is still missing.

The serious mathematical problems encountered in proving well-posedness basically originate from the discontinuity of the velocities at contact. The assumption of viscous material behavior allows at least the derivation of existence results for unilateral dynamic contact problems: Jarušek analyzed a frictionless viscoelastic body with singular memory [42, 44]. Viscoelastic materials satisfying a Kelvin-Voigt constitutive law were studied by Kuttler and Shillor [62] and Cocou [13]. Kuttler and Shillor proved existence for the case of frictional contact and a moving rigid foundation, while Cocou considered a problem with nonlocal friction. Migòrski and Ochal investigated a class of problems modeled by hemi-variational inequalities [74]. In 2008, Ahn and Stewart established existence for frictionless dynamical contact problems between a linearly viscoelastic body of Kelvin-Voigt type and a rigid obstacle [6]. A survey of existence and uniqueness results is given in the monograph [25] by Eck, Jarušek, and Krebeč.

The papers cited above primarily concern existence results for dynamical contact problems. Uniqueness and continuous dependence on the initial data have not been proven up to now, neither in the purely elastic nor in the viscoelastic case. The fundamental mathematical difficulties with such results can be traced back to the intrinsic non-smoothness of the problem emerging from Signorini's contact conditions. For this reason, the requirement of exact non-penetration of the bodies is often relaxed by using regularization techniques in the analytical models. However, for the medical applications discussed above, any violation of the contact constraints is unacceptable.

Numerical Integration. Over the last decades, a large amount of work has been done on the design of numerical methods for solving dynamical contact problems, which is and remains a challenging task. An overview on several known time discretization schemes can be found, e.g., in the monograph [65] or in the papers [22, 59]. Among them, the *classical Newmark method* is one of the most popular numerical solvers, which is also used in the wide-spread finite element analysis program NASTRAN. Unfortunately, it is well-known that this scheme may lead to an unphysical energy blow-up during time integration and numerical instabilities at dynamical contact boundaries may occur. For this reason, Kane, Repetto, Ortiz, and Marsden introduced a *contact–implicit* version which is energy dissipative in contact, but still unable to suppress the undesirable oscillations [46]. Recently, Deuflhard, Krause, and Ertel proposed a *contact–stabilized* variant, which avoids the unphysi-

cal oscillations at contact interfaces and is still energy dissipative [19]. For related stabilizations see [87, 88].

Laursen, Chawla, and Love have designed time integration schemes of Newmark type with predominant focus on energy conservation of the discretized solution [66, 67]. Such approaches typically lead to possible interpenetration originating from a discretized persistency condition. However, the biomedical applications in mind require strict non-penetration. For the same reason, enforcement with penalty methods or enforcement with contact conditions in velocities are ruled out.

A different approach for reducing artificial oscillations at contact boundaries has recently been suggested by Khenous, Laborde, and Renard [47, 48]. Their mass redistribution method is based on completely removing the mass in a small strip on the contact boundaries. The algorithm has been further improved by Hager, Hüeber, and Wohlmuth in view of computational cost [31]. However, the scheme is formulated within the method of lines framework, which in general inhibits the development of efficient adaptivity in space. In contrast, the contact–stabilization by Deuflhard et al. leaves the mass matrix unchanged and can easily be applied for arbitrary spatial discretization.

In the absence of contact, any symmetric variant of Newmark's method is equivalent to the Störmer-Verlet scheme, which is well-known to be second-order consistent and convergent (see, e.g., the textbook [33] of Hairer, Lubich, and Wanner). In the presence of contact, the question of consistency and convergence has not been solved yet for any of the discretization schemes presented above. This is due the high irregularities encountered at contact interfaces in the constrained problem, which inhibit the derivation of viable estimates for the local discretization errors via the classical approach.

Adaptivity. The efficient and reliable simulation of the motion of a human knee joint requires a stable numerical integrator for dynamical contact problems, which allows for adaptivity both in time and in space. An equidistant mesh can not be expected to be adequate for reaching a given accuracy of the approximation with a reasonable computational effort. However, until now, the topic of an adaptive timestep control for discretizations of dynamical contact problems has completely been avoided both in engineering and in mathematical literature. This is mainly due to the lack of perturbation and consistency results in the constrained situation.

The present thesis will work out an efficient adaptive time integrator for frictionless dynamical contact problems in viscoelasticity that are formulated on the basis of Signorini's contact conditions. Apart from medical treatment planning, the issue is of wide need in many different application areas such as structural mechanics or metal forming processes.

Outline

Chapter 1 will deal with the mathematical model used to describe frictionless dynamical contact between two viscoelastic bodies fulfilling the Kelvin-Voigt material law. Both the strong and weak problem formulation are presented, which are based on Signorini's contact conditions for bilateral contact. Moreover, conservation properties and the validity of a persistency condition will be discussed. *Chapter 2* will be devoted to the numerical integration of dynamical contact problems. Here, a detailed theoretical and numerical analysis of the classical, the contact–implicit, and the contact–stabilized Newmark method will be given. The presentation will motivate the development of an improved contact–stabilized version, which is the time discretization scheme of interest in this thesis.

In a first step towards an adaptive timestep control, a norm in function space has to be determined in which a perturbation result is satisfied even in the presence of contact. By reason of the present unclear situation in view of well-posedness of dynamical contact problems, *Chapter 3* will concentrate on a stability study under perturbations of the initial data for both the elastic and the viscoelastic case. This will necessitate the definition and interpretation of a stability condition that characterizes a suitable class of contact problems. In a second step, the construction of an adaptive timestep control requires the derivation of a consistency result and the corresponding consistency order. In order to fill the lack of such knowledge for Newmark methods under contact constraints, *Chapter 4* starts with an investigation of the Newmark schemes in function space. Then, consistency error estimates will be derived in the specific norm found in the earlier perturbation theory and in a further discrete norm. Moreover, the consistency behavior of the Newmark methods in the special case of permanent active contact will be analyzed. Subsequently, a novel proof technique will be introduced in *Chapter 5*, which allows showing convergence of the improved contact–stabilized Newmark methods in both norms. This requires in particular the derivation of perturbation results for the scheme, which are again based on a suitable stability condition.

Finally, in *Chapter 6*, an adaptive timestep control will be devised in the improved contact–stabilized Newmark method (ContacX). On the basis of a theoretical and numerical investigation of an asymptotic error expansion of the Newmark scheme, established extrapolation techniques will be transferred to the algorithm in order to construct a comparative scheme of higher-order accuracy. This allows the suggestion of a problem-adapted error estimator and timestep selection which also cover the presence of contact. Moreover, the actually achieved global discretization error of the adaptive timestep control will be discussed. In *Chapter 7*, an illustrative numerical example will be given followed by a prototype of a dynamical simulation of a human knee joint.

1. The Motion of the Human Knee as a Dynamical Contact Problem

The first chapter of this thesis is dedicated to the analytical model that is chosen to describe the main dynamics of a human knee joint. The considerations are restricted to the main mathematical challenge that is a frictionless dynamical contact problem between two viscoelastic bodies subject to Signorini's contact conditions.

Section 1.1 contains a brief presentation of the anatomical structure of a human knee related to the relevant biomechanical properties. After that, Section 1.2 deals with a description of linear viscoelasticity of Kelvin-Voigt type and the definition of linearized non-penetration conditions. The resulting dynamical contact problem will be stated both in the strong and in the weak formulation in Section 1.3. In Section 1.4, the so-called persistency condition and the conservation properties of the system will be discussed.

1.1. The Human Knee

Setting up a mathematical model for the movement of a human knee necessitates information on the existing anatomical and biomechanical system. Therefore, this section will overview the basic parts composing the complex knee joint particularly with regard to their biomechanics. A simplifying illustration of the anatomy is given in Figure 1.1. More details on this topic can be found, e.g., in [11, 78].

The knee is an example for a hinge joint and links the thighbone – the femur – and the two bones of the lower leg – the tibia and the fibula. In addition, the knee joint contains the patella bone, which is commonly known as kneecap. Composed of the tibiofemoral joint and the patellofemoral joint, the knee shows a two-joint structure. The bones are connected by ligaments across the articulation, which provide stability of the joint by controlling the relative motion of the bones.

In activities as walking and running, jumping, or stair climbing, the human knee is subjected to forces, which are mainly produced by body weight, muscle forces, and externally applied forces. In particular, the knee joint regularly sustains from high stresses and moments that originate from intermittent impacts. Muscles develop tensions, which are transmitted to bones via tendons attaching muscles to bones.

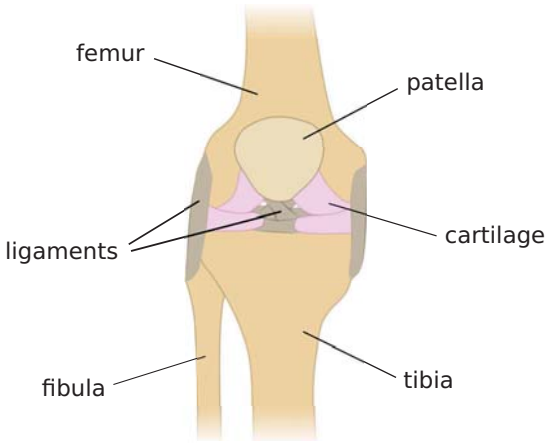

Figure 1.1.: Anatomy of the human knee.

The interacting surfaces of femur, tibia, and patella are covered with layers of articular cartilage. This tissue facilitates a smooth articulation by dissipating dangerous amounts of energy. Moreover, cartilage has low friction characteristics, which reduce sliding frictional forces in articulation such that a gliding movement occurs. In the middle of the knee are the disc-shaped menisci acting as additional shock absorbers. The joint is surrounded by a connective tissue capsule retaining synovial fluid. This provides lubrication to the articular surfaces, which leads to a further reduction of joint friction.

On the basis of this medical knowledge, the biomechanical behavior of the human knee joint with all interacting components can be modeled as a large and heterogeneous time-dependent contact problem. Due to the high complexity, the following considerations are focussed on the tibiofemoral joint, where the central mathematical difficulty is the correct modeling and simulation of articulation. For this reason, the thesis at hand concentrates on the dynamical interplay of the two bones and the covering cartilage. Bones mainly provide a simple linearly elastic material response such that the slight viscosity can be disregarded. By contrast, articulating cartilage displays both elastic and viscous properties [37]. Friction forces are negligible in a normal knee joint. For simplification, anisotropic and heterogeneous effects will also be neglected.

1.2. Basics of the Mathematical Model

In this section, an analytical model for the mechanical behavior of human bone and cartilage will be presented, which is based on the Kelvin-Voigt constitutive law of linear viscoelasticity. Moreover, the non-penetration constraints for modeling two-body contact will be introduced, which are formulated following Signorini's contact

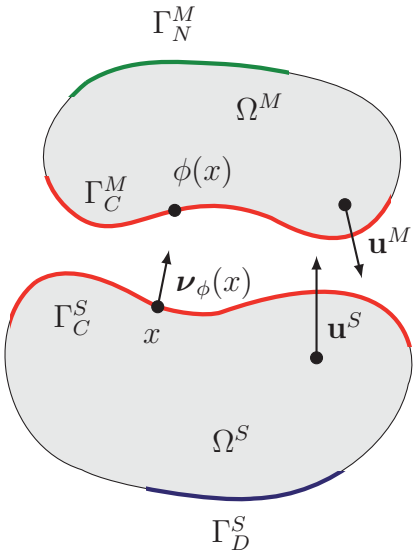

Figure 1.2.: Notation for the two-body contact problem.

conditions in displacements. The concepts have been described briefly in [51–53] for the viscoelastic case and in [19] for the purely elastic case.

At initial time $t = 0$, the volume of the two solid bodies under consideration is identified with the closure of some domains Ω^K, $K \in \{S, M\}$, which is called *reference configuration*. According to the context of mortar methods, the notations S and M stand for slave and master body, see, e.g. [90]. The domains are understood to be open, bounded, and connected subsets in $\mathbb{R}^d$ with dimension $d = 2, 3$. In addition, the bodies are assumed to have empty intersection. For the union of the two domains, the abbreviation $\Omega := \Omega^S \cup \Omega^M$ is used. The problem setting in the initial configuration is illustrated in Figure 1.2.

Notations. As is standard in literature on continuum mechanics, tensor- and vector-valued quantities are written in bold characters, e.g., $\boldsymbol{\sigma}$ and $\mathbf{v}$ with components σ_{ij} and v_i, respectively. Indices i, j, l, m are in the range from 1 to d. The scalar product in $\mathbb{R}^d$ is denoted by $(\cdot, \cdot)$, and the Euclidean vector norm is written as $|\cdot|$. The partial derivative with respect to the spatial variable x_j is indicated by a subindex j, e.g., $\mathbf{v}_{,j}$, and ∇ means the gradient of a vector field. The transpose of a vector $\mathbf{v}$ is denoted by $\mathbf{v}^T$. Derivatives with respect to the time t are indicated by dots ($\dot{}$). For the sake of clear arrangement, the abbreviation $\bar{\mathbf{v}} := (\mathbf{v}, \dot{\mathbf{v}})$ is set for a function $\mathbf{v}$ and its first time derivative $\dot{\mathbf{v}}$.

If the two bodies are subjected to initial velocities or to volume, surface, or contact forces, they will undergo some deformation when time proceeds and take on a new configuration. Hence, each material particle $\mathbf{x} \in \Omega$ of the bodies in the reference

configuration is assigned to a new position in the deformed configuration at time $t > 0$. The time interval of interest is $[0, T]$. In elasticity, the final position of every point is usually described by the *deformation* function

$$\boldsymbol{\varphi} : \Omega \times (0, T] \longrightarrow \mathbb{R}^d . \tag{1.1}$$

The *displacement* field is defined by the relation

$$\mathbf{u} : \Omega \times (0, T] \longrightarrow \mathbb{R}^d , \quad \mathbf{u}(\mathbf{x}, t) := \boldsymbol{\varphi}(\mathbf{x}, t) - \mathbf{x} . \tag{1.2}$$

This quantity commonly plays the role of unknowns in solid mechanics. The situation is sketched in Figure 1.3. According to the notation for the two bodies, the displacements (and their time derivatives) are decomposed via $\mathbf{u} := (\mathbf{u}^S, \mathbf{u}^M)$.

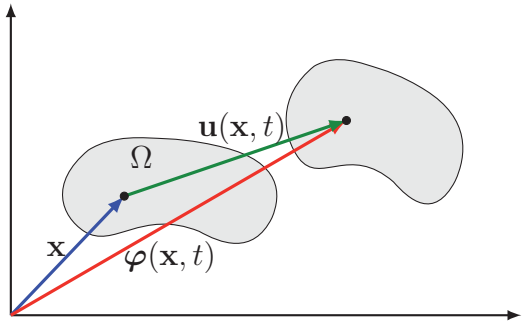

Figure 1.3.: Deformations and displacements.

Next, a short description of the basic concepts of linear viscoelasticity will be given, which will be utilized for modeling the mechanics of human bone and cartilage under deformation.

Linear Viscoelasticity. When the human knee is subjected to real physiological loadings, the bones typically undergo small deformations only. Hence, this thesis deals with the linearized second-order *strain tensor*

$$\boldsymbol{\varepsilon}(\mathbf{v}) := \frac{1}{2}\big(\nabla \mathbf{v} + (\nabla \mathbf{v})^T\big) . \tag{1.3}$$

By definition, the linearized strain is invariant under translations, but not under rotations. In particular, this means that the model used in the following is not invariant under rigid body motions: a deformation is called *rigid* if it is writable as a combination of translation and rotation around the origin.

The deformation of the two bodies under consideration causes stresses, which are described by the *stress tensor* $\boldsymbol{\sigma}$. The link between stress and strain is given by *constitutive relations* providing the specific properties of a material. A material is called *elastic*, if the stress tensor at a point $\mathbf{x} \in \Omega$ only depends on the gradient of

the displacements at $\mathbf{x}$ at the same time and possibly on $\mathbf{x}$ itself. By contrast, the stress tensor of *viscous* material depends on the gradient of the velocities. The term *viscoelasticity* means that the material presents both elastic and viscous properties. As justified in Section 1.1, bone and articulating cartilage can be assumed to consist of linearly elastic and viscoelastic material, respectively.

In rheology, elastic behavior is described by springs, which are elements providing a connection between stress and strain. Viscous behavior is modeled by dashpots, which exhibit a connection between stress and strain rate. In general, these elements can be combined in serial or in parallel [35]. Here, the latter construction is chosen. This leads to the *Kelvin-Voigt constitutive law*, where stress and strain or strain rate obey the linear relationship

$$\boldsymbol{\sigma}(\mathbf{u}, \dot{\mathbf{u}}) := \mathbf{E}\,\boldsymbol{\varepsilon}(\mathbf{u}) + \mathbf{V}\,\boldsymbol{\varepsilon}(\dot{\mathbf{u}})\,. \tag{1.4}$$

The proportionality factors $\mathbf{E}$ and $\mathbf{V}$ denote the fourth-order *elasticity tensor* and *viscosity tensor* characterizing the material, respectively (see, e.g., [35]). Both tensors are assumed to be sufficiently smooth, bounded, symmetric, and uniformly positive definite, i.e., there are constants $E_0, V_0 > 0$ such that

$$(\boldsymbol{E}\boldsymbol{\zeta}, \boldsymbol{\zeta}) \geq E_0|\boldsymbol{\zeta}|^2 \qquad (\boldsymbol{V}\boldsymbol{\zeta}, \boldsymbol{\zeta}) \geq V_0|\boldsymbol{\zeta}|^2 \tag{1.5}$$

for all symmetric second-order tensors $\boldsymbol{\zeta} = (\zeta_{ij})$, where $|\boldsymbol{\zeta}| = (\sum_{i,j} \zeta_{ij}^2)^{1/2}$. If the viscosity tensor vanishes, the constitutive law reduces to *Hooke's law* as used for purely linear elastic springs. If the elasticity tensor vanishes, the resulting linear relation between stress and strain rate is called *Newton's law*. If both tensors are equal to zero, the deformation of the material is rigid.

If the elasticity and viscosity tensors do not explicitly depend on the material point $\mathbf{x} \in \Omega$, i.e., if the material behaves the same at all points, the material is said to be *homogeneous*. If the tensors are invariant under rotations of the coordinate system for a fixed point $\mathbf{x} \in \Omega$, i.e., if the material shows the same behavior in all directions, the material is called *isotropic* at $\mathbf{x}$. For homogeneous and isotropic materials, the stress tensor for pure elasticity or viscosity is fully specified by only two material parameters via

$$\boldsymbol{\sigma} = \lambda\,(\mathrm{tr}\boldsymbol{\varepsilon})\,\mathbf{Id} + 2\mu\,\boldsymbol{\varepsilon}\,,$$

where $\mathbf{Id}$ denotes the identity and tr the trace of a tensor. Materials behaving like this are named *St. Venant-Kirchhoff materials*. The constants $\lambda > 0$ and $\mu > 0$ are called *Lamé parameters*. For the elasticity tensor, the notation

$$\mathbf{E}\,\boldsymbol{\varepsilon}(\mathbf{u}) = \frac{E\nu}{(1+\nu)(1-2\nu)}\,(\mathrm{tr}\boldsymbol{\varepsilon}(\mathbf{u}))\,\mathbf{Id} + \frac{E}{1+\nu}\,\boldsymbol{\varepsilon}(\mathbf{u}) \tag{1.6}$$

is more prevalently used in the engineering literature. The two parameters $E > 0$ and $0 < \nu < 1/2$ are called *Young's modulus* and *Poisson ratio* of the material,

respectively. For more information on elasticity see, e.g., [12, 16, 71]. The viscous component is usually expressed via

$$\mathbf{V}\,\boldsymbol{\varepsilon}(\dot{\mathbf{u}}) = \left(\mu_{\text{bulk}} - \frac{2}{3}\mu_{\text{shear}}\right)(\text{tr}\boldsymbol{\varepsilon}(\dot{\mathbf{u}}))\,\mathbf{Id} + 2\mu_{\text{shear}}\,\boldsymbol{\varepsilon}(\dot{\mathbf{u}}) \tag{1.7}$$

with the *shear viscosity* $\mu_{\text{shear}} > 0$ and the *bulk viscosity* $\mu_{\text{bulk}} > 0$ [30].

Each of the domain boundaries $\Gamma^K := \partial\Omega^K$, $K \in \{S, M\}$ is assumed to be decomposed into three pairwise disjoint open subsets via $\partial\Omega^K = \bar{\Gamma}_C^K \cup \bar{\Gamma}_N^K \cup \bar{\Gamma}_C^K$: Γ_D^K, the Dirichlet boundary, Γ_N^K, the Neumann boundary, and Γ_C^K, the possible contact boundary, see Figure 1.2. The actual contact boundary is an unknown of the problem, but is assumed to be contained in a compact strict subset of Γ_C^K. For abbreviation, $\Gamma_* := \Gamma_*^S \cup \Gamma_*^M$ with $* \in \{D, N, C\}$ is set in the following. Each boundary segment is assumed to be smooth, i.e., $\Gamma_*^K \in C^{0,1}$ (for a precise definition see, e.g., [95]). Then, Rademacher's theorem allows introducing an associated outward directed normal vector $\boldsymbol{\nu}_*^K \in \mathbf{L}^\infty$ almost everywhere on each of the boundaries, cf., e.g., [12].

At the possible contact interfaces Γ_C, the bodies may come into contact but must not penetrate each other. Therefore, the displacements have to fulfill a condition modeling the geometric non-penetration. A suitable formulation for dynamical contact between two bodies with curved surfaces is given below.

Non-penetration condition. The commonly employed linearized non-penetration condition [24] exploits the simplifying assumption of small deformations again. For a precise formulation of this constraint, assume the existence of a bijective and smooth *contact mapping*

$$\boldsymbol{\phi} : \Gamma_C^S \longrightarrow \Gamma_C^M\,, \tag{1.8}$$

which identifies a priori the two possible contact boundaries with each other, see Figure 1.2. If the bijection $\boldsymbol{\phi}$ is the identity, the contact surfaces coincide or one surface is contained in the other. The initial *gap function* in between the two bodies is defined as

$$g : \Gamma_C^S \longrightarrow \mathbb{R}\,, \quad g(\mathbf{x}) := |\mathbf{x} - \boldsymbol{\phi}(\mathbf{x})|\,, \tag{1.9}$$

and the corresponding normalized outward *normal vector* is given by

$$\boldsymbol{\nu}_{\boldsymbol{\phi}}(\mathbf{x}) := \begin{cases} \dfrac{\boldsymbol{\phi}(\mathbf{x}) - \mathbf{x}}{|\boldsymbol{\phi}(\mathbf{x}) - \mathbf{x}|}\,, & \text{if} \quad \mathbf{x} \neq \boldsymbol{\phi}(\mathbf{x})\,,\ \mathbf{x} \in \Gamma_C^S\,, \\ \boldsymbol{\nu}_C^S(\mathbf{x}) = -\boldsymbol{\nu}_C^M(\mathbf{x})\,, & \text{if} \quad \mathbf{x} = \boldsymbol{\phi}(\mathbf{x})\,,\ \mathbf{x} \in \Gamma_C^S\,. \end{cases} \tag{1.10}$$

With respect to the *relative displacement* in normal direction,

$$[\mathbf{u}(\mathbf{x}, t) \cdot \boldsymbol{\nu}]_{\boldsymbol{\phi}} := \left(\mathbf{u}^S(\mathbf{x}, t) - \mathbf{u}^M(\boldsymbol{\phi}(\mathbf{x}), t)\right) \cdot \boldsymbol{\nu}_{\boldsymbol{\phi}}(\mathbf{x})\,, \quad \mathbf{x} \in \Gamma_C^S\,,\ t \in [0, T]\,, \tag{1.11}$$

the *linearized non-penetration condition* is defined via

$$[\mathbf{u}(\mathbf{x},t)\cdot\boldsymbol{\nu}]_{\boldsymbol{\phi}} \leq g(\mathbf{x})\,, \quad \mathbf{x}\in\Gamma_C^S\,,\ t\in[0,T]\,. \tag{1.12}$$

In the following, the linearized non-penetration condition is also called *Signorini contact condition* for simplicity. Since the condition is formulated in terms of the reference configuration solely, the contact constraints can be computed easily. However, tangential displacements are not taken into account such that geometric penetration might occur.

If the assumption of small displacements is fulfilled, the possible contact boundaries on slave and master side are very close to each other, and the outer normals can be regarded to differ only slightly: $\boldsymbol{\nu}_C^S \approx -\boldsymbol{\nu}_C^M \circ \boldsymbol{\phi} \approx \boldsymbol{\nu}_{\boldsymbol{\phi}}$. Then, the linearized contact condition (1.12) is a close approximation of the geometrical non-penetration condition [24]. In this case, the quantity $[\mathbf{u}\cdot\boldsymbol{\nu}]_{\boldsymbol{\phi}}$ is called the *jump* of $\mathbf{u}$ in normal direction at the contact interfaces.

1.3. Strong and Variational Problem

In this section, a frictionless dynamical contact problem between two linearly viscoelastic bodies satisfying the Kelvin-Voigt material law will be stated, which is based on Signorini's contact conditions. In a first step, the strong problem formulation will be presented. Afterwards, the weak formulation will be introduced in terms of a variational inequality.

Contact stresses. The *boundary stresses* are defined as

$$\hat{\boldsymbol{\sigma}}(\mathbf{u},\dot{\mathbf{u}}) := \boldsymbol{\sigma}(\mathbf{u},\dot{\mathbf{u}})\cdot\boldsymbol{\nu} \text{ on } \Gamma\,, \tag{1.13}$$

and the *contact stresses* are given by

$$\hat{\boldsymbol{\sigma}}_C(\mathbf{u},\dot{\mathbf{u}}) := \hat{\boldsymbol{\sigma}}(\mathbf{u}^S,\dot{\mathbf{u}}^S) \text{ on } \Gamma_C^S\,. \tag{1.14}$$

The normal and tangential components of the contact stresses are denoted by

$$\sigma_{\nu_{\boldsymbol{\phi}}}(\mathbf{u},\dot{\mathbf{u}}) := \hat{\boldsymbol{\sigma}}_C(\mathbf{u},\dot{\mathbf{u}})\cdot\boldsymbol{\nu}_{\boldsymbol{\phi}} \text{ on } \Gamma_C^S \tag{1.15}$$

and

$$\boldsymbol{\sigma}_t(\mathbf{u},\dot{\mathbf{u}}) := \hat{\boldsymbol{\sigma}}_C(\mathbf{u},\dot{\mathbf{u}}) - \sigma_{\nu_{\boldsymbol{\phi}}}(\mathbf{u},\dot{\mathbf{u}})\cdot\boldsymbol{\nu}_{\boldsymbol{\phi}} \text{ on } \Gamma_C^S\,, \tag{1.16}$$

respectively.

With these definitions, the strong formulation of a two-body dynamical contact problem can be given [23, 49]. The problem amounts to the solution of a partial differential equation from elastodynamics with additional contact constraints.

Strong problem formulation.

$$\rho\ddot{\mathbf{u}} - \operatorname{div}\boldsymbol{\sigma}(\mathbf{u},\dot{\mathbf{u}}) = \rho\mathbf{f} \qquad \text{on } \Omega\times[0,T] \qquad (1.17a)$$

$$\mathbf{u} = \mathbf{0} \qquad \text{on } \Gamma_D\times[0,T] \qquad (1.17b)$$

$$\hat{\boldsymbol{\sigma}}(\mathbf{u},\dot{\mathbf{u}}) = \boldsymbol{\pi} \qquad \text{on } \Gamma_N\times[0,T] \qquad (1.17c)$$

$$[\mathbf{u}\cdot\boldsymbol{\nu}]_{\boldsymbol{\phi}} \le g \qquad \text{on } \Gamma_C^S\times[0,T] \qquad (1.17d)$$

$$\hat{\boldsymbol{\sigma}}\big(\mathbf{u}^M\circ\boldsymbol{\phi},\dot{\mathbf{u}}^M\circ\boldsymbol{\phi}\big) = -\hat{\boldsymbol{\sigma}}\big(\mathbf{u}^S,\dot{\mathbf{u}}^S\big) \qquad \text{on } \Gamma_C^S\times[0,T] \qquad (1.17e)$$

$$\big([\mathbf{u}\cdot\boldsymbol{\nu}]_{\boldsymbol{\phi}} - g\big)\,\sigma_{\nu_{\boldsymbol{\phi}}}(\mathbf{u},\dot{\mathbf{u}}) = 0 \qquad \text{on } \Gamma_C^S\times[0,T] \qquad (1.17f)$$

$$\sigma_{\nu_{\boldsymbol{\phi}}}(\mathbf{u},\dot{\mathbf{u}}) \le 0 \qquad \text{on } \Gamma_C^S\times[0,T] \qquad (1.17g)$$

$$\boldsymbol{\sigma}_t(\mathbf{u},\dot{\mathbf{u}}) = \mathbf{0} \qquad \text{on } \Gamma_C^S\times[0,T] \qquad (1.17h)$$

$$\mathbf{u}(0) = \mathbf{u}_0, \dot{\mathbf{u}}(0) = \dot{\mathbf{u}}_0 \qquad \text{on } \Omega \qquad (1.17i)$$

In the first instance, the problem consists of an equation of motion (1.17a) representing the balance law of momentum or Newton's second law. This equation is second-order in time and formulated on the undeformed reference configuration Ω. The density of external volume forces applied to the bodies is denoted by $\mathbf{f}$. The mass density is given by $\rho > 0$ and may generally vary with the material points $\mathbf{x}\in\Omega$. In what follows, $\rho = 1$ is set for ease of presentation.

With regard to mixed boundary conditions, the body is clamped at the Dirichlet boundaries Γ_D, where vanishing Dirichlet values are prescribed, see (1.17b). On the Neumann parts Γ_N of the boundaries, surface tractions $\boldsymbol{\pi}$ are acting, cf. (1.17c). The contact conditions are stated on the remaining contact boundaries Γ_C, where the two bodies may potentially get into contact. Bearing the non-penetration condition (1.12) in mind, the relative displacements in normal direction must not exceed the normal gap between the two bodies, cf. (1.17d). This constraint is the only primal contact condition arising in the problem.

The statement of the problem is accompanied by the dual conditions (1.17e)–(1.17h) on the boundary stresses developed at the possible contact boundaries. These stresses can be interpreted as the contact forces that are necessary to prevent interpenetration of the two bodies. By reason of Newton's second law, (1.17e) gives the equilibrium of the contact stresses at contact interfaces. The complementarity condition (1.17f) states that stresses in normal direction are only generated where contact is occurring. Finally, normal contact stresses have to be compressive or equal to zero, cf. (1.17g).

In a normal human knee joint, frictional effects at contact surfaces are negligible. Hence, the tangential stresses are assumed to be equal to zero, cf. (1.17h), which enables the bodies to move freely in tangential directions. The displacement and velocity fields at initial time are prescribed via (1.17i).

Notations. Let $L_2(\Omega^K)$ be the space of square-integrable functions with the vector-valued counterparts $\mathbf{L}_2(\Omega^K) := (L_2(\Omega^K))^d$, and the corresponding product space

$\mathbf{L}_2(\Omega) := \mathbf{L}_2(\Omega^S) \times \mathbf{L}_2(\Omega^M)$. The Sobolev space of weakly differentiable functions with derivatives in $\mathbf{L}_2(\Omega)$ is denoted by $\mathbf{H}^1(\Omega)$. The topological dual space is indicated as $(\mathbf{H}^1)^*(\Omega)$. Scalar products are written in the form $(\cdot,\cdot)_{\mathbf{L}_2}$ and $(\cdot,\cdot)_{\mathbf{H}^1}$ with induced norms $\|\mathbf{v}\|^2_{\mathbf{L}_2} := (\mathbf{v},\mathbf{v})_{\mathbf{L}_2}$ and $\|\mathbf{v}\|^2_{\mathbf{H}^1} := (\mathbf{v},\mathbf{v})_{\mathbf{H}^1}$, respectively. For the dual pairing, the notation $\langle\cdot,\cdot\rangle_{(\mathbf{H}^1)^*\times\mathbf{H}^1}$ is used, and the operator norm on $(\mathbf{H}^1)^*$ is written as $\|\cdot\|_{(\mathbf{H}^1)^*}$. For details concerning Sobolev spaces see, e.g., [5]. For given Banach space $\mathbf{V}$ and times $t_0 < t < \infty$, let $\mathbf{C}([t_0,t],\mathbf{V})$ be the continuous functions and $\mathbf{C}^k([t_0,t],\mathbf{V})$, $k \in \mathbb{N}$ the k-times continuously differentiable functions $\mathbf{v} : [t_0,t] \to \mathbf{V}$. The space $\mathbf{L}_2(t_0,t;\mathbf{V})$ consists of all measurable functions $\mathbf{v} : (t_0,t) \to \mathbf{V}$ for which

$$\|\mathbf{v}\|^2_{\mathbf{L}_2(t_0,t;\mathbf{V})} := \int_{t_0}^{t} \|\mathbf{v}(t)\|^2_{\mathbf{V}}\, dt < \infty$$

holds. Identifying $\mathbf{L}_2(\Omega)$ with its dual space yields the evolution triple

$$\mathbf{H}^1(\Omega) \subset \mathbf{L}_2(\Omega) \subset \left(\mathbf{H}^1\right)^*(\Omega)$$

with dense, continuous, and compact embeddings. With this in mind, the Sobolev space $\mathbf{W}^1_2(t_0,t;\mathbf{H}^1,\mathbf{L}_2)$ means the set of all functions $\mathbf{v} \in \mathbf{L}_2(t_0,t;\mathbf{H}^1(\Omega))$ that have generalized derivatives $\dot{\mathbf{v}} \in \mathbf{L}_2(t_0,t;(\mathbf{H}^1)^*(\Omega))$, cf., e.g., [93, Section 23.6].

Generalized boundary conditions. The weak formulation of the dynamical contact problem requires to deal with generalized boundary conditions for $\mathbf{H}^1(\Omega)$-functions. For this aim, a precise meaning of extensions of such functions to spaces of functions defined on the boundary segments Γ_D, Γ_N, and Γ_C is needed. The classical trace theorem [94, Appendix, Application (49)] states that, if $\Gamma \in C^{0,1}$, there exists a linear, continuous, and surjective operator $\boldsymbol{\gamma} : \mathbf{H}^1(\Omega) \to \mathbf{H}^{1/2}(\Gamma)$ such that $\boldsymbol{\gamma}(\mathbf{u})$ is the classical boundary function of $\mathbf{u}$ with respect to Γ for all $\mathbf{u} \in \mathbf{C}^1(\bar{\Omega})$. If $\mathbf{u} \in \mathbf{H}^1(\Omega)$, $\boldsymbol{\gamma}(\mathbf{u})$ is called the trace of $\mathbf{u}$. The trace is uniquely determined as an element of the space $\mathbf{L}_2(\Gamma)$, i.e., up to surface measure zero. Here, $\mathbf{L}_2(\Gamma)$ is the space of square-integrable functions on Γ. The definition of $\mathbf{H}^{1/2}(\Gamma)$ can also be found in [94]. In the following, $(\mathbf{H}^{1/2})^*(\Gamma)$ denotes the corresponding dual space, and the dual pairing is written as $\langle\cdot,\cdot\rangle_{(\mathbf{H}^{1/2})^*\times\mathbf{H}^{1/2}}$.

Let $\boldsymbol{\gamma}_*$ be the surjective trace maps that associate $\mathbf{v} \in \mathbf{H}^1(\Omega)$ with the restrictions $\boldsymbol{\gamma}_*(\mathbf{v})$ to $\mathbf{H}^{1/2}(\Gamma_*)$. Then, the Dirichlet boundary conditions give rise to the subspaces

$$\mathbf{H}^1_D(\Omega) := \left\{\mathbf{v} \in \mathbf{H}^1(\Omega) \,\middle|\, \boldsymbol{\gamma}_D(\mathbf{v}) = \mathbf{0} \text{ a.e. on } \boldsymbol{\Gamma}_D\right\} \subset \mathbf{H}^1(\Omega)\,. \tag{1.18}$$

This is the set of functions in $\mathbf{H}^1(\Omega)$ that are zero on Γ_D in the sense of traces.

The non-penetration condition (1.12) for contact problems of Signorini type affects only points at the possible contact boundaries of the domains. Hence, the definition of the set of admissible displacements in $\mathbf{H}^1_D(\Omega)$ has to make use of the trace operator

γ_C on Γ_C. Let $g \in \mathbf{H}^{1/2}(\Gamma_C)$ be a given positive gap function. Then, the solution space for displacements of the weak dynamical contact problem is the *admissible set*

$$\mathcal{K} := \left\{ \mathbf{v} \in \mathbf{H}^1_D(\Omega) \,\middle|\, [\boldsymbol{\gamma}_C(\mathbf{v}) \cdot \boldsymbol{\nu}]_{\boldsymbol{\phi}} \leq g \text{ a.e. on } \Gamma_C \right\} \subset \mathbf{H}^1(\Omega)\,. \tag{1.19}$$

The set is non-empty, closed, and convex due to the linearization of the contact constraints. For the above definition of the admissible set, the possible contact boundaries Γ_C have to be contained strictly in $\Gamma \backslash \Gamma_D$. Otherwise, the space $\mathbf{H}^{1/2}(\Gamma_C)$ is not appropriate for dealing with traces on Γ_C since the surjectivity of the trace operator from $\mathbf{H}^1_D(\Omega)$ to $\mathbf{H}^{1/2}(\Gamma_C)$ may be lost. This technical difficulty can be resolved by introducing a special subspace of $\mathbf{H}^{1/2}(\Gamma_C)$. For more details see [49,69].

Generalized forces. The internal forces can be written as a bilinear form

$$a(\mathbf{v}, \mathbf{w}) := \sum_{i,j,k,l} \int_\Omega E^K_{ijml} v^K_{i,j} w^K_{l,m}\, d\mathbf{x} = \int_\Omega \mathbf{E}\boldsymbol{\varepsilon}\big(\mathbf{v}^K\big) : \boldsymbol{\varepsilon}\big(\mathbf{w}^K\big) d\mathbf{x}\,, \quad \mathbf{v}, \mathbf{w} \in \mathbf{H}^1 \tag{1.20}$$

for the elastic part and

$$b(\mathbf{v}, \mathbf{w}) := \sum_{i,j,k,l} \int_\Omega V^K_{ijml} v^K_{i,j} w^K_{l,m}\; d\mathbf{x} = \int_\Omega \mathbf{V}\boldsymbol{\varepsilon}\big(\mathbf{v}^K\big) : \boldsymbol{\varepsilon}\big(\mathbf{w}^K\big)\, d\mathbf{x}\,, \quad \mathbf{v}, \mathbf{w} \in \mathbf{H}^1 \tag{1.21}$$

for the viscous part. Both bilinear forms are bounded in $\mathbf{H}^1$, i.e.,

$$|a(\mathbf{v}, \mathbf{w})| \leq E_\infty \|\mathbf{v}\|_{\mathbf{H}^1} \|\mathbf{w}\|_{\mathbf{H}^1}\,, \qquad \mathbf{v}, \mathbf{w} \in \mathbf{H}^1 \tag{1.22}$$

and

$$|b(\mathbf{v}, \mathbf{w})| \leq V_\infty \|\mathbf{v}\|_{\mathbf{H}^1} \|\mathbf{w}\|_{\mathbf{H}^1}\,, \qquad \mathbf{v}, \mathbf{w} \in \mathbf{H}^1\,, \tag{1.23}$$

where the constants E_∞ and V_∞ only depend on $\boldsymbol{E}$ and $\boldsymbol{V}$, respectively. The bilinear forms give rise to seminorms

$$\|\cdot\|_a^2 := a(\cdot, \cdot)\,, \qquad \|\cdot\|_b^2 := b(\cdot, \cdot)\,. \tag{1.24}$$

Since the elasticity and viscosity tensors are positive definite, cf. (1.5), Korn's second inequality (A.2) yields the ellipticity of the bilinear forms under the assumption that Γ_D has positive measure:

$$|a(\mathbf{v}, \mathbf{v})| \geq E_0 c_K \|\mathbf{v}\|^2_{\mathbf{H}^1}\,, \qquad \mathbf{v} \in \mathbf{H}^1$$

and

$$|b(\mathbf{v}, \mathbf{v})| \geq V_0 c_K \|\mathbf{v}\|^2_{\mathbf{H}^1}\,, \qquad \mathbf{v} \in \mathbf{H}^1\,.$$

In this case, $\|\cdot\|_{\mathbf{H}^1}$ and $\|\cdot\|_a$ or $\|\cdot\|_b$ are equivalent norms on $\mathbf{H}^1$.

For the data, assume that $\mathbf{f}(\cdot, t) \in (\mathbf{H}^1)^*(\Omega)$ and $\boldsymbol{\pi}(\cdot, t) \in (\mathbf{H}^{1/2})^*(\Gamma_N)$ for almost every $t \in [0, T]$, which accounts for the forces acting on the volume and the tractions

on the Neumann boundaries. The sum of the external forces is represented by the linear functional

$$f_{\text{ext}}(\mathbf{v}) := \langle \mathbf{f}, \mathbf{v} \rangle_{(\mathbf{H}^1)^*(\Omega)\times\mathbf{H}^1(\Omega)} + \langle \boldsymbol{\pi}, \boldsymbol{\gamma}_N(\mathbf{v}) \rangle_{\mathbf{H}^{-1/2}(\Gamma_N)\times\mathbf{H}^{1/2}(\Gamma_N)}\,, \qquad \mathbf{v} \in \mathbf{H}^1\,. \quad (1.25)$$

Moreover, it is convenient to write the sum of elastic and external forces as

$$\langle \mathbf{F}(\mathbf{w}), \mathbf{v} \rangle_{(\mathbf{H}^1)^*\times\mathbf{H}^1} := a(\mathbf{w}, \mathbf{v}) - f_{\text{ext}}(\mathbf{v})\,, \qquad \mathbf{v}, \mathbf{w} \in \mathbf{H}^1\,, \quad (1.26)$$

and the viscoelastic forces as

$$\langle \mathbf{G}(\mathbf{w}), \mathbf{v} \rangle_{(\mathbf{H}^1)^*\times\mathbf{H}^1} := b(\mathbf{w}, \mathbf{v})\,, \qquad \mathbf{v}, \mathbf{w} \in \mathbf{H}^1\,. \quad (1.27)$$

Variational problem formulation. The weak formulation of the contact problem can be derived via integration by parts and exploiting the boundary conditions [23, 49]. This leads to a hyperbolic variational inequality that can be written as follows: for almost every $t \in [0, T]$, find $\mathbf{u}(\cdot, t) \in \mathcal{K}$ with $\mathbf{u} \in \mathbf{C}([0, T], \mathbf{H}^1)$ and $\dot{\mathbf{u}} \in \mathbf{W}_2^1(0, T; \mathbf{H}^1, \mathbf{L}_2)$ such that for all $\mathbf{v} \in \mathcal{K}$

$$\langle \ddot{\mathbf{u}}, \mathbf{v} - \mathbf{u} \rangle_{(\mathbf{H}^1)^*\times\mathbf{H}^1} + \langle \mathbf{F}(\mathbf{u}), \mathbf{v} - \mathbf{u} \rangle_{(\mathbf{H}^1)^*\times\mathbf{H}^1} + \langle \mathbf{G}(\dot{\mathbf{u}}), \mathbf{v} - \mathbf{u} \rangle_{(\mathbf{H}^1)^*\times\mathbf{H}^1} \geq 0 \quad (1.28)$$

and

$$\mathbf{u}(0) = \mathbf{u}_0\,, \quad \dot{\mathbf{u}}(0) = \dot{\mathbf{u}}_0\,. \quad (1.29)$$

Alternatively, the variational problem can be defined on the whole space $\mathbf{H}^1$. To this end, the constraints $\mathbf{u}(\cdot, t) \in \mathcal{K}$ are incorporated by the characteristic functional

$$I_{\mathcal{K}}(\mathbf{u}) = \begin{cases} 0 & \text{if } \mathbf{u} \in \mathcal{K} \\ \infty & \text{else} \end{cases}\,, \qquad \mathbf{u} \in \mathbf{H}^1\,.$$

Then, the variational inequality (1.28) can equivalently be formulated as the variational inclusion

$$0 \in \ddot{\mathbf{u}} + \mathbf{F}(\mathbf{u}) + \mathbf{G}(\dot{\mathbf{u}}) + \partial I_{\mathcal{K}}(\mathbf{u}) \quad (1.30)$$

utilizing the set-valued subdifferential $\partial I_{\mathcal{K}}$ of $I_{\mathcal{K}}$ (see, e.g., [26]). The subdifferential enforces the fulfillment of the non-penetration condition by penalizing any inadmissible displacement with infinite energy.

For a given solution $\mathbf{u}$ of the variational inequality (1.28), the *contact forces* $\mathbf{F}_{\text{con}}(\mathbf{u}) \in (\mathbf{H}^1)^*$ are defined by

$$\langle \mathbf{F}_{\text{con}}(\mathbf{u}), \mathbf{v} \rangle_{(\mathbf{H}^1)^*\times\mathbf{H}^1} := \langle \ddot{\mathbf{u}} + \mathbf{F}(\mathbf{u}) + \mathbf{G}(\dot{\mathbf{u}}), \mathbf{v} \rangle_{(\mathbf{H}^1)^*\times\mathbf{H}^1}\,, \qquad \mathbf{v} \in \mathbf{H}^1 \quad (1.31)$$

for almost every $t \in [0, T]$. Upon exploiting (1.28),

$$\langle \mathbf{F}_{\text{con}}(\mathbf{u}), \mathbf{u} - \mathbf{v} \rangle_{(\mathbf{H}^1)^*\times\mathbf{H}^1} \leq 0 \quad (1.32)$$

for $\mathbf{v} \in \mathcal{K}$, and comparing (1.30) and (1.31) shows that $-\mathbf{F}_{\text{con}}(\mathbf{u}) \in \partial I_{\mathcal{K}}(\mathbf{u})$.

Provided the solution $\mathbf{u}$ is sufficiently smooth, the equivalence of the strong and variational formulation of the dynamical contact problem can be shown via integrating by parts with suitable smooth test functions.

Initial conditions. The generalized derivative $\dot{\mathbf{u}} \in \mathbf{W}_2^1(0,T;\mathbf{H}^1,\mathbf{L}_2)$ is only determined up to changes on a set of measure zero on $[0,T]$. Nevertheless, the initial conditions (1.29) for the velocities are formulated in a meaningful way: since the embedding $\mathbf{W}_2^1(0,T;\mathbf{H}^1,\mathbf{L}_2) \subset \mathbf{C}([0,T],\mathbf{L}_2)$ is continuous, cf. [94, Section 33.1], there exists a uniquely determined representative $\dot{\mathbf{u}} \in \mathbf{C}([0,T],\mathbf{L}_2)$. The initial conditions are to be understood in this sense.

Remark 1.3.1. In the simple case of pure elasticity and vanishing external forces, a solution of the dynamical contact problem (1.30) can be regarded as a stationary point of the action integral

$$\int_0^T \mathcal{L}(\mathbf{v}(t),\dot{\mathbf{v}}(t))\,dt$$

with the Lagrange functional

$$\mathcal{L}(\mathbf{v},\dot{\mathbf{v}}) := \frac{1}{2}\|\dot{\mathbf{v}}\|_{\mathbf{L}_2}^2 - a(\mathbf{v},\mathbf{v}) - I_{\mathcal{K}}(\mathbf{v}) \in \mathbb{R}\cup\{\infty\}$$

under suitable initial and boundary conditions [46, 70]. This principle can also be generalized to the viscoelastic problem.

As shown, for instance, in [6], the unilateral contact problem between a viscoelastic body and a rigid foundation has at least one weak solution. However, uniqueness and well-posedness are still open questions for solutions of dynamical contact problems.

Notation. In the following, for $t_n, t_{n+1} \in [0,T]$, the state of a solution $\bar{\mathbf{u}} = (\mathbf{u},\dot{\mathbf{u}})$ of (1.28) is represented by

$$\mathbf{u}(t_{n+1}) = \mathbf{\Phi}^{t_{n+1},t_n}(\mathbf{u}(t_n),\dot{\mathbf{u}}(t_n))\,, \quad \dot{\mathbf{u}}(t_{n+1}) = \dot{\mathbf{\Phi}}^{t_{n+1},t_n}(\mathbf{u}(t_n),\dot{\mathbf{u}}(t_n)) \tag{1.33}$$

with the *evolution operator*

$$\bar{\mathbf{\Phi}}^{t_{n+1},t_n} = (\mathbf{\Phi}^{t_{n+1},t_n},\dot{\mathbf{\Phi}}^{t_{n+1},t_n}) : \mathbf{H}^1\times\mathbf{L}_2 \longrightarrow \mathbf{H}^1\times\mathbf{L}_2\,. \tag{1.34}$$

1.4. Conservation Properties and Persistency Condition

In the final section of this introductory chapter, the influence of the contact constraints on the conservation of energy, linear and angular momentum in the system will be studied. In particular, the validity of a persistency condition for viscoelastic problems will be discussed in comparison with the purely elastic case.

Linear momentum. The *linear momentum* of a state $\bar{\mathbf{u}} = (\mathbf{u}, \dot{\mathbf{u}})$ is defined as

$$\boldsymbol{\mathcal{L}}(\dot{\mathbf{u}}) := \int_\Omega \dot{\mathbf{u}}(\mathbf{x})\, d\mathbf{x}\,. \tag{1.35}$$

In the case of non-vanishing external forces acting on the volume or stemming from Neumann or Dirichlet boundaries, the linear momentum cannot be expected to be constant in time. Excluding these situations, the linear momentum is a conserved quantity of the system as shown in the following theorem (compare, e.g., [66]).

Theorem 1.4.1. *The variational problem* (1.28) *with* $f_{\text{ext}} = 0$ *and* $\Gamma_D = \emptyset$ *conserves the linear momentum.*

Proof. Let $t_0, t \in [0,T]$ be arbitrary times, and $\mathbf{w} \in \Omega$ a test function that is constant in time and in space. Due to $\ddot{\mathbf{u}} \in \mathbf{W}_2^1(0,T;\mathbf{H}^1,\mathbf{L}_2)$, integration by parts yields, cf. [93, Proposition 23.23],

$$\begin{aligned}
&\big(\boldsymbol{\mathcal{L}}(\dot{\mathbf{u}}(t)) - \boldsymbol{\mathcal{L}}(\dot{\mathbf{u}}(t_0))\big)\cdot \mathbf{w}\\
&= (\dot{\mathbf{u}}(t) - \dot{\mathbf{u}}(t_0), \mathbf{w})_{\mathbf{L}_2}\\
&= \int_{t_0}^t \langle \ddot{\mathbf{u}}(s), \mathbf{w}\rangle_{(\mathbf{H}^1)^*\times\mathbf{H}^1}\, ds\\
&= -\int_{t_0}^t \langle \mathbf{F}(\mathbf{u}(s)), \mathbf{w}\rangle_{(\mathbf{H}^1)^*\times\mathbf{H}^1}\, ds - \int_{t_0}^t \langle \mathbf{G}(\mathbf{u}(s)), \mathbf{w}\rangle_{(\mathbf{H}^1)^*\times\mathbf{H}^1}\, ds\\
&\quad + \int_{t_0}^t \langle \mathbf{F}_{\text{con}}(\mathbf{u}(s)), \mathbf{w}\rangle_{(\mathbf{H}^1)^*\times\mathbf{H}^1}\, ds\\
&= -\int_{t_0}^t \Big(\int_\Omega \mathbf{E}\boldsymbol{\varepsilon}(\mathbf{u}(s)) \colon \boldsymbol{\varepsilon}(\mathbf{w})\, d\mathbf{x}\Big)\, ds - \int_{t_0}^t \Big(\int_\Omega \mathbf{V}\boldsymbol{\varepsilon}(\dot{\mathbf{u}}(s)) \colon \boldsymbol{\varepsilon}(\mathbf{w})\, d\mathbf{x}\Big)\, ds\\
&\quad + \int_{t_0}^t \langle \mathbf{F}_{\text{con}}(\mathbf{u}(s)), \mathbf{w}\rangle_{(\mathbf{H}^1)^*\times\mathbf{H}^1}\, ds\,,
\end{aligned}$$

where the problem formulation (1.31) has been used. The first two terms are equal to zero since $\boldsymbol{\varepsilon}(\mathbf{w}) = 0$ by definition. Second, $[\mathbf{w}\cdot\boldsymbol{\nu}]_{\boldsymbol{\phi}} = 0$ such that $\mathbf{w} \in \mathcal{K}$ and $-\mathbf{w} \in \mathcal{K}$. Thus, the last term including the contact forces vanishes as well due to (1.32). This gives the result of the theorem. □

Angular momentum. The *angular momentum* of a state $\bar{\mathbf{u}} = (\mathbf{u}, \dot{\mathbf{u}})$ is defined as

$$\boldsymbol{\mathcal{J}}(\bar{\mathbf{u}}) := \int_\Omega \mathbf{u} \times \dot{\mathbf{u}}\, d\mathbf{x}\,. \tag{1.36}$$

In order to examine the conservation properties of the angular momentum, let the external forces be central forces meaning that $\int_\Omega (\mathbf{f} + \boldsymbol{\pi}) \times \mathbf{u}\, dx = 0$ for $\mathbf{f},\ \boldsymbol{\pi} \in \mathbf{L}_2(\Omega)$.

Via integration by parts, the angular momentum at arbitrary times $t_0, t \in [0,T]$ tested with a constant function $\mathbf{w} \in \Omega$ can formally be written as

$$
\begin{aligned}
&\big(\boldsymbol{\mathcal{J}}(\bar{\mathbf{u}}(t)) - \boldsymbol{\mathcal{J}}(\bar{\mathbf{u}}(t_0))\big) \cdot \mathbf{w} \\
&= (\mathbf{u}(t) \times \dot{\mathbf{u}}(t) - \mathbf{u}(t_0) \times \dot{\mathbf{u}}(t_0), \mathbf{w})_{\mathbf{L}_2} \\
&= (\dot{\mathbf{u}}(s), \mathbf{w} \times \mathbf{u}(s))_{\mathbf{L}_2}\Big|_{s=t_0}^{s=t} \\
&= \int_{t_0}^{t} \langle \ddot{\mathbf{u}}(s), \mathbf{w} \times \mathbf{u}(s) \rangle_{(\mathbf{H}^1)^* \times \mathbf{H}^1} \, ds - \int_{t_0}^{t} (\mathbf{w}, \dot{\mathbf{u}}(s) \times \dot{\mathbf{u}}(s) \rangle_{(\mathbf{H}^1)^* \times \mathbf{H}^1} \, ds \\
&= -\int_{t_0}^{t} \langle \mathbf{F}(\mathbf{u}(s)), \mathbf{w} \times \mathbf{u}(s) \rangle_{(\mathbf{H}^1)^* \times \mathbf{H}^1} \, ds - \int_{t_0}^{t} \langle \mathbf{G}(\mathbf{u}(s)), \mathbf{w} \times \mathbf{u}(s) \rangle_{(\mathbf{H}^1)^* \times \mathbf{H}^1} \, ds \\
&\quad + \int_{t_0}^{t} \langle \mathbf{F}_{\mathrm{con}}(\mathbf{u}(s)), \mathbf{w} \times \mathbf{u}(s) \rangle_{(\mathbf{H}^1)^* \times \mathbf{H}^1} \, ds \\
&= -\int_{t_0}^{t} \Big(\int_{\Omega} \mathbf{E}\boldsymbol{\varepsilon}(\mathbf{u}(s)) \colon \boldsymbol{\varepsilon}(\mathbf{w} \times \mathbf{u}(s)) \, d\mathbf{x} \Big) \, ds - \int_{t_0}^{t} \Big(\int_{\Omega} \mathbf{V}\boldsymbol{\varepsilon}(\dot{\mathbf{u}}(s)) \colon \boldsymbol{\varepsilon}(\mathbf{w} \times \mathbf{u}(s)) \, d\mathbf{x} \Big) \, ds \\
&\quad + \int_{t_0}^{t} \langle \mathbf{F}_{\mathrm{con}}(\mathbf{u}(s)), \mathbf{w} \times \mathbf{u}(s) \rangle_{(\mathbf{H}^1)^* \times \mathbf{H}^1} \, ds
\end{aligned}
$$

by using definition (1.31). The first two integral terms are equal to zero by arguments from tensor analysis, see [66]. Hence, it remains to verify that the contact term

$$\int_{t_0}^{t} \langle \mathbf{F}_{\mathrm{con}}(\mathbf{u}(s)), \mathbf{w} \times \mathbf{u}(s) \rangle_{(\mathbf{H}^1)^* \times \mathbf{H}^1} \, ds$$

vanishes. In the presence of contact, this requires that $[(\mathbf{w} \times \mathbf{u}) \cdot \boldsymbol{\nu}]_{\boldsymbol{\phi}} = 0$ almost everywhere on $[t_0, t]$. This condition is equivalent to $[\mathbf{u}^S - \mathbf{u}^M(\boldsymbol{\phi})] \times \boldsymbol{\nu}_{\boldsymbol{\phi}} = 0$ on Γ_C^S. Hence, the gap $\mathbf{u}^S - \mathbf{u}^M \circ \boldsymbol{\phi}$ has to be parallel to the normal vector $\boldsymbol{\nu}_{\boldsymbol{\phi}}$. However, this parallelism cannot be expected to hold in general since the transfer operator $\boldsymbol{\phi}$ originates from the reference configuration. Instead, angular momentum conservation needs the utilization of an evolution dependent surface-to-surface mapping. Nevertheless, the linearized non-penetration condition is consistent with the overall modeling assumption of small deformations, where angular momenta are of less importance.

Energy. In the context of evolution problems in elasticity, the *total energy* of a state $\bar{\mathbf{u}} = (\mathbf{u}, \dot{\mathbf{u}})$ has the form

$$\mathcal{E}(\bar{\mathbf{u}}) := \mathcal{E}_{\mathrm{kin}}(\dot{\mathbf{u}}) + \mathcal{E}_{\mathrm{pot}}(\mathbf{u}) \tag{1.37}$$

with the *kinetic energy*

$$\mathcal{E}_{\mathrm{kin}}(\dot{\mathbf{u}}) := \frac{1}{2} \|\dot{\mathbf{u}}\|_{\mathbf{L}_2}^2 \tag{1.38}$$

and the *elastic potential energy*

$$\mathcal{E}_{\mathrm{pot}}(\mathbf{u}) := \frac{1}{2}\|\mathbf{u}\|_a^2 \,. \tag{1.39}$$

For problems in viscoelasticity, the additionally appearing *viscous energy* is induced by means of

$$\mathcal{E}_{\mathrm{visco}}(\dot{\mathbf{u}}) := \|\dot{\mathbf{u}}\|_b^2 \,. \tag{1.40}$$

In the case of pure linear elasticity, the total energy of the system is in general expected to be preserved throughout the evolution. However, up to now, energy conservation could only be shown for one-dimensional problems, where the contact boundaries reduce to a single point. In this case, the variation of total energy is equal to the work of the external forces, which particularly means that the contact forces do not contribute to any work [25, 68].

Persistency condition. In higher dimensions, a proof of energy conservation typically exploits the additional requirement

$$\sigma_{\nu_\phi} \frac{\mathrm{d}}{\mathrm{d}t}\big([\boldsymbol{\gamma}_C(\mathbf{u}) \cdot \boldsymbol{\nu}]_{\boldsymbol{\phi}} - g\big) = 0 \text{ on } \Gamma_C^S \times [0,T] \,, \tag{1.41}$$

which is commonly known as *persistency condition* [66]. This condition states that the relative velocities in normal direction have to be zero at active contact boundaries. The persistency condition is well-known to be sufficient for energy conservation, but widely disputed since the physical meaning is unclear [65].

Analyzing the proof in the later Theorem 1.4.3 shows that condition (1.41) can be weakened to the *generalized persistency condition*

$$\langle \mathbf{F}_{\mathrm{con}}(\mathbf{u}(t)), \dot{\mathbf{u}}(t) \rangle_{(\mathbf{H}^1)^* \times \mathbf{H}^1} = 0 \,, \text{ a.e. } t \in [0,T] \tag{1.42}$$

in function space. The validity of this condition is provable for solutions of the viscoelastic problem. For this aim, the next theorem adopts the presentation for unilateral contact problems in [6] and references therein.

Theorem 1.4.2. *A solution of the variational problem* (1.28) *satisfies the generalized persistency condition* (1.42)*.*

Proof. Definition (1.31) of the contact forces and the continuity of the linearly viscoelastic forces, see (1.22) and (1.23), lead to

$$\begin{aligned}
&\|\mathbf{F}_{\mathrm{con}}(\mathbf{u})\|_{\mathbf{L}_2(0,T;(\mathbf{H}^1)^*)} \\
&\leq c\big(\|\ddot{\mathbf{u}}\|_{\mathbf{L}_2(0,T;(\mathbf{H}^1)^*)} + \|\mathbf{F}(\mathbf{u})\|_{\mathbf{L}_2(0,T;(\mathbf{H}^1)^*)} + \|\mathbf{G}(\mathbf{u})\|_{\mathbf{L}_2(0,T;(\mathbf{H}^1)^*)}\big) \\
&\leq c\big(\|\ddot{\mathbf{u}}\|_{\mathbf{L}_2(0,T;(\mathbf{H}^1)^*)} + \|\mathbf{u}\|_{\mathbf{L}_2(0,T;\mathbf{H}^1)} + \|\dot{\mathbf{u}}\|_{\mathbf{L}_2(0,T;\mathbf{H}^1)}\big) \\
&< \infty
\end{aligned}$$

such that $\mathbf{F}_{\mathrm{con}}(\mathbf{u}) \in \mathbf{L}_2(0,T;(\mathbf{H}^1)^*)$. Since the generalized time derivative $\dot{\mathbf{u}}$ is contained in $\mathbf{L}_2(0,T;\mathbf{H}^1)$, $\dot{\mathbf{u}}(t)$ exists for almost every $t \in [0,T]$ even in the classical sense by reason of the generalized main theorem of calculus (compare, e.g., [93, Problem 23.5]). If t is chosen such that $\mathbf{F}_{\mathrm{con}}(\mathbf{u}(t))$ and $\dot{\mathbf{u}}(t)$ exists and condition (1.28) holds, then

$$\left\langle \mathbf{F}_{\mathrm{con}}(\mathbf{u}(t)), \frac{\mathbf{u}(t+h)-\mathbf{u}(t)}{h} \right\rangle_{(\mathbf{H}^1)^*\times\mathbf{H}^1} \begin{cases} \geq 0 & \text{if } h>0 \\ \leq 0 & \text{if } h<0 \end{cases}$$

and, for almost every $t \in [0,T]$,

$$\langle \mathbf{F}_{\mathrm{con}}(\mathbf{u}(t)), \dot{\mathbf{u}}(t) \rangle_{(\mathbf{H}^1)^*\times\mathbf{H}^1} = \lim_{h\to 0} \left\langle \mathbf{F}_{\mathrm{con}}(\mathbf{u}(t)), \frac{\mathbf{u}(t+h)-\mathbf{u}(t)}{h} \right\rangle_{(\mathbf{H}^1)^*\times\mathbf{H}^1} = 0\,.$$

□

The above proof of the generalized persistency condition requires the velocities to be sufficiently smooth, namely $\dot{\mathbf{u}} \in \mathbf{L}_2(0,T;\mathbf{H}^1)$. This regularity assumption is satisfied for solutions of the viscoelastic contact problem, but not for those of the purely elastic problem in general. However, the following theorem shows that the generalized persistency condition is necessary for energy conservation of dynamical contact problems. This result only requires to exclude that the bodies under consideration are exposed to external forces.

Theorem 1.4.3. *The variational problem* (1.28) *with* $f_{\mathrm{ext}} = 0$ *conserves the total energy including the viscous energy.*

Proof. Since $\ddot{\mathbf{u}} \in \mathbf{W}_2^1(0,T;\mathbf{H}^1,\mathbf{L}_2)$, integration by parts, cf. [93, Proposition 23.23], and definition (1.31) of the variational problem lead to

$$\begin{aligned}
&\mathcal{E}(\bar{\mathbf{u}}(t)) - \mathcal{E}(\bar{\mathbf{u}}(t_0)) \\
&= \frac{1}{2}\|\dot{\mathbf{u}}(t)\|_{\mathbf{L}_2}^2 + \frac{1}{2}\|\mathbf{u}(t)\|_a^2 - \frac{1}{2}\|\dot{\mathbf{u}}(t_0)\|_{\mathbf{L}_2}^2 - \frac{1}{2}\|\mathbf{u}(t_0)\|_a^2 \\
&= \int_{t_0}^t \langle \ddot{\mathbf{u}}(s), \dot{\mathbf{u}}(s) \rangle_{(\mathbf{H}^1)^*\times\mathbf{H}^1}\, ds + \int_{t_0}^t a(\mathbf{u}(s), \dot{\mathbf{u}}(s))\, ds \\
&= -\int_{t_0}^t b(\dot{\mathbf{u}}(s), \dot{\mathbf{u}}(s))\, ds + \int_{t_0}^t \langle \mathbf{F}_{\mathrm{con}}(\mathbf{u}(s)), \dot{\mathbf{u}}(s) \rangle_{(\mathbf{H}^1)^*\times\mathbf{H}^1}\, ds\,.
\end{aligned}$$

Exploiting the generalized persistency condition of Theorem 1.4.2 in the last line of this relation yields

$$\mathcal{E}(\bar{\mathbf{u}}(t)) + \int_{t_0}^t \mathcal{E}_{\mathrm{visco}}(\dot{\mathbf{u}}(s))\, ds = \mathcal{E}(\bar{\mathbf{u}}(t_0))\,.$$

□

As a consequence of the above investigations, the conservation of linear momentum and total energy and the validity of a discretized persistency condition will play a major role for a suitable realization of numerical integration in the subsequent chapter.

2. Newmark Methods

In the last decades, a large variety of algorithms has been proposed for the numerical solution of dynamical contact problems with Signorini's conditions. However, all these discretizations are uniform in space and in time, although adaptivity is strongly needed for the efficient simulation of many practical applications. In particular, adaptive mesh refinement is required at timepoints when contact is gained or lost and at spatial points near varying active contact boundaries.

There are two principal choices for an adaptive spatiotemporal integration of time-dependent partial differential equations (PDEs) [10,20,64]: the *method of lines* (MOL), which is still the more popular one, and the *method of time layers* (MOT), also known as *Rothe method*. As discussed below, the approaches differ in the sequence of discretization. For equidistant grids in space and in time, the sequence does not play a role by reason of commutativity.

MOL The method of lines is a wide-spread framework for the adaptive solution of time-dependent PDEs, where discretization is performed first in space and then in time. In general, this approach creates a large block-structured initial value problem of ordinary differential equations (ODEs) (see the schematic presentation in Figure 2.1, left). While adaptive time-stepping can be realized as in the case of ODEs, an appropriate updating of the spatial mesh from time to time is subject to severe limitations. Hence, the method of lines leads to considerable and well-known difficulties with regard to adaptivity both in space and in time.

MOT The method of time layers, first used by Rothe around 1930 [80], discretizes first the time and then the space (see Figure 2.1, right). Around 1990, the setting has been used by Bornemann to realize full adaptivity in space and time for parabolic equations [9, 10]. Ten years later, Lang extended the approach to nonlinear parabolic problems [64].

The underlying idea is to consider the time-dependent PDE as an abstract Cauchy problem in an appropriate function space. The initial value problem is virtually integrated by applying adaptive time-stepping schemes for ODEs in function space, while the sequence of stationary PDEs is assumed to be solved exactly. For an actual numerical realization, the elliptic boundary value problems in each timestep can be discretized efficiently by finite element methods.

In contrast to the method of lines, this gives the possibility to refine the spatial mesh adaptively over all time layers. From the analytical point of view, the time integration is considered as perturbed by the numerical solution of the elliptic subproblem. The magnitude of the perturbation can be controlled independent of the time discretization by prescribing a certain accuracy (the user-defined tolerance) to the finite element code.

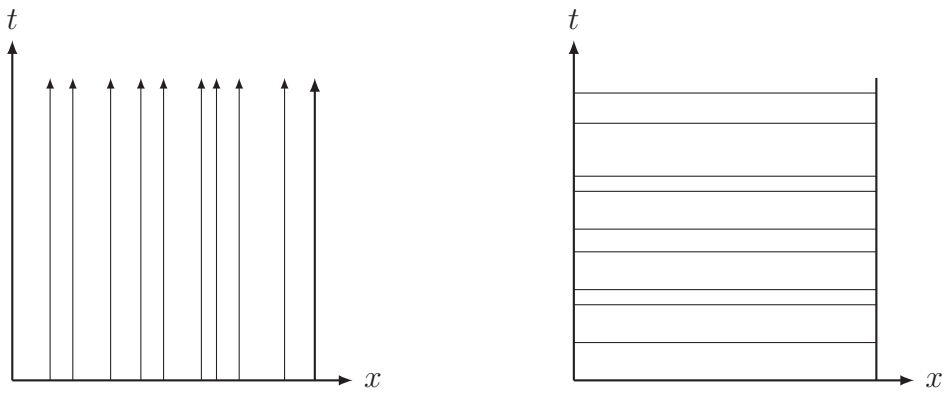

Figure 2.1.: Left: method of lines, right: method of time layers (inspired by [20]).

The method of time layers naturally allows combining adaptive integration in time with multigrid methods that are adaptive in space. Therefore, this setting is the favored spatiotemporal discretization for the dynamical contact problem posed in the previous chapter.

Many time-stepping schemes for dynamical contact problems are based on the most popular numerical integrator in structural dynamics: the classical Newmark method, which will be introduced in Section 2.1. However, in the presence of contact, the scheme leads to spurious instabilities at dynamical contact boundaries and even causes an uncontrollable behavior of the total energy during time integration. In the last years, several variants of Newmark's method have been designed to avoid these deficits. An energy dissipative modification will be described in Section 2.2. In Section 2.3, a contact–stabilization of this algorithm will be presented, which additionally prevents artificial oscillations at contact interfaces. Finally, the contact–stabilized Newmark method will be further improved with regard to a discrete persistency condition in Section 2.4. In order to complete the theoretical analysis of the four types of Newmark methods, in Section 2.5, the advantages and disadvantages will be confirmed by numerical findings for a Hertzian contact problem.

In the method of time layers, the space discretization has no influence on the time discretization apart from its perturbing character. From the algorithmic point of view, this allows using a finite element code as a black box for time integration.

Hence, only the semi-discretization in time is subject to the present thesis, while the spatial discretization is mostly ignored. However, the main cause for the occurrence of numerical instabilities in many Newmark methods is an undesirable interaction of space and time discretization. Therefore, in this chapter, the space-time discrete system will be examined.

Discretization in time. In order to fix notation, let the continuous time interval $[0, T]$ be subdivided by $N_\triangle + 1$ discrete timepoints

$$0 = t_0 < t_1 < \cdots < t_{N_\triangle} = T$$

forming a mesh $\triangle = \{t_0, t_1, \ldots, t_{N_\triangle}\}$ on $[0, T]$. In addition, let

$$\tau_n = t_{n+1} - t_n\,, \qquad n = 0, \ldots, N_\triangle$$

denote the (not necessarily equidistant) timesteps. The discrete quantities $\mathbf{u}^n$ and $\dot{\mathbf{u}}^n$ are assumed to be given by algorithmic approximations of the solution $\mathbf{u}(t_n)$ and the velocity $\dot{\mathbf{u}}(t_n)$.

Discretization in space. The discretization in space is realized by piecewise linear finite elements. Let Ω_h be a polyhedral domain partitioned into triangles or tetrahedra with $h > 0$ the maximal diameter, and let the sequence of triangulations be shape regular. Denote the corresponding finite element space by $\mathbf{S}_h$. In this setting, $\mathcal{K}_h \subset \mathbf{S}_h$ has to be understood as a discrete approximation of the set of admissible displacements. If $\mathcal{N}_h$ denotes the set of vertices contained in $\Omega_h \cup \Gamma_{h,N} \cup \Gamma_{h,C}$, then $\mathcal{K}_h$ means the set

$$\mathcal{K}_h := \left\{ \mathbf{v}_h \in \mathbf{S}_h \,\middle|\, [\mathbf{v}_h \cdot \boldsymbol{\nu}_h]_{\boldsymbol{\phi}_h} \leq g_h \quad \forall\, p \in \mathcal{N}_h \cap \Gamma_{h,C} \right\}, \tag{2.1}$$

where $\boldsymbol{\nu}_{\boldsymbol{\phi}_h}$, $\boldsymbol{\phi}_h$, and g_h are suitable approximations of $\boldsymbol{\nu}_{\boldsymbol{\phi}}$, $\boldsymbol{\phi}$, and g. Details of the spatial discretization are omitted here and can be found in [49, 56–58, 90].

2.1. Classical Newmark Method

The most wide-spread time-stepping scheme for solving dynamical contact problems is the family of classical Newmark methods as examined by Newmark in 1959 [76]. The algorithms form a subset of the Hilber-Hughes-Taylor (HHT) family of temporal integrators, which are sometimes also called α-methods [40, 41].

The underlying concept of the discretizations are Taylor expansions of displacements and velocities neglecting terms of higher order. For an arbitrary equation of motion, the discrete evolution is described by the finite difference equations

$$\begin{aligned} \mathbf{u}_h^{n+1} &= \mathbf{u}_h^n + \tau \dot{\mathbf{u}}_h^n + \frac{\tau^2}{2}\big((1-2\beta)\ddot{\mathbf{u}}_h^n + 2\beta \ddot{\mathbf{u}}_h^{n+1}\big) \\ \dot{\mathbf{u}}_h^{n+1} &= \dot{\mathbf{u}}_h^n + \tau\big((1-\gamma)\ddot{\mathbf{u}}_h^n + \gamma \ddot{\mathbf{u}}_h^{n+1}\big)\,, \end{aligned} \tag{2.2}$$

where τ is a given timestep and $\mathbf{u}_h^n$, $\dot{\mathbf{u}}_h^n$, and $\ddot{\mathbf{u}}_h^n$ are approximations of $\mathbf{u}(t_n)$, $\dot{\mathbf{u}}(t_n)$, and $\ddot{\mathbf{u}}(t_n)$, respectively. The traditional algorithmic parameters γ, $2\beta \in [0,1]$ determine the stability and accuracy characteristics of the schemes [65, 79]. The straightforward application of the Newmark integrators (2.2) to the variational inclusion (1.30) of the dynamical contact problem reads as follows.

Classical Newmark method (N-CL)$_h$.

$$\begin{aligned}
\mathbf{u}_{h,\mathrm{pred}}^{n+1} &= \mathbf{u}_h^n + \tau \dot{\mathbf{u}}_h^n \\
0 &\in \mathbf{u}_h^{n+1} - \mathbf{u}_{h,\mathrm{pred}}^{n+1} + \frac{\tau^2}{2}\big(\mathbf{F}^{2\beta}(\mathbf{u}_h^n, \mathbf{u}_h^{n+1}) + \mathbf{G}^{2\beta}(\dot{\mathbf{u}}_h^n, \dot{\mathbf{u}}_h^{n+1}) - \widetilde{\mathbf{F}}_{\mathrm{con}}^{2\beta}(\mathbf{u}_h^n, \mathbf{u}_h^{n+1})\big) \\
\dot{\mathbf{u}}_h^{n+1} &= \dot{\mathbf{u}}_h^n - \tau\big(\mathbf{F}^{\gamma}(\mathbf{u}_h^n, \mathbf{u}_h^{n+1}) + \mathbf{G}^{\gamma}(\dot{\mathbf{u}}_h^n, \dot{\mathbf{u}}_h^{n+1}) - \mathbf{F}_{\mathrm{con}}^{\gamma}(\mathbf{u}_h^n, \mathbf{u}_h^{n+1})\big)
\end{aligned} \tag{2.3}$$

where, for ease of writing, the shorthand notations

$$\mathbf{F}^{\lambda}(\mathbf{u}_h^n, \mathbf{u}_h^{n+1}) := (1-\lambda)\mathbf{F}(\mathbf{u}_h^n) + \lambda \mathbf{F}(\mathbf{u}_h^{n+1}), \qquad \lambda \in [0,1] \tag{2.4}$$

and

$$\widetilde{\mathbf{F}}_{\mathrm{con}}^{2\beta}(\mathbf{u}_h^n, \mathbf{u}_h^{n+1}) := (1-2\beta)\mathbf{F}_{\mathrm{con}}(\mathbf{u}_h^n) - 2\beta \partial I_{\mathcal{K}_h}(\mathbf{u}_h^{n+1}) \tag{2.5}$$

are introduced.

Clearly, implicit Newmark methods with $2\beta > 0$ require the solution of a variational inclusion in the second line of (2.3) in each timestep. Once the problem is solved, the contact forces $\mathbf{F}_{\mathrm{con}}(\mathbf{u}_h^{n+1})$ are defined via

$$\begin{aligned}
\frac{\tau^2}{2}\big\langle 2\beta \mathbf{F}_{\mathrm{con}}(\mathbf{u}_h^{n+1}), \mathbf{v}_h \big\rangle := \Big\langle \mathbf{u}_h^{n+1} - \mathbf{u}_{h,\mathrm{pred}}^{n+1} + \frac{\tau^2}{2}\big(\mathbf{F}^{2\beta}(\mathbf{u}_h^n, \mathbf{u}_h^{n+1}) + \mathbf{G}^{2\beta}(\dot{\mathbf{u}}_h^n, \dot{\mathbf{u}}_h^{n+1}) \\
- (1-2\beta)\mathbf{F}_{\mathrm{con}}(\mathbf{u}_h^n)\big), \mathbf{v}_h \Big\rangle, \qquad \mathbf{v}_h \in \mathbf{H}^1 .
\end{aligned} \tag{2.6}$$

Hence, the contact forces $\mathbf{F}_{\mathrm{con}}^{\gamma}(\mathbf{u}_h^n, \mathbf{u}_h^{n+1})$ entering in the algebraic expression for the velocities in the third line of (2.3) are provided by the residual of the variational inclusion in the second line.

Due to the high nonlinearity of the non-penetration constraints, the most expensive part of the time discretization scheme is the solving of the variational problem. The choice of a suitable algorithm will be discussed in Section 2.5.

For $n > 0$, the discrete displacements and velocities $\mathbf{u}_h^n$ and $\dot{\mathbf{u}}_h^n$ and the contact forces $\mathbf{F}_{\mathrm{con}}(\mathbf{u}_h^n)$ are known from the calculation of the previous timestep. In the first step, $\mathbf{u}_h^0$ and $\dot{\mathbf{u}}_h^0$ are given by the initial values of the variational problem (1.28). The contact forces $\mathbf{F}_{\mathrm{con}}(\mathbf{u}_h^0)$ are zero if no contact is detected at initial time. Otherwise, a suitable approximation of this quantity is needed in the initial configuration.

Trapezoidal rule. The Newmark family contains many well-known and widely-used algorithms as special cases, which correspond to different available choices of the parameters. The most popular member in structural dynamics applications is the *trapezoidal rule* or *average acceleration method*, which is obtained by setting the symmetric parameters $2\beta = \gamma = \frac{1}{2}$ [41,65,86]. The resulting scheme is an example for an implicit integrator, and the second and the third line of algorithm (2.3) decouple for viscoelastic materials, cf. Remark 2.2.1.

In the unconstrained case, the method is second-order consistent and unconditionally stable [65]. Moreover, linear momentum and total energy of the discrete evolution are preserved, see [33, 65] for the purely elastic case. Proofs of these conservation properties in viscoelasticity are presented in Theorem 2.4.1 and Theorem 2.4.2. By reason of the excellent characteristics in the absence of contact, the symmetric Newmark scheme is of great practical interest and prevalent in common use in the community of computational mechanics. In the case of contact constraints, however, the situation must be reexamined.

Conservation properties. Also in the presence of contact, the family of Newmark integrators conserves the linear momentum of the discrete evolution. A proof in the case of pure elasticity can be found in [59] for $2\beta = \gamma = \frac{1}{2}$. This proof can easily be transferred to arbitrary choices of parameters as well as linear viscoelasticity, compare Theorem 2.4.1. As discussed in Section 1.4 for the continuous problem, the angular momentum is not expected to be preserved by the discretized system.

The desirable energy conserving property in pure elasticity only holds in the case of permanent contact, i.e., if the active contact boundaries do not change during the timestep [65]: while the detection of a new contact point decreases the energy of the discretized system, the release of an existing contact point increases the energy. Unfortunately, loss and regain of energy do not balance such that the energy cannot be guaranteed to remain bounded during time integration. In particular, an unwanted energy blow-up may occur.

Artificial oscillations. Depending on parameter specification, the improper handling of the non-penetration condition by Newmark methods evokes instabilities at contact boundaries. These show up as unwanted oscillations in displacements, velocities, and contact stresses, see [19,59] and the numerical tests in Section 2.5. The phenomenon, known as *bouncing*, can be attenuated by increasing γ to values larger than $1/2$ at the expense of degrading the order of accuracy.

Throughout this thesis, the trapezoidal rule with symmetric parameters is identified as classical Newmark method. This algorithm is chosen due to its valuable numerical features in the unconstrained situation. A reliable time discretization scheme should not trigger spurious oscillations during the phase of contact. In addition, a tight energy conservation should be achieved to guarantee a good long-time

behavior of the discrete evolution. These demands have motivated the design of alternative time integrators in the last years, which will be described in the following sections.

2.2. Contact–Implicit Newmark Method

In order to overcome the poor energy conservation of the classical Newmark method, Kane, Repetto, Ortiz, and Marsden [46] developed an energy-dissipative version of the algorithm in 1999. For the purely elastic problem, they proposed a fully implicit treatment of the contact forces by replacing the term $\widetilde{\mathbf{F}}^{1/2}_{\mathrm{con}}(\mathbf{u}_h^n, \mathbf{u}_h^{n+1})$ in the classical scheme with the subdifferential $\partial I_{\mathcal{K}}(\mathbf{u}_h^{n+1})$. The generalization to viscoelasticity has been given in [53] and can be found below.

Contact–implicit Newmark method (N-CI)$_h$.

$$
\begin{aligned}
&\mathbf{u}_{h,\mathrm{pred}}^{n+1} = \mathbf{u}_h^n + \tau \dot{\mathbf{u}}_h^n \\
&0 \in \mathbf{u}_h^{n+1} - \mathbf{u}_{h,\mathrm{pred}}^{n+1} + \frac{\tau^2}{2}\big(\mathbf{F}^{1/2}(\mathbf{u}_h^n, \mathbf{u}_h^{n+1}) + \mathbf{G}^{1/2}(\dot{\mathbf{u}}_h^n, \dot{\mathbf{u}}_h^{n+1}) + \partial I_{\mathcal{K}_h}(\mathbf{u}_h^{n+1})\big) \qquad (2.7)\\
&\dot{\mathbf{u}}_h^{n+1} = \dot{\mathbf{u}}_h^n - \tau\big(\mathbf{F}^{1/2}(\mathbf{u}_h^n, \mathbf{u}_h^{n+1}) + \mathbf{G}^{1/2}(\dot{\mathbf{u}}_h^n, \dot{\mathbf{u}}_h^{n+1}) - \mathbf{F}_{\mathrm{con}}(\mathbf{u}_h^{n+1})\big)
\end{aligned}
$$

where the contact forces $\mathbf{F}_{\mathrm{con}}(\mathbf{u}_h^{n+1})$ are defined via

$$
\begin{aligned}
\frac{\tau^2}{2}\big\langle \mathbf{F}_{\mathrm{con}}(\mathbf{u}_h^{n+1}), \mathbf{v}_h\big\rangle_{(\mathbf{H}^1)^*\times\mathbf{H}^1} := \Big\langle \mathbf{u}_h^{n+1} - \mathbf{u}_{h,\mathrm{pred}}^{n+1} + \frac{\tau^2}{2}\big(\mathbf{F}^{1/2}(\mathbf{u}_h^n, \mathbf{u}_h^{n+1}) \qquad (2.8)\\
+\mathbf{G}^{1/2}(\dot{\mathbf{u}}_h^n, \dot{\mathbf{u}}_h^{n+1})\big), \mathbf{v}_h\Big\rangle_{(\mathbf{H}^1)^*\times\mathbf{H}^1}, \qquad \mathbf{v}_h \in \mathbf{H}^1 .
\end{aligned}
$$

Remark 2.2.1. A simple calculation shows that for (N-CL)$_h$ and (N-CI)$_h$

$$
\dot{\mathbf{u}}_h^{n+1} = \dot{\mathbf{u}}_h^n + \frac{2}{\tau}\big(\mathbf{u}_h^{n+1} - \mathbf{u}_{h,\mathrm{pred}}^{n+1}\big) = -\dot{\mathbf{u}}_h^n + \frac{2}{\tau}\big(\mathbf{u}_h^{n+1} - \mathbf{u}_h^n\big) .
$$

Hence, the viscoelastic part $\mathbf{G}^{1/2}(\dot{\mathbf{u}}_h^n, \dot{\mathbf{u}}_h^{n+1})$ is identical to $\mathbf{G}\big(\frac{\mathbf{u}_h^{n+1}-\mathbf{u}_h^n}{\tau}\big)$, which results in a decoupling of the second and the third line of the schemes.

Energy dissipativity. In contrast to (N-CL)$_h$, the implicit handling of the non-penetration constraints in (N-CI)$_h$ leads to energy dissipativity of the discrete evolution in the presence of contact. If $\mathbf{u}_h^{n+1}$ is not in contact or if $\mathbf{u}_h^{n+1}$ is only in contact where $\mathbf{u}_h^n$ has already been in contact, the algorithm is even energy conserving (including the viscous energy). Hence, the largest loss of energy is expected when the two bodies get in contact for the first time, compare the numerical investigations in Section 2.5. Furthermore, the modification (N-CI)$_h$ still preserves the linear momentum of the system. For pure elasticity, the conservation properties of the scheme have been verified in [19]. The proofs can be transferred to viscoelasticity as in Theorem 2.4.1 and in Theorem 2.4.2.

Artificial oscillations. Unfortunately, the instabilities of $(\text{N-CL})_h$ at contact interfaces are still present in $(\text{N-CI})_h$, cf. [19] and the numerical computations in Section 2.5. In view of the construction of a stable Newmark scheme in the following section, a simple geometric argument is given here, which explains the origin of the spurious oscillations for both $(\text{N-CL})_h$ and $(\text{N-CI})_h$.

Assume that contact is found over several timesteps so that

$$\mathbf{u}_h^n \cdot \boldsymbol{\nu}_{\phi_h} = \mathbf{u}_h^{n+1} \cdot \boldsymbol{\nu}_{\phi_h} \quad \text{on } \Gamma_{C,h}\,.$$

Then, Remark 2.2.1 yields an undesirable reversion of the normal component of the discrete velocities at contact boundaries:

$$\dot{\mathbf{u}}_h^{n+1} \cdot \boldsymbol{\nu}_{\phi_h} = -\dot{\mathbf{u}}_h^n \cdot \boldsymbol{\nu}_{\phi_h} + \frac{2}{\tau}\big(\mathbf{u}_h^{n+1} - \mathbf{u}_h^n\big) \cdot \boldsymbol{\nu}_{\phi_h} = -\dot{\mathbf{u}}_h^n \cdot \boldsymbol{\nu}_{\phi_h} \quad \text{on } \Gamma_{C,h} \tag{2.9}$$

(the formal calculation also holds for the tangential components). Therefore, new contact points of $(\text{N-CL})_h$ and $(\text{N-CI})_h$ are likely to be detached in the next but one timestep. The zigzagging of the velocities can be confirmed by numerical tests as well, cf. Section 2.5.

2.3. Contact–Stabilized Newmark Method

In 2007, Deuflhard, Krause, and Ertel [19] designed a contact–stabilized variant of the contact–implicit Newmark method in linear elasticity, which completely removes the spurious oscillations at contact boundaries and is still energy dissipative in the presence of contact. The generalization to the viscoelastic case has been devised in [53].

The key idea for the achievement of the stabilization does not only originate from the above geometric argument, but also from a physical reason for the oscillations observed in $(\text{N-CL})_h$ and $(\text{N-CI})_h$. In a dynamical contact problem, the contact forces $\mathbf{F}_{\text{con}}$ equilibrate the internal and external forces $\mathbf{F}+\mathbf{G}$ on account of Newton's third law of motion [28]. For the construction of a time discretization scheme, this translates to the physically reasonable requirement that the normal components of the discrete forces balance at the contact interfaces, i.e.,

$$\mathbf{F}^{1/2}\big(\mathbf{u}_h^n, \mathbf{u}_h^{n+1}\big) \cdot \boldsymbol{\nu}_{\phi_h} + \mathbf{G}\Big(\frac{\mathbf{u}_h^{n+1} - \mathbf{u}_h^n}{\tau}\Big) \cdot \boldsymbol{\nu}_{\phi_h} = \mathbf{F}_{\text{con}}\big(\mathbf{u}_h^{n+1}\big) \cdot \boldsymbol{\nu}_{\phi_h} \quad \text{on } \Gamma_{C,h}\,. \tag{2.10}$$

Discretization in space assigns a mass to the discrete boundaries, although they have measure zero in the continuous problem. Thus, the contact forces in $(\text{N-CL})_h$ and $(\text{N-CI})_h$ take effect on $\mathbf{u}_h^n + \tau\dot{\mathbf{u}}_h^n$ if this quantity causes penetration of the bodies. In other words, the entries of the mass matrix at contact boundaries are transferred into contributions to the contact forces without any physical meaning. Hence, the

interaction of the discretization in space and time can be understood to be the main cause for the undesirable oscillations in Newmark methods.

The lack of the force equilibrium (2.10) suggests the adding of a stabilization procedure on the energy dissipative scheme $(\text{N-CI})_h$, which removes the unphysical part of the discrete contact forces. The modification of Deuflhard et al. can easily be incorporated into $(\text{N-CI})_h$ by replacing the linear predictor step in the first line of algorithm (2.7) by a special nonlinear one, while the remaining steps are left unchanged. The contact–stabilized version of Newmark's method reads as follows.

Contact–stabilized Newmark method $(\text{N-CS})_h$.

$$
\begin{aligned}
&0 \in \mathbf{u}_{h,\mathrm{pred}}^{n+1} - \big(\mathbf{u}_h^n + \tau\dot{\mathbf{u}}_h^n\big) + \partial I_{\mathcal{K}_h}\big(\mathbf{u}_{h,\mathrm{pred}}^{n+1}\big)\\
&0 \in \mathbf{u}_h^{n+1} - \mathbf{u}_{h,\mathrm{pred}}^{n+1} + \frac{\tau^2}{2}\Big(\mathbf{F}^{1/2}\big(\mathbf{u}_h^n, \mathbf{u}_h^{n+1}\big) + \mathbf{G}\Big(\frac{\mathbf{u}_h^{n+1} - \mathbf{u}_h^n}{\tau}\Big) + \partial I_{\mathcal{K}_h}\big(\mathbf{u}_h^{n+1}\big)\Big)\\
&\dot{\mathbf{u}}_h^{n+1} = \dot{\mathbf{u}}_h^n - \tau\Big(\mathbf{F}^{1/2}\big(\mathbf{u}_h^n, \mathbf{u}_h^{n+1}\big) + \mathbf{G}\Big(\frac{\mathbf{u}_h^{n+1} - \mathbf{u}_h^n}{\tau}\Big) - \mathbf{F}_{\mathrm{con}}\big(\mathbf{u}_h^{n+1}\big)\Big)
\end{aligned}
\tag{2.11}
$$

with contact forces

$$
\begin{aligned}
\frac{\tau^2}{2}\big\langle \mathbf{F}_{\mathrm{con}}(\mathbf{u}_h^{n+1}), \mathbf{v}_h\big\rangle_{(\mathbf{H}^1)^*\times\mathbf{H}^1} := \Big\langle \mathbf{u}_h^{n+1} - \mathbf{u}_{h,\mathrm{pred}}^{n+1} + \frac{\tau^2}{2}\Big(\mathbf{F}^{1/2}\big(\mathbf{u}_h^n, \mathbf{u}_h^{n+1}\big)\\
+\mathbf{G}\Big(\frac{\mathbf{u}_h^{n+1} - \mathbf{u}_h^n}{\tau}\Big)\Big), \mathbf{v}_h\Big\rangle_{(\mathbf{H}^1)^*\times\mathbf{H}^1}, \mathbf{v}_h \in \mathbf{H}^1\,.
\end{aligned}
\tag{2.12}
$$

The additional variational inclusion in the predictor step can equivalently be written as the convex minimization problem

$$
\min_{\mathbf{v}_h\in\mathcal{K}_h} \big\|\mathbf{v}_h - \mathbf{u}_h^n - \tau\dot{\mathbf{u}}_h^n\big\|_{\mathbf{L}_2(\Omega_h)}\,. \tag{2.13}
$$

Hence, the contact–stabilized predictor can be considered as the $\mathbf{L}_2$-projection of the standard predictor onto the discrete admissible set $\mathcal{K}_h$ in each timestep.

Due to the definition (2.1) of $\mathcal{K}_h$, the discrete $\mathbf{L}_2$-projection requires the evaluation of the normal trace of $\mathbf{u}_h^n + \tau\dot{\mathbf{u}}_h^n$. The trace on contact boundaries is well-defined for finite element functions in $\mathbf{S}_h$, but not for arbitrary $\mathbf{L}_2$-functions. However, the effect of the $\mathbf{L}_2$-projection vanishes if the spatial grid is refined, see Section 4.1, which is another strong hint that the oscillations in $(\text{N-CL})_h$ and $(\text{N-CI})_h$ are caused by the spatial discretization solely. In consequence, the discrete boundary mass causes artificial oscillations at contact interfaces on the one hand, but allows removing the oscillations by means of the discrete $\mathbf{L}_2$-projection on the other hand.

The projection is defined on the whole domain Ω_h, while $\mathcal{K}_h$ only acts as a restriction to the points at possible contact boundaries. Hence, during the predictor step, the approximated solution may temporarily penetrate the interior of the domain, although $\mathbf{u}_{h,\mathrm{pred}}^{n+1} \in \mathcal{K}_h$ is admissible in the sense of the definition of $\mathcal{K}_h$. This is due to the fact that the contact–stabilized predictor was not constructed to guarantee non-penetration, but to achieve a force balance on the contact boundaries.

Remark 2.3.1. If the $\mathbf{L}_2$-projection is realized with the full mass matrix, the constrained minimization problem can be solved with optimal complexity by using a monotone multigrid method [57]. If a lumped mass matrix is used instead, the variational inclusion is interpretable as a local projection onto the set of admissible displacements. In this case, all unknowns decouple, and the nonlinear predictor step can be carried out pointwise on the possible contact boundaries. Hence, the costs for solving the additional variational problem are negligible and do not influence the overall efficiency of the Newmark method.

Energy dissipativity. The contact–stabilized scheme $(\text{N-CS})_h$ is still energy dissipative in the presence of contact and energy conserving if $\mathbf{u}_{h,\text{pred}}^{n+1}$ and $\mathbf{u}_h^{n+1}$ are not in contact (including the viscous energy). In addition, the energy of the discrete evolution is preserved when the contact boundaries predicted by $\mathbf{u}_{\text{pred}}^{n+1}$ and $\mathbf{u}_h^{n+1}$ coincide with those given by $\mathbf{u}_h^n$. Therefore, most of the total energy is expected to be lost in the phase of detaching, which is in contrast to the behavior of $(\text{N-CI})_h$, cf. Section 2.5. The energy conservation of $(\text{N-CS})_h$ has been analyzed for the purely elastic case in [19]. A corresponding result in viscoelasticity can be derived by following the proof of Theorem 2.4.2. The linear momentum of the system is also preserved, for a proof compare Theorem 2.4.1.

Avoidance of artificial oscillations and a discrete persistency condition. In contrast to $(\text{N-CL})_h$ and $(\text{N-CI})_h$, the validity of the force equilibrium (2.10) in $(\text{N-CS})_h$ immediately prevents the occurrence of spurious oscillations.

Assume that $\mathbf{u}_{h,\text{pred}}^{n+1}$ predicts $\mathbf{u}_h^{n+1}$ at the contact boundaries, i.e.,

$$\mathbf{u}_{h,\text{pred}}^{n+1} \cdot \boldsymbol{\nu}_{\phi_h} = \mathbf{u}_h^{n+1} \cdot \boldsymbol{\nu}_{\phi_h} \quad \text{on } \Gamma_{C,h}\,.$$

The update formula for the velocities, third line of algorithm (2.11), leads to

$$\dot{\mathbf{u}}_h^{n+1} = \dot{\mathbf{u}}_h^n + \frac{2}{\tau}\big(\mathbf{u}_h^{n+1} - \mathbf{u}_{h,\text{pred}}^{n+1}\big)\,.$$

This directly yields the conservation of the normal components of the velocities during the phase of contact:

$$\dot{\mathbf{u}}_h^{n+1} \cdot \boldsymbol{\nu}_{\phi_h} = \dot{\mathbf{u}}_h^n \cdot \boldsymbol{\nu}_{\phi_h} + \frac{2}{\tau}\big(\mathbf{u}_h^{n+1} - \mathbf{u}_{h,\text{pred}}^{n+1}\big) \cdot \boldsymbol{\nu}_{\phi_h} = \dot{\mathbf{u}}_h^n \cdot \boldsymbol{\nu}_{\phi_h} \quad \text{on } \Gamma_{C,h}\,. \tag{2.14}$$

The relation corresponds to the discretized version (2.10) of Newton's axiom of equilibrium forces. As a result, the spurious oscillations in displacements and contact forces disappear in $(\text{N-CS})_h$, see the numerical example in Section 2.5.

The constant velocities at active contact boundaries result in the relation

$$\big\langle \mathbf{F}_{\text{con}}(\mathbf{u}_h^{n+1}), \dot{\mathbf{u}}_h^{n+1} \big\rangle_{(\mathbf{H}^1)^* \times \mathbf{H}^1} = \big\langle \mathbf{F}_{\text{con}}(\mathbf{u}_h^{n+1}), \dot{\mathbf{u}}_h^{n} \big\rangle_{(\mathbf{H}^1)^* \times \mathbf{H}^1} \tag{2.15}$$

if $\mathbf{u}_{h,\mathrm{pred}}^{n+1}$ is in contact wherever $\mathbf{u}_h^{n+1}$ is in contact. Thus, $(\text{N-CS})_h$ does not fulfill a *discrete persistency condition*

$$\mathrm{P}_h^{n+1} := \big\langle \mathbf{F}_{\mathrm{con}}(\mathbf{u}_h^{n+1}), \dot{\mathbf{u}}_h^{n+1} \big\rangle_{(\mathbf{H}^1)^* \times \mathbf{H}^1} = 0 \tag{2.16}$$

during phases of permanent contact as does the continuous problem, cf. Section 1.4. For $(\text{N-CL})_h$ and $(\text{N-CI})_h$, the sign of P_h^{n+1} is even alternating by reason of the zigzagging (2.9) of the velocities. The observations signify the lack of a discrete persistency condition for all three types of Newmark methods.

2.4. Improved Contact–Stabilized Newmark Method

The violation of a discrete persistency condition by the previous Newmark methods stimulates to improve the energy dissipative and contact–stabilized scheme, which is the topic of the present section.

For space-time discretizations, condition (2.16) is only fulfilled at permanent active contact boundaries if the normal components of the velocities vanish, i.e.,

$$\dot{\mathbf{u}}_h^{n+1} \cdot \boldsymbol{\nu}_{\phi_h} = 0 \quad \text{on } \Gamma_{C,h} \qquad \text{if } \ \mathbf{u}_h^n \cdot \boldsymbol{\nu}_{\phi_h} = \mathbf{u}_h^{n+1} \cdot \boldsymbol{\nu}_{\phi_h} \quad \text{on } \Gamma_{C,h}\,.$$

The contact–stabilization in $(\text{N-CS})_h$ leads to constant velocities during phases of active contact, cf. (2.14), but the values are not equal to zero. In order to overcome this deficiency, the update formula for the velocities in the third line of algorithm (2.11) has to be modified adequately. For this purpose, the contact–stabilized predictor can be reused, which is interpretable as a correction of the discrete velocities of the last step.

Improved contact–stabilized Newmark method $(\text{N-CS}+)_h$.

$$\begin{aligned}
&0 \in \mathbf{u}_{h,\mathrm{pred}}^{n+1} - \big(\mathbf{u}_h^n + \tau \dot{\mathbf{u}}_h^n\big) + \partial I_{\mathcal{K}_h}\big(\mathbf{u}_{h,\mathrm{pred}}^{n+1}\big) \\
&0 \in \mathbf{u}_h^{n+1} - \mathbf{u}_{h,\mathrm{pred}}^{n+1} + \frac{\tau^2}{2}\Big(\mathbf{F}^{1/2}\big(\mathbf{u}_h^n, \mathbf{u}_h^{n+1}\big) + \mathbf{G}\Big(\frac{\mathbf{u}_h^{n+1} - \mathbf{u}_h^n}{\tau}\Big) + \partial I_{\mathcal{K}_h}\big(\mathbf{u}_h^{n+1}\big)\Big) \\
&\dot{\mathbf{u}}_h^{n+1} = \dot{\mathbf{u}}_h^n + \mathbf{G}_{\mathrm{con}}\big(\mathbf{u}_{h,\mathrm{pred}}^{n+1}\big) - \tau\Big(\mathbf{F}^{1/2}\big(\mathbf{u}_h^n, \mathbf{u}_h^{n+1}\big) + \mathbf{G}\Big(\frac{\mathbf{u}_h^{n+1} - \mathbf{u}_h^n}{\tau}\Big) - \mathbf{F}_{\mathrm{con}}\big(\mathbf{u}_h^{n+1}\big)\Big)
\end{aligned} \tag{2.17}$$

where the contact forces $\mathbf{F}_{\mathrm{con}}(\mathbf{u}_h^{n+1})$ are defined by (2.12). In this spirit, the variational inclusion in the contact–stabilized predictor step is also characterized in terms of some element $\mathbf{G}_{\mathrm{con}}(\mathbf{u}_{h,\mathrm{pred}}^{n+1}) \in \partial I_{\mathcal{K}_h}(\mathbf{u}_{h,\mathrm{pred}}^{n+1})$ via

$$\tau\big(\mathbf{G}_{\mathrm{con}}(\mathbf{u}_{h,\mathrm{pred}}^{n+1}), \mathbf{v}_h\big)_{\mathbf{L}_2} := \big(\mathbf{u}_{h,\mathrm{pred}}^{n+1} - \mathbf{u}_h^n - \tau \dot{\mathbf{u}}_h^n, \mathbf{v}_h\big)_{\mathbf{L}_2}\,, \quad \mathbf{v}_h \in \mathbf{L}_2\,. \tag{2.18}$$

The variational problem in the second line of (2.17) can equivalently be formulated as the variational inequality

$$\left\langle \mathbf{F}_{\mathrm{con}}(\mathbf{u}_h^{n+1}), \mathbf{u}_h^{n+1} - \mathbf{v}_h \right\rangle_{(\mathbf{H}^1)^* \times \mathbf{H}^1} \leq 0\,, \qquad \forall \mathbf{v}_h \in \mathcal{K}_h\,, \tag{2.19}$$

and the predictor step can be rewritten as

$$\left(\mathbf{G}_{\mathrm{con}}(\mathbf{u}_{h,\mathrm{pred}}^{n+1}), \mathbf{u}_{h,\mathrm{pred}}^{n+1} - \mathbf{v}_h\right)_{\mathbf{L}_2} \leq 0\,, \qquad \forall \mathbf{v}_h \in \mathcal{K}_h\,. \tag{2.20}$$

Avoidance of artificial oscillations and fulfillment of a discrete persistency condition. In contrast to the three previous Newmark methods, the suggested modification (N-CS+)$_h$ of the contact–stabilized scheme enables vanishing normal components of the velocities at contact boundaries: assume that contact is found over several timesteps such that

$$\mathbf{u}_h^n \cdot \boldsymbol{\nu}_{\boldsymbol{\phi}_h} = \mathbf{u}_{h,\mathrm{pred}}^{n+1} \cdot \boldsymbol{\nu}_{\boldsymbol{\phi}_h} = \mathbf{u}_h^{n+1} \cdot \boldsymbol{\nu}_{\boldsymbol{\phi}_h} \quad \text{on } \Gamma_{C,h}\,.$$

Then, the modified update formula for the velocities in the third line of algorithm (2.17) leads to

$$\dot{\mathbf{u}}_h^{n+1} - \frac{\mathbf{u}_{h,\mathrm{pred}}^{n+1} - \mathbf{u}_h^n}{\tau} = \frac{2}{\tau}\big(\mathbf{u}_h^{n+1} - \mathbf{u}_{h,\mathrm{pred}}^{n+1}\big)\,,$$

which directly yields the desired property

$$\dot{\mathbf{u}}_h^{n+1} \cdot \boldsymbol{\nu}_{\boldsymbol{\phi}_h} = \frac{\mathbf{u}_{h,\mathrm{pred}}^{n+1} - \mathbf{u}_h^n}{\tau} \cdot \boldsymbol{\nu}_{\boldsymbol{\phi}_h} + \frac{2}{\tau}\big(\mathbf{u}_h^{n+1} - \mathbf{u}_{h,\mathrm{pred}}^{n+1}\big) \cdot \boldsymbol{\nu}_{\boldsymbol{\phi}_h} = 0 \quad \text{on } \Gamma_{C,h} \tag{2.21}$$

in the case of permanent active contact. Figure 2.2 shows a comparative illustration of this issue for the four Newmark schemes under consideration.

As a consequence, the validity of a discrete persistency condition follows immediately:

$$\mathrm{P}_h^{n+1} = \left\langle \mathbf{F}_{\mathrm{con}}(\mathbf{u}_h^{n+1}), \dot{\mathbf{u}}_h^{n+1} \right\rangle_{(\mathbf{H}^1)^* \times \mathbf{H}^1} = 0 \quad \text{on } \Gamma_{C,h} \tag{2.22}$$

if $\mathbf{u}_h^n$ and $\mathbf{u}_{h,\mathrm{pred}}^{n+1}$ are in contact wherever $\mathbf{u}_h^{n+1}$ is in contact. In particular, this covers the situation of permanent active contact, but probably not the timestep when contact is found initially. This leads to the conjecture that the poor energy conservation of (N-CS)$_h$ is improved by (N-CS+)$_h$ in the phase of detaching, but not when contact is detected for the first time. The conjecture will be verified by the numerical tests in Section 2.5.

The new variant of Newmark's method still preserves the linear momentum of the system as proven in the following theorem.

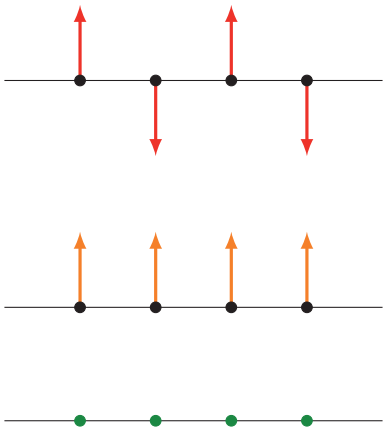

Figure 2.2.: Normal component of velocities at permanent active contact boundaries. Top: $(\text{N-CL})_h$ and $(\text{N-CI})_h$, middle: $(\text{N-CS})_h$, bottom: $(\text{N-CS+})_h$.

Theorem 2.4.1 (Linear momentum conservation). *The improved contact–stabilized Newmark method* $(\text{N-CS+})_h$ *conserves the linear momentum if* $f_{\text{ext}} = 0$ *and* $\Gamma_D = \emptyset$.

Proof. The change of the linear momentum in two successive timesteps is tested against an arbitrary vector $\mathbf{w} \in \mathbf{H}^1$ that is constant in space and in time. Inserting the third line of (2.17) into this quantity yields

$$
\begin{aligned}
&\big(\boldsymbol{\mathcal{L}}(\dot{\mathbf{u}}_h^{n+1}) - \boldsymbol{\mathcal{L}}(\dot{\mathbf{u}}_h^{n})\big) \cdot \mathbf{w} \\
&= \big(\dot{\mathbf{u}}_h^{n+1} - \dot{\mathbf{u}}_h^{n}, \mathbf{w}\big)_{\mathbf{L}_2} \\
&= -\tau \big\langle \mathbf{F}^{1/2}(\mathbf{u}_h^{n}, \mathbf{u}_h^{n+1}), \mathbf{w} \big\rangle_{(\mathbf{H}^1)^* \times \mathbf{H}^1} - \tau \Big\langle \mathbf{G}\Big(\frac{\mathbf{u}_h^{n+1} - \mathbf{u}_h^{n}}{\tau}\Big), \mathbf{w} \Big\rangle_{(\mathbf{H}^1)^* \times \mathbf{H}^1} \\
&\quad + \tau \big\langle \mathbf{G}_{\text{con}}(\mathbf{u}_{h,\text{pred}}^{n+1}), \mathbf{w} \big\rangle_{(\mathbf{H}^1)^* \times \mathbf{H}^1} + \tau \big\langle \mathbf{F}_{\text{con}}(\mathbf{u}_h^{n+1}), \mathbf{w} \big\rangle_{(\mathbf{H}^1)^* \times \mathbf{H}^1} \\
&= -\tau \int_\Omega \mathbf{E}\boldsymbol{\varepsilon}\Big(\frac{\mathbf{u}_h^{n} + \mathbf{u}_h^{n+1}}{2}\Big) : \boldsymbol{\varepsilon}(\mathbf{w})\, d\mathbf{x} - \tau \int_\Omega \mathbf{V}\boldsymbol{\varepsilon}\Big(\frac{\mathbf{u}_h^{n+1} - \mathbf{u}_h^{n}}{\tau}\Big) : \boldsymbol{\varepsilon}(\mathbf{w})\, d\mathbf{x} \\
&\quad + \tau \big\langle \mathbf{G}_{\text{con}}(\mathbf{u}_{h,\text{pred}}^{n+1}), \mathbf{w} \big\rangle_{(\mathbf{H}^1)^* \times \mathbf{H}^1} + \tau \big\langle \mathbf{F}_{\text{con}}(\mathbf{u}_h^{n+1}), \mathbf{w} \big\rangle_{(\mathbf{H}^1)^* \times \mathbf{H}^1} .
\end{aligned}
$$

The first two terms vanish by the choice of the test function since $\boldsymbol{\varepsilon}(\mathbf{w}) = 0$. Due to $[\mathbf{w} \cdot \boldsymbol{\nu}_h]_{\phi_h} = 0$ on $\boldsymbol{\Gamma}_{C,h}$, both $\mathbf{w} \in \mathcal{K}_h$ and $-\mathbf{w} \in \mathcal{K}_h$. Therefore, the last two terms containing $\mathbf{G}_{\text{con}}(\mathbf{u}_{h,\text{pred}}^{n+1})$ and $\mathbf{F}_{\text{con}}(\mathbf{u}_h^{n+1})$ are also equal to zero by reason of (2.19) and (2.20), respectively. This leads to the wanted linear momentum conservation. □

The next theorem shows that the modification of the velocity update in $(\text{N-CS+})_h$ does not change the energy dissipativity of the contact–stabilization in the presence of contact.

Theorem 2.4.2 (**Energy dissipativity**). *Consider the improved contact–stabilized Newmark method* (N-CS+)$_h$ *with* $f_{\text{ext}} = 0$. *If* $\mathbf{u}_{h,\text{pred}}^{n+1}$ *and* $\mathbf{u}_h^{n+1}$ *are not in contact, the algorithm is energy conserving (including the viscous energy). If* $\mathbf{u}_{h,\text{pred}}^{n+1}$ *and* $\mathbf{u}_h^{n+1}$ *are only in contact where* $\mathbf{u}_h^n$ *has already been in contact, the algorithm is also energy conserving. Otherwise, the algorithm is energy dissipative.*

Proof. Combining the second and the third line of algorithm (2.17) leads to

$$\begin{aligned}\dot{\mathbf{u}}_h^{n+1} - \dot{\mathbf{u}}_h^n &= \frac{2}{\tau}\big(\mathbf{u}_h^{n+1} - \mathbf{u}_{h,\text{pred}}^{n+1}\big) + \mathbf{G}_{\text{con}}\big(\mathbf{u}_{h,\text{pred}}^{n+1}\big)\\ \dot{\mathbf{u}}_h^{n+1} + \dot{\mathbf{u}}_h^n &= \frac{2}{\tau}\big(\mathbf{u}_h^{n+1} - \mathbf{u}_h^n\big) - \mathbf{G}_{\text{con}}\big(\mathbf{u}_{h,\text{pred}}^{n+1}\big)\,.\end{aligned}$$

Thus, the change in kinetic and potential energy between two successive timesteps can be written as

$$\begin{aligned}&\big(\mathcal{E}_{\text{kin}}(\dot{\mathbf{u}}_h^{n+1}) + \mathcal{E}_{\text{pot}}(\mathbf{u}_h^{n+1})\big) - \big(\mathcal{E}_{\text{kin}}(\dot{\mathbf{u}}_h^n) + \mathcal{E}_{\text{pot}}(\mathbf{u}_h^n)\big)\\ &= \frac{1}{2}\big(\dot{\mathbf{u}}_h^{n+1} - \dot{\mathbf{u}}_h^n, \dot{\mathbf{u}}_h^{n+1} + \dot{\mathbf{u}}_h^n\big)_{\mathbf{L}_2} + \frac{1}{2}a\big(\mathbf{u}_h^{n+1} + \mathbf{u}_h^n, \mathbf{u}_h^{n+1} - \mathbf{u}_h^n\big)\\ &= \frac{2}{\tau^2}\big(\mathbf{u}_h^{n+1} - \mathbf{u}_{h,\text{pred}}^{n+1}, \mathbf{u}_h^{n+1} - \mathbf{u}_h^n\big)_{\mathbf{L}_2} + \frac{1}{\tau}\big(\mathbf{G}_{\text{con}}(\mathbf{u}_{h,\text{pred}}^{n+1}), \mathbf{u}_{h,\text{pred}}^{n+1} - \mathbf{u}_h^n\big)_{\mathbf{L}_2}\\ &\quad - \frac{1}{2}\big(\mathbf{G}_{\text{con}}(\mathbf{u}_{h,\text{pred}}^{n+1}), \mathbf{G}_{\text{con}}(\mathbf{u}_{h,\text{pred}}^{n+1})\big)_{\mathbf{L}_2} + \big\langle \mathbf{F}^{1/2}(\mathbf{u}_h^n, \mathbf{u}_h^{n+1}), \mathbf{u}_h^{n+1} - \mathbf{u}_h^n\big\rangle_{(\mathbf{H}^1)^*\times\mathbf{H}^1}\end{aligned}$$

$$\begin{aligned}&= -\Big\langle \mathbf{G}\Big(\frac{\mathbf{u}_h^{n+1} - \mathbf{u}_h^n}{\tau}\Big), \mathbf{u}_h^{n+1} - \mathbf{u}_h^n\Big\rangle_{(\mathbf{H}^1)^*\times\mathbf{H}^1} + \big\langle \mathbf{F}_{\text{con}}(\mathbf{u}_h^{n+1}), \mathbf{u}_h^{n+1} - \mathbf{u}_h^n\big\rangle_{(\mathbf{H}^1)^*\times\mathbf{H}^1}\\ &\quad + \frac{1}{\tau}\big(\mathbf{G}_{\text{con}}(\mathbf{u}_{h,\text{pred}}^{n+1}), \mathbf{u}_{h,\text{pred}}^{n+1} - \mathbf{u}_h^n\big)_{\mathbf{L}_2} - \frac{1}{2}\big(\mathbf{G}_{\text{con}}(\mathbf{u}_{h,\text{pred}}^{n+1}), \mathbf{G}_{\text{con}}(\mathbf{u}_{h,\text{pred}}^{n+1})\big)_{\mathbf{L}_2}\end{aligned}$$

by using the third line of (2.17). If viscous energy is taken into account, the energy balance is of the form

$$\begin{aligned}&\mathcal{E}\big(\bar{\mathbf{u}}_h^{n+1}\big) + \tau\mathcal{E}_{\text{visco}}\Big(\frac{\mathbf{u}_h^{n+1} - \mathbf{u}_h^n}{\tau}\Big) - \mathcal{E}\big(\bar{\mathbf{u}}_h^n\big)\\ &= \big\langle \mathbf{F}_{\text{con}}(\mathbf{u}_h^{n+1}), \mathbf{u}_h^{n+1} - \mathbf{u}_h^n\big\rangle_{(\mathbf{H}^1)^*\times\mathbf{H}^1} + \frac{1}{\tau}\big(\mathbf{G}_{\text{con}}(\mathbf{u}_{h,\text{pred}}^{n+1}), \mathbf{u}_{h,\text{pred}}^{n+1} - \mathbf{u}_h^n\big)_{\mathbf{L}_2}\\ &\quad - \frac{1}{2}\Big\|\frac{\mathbf{u}_{h,\text{pred}}^{n+1} - \mathbf{u}_h^n}{\tau}\Big\|_{\mathbf{L}_2}\,.\end{aligned}$$

By exploiting (2.19) and (2.20) with $\mathbf{v}_h = \mathbf{u}_h^n$, the right-hand side of the expression is less or equal to zero,

$$\mathcal{E}\big(\bar{\mathbf{u}}_h^{n+1}\big) + \tau\mathcal{E}_{\text{visco}}\Big(\frac{\mathbf{u}_h^{n+1} - \mathbf{u}_h^n}{\tau}\Big) \le \mathcal{E}\big(\bar{\mathbf{u}}_h^n\big)\,,$$

which yields energy dissipativity of the scheme. □

	$(\text{N-CL})_h$	$(\text{N-M})_h$	$(\text{N-CS})_h$	$(\text{N-CS+})_h$
linear momentum	conserved	conserved	conserved	conserved
energy	blow-up	dissipative	dissipative	dissipative
contact	instable	instable	stable	stable
persistency condition	no	no	no	fulfilled

Table 2.1.: Comparison of the Newmark methods.

In Table 2.1, the numerical characteristics of the four Newmark methods are summarized. Throughout this thesis, the improved contact–stabilized Newmark method is the time integration scheme of interest due to its benefits.

2.5. Numerical Comparison

In the foregoing sections of this chapter, four variants of the Newmark method have been presented, analyzed, and compared with regard to the most relevant physical properties of the system. Now, a numerical study of the energy conservation, the stability behavior, and the fulfillment of a discrete persistency condition will be performed.

Stationary contact problems. The nonlinear variational problem in the second line of the four Newmark methods can be rewritten as a static two-body contact problem discretized in space, which is of the form

$$\mathbf{u} \in \mathcal{K}_h : \qquad \mathcal{J}(\mathbf{u}) \leq \mathcal{J}(\mathbf{v}) \qquad \forall\, \mathbf{v} \in \mathcal{K}_h$$

with a quadratic functional

$$\mathcal{J}(\mathbf{v}) = \frac{1}{2} a(\mathbf{v}, \mathbf{v}) - l(\mathbf{v}) \,,$$

where $a(\cdot, \cdot)$ is a self-adjoint, positive definite bilinear form, and l is a linear functional on $\mathbf{S}_h$ (cf., e.g., [57]). Constrained minimization problems of this type are known to admit a unique solution [8, 36].

Stationary contact problems can be solved efficiently by using the adaptive monotone multigrid methods developed by Kornhuber and Krause [55–58]. These methods discretize the problem without any regularization of the Signorini constraints

such that no algorithmic parameters have to be chosen. Moreover, the nonlinear problems are solved with optimal multigrid complexity, i.e., at the cost of solving a linear system of equations. Recently, the algorithm has been further improved by Gräser and Kornhuber to the so-called truncated nonsmooth Newton multigrid method (TNNMG) [29]. This solver enters the fast linear convergence speed almost immediately in practical applications. The resulting space-time discretization provides stability, accuracy, and efficiency.

Algorithmic realization. The implementation of the different integration schemes is carried out within the frame of the Distributed and Unified Numerics Environment DUNE [2]. For discretization in space, the finite element toolbox UG [3] is utilized. The information transfer at the contact interfaces Γ_C is realized by means of nonconforming domain decomposition or mortar methods, see [89, 90]. Among the possible solvers for variational inequalities, TNMMG is selected. For the $\mathbf{L}_2$-scalar product, a lumped mass matrix is used, which reduces the cost for computing the contact–stabilized predictor steps of $(\text{N-CS})_h$ and $(\text{N-CS+})_h$, cf. Remark 2.3.1.

Hertzian contact. In 1882, Heinrich Hertz published one of the first works in classical contact mechanics [39], where he treated a static contact problem in elasticity. Hertz considered two bodies pressed to each other, which have a symmetry such that the problem effectively reduces to a two-dimensional geometry. In addition, he assumed that the section of the contact surfaces through the plane perpendicular to the symmetry axis is conic. His analytical computations of some characteristic quantities can be applied to several special applications as, e.g., the contact of a circular cylinder, a half-cylinder, or a sphere with a rigid foundation. Such problems are commonly referred to as *Hertz-type* or *Hertzian contact* [49].

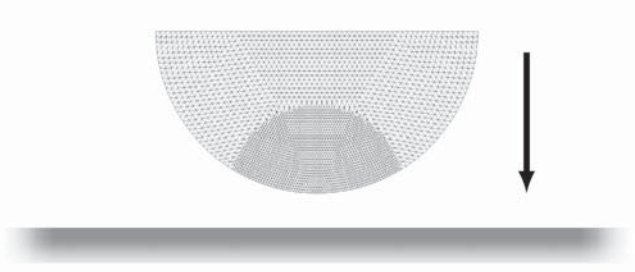

Figure 2.3.: Computational mesh of the test problem.

In the following numerical comparison of the four Newmark methods, a Hertzian contact in two space dimensions is selected as an illustrative test problem. The initial configuration at time $t_0 = 0$ is a semicircle with radius 0.15. The semicircle has an initial distance 0.05 to a rigid plate in the horizontal and is moving downwards at

speed $\dot{\mathbf{u}}_0 = (0, -1)$. The specifications of the elastic and viscous material parameters are listed in Table 2.2. The underlying triangulation results from 5 refinement steps of a coarse grid triangulation with 3 vertices. Within a circle of radius 0.08 around the bottom of the semicircle, the grid is refined further two times. The computational mesh is shown in Figure 2.3. A sixth circle of the boundary located at the bottom is considered as the possible contact boundary. The remaining part of the boundary is traction-free and no volume forces occur, i.e., $f_{\text{ext}} = 0$. For discretization in time, the constant timestep $\tau = 5 \cdot 10^{-4}$ is chosen, and the computations are carried out until $T = 0.015$.

parameter	value
Young's modulus	10^4
Poisson ratio	0.3
shear viscosity	10^{-3}
bulk viscosity	10^{-3}

Table 2.2.: Material specifications of the test problem.

In the following, the properties of the four Newmark's algorithms will be examined for the above test problem. The considered characteristics are the temporal evolutions of the total energy, the number of active contact points, and the contact forces and velocities at contact boundaries.

Total energy. Figure 2.4 illustrates the temporal evolution of the total energy of the Newmark methods normalized to the initial energy of the system (including the viscous energy). During the phase of contact, the classical scheme $(\text{N-CL})_h$ produces an energy blow-up of more than 50% together with appreciable oscillations. The three variants $(\text{N-CI})_h$, $(\text{N-CS})_h$, and $(\text{N-CS+})_h$ are dissipative in the presence of contact with a slight energy loss of about 0.02%. Moreover, there is clear numerical evidence that the loss of energy stems from the variation of the active contact boundary: for $(\text{N-CS})_h$, the largest energy dissipation is generated when the semicircle leaves the plate. In contrast, $(\text{N-CI})_h$ and $(\text{N-CS+})_h$ loose most energy in the moment when the semicircle gets in contact with the plate for the first time. This behavior is more in accordance with the mathematical and physical structure of the problem since finding contact is much more nonlinear and irregular than detaching contact. In the absence of contact, all Newmark methods preserve the total energy of the system.

Active contact. In Figure 2.5, the number of active contact points is given over a selective interval of time for all four Newmark methods. In more detail, this is the number of vertices at boundaries where contact actually occurs. Although the quantity should behave smooth, the classical scheme $(\text{N-CL})_h$ generates numerous

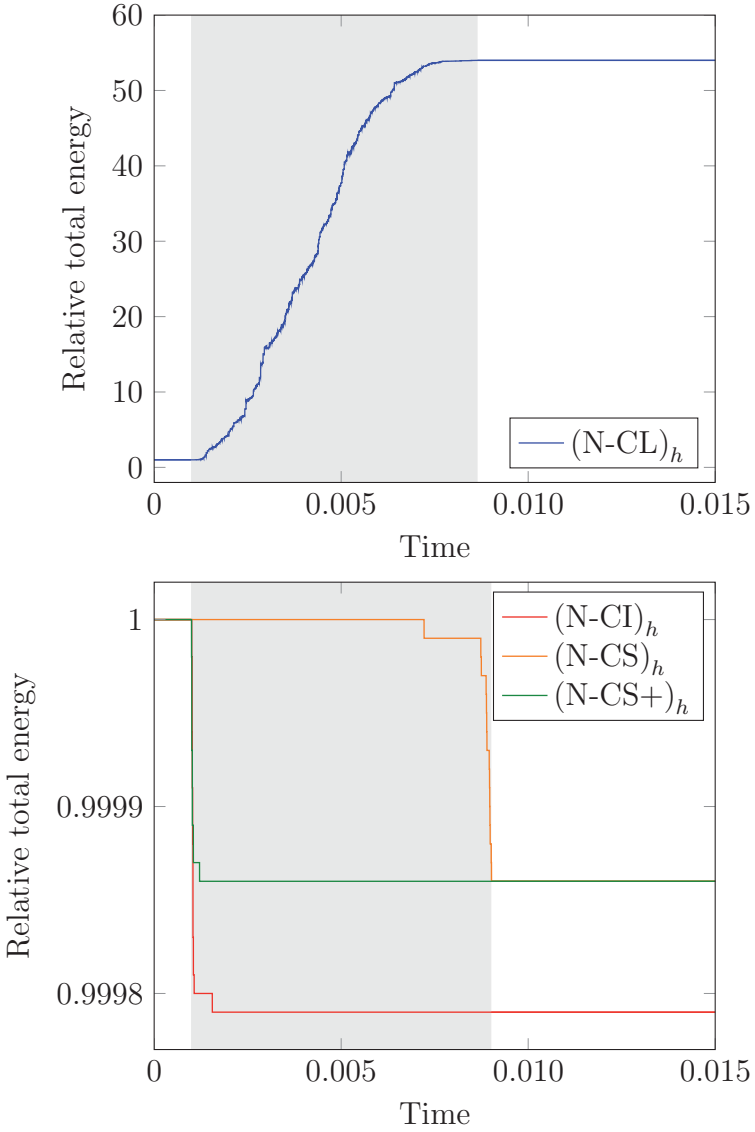

Figure 2.4.: Comparison of the total energy normalized to total energy at initial time including viscous energy (grey: phase of contact).

artificial oscillations (1232) in displacements. The dissipative modification $(\text{N-CI})_h$ produces a much more stable active contact boundary, but still exhibits some oscillations (242). Only the contact–stabilized versions $(\text{N-CS})_h$ and $(\text{N-CS+})_h$ do not show any spurious oscillations (0) on the whole time interval.

Contact forces. Figure 2.6 presents the normal components of the contact forces evaluated at the south pole of the semicircle for the four Newmark methods. The classical scheme $(\text{N-CL})_h$ produces high artificial oscillations in the contact forces during the whole phase of contact. The contact forces of $(\text{N-CI})_h$ show extremely large values in the initial phase of contact and a highly oscillatory zigzagging during the remaining contact phase. The contact–stabilization in $(\text{N-CS})_h$ and $(\text{N-CS+})_h$ clearly eliminates both the overshooting phenomenon and the spurious oscillations.

Velocities. A deeper insight into the origin of the undesirable instabilities in active contact and in contact forces can be gained from Figure 2.7. Here, the normal components of the velocities of $(\text{N-CI})_h$, $(\text{N-CS})_h$, and $(\text{N-CS+})_h$ at the south pole are plotted over a segment of timesteps. While the sign of the velocities of $(\text{N-CI})_h$ is zigzagging in every timestep, the contact–stabilization does not evoke any artificial oscillations: once a node is in contact, the velocities of $(\text{N-CS})_h$ remain the same during the phase of contact. The improved variant $(\text{N-CS+})_h$ even features vanishing normal components of the velocities. This reflects the actual physical behavior of the system.

Discrete persistency condition. In Figure 2.8, the time evolution of the discrete quantity P_h introduced in (2.16) is plotted for all four types of Newmark's method. As expected by the investigations of the contact forces and velocities at the south pole, the classical scheme $(\text{N-CL})_h$ shows an extremely oscillatory behavior of this quantity. The modification $(\text{N-CI})_h$ produces a large peak in P_h when the bodies get into contact followed by a zigzagging in the remaining contact phase. The evolution of P_h for the contact–stabilization $(\text{N-CS})_h$ is similar to the one of the contact force at the south pole. Finally, the improved contact–stabilized method $(\text{N-CS+})_h$ fulfills the discrete persistency condition (2.16) over large phases of active contact.

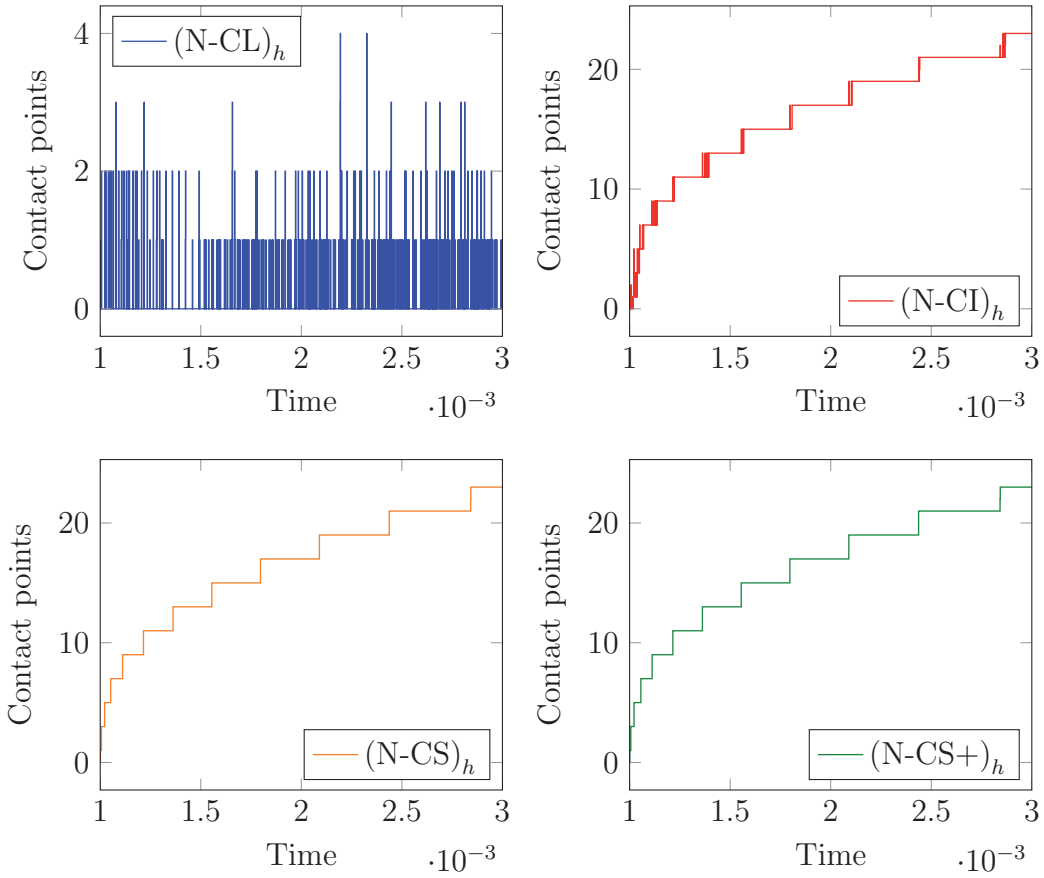

Figure 2.5.: Comparison of the number of active contact points (zoom).

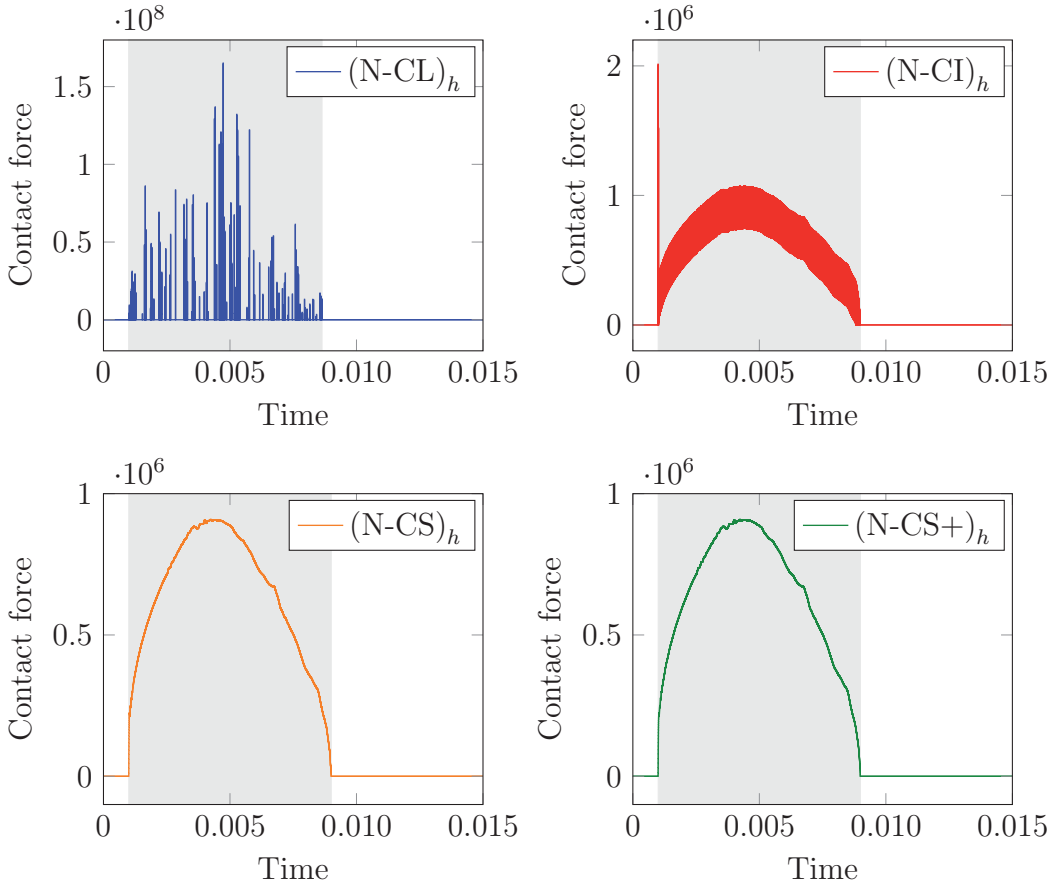

Figure 2.6.: Comparison of the normal components of the contact forces at the south pole (grey: phase of contact).

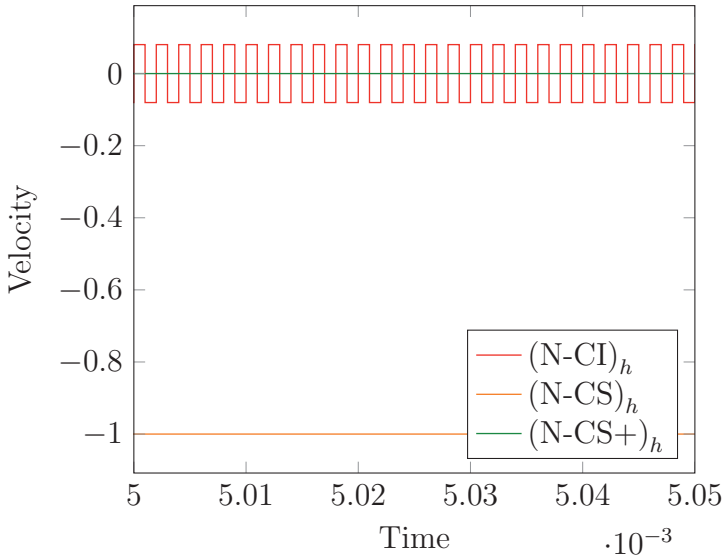

Figure 2.7.: Comparison of the normal components of the velocities at the south pole (zoom).

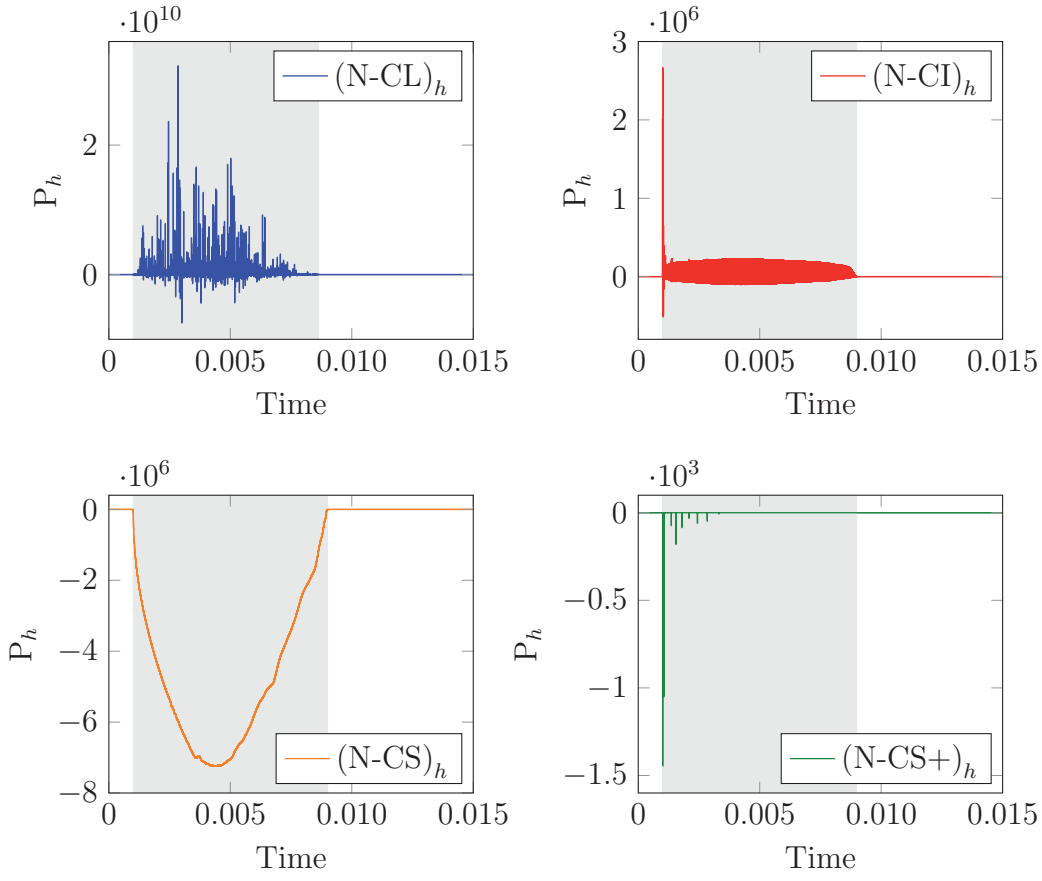

Figure 2.8.: Comparison of P_h (grey: phase of contact).

3. A Perturbation Result – Viscosity and Physical Energy Norm

In order to cope with the challenge of an efficient simulation of real life problems as, e.g., the motion of the human knee, an adaptive control of timesteps for the improved contact–stabilized Newmark method is desirable. Primarily, this purpose requires a realistic estimation of the local discretization error within a problem-adapted norm [18]. Hence, a necessary preparatory step is to find a norm in which a perturbation result for dynamical contact problems can be expected. Such a norm will moreover provide the basis for a proof of convergence of the improved contact–stabilized Newmark method by applying the established proof technique for discretizations of evolution problems by Hairer, Nørsett, and Wanner (also known as "Lady Windermere's Fan", cf. [34]).

Unfortunately, results concerning the continuous dependence of dynamical contact problems with Signorini conditions on the initial data are not yet existing in mathematical literature, neither in the purely elastic nor in the viscoelastic case. The lack of well-posedness results mainly originates from the Signorini contact conditions on the unknown displacement field. The constraints lead to nonsmooth and nonlinear variational inequalities of hyperbolic structure, which inhibit a general regularity of the solution at contact interfaces and lead to shock waves after impacts. This causes serious and unresolved mathematical difficulties in the analysis of these problems.

The present chapter is intended to be a first step towards the stability of dynamical contact problems with Signorini conditions under perturbations of the initial data [50, 51]. In Section 3.1, the essential mathematical problems in the derivation of a perturbation result for linearly elastic bodies in the presence of contact will be pointed out. To this end, the focus is on viscoelastic materials fulfilling the Kelvin-Voigt constitutive law. In Section 3.2, a class of problems will be found that satisfy a perturbation result in a non-trivial choice of mixed norms in function space. This characterization will be given in form of a stability condition on the contact stresses at the contact boundaries and will be interpreted in Section 3.3. Finally, in Section 3.4, two well-established approximations of the classical Signorini condition in linear viscoelasticity will be discussed, the Signorini condition formulated in velocities and the model of normal compliance. Both problems are even satisfying a

sharper version of the stability condition, and a perturbation result can be proven by application of the same techniques.

3.1. Elasticity

The first three sections of this chapter deal with the continuous dependence on the initial data for dynamical contact problems with Signorini conditions in displacements. In a first step, the classical contact problem in pure linear elasticity is under consideration. Here, the fundamental difficulties with a characterization of a class of problems satisfying a perturbation result will be analyzed.

The underlying mathematical model of dynamical contact between two linearly elastic bodies based on Signorini's contact conditions is formulated as follows (compare Section 1.3 for the viscoelastic case). For almost every $t \in [0,T]$, find $\mathbf{u}(\cdot,t) \in \mathcal{K}$ with $\ddot{\mathbf{u}}(\cdot,t) \in (\mathbf{H}^1)^*$ such that

$$\langle \ddot{\mathbf{u}}, \mathbf{v}-\mathbf{u}\rangle_{(\mathbf{H}^1)^*\times\mathbf{H}^1} + \langle \mathbf{F}(\mathbf{u}), \mathbf{v}-\mathbf{u}\rangle_{(\mathbf{H}^1)^*\times\mathbf{H}^1} \geq 0\,, \qquad \forall\, \mathbf{v} \in \mathcal{K} \tag{3.1}$$

and

$$\mathbf{u}(0) = \mathbf{u}_0,\ \dot{\mathbf{u}}(0) = \dot{\mathbf{u}}_0\,. \tag{3.2}$$

The contact forces $\mathbf{F}_{\mathrm{con}}(\mathbf{u}) \in (\mathbf{H}^1)^*$ for a given solution $\mathbf{u}$ of this variational inequality are defined via

$$\langle \mathbf{F}_{\mathrm{con}}(\mathbf{u}), \mathbf{v}\rangle_{(\mathbf{H}^1)^*\times\mathbf{H}^1} := \langle \ddot{\mathbf{u}} + \mathbf{F}(\mathbf{u}), \mathbf{v}\rangle_{(\mathbf{H}^1)^*\times\mathbf{H}^1}\,, \qquad \mathbf{v} \in \mathbf{H}^1 \tag{3.3}$$

for almost every $t \in [0,T]$.

Notation. Consider a quantity $\mathbf{v}$ and its perturbation $\tilde{\mathbf{v}}$. Then,

$$\delta\mathbf{v} := \mathbf{v} - \tilde{\mathbf{v}}\,. \tag{3.4}$$

The study of stability starts with a formal derivation of a relation that describes the dynamical behavior of an initial perturbation in the energy norm of the system. Let $\mathbf{u}$ and $\tilde{\mathbf{u}}$ be two solutions of the linearly elastic contact problem (3.1) with initial values $\mathbf{u}(0) = \mathbf{u}_0$, $\dot{\mathbf{u}}(0) = \dot{\mathbf{u}}_0$ and $\tilde{\mathbf{u}}(0) = \tilde{\mathbf{u}}_0$, $\dot{\tilde{\mathbf{u}}}(0) = \dot{\tilde{\mathbf{u}}}_0$. Assume that $\delta\dot{\mathbf{u}}$ is contained in $\mathbf{W}_2^1(0,T;\mathbf{H}^1,\mathbf{L}_2)$, which may not be satisfied in general. Nevertheless, integrating (1.31) from 0 to t with $t \in [0,T]$ and using $\mathbf{v} = \delta\dot{\mathbf{u}}$ as a trial function yields

$$\begin{aligned}
&\int_0^t \langle \ddot{\mathbf{u}}(s), \delta\dot{\mathbf{u}}(s)\rangle_{(\mathbf{H}^1)^*\times\mathbf{H}^1}\, ds + \int_0^t a(\mathbf{u}(s), \delta\dot{\mathbf{u}}(s))\, ds \\
&= \int_0^t f_{\mathrm{ext}}(\delta\dot{\mathbf{u}}(s))\, ds + \int_0^t \langle \mathbf{F}_{\mathrm{con}}(\mathbf{u}(s)), \delta\dot{\mathbf{u}}(s)\rangle_{(\mathbf{H}^1)^*\times\mathbf{H}^1}\, ds\,.
\end{aligned}$$

After performing the same formal calculation with (1.31) for $\tilde{\mathbf{u}}$ instead of $\mathbf{u}$, the resulting equation for $\tilde{\mathbf{u}}$ can be subtracted from the equation for $\mathbf{u}$ above. The linearity of the functional f_{ext} leads to

$$\begin{aligned}&\int_0^t \langle \delta\ddot{\mathbf{u}}(s), \delta\dot{\mathbf{u}}(s)\rangle_{(\mathbf{H}^1)^*\times\mathbf{H}^1}\, ds + \int_0^t a(\delta\mathbf{u}(s), \delta\dot{\mathbf{u}}(s))\, ds \\ &= \int_0^t \langle \delta\mathbf{F}_{\text{con}}(\mathbf{u}(s)), \delta\dot{\mathbf{u}}(s)\rangle_{(\mathbf{H}^1)^*\times\mathbf{H}^1}\, ds\,.\end{aligned}$$

Under the regularity assumption $\delta\dot{\mathbf{u}} \in \mathbf{W}_2^1(0,T;\mathbf{H}^1,\mathbf{L}_2)$ on the velocities and accelerations, the left-hand side of the expression can be reformulated by applying integration by parts in time (see, e.g., [93, Proposition 23.23]). The calculation yields the following result.

Lemma 3.1.1. *Let* $\mathbf{u}$ *and* $\tilde{\mathbf{u}}$ *be two solutions of* (1.28) *with initial values* $\mathbf{u}(0) = \mathbf{u}_0$, $\dot{\mathbf{u}}(0) = \dot{\mathbf{u}}_0$ *and* $\tilde{\mathbf{u}}(0) = \tilde{\mathbf{u}}_0$, $\dot{\tilde{\mathbf{u}}}(0) = \dot{\tilde{\mathbf{u}}}_0$, *respectively. Furthermore, assume that* $\delta\dot{\mathbf{u}} \in \mathbf{W}_2^1(0,T;\mathbf{H}^1,\mathbf{L}_2)$. *Then, for all* $t \in [0,T]$,

$$\begin{aligned}&\frac{1}{2}\|\delta\dot{\mathbf{u}}(t)\|_{\mathbf{L}_2}^2 + \frac{1}{2}\|\delta\mathbf{u}(t)\|_a^2 \\ &= \frac{1}{2}\|\delta\dot{\mathbf{u}}_0\|_{\mathbf{L}_2}^2 + \frac{1}{2}\|\delta\mathbf{u}_0\|_a^2 + \int_0^t \langle \delta\mathbf{F}_{\text{con}}(\mathbf{u}(s)), \delta\dot{\mathbf{u}}(s)\rangle_{(\mathbf{H}^1)^*\times\mathbf{H}^1}\, ds\,.\end{aligned} \tag{3.5}$$

In the absence of contact, the two left-hand terms and the first two right-hand terms in (3.5) show the continuous dependence of the solution on the initial values. In the presence of contact, this structure is disturbed by the additional contact term on the right-hand side.

In order to gain some insight into this result, the focus is turned to the simpler problem of ordinary differential equations. In this case, the impulsive constraint forces $\mathbf{F}_{\text{con}}$ concentrate at times when the (rigid) bodies collide, see Figure 3.1. From the analytical point of view, these forces cannot be modeled as functions in time anymore, but rather as distributions or measures.

From the numerical point of view, the given situation is treated in terms of *"switching functions"* used to identify *"switching points"* as their local zeros. Once these points are determined, they can be used to restart the integration (cf., e.g., [18, Chapter 8.2]). If such methods are not applied, a loss of regularity would occur even in the ODE case. In the PDE case, each spatial point gives rise to a corresponding switching time, which is why such a treatment cannot carry over. However, the contact forces can still be expected to be very irregular.

In order to estimate the contact term, information on the time derivatives of the displacements at the contact boundaries are needed. Unfortunately, a purely

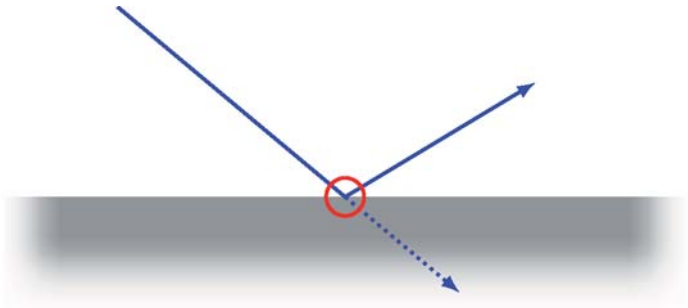

Figure 3.1.: Switching point for a trajectory in the ODE case.

elastic formulation is in general not capable of providing such information. This fact originates from the underlying assumption that the dependence of internal stresses on velocities can be neglected. Therefore, there is no way to define a class of elastic contact problems just by demanding a kind of stability on the contact stresses. A perturbation result for linearly elastic contact problems would necessarily require estimates on the velocities at the contact boundaries.

Actually, the problem is linked to the additional regularity assumption on the solutions, which is needed for the validity of Lemma 3.1.1. Due to the hyperbolic structure of purely elastic contact problems, the Signorini solutions are not as smooth as the initial data allow. Therefore, in the following section, attention will be directed to materials with viscoelastic behavior as they are commonly used for modeling articular cartilage in the human knee joint (compare the introductory Chapter 1).

3.2. Viscoelasticity

In this section, a class of linearly viscoelastic contact problems with Signorini conditions will be characterized that satisfy continuous dependence on the initial data. Under a stability condition on the contact stresses, a perturbation result in a special mix of norms in function space will be proven.

Viscosity leads to higher regularity of the solutions, which justifies the formal calculation for purely elastic problems as performed in Section 3.1. Furthermore, viscoelastic models are in general capable of providing information on the time derivatives of the solutions at the contact boundaries.

At first, a result for the viscoelastic problem will be given that corresponds to Lemma 3.1.1 in the purely elastic case.

Lemma 3.2.1. *Let* $\mathbf{u}$ *and* $\tilde{\mathbf{u}}$ *be two solutions of* (1.28) *with initial values* $\mathbf{u}(0) = \mathbf{u}_0$,

$\dot{\mathbf{u}}(0) = \dot{\mathbf{u}}_0$ *and* $\tilde{\mathbf{u}}(0) = \tilde{\mathbf{u}}_0$, $\dot{\tilde{\mathbf{u}}}(0) = \dot{\tilde{\mathbf{u}}}_0$, *respectively. Then, for all* $t \in [0,T]$,

$$\begin{aligned}&\frac{1}{2}\|\delta\dot{\mathbf{u}}(t)\|_{\mathbf{L}_2}^2 + \frac{1}{2}\|\delta\mathbf{u}(t)\|_a^2 + \int_0^t \|\delta\dot{\mathbf{u}}(s)\|_b^2\, ds \\ &= \frac{1}{2}\|\delta\dot{\mathbf{u}}_0\|_{\mathbf{L}_2}^2 + \frac{1}{2}\|\delta\mathbf{u}_0\|_a^2 + \int_0^t \langle \delta\mathbf{F}_{\mathrm{con}}(\mathbf{u}(s)), \delta\dot{\mathbf{u}}(s)\rangle_{(\mathbf{H}^1)^*\times\mathbf{H}^1}\, ds\,.\end{aligned}$$

Proof. As in the purely elastic case, the viscoelasticity equations (1.28) for $\mathbf{u}$ and $\tilde{\mathbf{u}}$ are integrated from 0 to t and tested with $\mathbf{v} = \delta\dot{\mathbf{u}}$. Then, subtracting one from the other gives

$$\begin{aligned}&\int_0^t \langle \delta\ddot{\mathbf{u}}(s), \delta\dot{\mathbf{u}}(s)\rangle_{(\mathbf{H}^1)^*\times\mathbf{H}^1}\, ds + \int_0^t a(\delta\mathbf{u}(s), \delta\dot{\mathbf{u}}(s))\, ds + \int_0^t b(\delta\dot{\mathbf{u}}(s), \delta\dot{\mathbf{u}}(s))\, ds \\ &= \int_0^t \langle \delta\mathbf{F}_{\mathrm{con}}(\mathbf{u}(s)), \delta\dot{\mathbf{u}}(s)\rangle_{(\mathbf{H}^1)^*\times\mathbf{H}^1}\, ds\end{aligned}$$

due to the linearity of the external forces. Integration by parts (see, e.g., [93, Proposition 23.23]) leads to the expression of the lemma. □

This result motivates the introduction of the following mix of norms in function space.

Physical energy norm. For a function $\bar{\mathbf{v}} = (\mathbf{v}, \dot{\mathbf{v}}) : [t, t+\tau] \to \mathbf{H}^1 \times \mathbf{L}_2$ with $\dot{\mathbf{v}} \in \mathbf{L}_2(t, t+\tau; \mathbf{H}^1)$, define

$$\|\bar{\mathbf{v}}\|_{\mathcal{E}(t,\tau)}^2 := \|\bar{\mathbf{v}}(t+\tau)\|_E^2 + \int_t^{t+\tau} \|\dot{\mathbf{v}}(s)\|_b^2\, ds \tag{3.6}$$

in terms of the *reduced* norm

$$\|\bar{\mathbf{v}}(t+\tau)\|_E^2 := \frac{1}{2}\|\dot{\mathbf{v}}(t+\tau)\|_{\mathbf{L}_2}^2 + \frac{1}{2}\|\mathbf{v}(t+\tau)\|_a^2\,. \tag{3.7}$$

Obviously, this norm may be interpreted as a sum of the kinetic energy, measured in $\mathbf{L}_2$, and the potential energy, measured in the usual energy norm in $\mathbf{H}^1$, including the viscoelastic part. Therefore, it will be called the *physical energy norm* throughout this thesis.

Even in the case of linear viscoelasticity, the dynamical contact problem with Signorini conditions in displacements may be ill-posed in the presence of contact.

Hence, a characterization of problems will be given for which the continuous dependence of the solutions on the initial values holds. The result presented in the lemma above shows that a stability condition is necessary for the time integral over the contact forces applied to the velocities. The perturbations in displacements and velocities will be measured in the canonical norm on $\mathbf{L}_2(0,T;\mathbf{H}^1)$.

Stability condition. Let

$$\begin{aligned} &\Big| \int_0^t \langle \delta \mathbf{F}_{\mathrm{con}}(\mathbf{u}(s)), \delta \dot{\mathbf{u}}(s) \rangle_{(\mathbf{H}^1)^* \times \mathbf{H}^1} \, ds \Big| \\ &\leq \varepsilon \big(\kappa \|\delta \mathbf{u}\|_{\mathbf{L}_2(0,t;\mathbf{H}^1)} + \|\delta \dot{\mathbf{u}}\|_{\mathbf{L}_2(0,t;\mathbf{H}^1)} \big) \|\delta \dot{\mathbf{u}}\|_{\mathbf{L}_2(0,t;\mathbf{H}^1)} \end{aligned} \tag{3.8}$$

hold for all $t \in [0,T]$ with $\varepsilon \geq 0$ sufficiently small and $\kappa \geq 0$.

The precise meaning of the requirement "ε sufficiently small" will be given in the following perturbation theorem. The validity of this demand will be found to be absolutely fundamental for the derivation of a perturbation result in the viscoelastic case. The stability condition on the contact forces is formulated in integrals over time, and hence, the assumption does not have a meaning for every single timepoint. Especially, this is true for the basic requirement that ε is small. A detailed interpretation and motivation of the stability condition will be presented in the following Section 3.3.

For the class of viscoelastic problems satisfying the stability condition above, the following perturbation result holds.

Theorem 3.2.2. *Let* $\bar{\mathbf{u}} = (\mathbf{u}, \dot{\mathbf{u}})$ *and* $\tilde{\bar{\mathbf{u}}} = (\tilde{\mathbf{u}}, \dot{\tilde{\mathbf{u}}})$ *be two solutions of* (1.28) *with initial values* $\mathbf{u}(0) = \mathbf{u}_0$, $\dot{\mathbf{u}}(0) = \dot{\mathbf{u}}_0$ *and* $\tilde{\mathbf{u}}(0) = \tilde{\mathbf{u}}_0$, $\dot{\tilde{\mathbf{u}}}(0) = \dot{\tilde{\mathbf{u}}}_0$, *respectively. Furthermore, assume the stability condition* (3.8) *with* $\frac{\varepsilon}{V_0 \, c_K} < 1$. *Then, for all* $t \in [0,T]$,

$$\|\delta \bar{\mathbf{u}}(t)\|_E^2 + \alpha \int_0^t \|\delta \dot{\mathbf{u}}(s)\|_b^2 \, ds \leq \big(\|\delta \bar{\mathbf{u}}_0\|_E^2 + ct \|\delta \mathbf{u}_0\|_{\mathbf{L}_2}^2 \big) \cdot e^{\tilde{\kappa}^2 t} \tag{3.9}$$

with $\alpha \in [0,1)$, $c \geq 0$, *and* $\tilde{\kappa} \geq 0$.

Remark 3.2.3. If the Dirichlet boundaries do not vanish, i.e., if $\mathrm{meas}(\Gamma_D) > 0$, or if a part of the contact boundaries is active in the whole time interval $[0,T]$, then

$$\|\delta \bar{\mathbf{u}}(t)\|_E^2 + \alpha \int_0^t \|\delta \dot{\mathbf{u}}(s)\|_b^2 \, ds \leq \|\delta \bar{\mathbf{u}}_0\|_E^2 \cdot e^{\tilde{\kappa}^2 t} \, . \tag{3.10}$$

In this case, the propagated perturbation of the solution measured in physical energy norm does no longer depend on the initial perturbation of the displacements in $\mathbf{L}_2$-norm [51].

Proof. By means of Lemma 3.2.1, the stability condition (3.8) leads to

$$\begin{aligned}
&\|\delta\bar{\mathbf{u}}(t)\|_E^2 + \int_0^t \|\delta\dot{\mathbf{u}}(s)\|_b^2\, ds \\
&\leq \|\delta\bar{\mathbf{u}}_0\|_E^2 + \Big| \int_0^t \langle \delta\mathbf{F}_{\mathrm{con}}(\mathbf{u}(s)), \delta\dot{\mathbf{u}}(s)\rangle_{(\mathbf{H}^1)^*\times\mathbf{H}^1}\, ds \Big| \\
&\leq \|\delta\bar{\mathbf{u}}_0\|_E^2 + \varepsilon\kappa \|\delta\mathbf{u}\|_{\mathbf{L}_2(0,t;\mathbf{H}^1)} \|\delta\dot{\mathbf{u}}\|_{\mathbf{L}_2(0,t;\mathbf{H}^1)} + \varepsilon \|\delta\dot{\mathbf{u}}\|^2_{\mathbf{L}_2(0,t;\mathbf{H}^1)}
\end{aligned}$$

for all $t \in (0,T)$. For an arbitrary parameter $\alpha < 1$, Young's inequality in the form

$$ab \leq \frac{1}{4\, V_0\, c_K\, (1-\alpha)}\, a^2 + V_0\, c_K\, (1-\alpha)\, b^2$$

gives

$$\begin{aligned}
&\|\delta\bar{\mathbf{u}}(t)\|_E^2 + \int_0^t \|\delta\dot{\mathbf{u}}(s)\|_b^2\, ds \\
&\leq \|\delta\bar{\mathbf{u}}_0\|_E^2 + \frac{\varepsilon^2\kappa^2}{4\, V_0\, c_K\, (1-\alpha)} \|\delta\mathbf{u}\|^2_{\mathbf{L}_2(0,t;\mathbf{H}^1)} + (\varepsilon + V_0\, c_K\, (1-\alpha)) \, \|\delta\dot{\mathbf{u}}\|^2_{\mathbf{L}_2(0,t;\mathbf{H}^1)} .
\end{aligned}$$

For almost every $t > 0$, the velocities $\dot{\mathbf{u}}(t)$ and $\dot{\tilde{\mathbf{u}}}(t)$ are contained in $\mathbf{H}^1$ with a trace on the boundary. If $\mathrm{meas}(\Gamma_D) > 0$ or if a part of the contact boundaries remains active in the time interval, then $\delta\mathbf{u}(t) = 0$ leads to $\delta\dot{\mathbf{u}}(t) = 0$ for almost every t on the segment of the boundaries. Thus, the simplified Korn's inequality (A.2) can be applied [51]. In the general case, inequality (A.1) and the estimate (1.5) yield

$$\begin{aligned}
&\|\delta\bar{\mathbf{u}}(t)\|_E^2 + \int_0^t \|\delta\dot{\mathbf{u}}(s)\|_b^2\, ds \\
&\leq \|\delta\bar{\mathbf{u}}_0\|_E^2 + \frac{\varepsilon^2\kappa^2}{4\, V_0\, c_K^2\, (1-\alpha)} \int_0^t \Big(\frac{1}{E_0} \|\delta\mathbf{u}(s)\|_a^2 + \|\delta\mathbf{u}(s)\|^2_{\mathbf{L}_2} \Big) ds \\
&\quad + \Big(\frac{\varepsilon}{c_K} + V_0\, (1-\alpha) \Big) \int_0^t \Big(\frac{1}{V_0} \|\delta\dot{\mathbf{u}}(s)\|_b^2 + \|\delta\dot{\mathbf{u}}(s)\|^2_{\mathbf{L}_2} \Big)\, ds\,,
\end{aligned}$$

which is equivalent to

$$\|\delta\bar{\mathbf{u}}(t)\|_E^2 + \tilde{\alpha}\int_0^t \|\delta\dot{\mathbf{u}}(s)\|_b^2\,ds$$
$$\leq \|\delta\bar{\mathbf{u}}_0\|_E^2 + \frac{c}{2\,E_0}\int_0^t \|\delta\mathbf{u}(s)\|_a^2\,ds + \frac{c}{2}\int_0^t \|\delta\mathbf{u}(s)\|_{\mathbf{L}_2}^2 ds + V_0(1-\tilde{\alpha})\int_0^t \|\delta\dot{\mathbf{u}}(s)\|_{\mathbf{L}_2}^2\,ds$$

with constants

$$\tilde{\alpha} = \alpha - \frac{\varepsilon}{V_0\,c_K}\,, \quad c = \frac{\varepsilon^2\kappa^2}{2\,V_0\,c_K^2\,(1-\alpha)}\,.$$

In order to ensure the non-negativity of the integral term on the left-hand side, let ε be such small that $\frac{\varepsilon}{V_0\,c_K} < 1$ and choose $\alpha < 1$ such that $\tilde{\alpha} \geq 0$. The inequalities of Young and Hölder lead to

$$\begin{aligned}
\|\delta\mathbf{u}(s)\|_{\mathbf{L}_2}^2 &= \Big\|\delta\mathbf{u}(0) + \int_0^s \delta\dot{\mathbf{u}}(\eta)\,d\eta\Big\|_{\mathbf{L}_2}^2 \\
&\leq \Big(\|\delta\mathbf{u}(0)\|_{\mathbf{L}_2} + \int_0^s \|\delta\dot{\mathbf{u}}(\eta)\|_{\mathbf{L}_2}\,d\eta\Big)^2 \\
&\leq 2\Big(\|\delta\mathbf{u}(0)\|_{\mathbf{L}_2}^2 + \Big(\int_0^s \|\delta\dot{\mathbf{u}}(\eta)\|_{\mathbf{L}_2}\,d\eta\Big)^2\Big) \\
&\leq 2\Big(\|\delta\mathbf{u}(0)\|_{\mathbf{L}_2}^2 + s\int_0^s \|\delta\dot{\mathbf{u}}(\eta)\|_{\mathbf{L}_2}^2\,d\eta\Big)
\end{aligned}$$

and

$$\|\delta\bar{\mathbf{u}}(t)\|_E^2 + \tilde{\alpha}\int_0^t \|\delta\dot{\mathbf{u}}(s)\|_b^2\,ds$$
$$\leq \|\delta\bar{\mathbf{u}}_0\|_E^2 + ct\|\delta\mathbf{u}_0\|_{\mathbf{L}_2}^2 + \frac{c}{2\,E_0}\int_0^t \|\delta\mathbf{u}(s)\|_a^2\,ds + \big(ct^2 + V_0(1-\tilde{\alpha})\big)\int_0^t \|\delta\dot{\mathbf{u}}(s)\|_{\mathbf{L}_2}^2\,ds\,.$$

This yields

$$\|\delta\bar{\mathbf{u}}(t)\|_E^2 + \tilde{\alpha}\int_0^t \|\delta\dot{\mathbf{u}}(s)\|_b^2\,ds \leq \|\delta\bar{\mathbf{u}}_0\|_E^2 + ct\|\delta\mathbf{u}_0\|_{\mathbf{L}_2}^2 + \tilde{\kappa}^2\int_0^t \|\delta\bar{\mathbf{u}}(s)\|_E^2 ds$$

with

$$\tilde{\kappa}^2 = \max\Big(\frac{c}{2\,E_0}, cT^2 + V_0(1-\tilde{\alpha})\Big)\,.$$

Note that $\mathbf{u} \in \mathbf{C}([0,T],\mathbf{H}^1)$ and $\dot{\mathbf{u}} \in \mathbf{C}([0,T],\mathbf{L}_2)$. Together with Lebesgue's theorem of calculus (cf., e.g., [94, Appendix, Application (25c)]) and $\dot{\mathbf{u}} \in \mathbf{L}_2(0,T;\mathbf{H}^1)$, this fact gives the continuity of the left-hand side with respect to $t \in [0,T]$. Now, the result of the theorem is a direct consequence of Gronwall's lemma as presented in Appendix A. □

The perturbation theorem given above is the main result of this section and suggests to use viscoelastic modeling throughout this thesis. Coming back to dynamical contact problems in the context of orthopaedic surgery planning mentioned in the introduction (the motion of the knee), cartilage may be interpreted as the nature's reflection of the above mathematical insight.

3.3. Interpretation of the Stability Condition

In order to interpret and to motivate the stability condition (3.8), the first aim is to localize the contact stresses on a segment of the possible contact boundaries. On the basis of such a localization, a sufficient criterion for the validity of the stability condition will be given.

The considerations are motivated by the intuition that perturbations in the contact forces are effective only on a small part of the contact boundaries, namely where the original solution is in contact and the perturbed is not, or vice versa. However, due to the lack of regularity of the solutions, the following presentation is more a heuristic argumentation rather than a rigorous proof. For simplification, let the possible contact boundaries and the bijective mappings between the two possible contact boundaries coincide, i.e., $\Gamma_C = \tilde{\Gamma}_C$ and $\boldsymbol{\phi} = \tilde{\boldsymbol{\phi}}$. This is the case of interest with regard to the analysis of the global discretization error in Chapter 5 and in Chapter 6.

In a first step, the purpose is to conceptualize the part of the possible contact boundaries where the solution of the dynamical contact problem (1.28) is actually in contact. For almost every $t \geq 0$, the natural definition of the active contact boundaries of a displacement $\mathbf{u}$ is

$$\Gamma_C(t) = \left\{ x \in \Gamma_C \,\middle|\, [\mathbf{u} \cdot \boldsymbol{\nu}]_{\boldsymbol{\phi}} = g \right\} \subset \Gamma_C \,.$$

In the general case, the lack of regularity results for dynamical contact problems prohibits the introduction of actual contact boundaries in this way. This is due to the fact that definition (1.19) of the admissible set only yields a non-penetration condition up to boundary sets of measure zero. Hence, the definition above necessitates the additional assumption that the solution is continuous on the possible contact boundaries, which is satisfied, e.g., if $\mathbf{u} \in \mathbf{L}_2(0,T;\mathbf{H}^2(\Omega))$ (for a definition of this space see, e.g., [5, 93]). A general definition of segments of the boundaries requires a more subtle mathematical approach.

The key for understanding the local behavior of functions in $\mathbf{H}^1(\Omega)$ is the concept of (Sobolev) capacity. The elements in the Sobolev space are equivalence classes of functions that agree almost everywhere in Ω. By using the notion of capacity, the almost everywhere equivalence can be refined.

Sobolev capacity. Let E be a subset of $\mathbb{R}^d$, and

$$\mathbf{S}(\mathrm{E}) := \left\{ \mathbf{u} \in \mathbf{H}^1(\mathbb{R}^d) \,\middle|\, \mathbf{u} = 1 \text{ on an open set containing E} \right\}. \tag{3.11}$$

Then, the *Sobolev capacity* of E is defined as

$$\mathrm{cap}(\mathrm{E}) := \inf_{\mathbf{u} \in \mathbf{S}(\mathrm{E})} \|\mathbf{u}\|^2_{\mathbf{H}^1(\mathbb{R}^d)} \in [0, \infty]. \tag{3.12}$$

A property is said to hold *quasieverywhere*, abbreviated q.e., if it holds except on a set $\mathrm{E} \subset \Omega$ of capacity zero. It easily follows from the Poincare inequality that each set of capacity zero has Lebesgue measure zero as well. For each $\mathbf{u} \in \mathbf{H}^1(\Omega)$, there is a function $\mathbf{v} \in \mathbf{H}^1(\Omega)$ such that $\mathbf{u} = \mathbf{v}$ almost everywhere, and $\mathbf{v}$ is *quasicontinuous*, i.e., $\mathbf{v}$ is continuous when restricted to a set whose complement has arbitrary small capacity. This quasicontinuous representative is unique up to a set of capacity zero. For details concerning Sobolev capacity see, e.g., [38].

By means of the notion of capacity, the item of active contact boundaries for dynamical contact problems can be introduced as follows.

Active contact boundaries. For almost every $t \geq 0$, the *active contact boundaries* of a solution $\mathbf{u}$ of (1.28) are defined as

$$\Gamma_C(t) := \left\{ \mathbf{x} \in \Gamma_C \,\middle|\, [\mathbf{u} \cdot \boldsymbol{\nu}]_{\boldsymbol{\phi}} = g \right\} \text{ q.e.} \tag{3.13}$$

or

$$\tilde{\Gamma}_C(t) := \left\{ \mathbf{x} \in \Gamma_C \,\middle|\, [\tilde{\mathbf{u}} \cdot \boldsymbol{\nu}]_{\boldsymbol{\phi}} = g \right\} \text{ q.e.} \tag{3.14}$$

for a perturbed solution $\tilde{\mathbf{u}}$.

The critical part of the actual contact boundaries means the set where the solution is in contact and the perturbed solution is not, or vice versa, see Figure 3.2.

Critical contact boundaries. The *critical contact boundaries* are given by the symmetric difference

$$\Gamma^*_C(t) := (\Gamma_C(t) \cup \tilde{\Gamma}_C(t)) \setminus (\Gamma_C(t) \cap \tilde{\Gamma}_C(t)) \tag{3.15}$$

for almost every $t \geq 0$. This set can equivalently be written as

$$\begin{aligned} \Gamma^*_C(t) = \Big\{ \mathbf{x} \in \Gamma_C \,\Big|\, & [\mathbf{u}(t) \cdot \boldsymbol{\nu}]_{\boldsymbol{\phi}} < g,\ [\tilde{\mathbf{u}}(t) \cdot \boldsymbol{\nu}]_{\boldsymbol{\phi}} = g \text{ or} \\ & [\mathbf{u}(t) \cdot \boldsymbol{\nu}]_{\boldsymbol{\phi}} = g,\ [\tilde{\mathbf{u}}(t) \cdot \boldsymbol{\nu}]_{\boldsymbol{\phi}} < g \Big\} \text{ q.e.} \end{aligned}$$

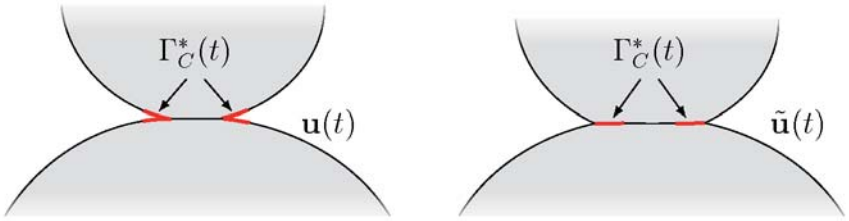

Figure 3.2.: Critical contact boundaries $\Gamma_C^*(t)$.

Localization of contact stresses. Using the preliminary definitions, the difference of the contact forces is intended to be written as an operator acting on the critical contact boundaries $\Gamma_C^*(t)$ only, i.e.,

$$\begin{aligned}&\int_0^t \langle \delta \mathbf{F}_{\mathrm{con}}(\mathbf{u}(s)), \delta\dot{\mathbf{u}}(s)\rangle_{(\mathbf{H}^1)^*(\Omega)\times\mathbf{H}^1(\Omega)}\, ds \\ &= \langle \delta\hat{\boldsymbol{\sigma}}^*(\mathbf{u},\dot{\mathbf{u}}), \delta\dot{\mathbf{u}}\rangle_{\mathbf{L}_2(0,t;(\mathbf{H}^{1/2})^*(\Gamma_C^*(s)))\times\mathbf{L}_2(0,t;\mathbf{H}^{1/2}(\Gamma_C^*(s)))}\end{aligned} \tag{3.16}$$

for all $t \geq 0$ with a functional $\delta\hat{\boldsymbol{\sigma}}^*(\mathbf{u},\dot{\mathbf{u}}) \in \mathbf{L}_2(0,t;(\mathbf{H}^{1/2})^*(\Gamma_C^*(s)))$. The proof of this representation is based on a trace theorem that generalizes the definition of the normal stresses. Several formulations of such a theorem can be found, e.g., in [7] and [49]. Under less strict assumptions, a generalized version of the theorem will be derived in Appendix B. Here, only a brief sketch how to validate (3.16) is given due to the technicality of the proof.

The first idea of the argumentation is the fact that the support of the contact forces is given by the union $\Gamma_C(t) \cup \tilde{\Gamma}_C(t)$ of the actual contact boundaries. This yields a representation of the contact forces via a functional in $\mathbf{L}_2(0,T;(\mathbf{H}^{1/2})^*(\Gamma_C(t) \cup \tilde{\Gamma}_C(t)))$. In a second step, the reduction of the contact forces onto the critical subset $\Gamma_C^*(t)$ is motivated in analogy to the persistency condition in Section 1.4: if it holds $[\delta\mathbf{u}(t)\cdot\boldsymbol{\nu}]_{\boldsymbol{\phi}} = 0$ on $\Gamma_C(t)\cap\tilde{\Gamma}_C(t)$, then even $[\delta\dot{\mathbf{u}}(t)\cdot\boldsymbol{\nu}]_{\boldsymbol{\phi}} = 0$ for almost every t. Under the additional regularity assumption $\operatorname{div}\boldsymbol{\sigma}(\mathbf{u},\dot{\mathbf{u}})$, $\operatorname{div}\boldsymbol{\sigma}(\tilde{\mathbf{u}},\dot{\tilde{\mathbf{u}}}) \in \mathbf{L}_2(0,T;\mathbf{L}_2(\Omega))$, the trace theorem mentioned above gives a representation of the contact forces in the form (3.16).

By means of the localization of the contact stresses, Lemma 3.2.1 can be reformulated in the following way.

Lemma 3.3.1. *Let* $\bar{\mathbf{u}} = (\mathbf{u},\dot{\mathbf{u}})$ *and* $\bar{\tilde{\mathbf{u}}} = (\tilde{\mathbf{u}},\dot{\tilde{\mathbf{u}}})$ *be two solutions of* (1.28) *with initial values* $\mathbf{u}(0) = \mathbf{u}_0$, $\dot{\mathbf{u}}(0) = \dot{\mathbf{u}}_0$ *and* $\tilde{\mathbf{u}}(0) = \tilde{\mathbf{u}}_0$, $\dot{\tilde{\mathbf{u}}}(0) = \dot{\tilde{\mathbf{u}}}_0$, *respectively. Furthermore, assume that* (3.16) *is valid. Then, for all* $t \in [0,T]$,

$$\begin{aligned} &\|\delta\bar{\mathbf{u}}(t)\|_E^2 + \int_0^t \|\delta\dot{\mathbf{u}}(s)\|_b^2 \, ds \\ &= \|\delta\bar{\mathbf{u}}_0\|_E^2 + \langle \delta\hat{\boldsymbol{\sigma}}^*(\mathbf{u},\dot{\mathbf{u}}), \delta\dot{\mathbf{u}} \rangle_{\mathbf{L}_2(0,t;(\mathbf{H}^{1/2})^*(\Gamma_C^*(s)))\times\mathbf{L}_2(0,t;\mathbf{H}^{1/2}(\Gamma_C^*(s)))} \,. \end{aligned} \tag{3.17}$$

Using this new representation of the integral term on the right-hand side, a variant of the original stability condition (3.8) on the contact stresses can be found.

Localized stability condition. Let

$$\|\delta\hat{\boldsymbol{\sigma}}^*(\mathbf{u},\dot{\mathbf{u}})\|_{\mathbf{L}_2(0,t;(\mathbf{H}^{1/2})^*(\Gamma_C^*(s)))} \le \varepsilon\big(\kappa\|\delta\mathbf{u}\|_{\mathbf{L}_2(0,t;\mathbf{H}^1(\Omega))} + \|\delta\dot{\mathbf{u}}\|_{\mathbf{L}_2(0,t;\mathbf{H}^1(\Omega))}\big) \tag{3.18}$$

hold for all $t \in [0,T]$ with $\varepsilon \ge 0$ sufficiently small and $\kappa \ge 0$.

In order to show that the stability condition (3.18) is reasonable, the special case of quasistatic contact problems in viscoelasticity will be discussed.

Quasistatic contact problems. This type of problems results from the dynamical contact problem (1.28) by setting

$$\ddot{\mathbf{u}} = 0 \,,$$

which yields the following problem formulation in the form of a variational inequality: for almost every $t \in [0,T]$, find $\mathbf{u}(\cdot,t) \in \mathcal{K}$ with $\mathbf{u}(\cdot,t) \in \mathbf{C}([0,T],\mathbf{H}^1)$ and $\dot{\mathbf{u}} \in \mathbf{L}_2(0,T;\mathbf{H}^1)$ such that

$$\langle \mathbf{F}(\mathbf{u}), \mathbf{v}-\mathbf{u}\rangle_{(\mathbf{H}^1)^*\times\mathbf{H}^1} + \langle \mathbf{G}(\dot{\mathbf{u}}), \mathbf{v}-\mathbf{u}\rangle_{(\mathbf{H}^1)^*\times\mathbf{H}^1} \ge 0 \,, \qquad \forall\, \mathbf{v} \in \mathbf{H}^1 \tag{3.19}$$

and

$$\mathbf{u}(0) = \mathbf{u}_0,\ \dot{\mathbf{u}}(0) = \dot{\mathbf{u}}_0 \,. \tag{3.20}$$

The corresponding contact forces $\mathbf{F}_{\mathrm{con}}(\mathbf{u}) \in (\mathbf{H}^1)^*$ are given by

$$\langle \mathbf{F}_{\mathrm{con}}(\mathbf{u}), \mathbf{v}\rangle_{(\mathbf{H}^1)^*\times\mathbf{H}^1} := \langle \mathbf{F}(\mathbf{u}), \mathbf{v}\rangle_{(\mathbf{H}^1)^*\times\mathbf{H}^1} + \langle \mathbf{G}(\dot{\mathbf{u}}), \mathbf{v}\rangle_{(\mathbf{H}^1)^*\times\mathbf{H}^1} \,, \qquad \mathbf{v} \in \mathbf{H}^1 \tag{3.21}$$

for almost every $t \in [0,T]$.

If the contact forces can be characterized as stresses on the active contact boundaries, i.e.,

$$\|\delta\mathbf{F}_{\mathrm{con}}(\mathbf{u})\|_{\mathbf{L}_2(0,t;(\mathbf{H}^1)^*(\Omega))} = \|\delta\hat{\boldsymbol{\sigma}}(\mathbf{u},\dot{\mathbf{u}})\|_{\mathbf{L}_2(0,t;(\mathbf{H}^{1/2})^*(\Gamma_C(s)\cup\tilde{\Gamma}_C(s)))}$$

for all $t \in [0,T]$, then the definition (3.21) of the contact forces and the continuity of the linearly viscoelastic forces, cf. (1.22) and (1.23), directly lead to

$$\begin{aligned} &\|\delta\hat{\boldsymbol{\sigma}}(\mathbf{u},\dot{\mathbf{u}})\|_{\mathbf{L}_2(0,t;(\mathbf{H}^{1/2})^*(\Gamma_C(s)\cup\tilde{\Gamma}_C(s)))} \\ &\le c\big(\|\delta\mathbf{F}(\mathbf{u})\|_{\mathbf{L}_2(0,t;(\mathbf{H}^1)^*(\Omega))} + \|\delta\mathbf{G}(\dot{\mathbf{u}})\|_{\mathbf{L}_2(0,t;(\mathbf{H}^1)^*(\Omega))}\big) \\ &\le c\big(\|\delta\mathbf{u}\|_{\mathbf{L}_2(0,t;\mathbf{H}^1(\Omega))} + \|\delta\dot{\mathbf{u}}\|_{\mathbf{L}_2(0,t;\mathbf{H}^1(\Omega))}\big) \,. \end{aligned}$$

Moreover, assume that

$$\|\delta\hat{\boldsymbol{\sigma}}^*(\mathbf{u},\dot{\mathbf{u}})\|_{\mathbf{L}_2(0,t;(\mathbf{H}^{1/2})^*(\Gamma_C^*(s)))} \leq \varepsilon \|\delta\hat{\boldsymbol{\sigma}}(\mathbf{u},\dot{\mathbf{u}})\|_{\mathbf{L}_2(0,t;(\mathbf{H}^{1/2})^*(\Gamma_C(s)\cup\tilde{\Gamma}_C(s)))}$$

is satisfied for all $t \in [0,T]$ with ε small. This yields the perturbation estimate

$$\|\delta\hat{\boldsymbol{\sigma}}^*(\mathbf{u},\dot{\mathbf{u}})\|_{\mathbf{L}_2(0,t;(\mathbf{H}^{1/2})^*(\Gamma_C^*(s)))} \leq \varepsilon\, c\big(\|\delta\mathbf{u}\|_{\mathbf{L}_2(0,t;\mathbf{H}^1(\Omega))} + \|\delta\dot{\mathbf{u}}\|_{\mathbf{L}_2(0,t;\mathbf{H}^1(\Omega))}\big)\,. \tag{3.22}$$

In the quasistatic case, the validity of the localized stability condition is found to be equivalent to the requirement that "ε is sufficiently small" for all $t \in [0,T]$. This condition corresponds to the intuition that, for small perturbations, the critical part of the actual contact boundaries is only a small part of the possible contact boundaries. The requirement is formulated for an integral over time, which cannot be referred to every single timepoint in general. Thus, the critical part of the actual contact boundaries only needs to be small for almost every timepoint, but points of exception may arise.

The characterization of a class of viscoelastic contact problems suggested above seems to be reasonable at least in the case of a small variation in the velocities. Thus, if the dynamical problem shows a behavior similar to the one of the quasistatic problem, continuous dependence on the initial data might be satisfied in the viscoelastic case.

3.4. Approximations of the Signorini Condition

In the last section of this chapter, two well-established approximations of the viscoelastic contact problem with the classical Signorini condition in displacements will be discussed, which have been suggested in the recent years.

Jarušek and Eck investigated dynamical contact problems with unilateral contact constraints formulated on the field of velocities instead of displacements (see, e.g., [43, 45] for solvability and the monograph [25]). This approach leads to a much simpler mathematical structure due to the monotonicity of the corresponding multivalued contact operator. Unfortunately, employing the Signorini contact conditions in velocities describes the physical behavior correctly only in a short period of time. Once the two bodies have lost contact, they will never regain it. Thus, the bodies can only get into contact if they touch each other already at initial time. The model of Jarušek and Eck is actually only applicable to the process of loosing contact, which is entirely improper for biomechanical modeling of, e.g., the motion of the human knee. However, a perturbation result in physical energy norm was proven [50], which gives the unique solvability of the dynamical contact problem with Signorini's condition in velocities. This leads to the conjecture that the stability condition is mainly necessary in the initial phase of finding contact.

Martins and Oden proposed the widely-used normal compliance condition of contact [72]. This model is based on a penalization of the exact Signorini condition in

displacements, which leads to a much simpler mathematical problem. The model assumes that the normal stresses on the contact boundaries only depend on the normal displacement field, which results in a relaxation of the non-penetration of mass. One of its main advantages is the higher regularity of the solutions in time [63]. Martins and Oden presented existence and uniqueness results for both linearly elastic and viscoelastic materials, but their proof of uniqueness unfortunately exhibits a fundamental error in the estimation of norms (they used a norm inequality in the wrong direction). The model of normal compliance was utilized in various papers, see, e.g., [14, 54, 60, 61] and the monograph [49]. However, for the medical applications in mind (such as the movement of the knee joint), a mutual interpenetration of the bodies is unacceptable, and normal compliance models are ruled out. Nevertheless, a perturbation result in physical energy norm was proven for this penalty approach [51], which leads to the uniqueness of the normal compliance problem for two viscoelastic bodies. The result further motivates the stability condition used in this section since the approximating penalty solution satisfies the assumption even in a sharper version.

4. Consistency – Bounded Variation

In this chapter, interest is focused on the consistency behavior of the classical Newmark method, the improved energy dissipative version due to Kane et al., the contact–stabilized Newmark method suggested by Deuflhard et al., and its improved variant in the presence of contact [53]. The results will have numerical consequences for the construction of an adaptive timestep control, which will be worked out in Chapter 6.

In the unconstrained situation, the symmetric Newmark scheme is equivalent to the Störmer-Verlet scheme, which is well-known to have consistency two (see, e.g., the textbook [33]). However, in the constrained situation, the question of consistency of Newmark methods has not been addressed up to now, neither in the engineering nor in the mathematical literature. The classical discretization error analysis would not supply any consistency at all because of the intrinsic discontinuities at contact interfaces.

The present chapter fills this gap by means of a novel proof technique. As a preparatory step, the stability of dynamical contact problems under perturbations of the initial data has been studied in Chapter 3. This has led to the idea about the physical energy norm in function space, which will be exploited for the following error analysis. In Section 4.1, all four variants of Newmark methods will be compared in detail in the method of time layers framework. Section 4.2 contains the main consistency result in physical energy norm. This estimate requires a regularity assumption on the solution and its derivatives, which is quite different from the classical approach. In Section 4.3, consistency results will be given in some norm of the local error in displacements only. Finally, in Section 4.4, the consistency error will be estimated in the special case of permanent active contact boundaries.

4.1. Newmark Methods in Function Space

As indicated in Chapter 2, this thesis uses the method of time layers, in which discretization is performed first in time and then in space. A crucial ingredient of this approach is the existence of a continuous counterpart of the implementable, space-discretized time integration scheme. Hence, in this section, focus is on the limit $h \to 0$ of the Newmark methods $(\text{N-CL})_h$, $(\text{N-CI})_h$, $(\text{N-CS})_h$, and $(\text{N-CS+})_h$,

which will be discussed in the following setting: let τ be a fixed temporal step size, $\mathbf{S}_H$ a fixed space discretization via finite elements, and $\mathbf{u}_H^n$, $\dot{\mathbf{u}}_H^n$ fixed initial values. Now, consider a family of quasi-uniform refinements $\mathbf{S}_h$ of $\mathbf{S}_H$ with $h \to 0$. The analysis will turn out that the solution $\mathbf{u}_{h,\mathrm{CL}}^{n+1}$ has a limit $\mathbf{u}_{\mathrm{CL}}^{n+1}$ and interestingly, $\mathbf{u}_{h,\mathrm{CI}}^{n+1}$ and $\mathbf{u}_{h,\mathrm{CS}(+)}^{n+1}$ possess a common limit, which will be called $\mathbf{u}_{\mathrm{CI/CS}(+)}^{n+1}$. This leads to only two numerical methods in function space, which will be called (N-CL) and (N-CI/CS(+)) in the following.

In a first step, the different predictor steps will be compared. Summarizing the predictors of all four methods and taking into account the initial values $\mathbf{u}_H^n$, $\dot{\mathbf{u}}_H^n$, gives

$$\begin{aligned}\mathbf{u}_{h,\mathrm{pred,CL/CI}}^{n+1} &= \mathbf{u}_H^n + \tau\dot{\mathbf{u}}_H^n \\ 0 \in \mathbf{u}_{h,\mathrm{pred,CS}(+)}^{n+1} &- \left(\mathbf{u}_H^n + \tau\dot{\mathbf{u}}_H^n\right) + \partial I_{\mathcal{K}_h}\left(\mathbf{u}_{h,\mathrm{pred,CS}(+)}^{n+1}\right),\end{aligned}$$

i.e., $(\text{N-CL})_h$ and $(\text{N-CI})_h$ have the same predictors, which remain constant as h tends to zero, while the predictor step of $(\text{N-CS}(+))_h$ contains a variational inclusion and changes, as h tends to zero, since $\mathcal{K}_h$ changes. This variational inclusion is necessarily defined after discretization in space via finite elements, since the normal trace of a $\mathbf{L}_2$-function is not evaluable in general. As noted in (2.13), the predictor step of $(\text{N-CS}(+))_h$ can equivalently be formulated as the $\mathbf{L}_2$-projection of the given finite element function $\mathbf{u}_H^n + \tau\dot{\mathbf{u}}_H^n$ onto the discrete admissible set $\mathcal{K}_h$. By definition (2.1), this set is related to the pointwise behavior of elements in $\mathbf{S}_h$ along the possible contact boundaries. Therefore, a modification of the classical predictor is mainly caused near the contact interfaces, while the nodes in the interior of the domain are changed only slightly.

Now, an important result concerning the predictor step of $(\text{N-CS}(+))_h$ in comparison to the one of $(\text{N-CL})_h$ and $(\text{N-CI})_h$ will be proven in the spatial limit $h \to 0$: the predictor $\mathbf{u}_{h,\mathrm{pred,CS}(+)}^{n+1}$ converges to $\mathbf{u}_{h,\mathrm{pred,CL/CI}}^{n+1}$ in $\mathbf{L}_2$. This is due to the fact that the contact boundaries have measure zero.

Lemma 4.1.1. *Consider $\mathbf{u}_H^n, \dot{\mathbf{u}}_H^n \in \mathbf{S}_H$ and a family of quasiuniform refinements $\mathbf{S}_h$ of $\mathbf{S}_H$. Then, the predictor $\mathbf{u}_{h,\mathrm{pred,CS}(+)}^{n+1}$ converges to $\mathbf{u}_{h,\mathrm{pred,CL/CI}}^{n+1}$ for $h \to 0$, i.e.,*

$$\lim_{h\to 0} \left\| \mathbf{u}_{h,\mathrm{pred,CS}(+)}^{n+1} - \mathbf{u}_{h,\mathrm{pred,CL/CI}}^{n+1} \right\|_{\mathbf{L}_2} = 0\,.$$

Proof. Due to the properties of the discrete $\mathbf{L}_2$-projection defined in (2.13),

$$\left\| \mathbf{u}_{h,\mathrm{pred,CS}(+)}^{n+1} - \mathbf{u}_H^n - \tau\dot{\mathbf{u}}_H^n \right\|_{\mathbf{L}_2} \leq \left\| \mathbf{v}_h - \mathbf{u}_H^n - \tau\dot{\mathbf{u}}_H^n \right\|_{\mathbf{L}_2}$$

for all admissible $\mathbf{v}_h \in \mathcal{K}_h$. Let $\mathbf{v}_h$ such that $\mathbf{v}_h = \mathbf{u}_H^n + \tau\dot{\mathbf{u}}_H^n$ at the nodes in the interior of the domain and $\mathbf{v}_h = \mathbf{u}_H^n$ at the nodes of the possible contact boundaries. This function is admissible due to the fact that non-penetration refers only to the

possible contact boundaries, compare (2.1). Denoting by S_h the small stripe of finite elements along the contact boundaries, $\mathbf{v}_h$ coincides with $\mathbf{u}_H^n + \tau\dot{\mathbf{u}}_H^n$ on $\Omega_h \setminus S_h$. This gives the estimate

$$\big\|\mathbf{u}_{h,\mathrm{pred,CS}(+)}^{n+1} - \mathbf{u}_H^n - \tau\dot{\mathbf{u}}_H^n\big\|_{\mathbf{L}_2} \le \big\|\tau\dot{\mathbf{u}}_H^n\big\|_{\mathbf{L}_2(S_h)}\,.$$

Applying the Hölder inequality with $\mathrm{meas}(S_h) = O(h)$ leads to

$$\tau\big\|\dot{\mathbf{u}}_H^n\big\|_{\mathbf{L}_2(S_h)} \le (\mathrm{meas}(S_h))^{\frac{1}{2}-\frac{1}{p}}\big\|\tau\dot{\mathbf{u}}_H^n\big\|_{\mathbf{L}_p(S_h)} \le Ch^{\frac{1}{2}-\frac{1}{p}}\big\|\tau\dot{\mathbf{u}}_H^n\big\|_{\mathbf{L}_p}$$

with the Lebesgue space $\mathbf{L}_p$ for $p > 2$ (see, e.g., [5, Theorem 2.14]). Since $\dot{\mathbf{u}}_H^n \in \mathbf{H}^1$ and $\mathbf{H}^1 \hookrightarrow \mathbf{L}_p$ for $p < \frac{2d}{d-2}$ with the space dimension $d = 2, 3$ (Sobolev embedding, cf., e.g., [5]), there exists a constant C independent of h such that

$$\big\|\mathbf{u}_{h,\mathrm{pred,CS}(+)}^{n+1} - \mathbf{u}_H^n - \tau\dot{\mathbf{u}}_H^n\big\|_{\mathbf{L}_2} \le Ch^{\frac{1}{2}-\frac{1}{p}}\big\|\tau\dot{\mathbf{u}}_H^n\big\|_{\mathbf{L}_p} \le Ch^{\frac{1}{2}-\frac{1}{p}} \longrightarrow 0$$

for $2 < p < \frac{2d}{d-2}$. Since $\mathbf{u}_{h,\mathrm{pred,CL/CI}}^{n+1} = \mathbf{u}_H^n + \tau\dot{\mathbf{u}}_H^n$ by definition, this yields the result of the proposition. □

As a next step, the aim is to prove that the difference between $(\text{N-CS}(+))_h$ and $(\text{N-CI})_h$ becomes smaller and smaller for $h \to 0$.

Lemma 4.1.2. *Consider $\mathbf{u}_H^n, \dot{\mathbf{u}}_H^n \in \mathbf{S}_H$ and a family of quasiuniform refinements $\mathbf{S}_h$ of $\mathbf{S}_H$. Then,*

$$\lim_{h\to 0}\big(\big\|\mathbf{u}_{h,\mathrm{CI}}^{n+1} - \mathbf{u}_{h,\mathrm{CS}(+)}^{n+1}\big\|_{\mathbf{H}^1} + \big\|\dot{\mathbf{u}}_{h,\mathrm{CI}}^{n+1} - \dot{\mathbf{u}}_{h,\mathrm{CS}(+)}^{n+1}\big\|_{\mathbf{L}_2}\big) = 0\,.$$

Proof. After discretization in space, the variational inclusions in the second line of (2.7), (2.11), and (2.17) can be written as the variational inequality, cf. (2.19),

$$\begin{aligned}
&\big(\mathbf{u}_h^{n+1}, \mathbf{u}_h^{n+1} - \mathbf{v}_h\big)_{\mathbf{L}_2} \\
&\le \big(\mathbf{u}_{h,\mathrm{pred}}^{n+1}, \mathbf{u}_h^{n+1} - \mathbf{v}_h\big)_{\mathbf{L}_2} \\
&\quad - \frac{1}{2}\tau^2\Big\langle \mathbf{F}^{1/2}\big(\mathbf{u}_h^n, \mathbf{u}_h^{n+1}\big) + \mathbf{G}\Big(\frac{\mathbf{u}_h^{n+1} - \mathbf{u}_h^n}{\tau}\Big), \mathbf{u}_h^{n+1} - \mathbf{v}_h\Big\rangle_{(\mathbf{H}^1)^*\times\mathbf{H}^1}\,, \qquad \forall\, \mathbf{v}_h \in \mathcal{K}_h\,,
\end{aligned}$$

where $\mathbf{u}_h^{n+1}$ denotes the algorithmic solutions of $(\text{N-CI})_h$, $(\text{N-CS})_h$, or $(\text{N-CS}+)_h$. Set $\mathbf{v}_h = \mathbf{u}_{h,\mathrm{CS}(+)}^{n+1}$ in the inequality for $\mathbf{u}_{h,\mathrm{CI}}^{n+1}$ and $\mathbf{v}_h = \mathbf{u}_{h,\mathrm{CI}}^{n+1}$ in the inequality for $\mathbf{u}_{h,\mathrm{CS}(+)}^{n+1}$. Then, adding both inequalities yields the estimate

$$\begin{aligned}
&\big\|\mathbf{u}_{h,\mathrm{CI}}^{n+1} - \mathbf{u}_{h,\mathrm{CS}(+)}^{n+1}\big\|_{\mathbf{L}_2}^2 + \frac{\tau^2}{4}\big\|\mathbf{u}_{h,\mathrm{CI}}^{n+1} - \mathbf{u}_{h,\mathrm{CS}(+)}^{n+1}\big\|_a^2 + \frac{\tau}{2}\big\|\mathbf{u}_{h,\mathrm{CI}}^{n+1} - \mathbf{u}_{h,\mathrm{CS}(+)}^{n+1}\big\|_b^2 \\
&\le \big(\mathbf{u}_{h,\mathrm{pred,CI}}^{n+1} - \mathbf{u}_{h,\mathrm{pred,CS}(+)}^{n+1}, \mathbf{u}_{h,\mathrm{CI}}^{n+1} - \mathbf{u}_{h,\mathrm{CS}(+)}^{n+1}\big)_{\mathbf{L}_2}\,.
\end{aligned}$$

The inequalities of Cauchy-Schwarz and Korn (A.1) lead to

$$\big\|\mathbf{u}_{h,\mathrm{CI}}^{n+1}-\mathbf{u}_{h,\mathrm{CS}(+)}^{n+1}\big\|_{\mathbf{H}^1}\leq C\big\|\mathbf{u}_{h,\mathrm{pred,CI}}^{n+1}-\mathbf{u}_{h,\mathrm{pred,CS}(+)}^{n+1}\big\|_{\mathbf{L}_2}$$

with a constant $C>0$ independent of h, and Lemma 4.1.1 gives

$$\begin{aligned}&\big\|\mathbf{u}_{h,\mathrm{CI}}^{n+1}-\mathbf{u}_{h,\mathrm{CS}(+)}^{n+1}\big\|_{\mathbf{H}^1}\\&\leq C\big(\big\|\mathbf{u}_{h,\mathrm{pred,CI}}^{n+1}-\mathbf{u}_H^n-\tau\dot{\mathbf{u}}_H^n\big\|_{\mathbf{L}_2}+\big\|\mathbf{u}_{h,\mathrm{pred,CS}(+)}^{n+1}-\mathbf{u}_H^n-\tau\dot{\mathbf{u}}_H^n\big\|_{\mathbf{L}_2}\big)\\&\quad\longrightarrow 0\,.\end{aligned}$$

In order to prove the corresponding result for the velocities, a simple calculation shows that for (N-CI)$_h$ and (N-CS)$_h$

$$\dot{\mathbf{u}}_{h,\mathrm{CI/CS}}^{n+1}=\dot{\mathbf{u}}_H^n+\frac{2}{\tau}\big(\mathbf{u}_{h,\mathrm{CI/CS}}^{n+1}-\mathbf{u}_{h,\mathrm{pred,CI/CS}}^{n+1}\big)$$

and for (N-CS+)

$$\dot{\mathbf{u}}_{h,\mathrm{CS+}}^{n+1}=\frac{1}{\tau}\big(\mathbf{u}_{h,\mathrm{pred,CI/CS}(+)}^{n+1}-\mathbf{u}_H^n\big)+\frac{2}{\tau}\big(\mathbf{u}_{h,\mathrm{CS+}}^{n+1}-\mathbf{u}_{h,\mathrm{pred,CS+})}^{n+1}\big)$$

in $\mathbf{L}_2$ such that

$$\lim_{h\to 0}\big\|\dot{\mathbf{u}}_{h,\mathrm{CI}}^{n+1}-\dot{\mathbf{u}}_{h,\mathrm{CS}(+)}^{n+1}\big\|_{\mathbf{L}_2}=\lim_{h\to 0}\frac{2}{\tau}\big\|\mathbf{u}_{h,\mathrm{CI}}^{n+1}-\mathbf{u}_{h,\mathrm{CS}(+)}^{n+1}\big\|_{\mathbf{L}_2}=0\,.$$

□

In order to present the main result of this section, the corresponding Newmark algorithms are formulated in function space. Naturally, these schemes are completely independent of any spatial discretization argument.

Classical Newmark method (N-CL).

$$\begin{aligned}&\mathbf{u}_{\mathrm{pred}}^{n+1}=\mathbf{u}^n+\tau\dot{\mathbf{u}}^n\\&0\in\mathbf{u}^{n+1}-\mathbf{u}_{\mathrm{pred}}^{n+1}+\frac{\tau^2}{2}\Big(\mathbf{F}^{1/2}\big(\mathbf{u}^n,\mathbf{u}^{n+1}\big)+\mathbf{G}\Big(\frac{\mathbf{u}^{n+1}-\mathbf{u}^n}{\tau}\Big)-\widetilde{\mathbf{F}}_{\mathrm{con}}^{1/2}\big(\mathbf{u}^n,\mathbf{u}^{n+1}\big)\Big)\\&\dot{\mathbf{u}}^{n+1}=\dot{\mathbf{u}}^n-\tau\Big(\mathbf{F}^{1/2}\big(\mathbf{u}^n,\mathbf{u}^{n+1}\big)+\mathbf{G}\Big(\frac{\mathbf{u}^{n+1}-\mathbf{u}^n}{\tau}\Big)-\mathbf{F}_{\mathrm{con}}^{1/2}\big(\mathbf{u}^n,\mathbf{u}^{n+1}\big)\Big)\end{aligned}\tag{4.1}$$

where the contact forces $\mathbf{F}_{\mathrm{con}}(\mathbf{u}^{n+1})$ are defined via

$$\begin{aligned}\frac{\tau^2}{2}\big\langle\mathbf{F}_{\mathrm{con}}(\mathbf{u}^{n+1}),\mathbf{v}\big\rangle_{(\mathbf{H}^1)^*\times\mathbf{H}^1}:=\Big\langle\mathbf{u}^{n+1}-\mathbf{u}_{\mathrm{pred}}^{n+1}+\frac{1}{2}\tau^2\Big(\mathbf{F}^{1/2}\big(\mathbf{u}^n,\mathbf{u}^{n+1}\big)\\+\mathbf{G}\Big(\frac{\mathbf{u}^{n+1}-\mathbf{u}^n}{\tau}\Big)\Big),\mathbf{v}\Big\rangle_{(\mathbf{H}^1)^*\times\mathbf{H}^1},\qquad\mathbf{v}\in\mathbf{H}^1\,.\end{aligned}\tag{4.2}$$

Due to Lemma 4.1.2, (N-CI)$_h$, (N-CS)$_h$, and (N-CS+)$_h$ correspond to the same method in function space:

Contact–implicit and (improved) contact–stabilized Newmark method (N-CI/CS(+)).

$$
\begin{aligned}
&\mathbf{u}_{\mathrm{pred}}^{n+1} = \mathbf{u}^n + \tau\dot{\mathbf{u}}^n \\
&0 \in \mathbf{u}^{n+1} - \mathbf{u}_{\mathrm{pred}}^{n+1} + \frac{1}{2}\tau^2\Big(\mathbf{F}^{1/2}\big(\mathbf{u}^n,\mathbf{u}^{n+1}\big) + \mathbf{G}\Big(\frac{\mathbf{u}^{n+1}-\mathbf{u}^n}{\tau}\Big) + \partial I_{\mathcal{K}}\big(\mathbf{u}^{n+1}\big)\Big) \\
&\dot{\mathbf{u}}^{n+1} = \dot{\mathbf{u}}^n - \tau\Big(\mathbf{F}^{1/2}\big(\mathbf{u}^n,\mathbf{u}^{n+1}\big) + \mathbf{G}\Big(\frac{\mathbf{u}^{n+1}-\mathbf{u}^n}{\tau}\Big) - \mathbf{F}_{\mathrm{con}}\big(\mathbf{u}^{n+1}\big)\Big)
\end{aligned}
\tag{4.3}
$$

with contact forces

$$
\begin{aligned}
\frac{\tau^2}{2}\big\langle \mathbf{F}_{\mathrm{con}}(\mathbf{u}^{n+1}),\mathbf{v}\big\rangle_{(\mathbf{H}^1)^*\times\mathbf{H}^1} := \Big\langle \mathbf{u}^{n+1} - \mathbf{u}_{\mathrm{pred}}^{n+1} + \frac{1}{2}\tau^2\Big(\mathbf{F}^{1/2}\big(\mathbf{u}^n,\mathbf{u}^{n+1}\big) \\
+\mathbf{G}\Big(\frac{\mathbf{u}^{n+1}-\mathbf{u}^n}{\tau}\Big)\Big),\mathbf{v}\Big\rangle_{(\mathbf{H}^1)^*\times\mathbf{H}^1}, \qquad \mathbf{v}\in\mathbf{H}^1\,.
\end{aligned}
\tag{4.4}
$$

The variational problems in the second line of (N-CL) and (N-CI/CS(+)) admit a unique solution [49]. Moreover, the variational inclusions can equivalently be formulated as the variational inequalities

$$
\big\langle \mathbf{F}_{\mathrm{con}}(\mathbf{u}^{n+1}),\mathbf{u}^{n+1}-\mathbf{v}\big\rangle_{(\mathbf{H}^1)^*\times\mathbf{H}^1} \le 0\,, \qquad \forall\,\mathbf{v}\in\mathcal{K}\,. \tag{4.5}
$$

Finally, assume that the closed convex set $\mathcal{K}\subset\mathbf{H}^1_D$ is approximated by the closed convex sets $\mathcal{K}_h\subset\mathbf{S}_h$ in the following way (compare [49, Remark 4.2.2]).

Assumption 4.1.3.

(i) $\forall\,\mathbf{v}\in\mathcal{K}$, $\exists\,\mathbf{v}_h\in\mathcal{K}_h$ such that $\|\mathbf{v}_h-\mathbf{v}\|_{\mathbf{H}^1}\to 0$ as $h\to 0$, and
(ii) for $\mathbf{w}_h\in\mathcal{K}_h$ "$\mathbf{w}_h\to\mathbf{w}$ weakly as $h\to 0$" implies $\mathbf{w}\in\mathcal{K}$

This leads to a convergence result concerning the spatial limit $h\to 0$ of the space-discretized Newmark schemes.

Theorem 4.1.4. *Let Assumption* 4.1.3 *hold. Then, the Newmark method* (N-CL)$_h$ *converges for* $h\to 0$ *to* (N-CL)*, i.e.,*

$$
\lim_{h\to 0}\big(\big\|\mathbf{u}_{h,\mathrm{CL}}^{n+1}-\mathbf{u}_{\mathrm{CL}}^{n+1}\big\|_{\mathbf{H}^1} + \big\|\dot{\mathbf{u}}_{h,\mathrm{CL}}^{n+1}-\dot{\mathbf{u}}_{\mathrm{CL}}^{n+1}\big\|_{\mathbf{L}_2}\big) = 0\,, \tag{4.6}
$$

and the Newmark methods (N-CI)$_h$, (N-CS)$_h$, *and* (N-CS+)$_h$ *converge for* $h\to 0$ *to the same limit* (N-CI/CS(+))*, i.e.,*

$$
\lim_{h\to 0}\big(\big\|\mathbf{u}_{h,\mathrm{CI}}^{n+1}-\mathbf{u}_{\mathrm{CI/CS(+)}}^{n+1}\big\|_{\mathbf{H}^1} + \big\|\dot{\mathbf{u}}_{h,\mathrm{CI}}^{n+1}-\dot{\mathbf{u}}_{\mathrm{CI/CS(+)}}^{n+1}\big\|_{\mathbf{L}_2}\big) = 0 \tag{4.7}
$$

and

$$
\lim_{h\to 0}\big(\big\|\mathbf{u}_{h,\mathrm{CS(+)}}^{n+1}-\mathbf{u}_{\mathrm{CI/CS(+)}}^{n+1}\big\|_{\mathbf{H}^1} + \big\|\dot{\mathbf{u}}_{h,\mathrm{CS(+)}}^{n+1}-\dot{\mathbf{u}}_{\mathrm{CI/CS(+)}}^{n+1}\big\|_{\mathbf{L}_2}\big) = 0\,. \tag{4.8}
$$

Proof. The second line of all four Newmark methods consists of an elliptic variational inequality. For $(\text{N-CL})_h$, this inequality is given by

$$\begin{aligned}
&\big(\mathbf{u}_h^{n+1} - \mathbf{u}_{h,\text{pred}}^{n+1}, \mathbf{v}_h - \mathbf{u}_h^{n+1}\big) + \frac{\tau^2}{2} a\Big(\frac{\mathbf{u}_h^n + \mathbf{u}_h^{n+1}}{2}, \mathbf{v}_h - \mathbf{u}_h^{n+1}\Big) \\
&+ \frac{\tau^2}{2} b\Big(\frac{\mathbf{u}_h^{n+1} - \mathbf{u}_h^n}{\tau}, \mathbf{v}_h - \mathbf{u}_h^{n+1}\Big) \\
&\geq \frac{\tau^2}{2} f_{\text{ext}}\big(\mathbf{v}_h - \mathbf{u}_h^{n+1}\big) + \frac{\tau^2}{2} \Big\langle \frac{1}{2} \widetilde{\mathbf{F}}_{\text{con}}\big(\mathbf{u}_h^n\big), \mathbf{v}_h - \mathbf{u}_h^{n+1} \Big\rangle_{(\mathbf{H}^1)^* \times \mathbf{H}^1}, \qquad \forall\, \mathbf{v}_h \in \mathcal{K}_h
\end{aligned}$$

while for $(\text{N-CI})_h$ and $(\text{N-CS}(+))_h$ the problem reads

$$\begin{aligned}
&\big(\mathbf{u}_h^{n+1} - \mathbf{u}_{h,\text{pred}}^{n+1}, \mathbf{v}_h - \mathbf{u}_h^{n+1}\big) + \frac{\tau^2}{2} a\Big(\frac{\mathbf{u}_h^n + \mathbf{u}_h^{n+1}}{2}, \mathbf{v}_h - \mathbf{u}_h^{n+1}\Big) \\
&+ \frac{\tau^2}{2} b\Big(\frac{\mathbf{u}_h^{n+1} - \mathbf{u}_h^n}{\tau}, \mathbf{v}_h - \mathbf{u}_h^{n+1}\Big) \\
&\geq \frac{\tau^2}{2} f_{\text{ext}}\big(\mathbf{v}_h - \mathbf{u}_h^{n+1}\big), \qquad \forall\, \mathbf{v}_h \in \mathcal{K}_h .
\end{aligned}$$

For all four Newmark methods, the bilinear forms on the left-hand side of the inequalities are continuous and elliptic on $\mathbf{H}_D^1$, while the right-hand side contains a bounded, linear functional on $\mathbf{H}_D^1$. Under the approximation assumptions made above, a convergence theory for $h \to 0$ is well-known for both minimization problems (cf. [49, Remark 4.2.2]). This theory yields that the solutions of all four Newmark schemes $(\text{N-CL})_h$, $(\text{N-CI})_h$, $(\text{N-CS})_h$, and $(\text{N-CS}+)_h$ converge to the solution of the corresponding scheme in function space for $h \to 0$. For $(\text{N-CL})_h$, this means that

$$\big\|\mathbf{u}_{h,\text{CL}}^{n+1} - \mathbf{u}_{\text{CL}}^{n+1}\big\|_{\mathbf{H}^1} \longrightarrow 0 \ \text{ for } h \to 0 .$$

In addition,

$$\dot{\mathbf{u}}_{h,\text{CL}}^{n+1} = -\dot{\mathbf{u}}_{h,\text{CL}}^{n} + \frac{2}{\tau}\big(\mathbf{u}_h^{n+1} - \dot{\mathbf{u}}_{h,\text{CL}}^{n}\big)$$

and

$$\dot{\mathbf{u}}_{\text{CL}}^{n+1} = -\dot{\mathbf{u}}_{\text{CL}}^{n} + \frac{2}{\tau}\big(\mathbf{u}^{n+1} - \dot{\mathbf{u}}_{\text{CL}}^{n}, \big)$$

yield

$$\big\|\dot{\mathbf{u}}_{h,\text{CL}}^{n+1} - \dot{\mathbf{u}}_{\text{CL}}^{n+1}\big\|_{\mathbf{L}_2} \longrightarrow 0 .$$

Concerning the spatial limit of $(\text{N-CI})_h$ and $(\text{N-CS}(+))_h$ for $h \to 0$, Lemma 4.1.2 shows that the limit of all three methods is equal. Since the limit of $(\text{N-CI})_h$ is given by the solution of (N-CI/CS(+)), the spatial limit of $(\text{N-CS}(+))_h$ is also identical to the solution of (N-CI/CS(+)), i.e.,

$$\big\|\mathbf{u}_{h,\text{CI}}^{n+1} - \mathbf{u}_{\text{CI/CS(+)}}^{n+1}\big\|_{\mathbf{H}^1} \longrightarrow 0 , \qquad \big\|\mathbf{u}_{h,\text{CS(+)}}^{n+1} - \mathbf{u}_{\text{CI/CS(+)}}^{n+1}\big\|_{\mathbf{H}^1} \longrightarrow 0 .$$

Following the same argumentation for the velocities as presented for (N-CL)$_h$ yields

$$\left\|\dot{\mathbf{u}}_{h,\mathrm{CI}}^{n+1} - \dot{\mathbf{u}}_{\mathrm{CI/CS(+)}}^{n+1}\right\|_{\mathbf{L}_2} \longrightarrow 0\,, \qquad \left\|\dot{\mathbf{u}}_{h,\mathrm{CS(+)}}^{n+1} - \dot{\mathbf{u}}_{\mathrm{CI/CS(+)}}^{n+1}\right\|_{\mathbf{L}_2} \longrightarrow 0\,.$$

□

In consequence of this result, the following analysis of consistency errors within the framework of the method of time layers only refers to (N-CL) and (N-CI/CS(+)).

Remark 4.1.5. (N-CL) and (N-CI/CS(+)) satisfy the relation

$$\frac{\mathbf{u}^{n+1} - \mathbf{u}^n}{\tau} = \frac{\dot{\mathbf{u}}^n + \dot{\mathbf{u}}^{n+1}}{2}\,.$$

Notations. For the proofs to follow, define the *discrete evolution operator*

$$\bar{\mathbf{\Psi}}^{t_{n+1},t_n} = \left(\mathbf{\Psi}^{t_{n+1},t_n}, \dot{\mathbf{\Psi}}^{t_{n+1},t_n}\right) : \mathbf{H}^1 \times \mathbf{L}_2 \longrightarrow \mathbf{H}^1 \times \mathbf{L}_2 \tag{4.9}$$

of (N-CL) and (N-CI/CS(+)) for $t_n, t_{n+1} \in \triangle_\tau$ via

$$\mathbf{u}^{n+1} = \mathbf{\Psi}^{t_{n+1},t_n}\left(\mathbf{u}^n, \dot{\mathbf{u}}^n\right), \qquad \dot{\mathbf{u}}^{n+1} = \dot{\mathbf{\Psi}}^{t_{n+1},t_n}\left(\mathbf{u}^n, \dot{\mathbf{u}}^n\right) \tag{4.10}$$

in analogy to the continuous problem. Furthermore, let

$$\boldsymbol{\epsilon}(t, \bar{\mathbf{u}}, \tau) = (\boldsymbol{\epsilon}(t, \mathbf{u}, \tau), \boldsymbol{\epsilon}(t, \dot{\mathbf{u}}, \tau)) \tag{4.11}$$

denote the *consistency error* with

$$\boldsymbol{\epsilon}(t, \mathbf{u}, \tau) := \mathbf{\Psi}^{t+\tau,t}\bar{\mathbf{u}}(t) - \mathbf{\Phi}^{t+\tau,t}\bar{\mathbf{u}}(t) \tag{4.12}$$

the *consistency error in position variables* and

$$\boldsymbol{\epsilon}(t, \dot{\mathbf{u}}, \tau) := \dot{\mathbf{\Psi}}^{t+\tau,t}\bar{\mathbf{u}}(t) - \dot{\mathbf{\Phi}}^{t+\tau,t}\bar{\mathbf{u}}(t) \tag{4.13}$$

the *consistency error in velocity variables*. For ease of presentation, the quantity

$$\tilde{\boldsymbol{\epsilon}}(s, \dot{\mathbf{u}}, \tau) := \frac{\mathbf{u}^{n+1} - \mathbf{u}^n}{\tau} - \dot{\mathbf{u}}(s)\,, \qquad s \in [t, t+\tau] \tag{4.14}$$

is introduced.

4.2. Consistency Error in Physical Energy Norm

This section contains the main consistency results, in the presence of contact, for the classical, the contact–implicit, and the (improved) contact–stabilized Newmark method. Within the physical energy norm suggested by the previous perturbation result in Chapter 3, an estimate for the local discretization error will be derived.

The presentation starts with the analysis of the discretization error for the Newmark scheme (N-CI/CS(+)), which afterwards will be transferred to the classical scheme (N-CL).

Lemma 4.2.1. *Assume that* $\ddot{\mathbf{u}}(\cdot,t)$, $\mathbf{F}_{\mathrm{con}}(\mathbf{u}(\cdot,t)) \in (\mathbf{H}^1)^*$ *for all* $t \in [0,T]$. *Then, for initial values* $\mathbf{u}^n = \mathbf{u}(t)$ *and* $\dot{\mathbf{u}}^n = \dot{\mathbf{u}}(t)$, *the local error* $\bar{\boldsymbol{\Psi}} - \bar{\boldsymbol{\Phi}} = (\boldsymbol{\Psi} - \boldsymbol{\Phi}, \dot{\boldsymbol{\Psi}} - \dot{\boldsymbol{\Phi}})$ *of* (N-CI/CS(+)) *satisfies*

$$
\begin{aligned}
&\big\|\bar{\boldsymbol{\Psi}}^{t+\tau,t}\bar{\mathbf{u}}(t) - \bar{\boldsymbol{\Phi}}^{t+\tau,t}\bar{\mathbf{u}}(t)\big\|_E^2 + \int_t^{t+\tau} \|\tilde{\boldsymbol{\epsilon}}(s,\dot{\mathbf{u}},\tau)\|_b^2\, ds \\
&- \big\langle \mathbf{F}_{\mathrm{con}}(\mathbf{u}^{n+1}) - \mathbf{F}_{\mathrm{con}}(\mathbf{u}(t+\tau)), \mathbf{u}^{n+1} - \mathbf{u}(t+\tau)\big\rangle_{(\mathbf{H}^1)^*\times\mathbf{H}^1} \\
&= \int_t^{t+\tau} a\Big(\mathbf{u}(s) - \frac{\mathbf{u}(t)+\mathbf{u}(t+\tau)}{2}, \tilde{\boldsymbol{\epsilon}}(s,\dot{\mathbf{u}},\tau)\Big)\, ds \\
&\quad - \int_t^{t+\tau} \langle \mathbf{F}_{\mathrm{con}}(\mathbf{u}(s)) - \mathbf{F}_{\mathrm{con}}(\mathbf{u}(t+\tau)), \tilde{\boldsymbol{\epsilon}}(s,\dot{\mathbf{u}},\tau)\rangle_{(\mathbf{H}^1)^*\times\mathbf{H}^1}\, ds \\
&\quad + \int_t^{t+\tau} \Big(1 - \frac{2(s-t)}{\tau}\Big) \langle \ddot{\mathbf{u}}(s) - \ddot{\mathbf{u}}(t+\tau), \tilde{\boldsymbol{\epsilon}}(t,\dot{\mathbf{u}},\tau)\rangle_{(\mathbf{H}^1)^*\times\mathbf{H}^1}\, ds\,.
\end{aligned}
\tag{4.15}
$$

Remark 4.2.2. If the active contact boundaries do not change during the time interval of interest, the result of the lemma above simplifies in the following manner. The term on the right-hand side of the estimate that is containing the contact forces can be written as

$$
\begin{aligned}
&- \int_t^{t+\tau} \langle \mathbf{F}_{\mathrm{con}}(\mathbf{u}(s)) - \mathbf{F}_{\mathrm{con}}(\mathbf{u}(t+\tau)), \tilde{\boldsymbol{\epsilon}}(s,\dot{\mathbf{u}},\tau)\rangle_{(\mathbf{H}^1)^*\times\mathbf{H}^1}\, ds \\
&= -\frac{1}{\tau} \int_t^{t+\tau} \big\langle \mathbf{F}_{\mathrm{con}}(\mathbf{u}(s)), \mathbf{u}^{n+1} - \mathbf{u}^n\big\rangle_{(\mathbf{H}^1)^*\times\mathbf{H}^1}\, ds \\
&\quad + \big\langle \mathbf{F}_{\mathrm{con}}(\mathbf{u}(t+\tau)), \mathbf{u}^{n+1} - \mathbf{u}(t+\tau)\big\rangle_{(\mathbf{H}^1)^*\times\mathbf{H}^1}
\end{aligned}
$$

due to the persistency condition (cf. Theorem 1.4.2). Under the assumption that $[(\mathbf{u}^{n+1} - \mathbf{u}^n)\cdot\boldsymbol{\nu}]_{\boldsymbol{\phi}} = g - g = 0$ on Γ_C, both $\mathbf{u}^{n+1} - \mathbf{u}^n \in \mathcal{K}$ and $-(\mathbf{u}^{n+1} - \mathbf{u}^n) \in \mathcal{K}$.

The same is valid for the difference $\mathbf{u}^{n+1} - \mathbf{u}(t+\tau)$ if $[(\mathbf{u}^{n+1} - \mathbf{u}(t+\tau)) \cdot \boldsymbol{\nu}]_{\boldsymbol{\phi}} = 0$ on Γ_C. Hence, the signs of the contact forces, cf. (1.31), yield the relation

$$\int_t^{t+\tau} \langle \mathbf{F}_{\mathrm{con}}(\mathbf{u}(s)) - \mathbf{F}_{\mathrm{con}}(\mathbf{u}(t+\tau)), \tilde{\boldsymbol{\epsilon}}(s, \dot{\mathbf{u}}, \tau) \rangle_{(\mathbf{H}^1)^* \times \mathbf{H}^1} \, ds = 0 \,.$$

This observation leads to the conjecture that, in the special case of permanent active contact, a much better consistency order can be proven. A detailed discussion of this problem will be presented in Section 4.4. The knowledge will become important for the construction of an adaptive timestep control for the improved contact–stabilized Newmark method in Chapter 6.

Proof. The local error of the velocities in $\mathbf{L}_2$-norm can be written as

$$\frac{1}{2} \big\| \dot{\mathbf{u}}^{n+1} - \dot{\mathbf{u}}(t+\tau) \big\|_{\mathbf{L}_2}^2 = \frac{1}{2} \Big\| \dot{\mathbf{u}}^n + \frac{2}{\tau} \big(\mathbf{u}^{n+1} - \mathbf{u}^n - \tau \dot{\mathbf{u}}^n \big) - \dot{\mathbf{u}}(t+\tau) \Big\|_{\mathbf{L}_2}^2 ,$$

cf. Remark 4.1.5. Since $\dot{\mathbf{u}} \in \mathbf{W}_2^1(0, T; \mathbf{H}^1, \mathbf{L}_2)$, integration by parts (see, e.g., [93, Proposition 23.23]) yields

$$\begin{aligned}
&\frac{1}{2} \big\| \dot{\mathbf{u}}^{n+1} - \dot{\mathbf{u}}(t+\tau) \big\|_{\mathbf{L}_2}^2 \\
&= \frac{1}{2} \Big\| \dot{\mathbf{u}}^n + \frac{2(s-t)}{\tau^2} \big(\mathbf{u}^{n+1} - \mathbf{u}^n - \tau \dot{\mathbf{u}}^n \big) - \dot{\mathbf{u}}(s) \Big\|_{\mathbf{L}_2}^2 \Big|_{s=t}^{s=t+\tau} \\
&= \int_t^{t+\tau} \Big\langle \frac{2}{\tau^2} \big(\mathbf{u}^{n+1} - \mathbf{u}^n - \tau \dot{\mathbf{u}}^n \big) - \ddot{\mathbf{u}}(s), \\
&\qquad\qquad \dot{\mathbf{u}}^n + \frac{2(s-t)}{\tau^2} \big(\mathbf{u}^{n+1} - \mathbf{u}^n - \tau \dot{\mathbf{u}}^n \big) - \dot{\mathbf{u}}(s) \Big\rangle_{(\mathbf{H}^1)^* \times \mathbf{H}^1} \, ds \,.
\end{aligned}$$

By means of

$$\begin{aligned}
&\dot{\mathbf{u}}^n + \frac{2(s-t)}{\tau^2} \big(\mathbf{u}^{n+1} - \mathbf{u}^n - \tau \dot{\mathbf{u}}^n \big) - \dot{\mathbf{u}}(s) \\
&= \frac{\mathbf{u}^{n+1} - \mathbf{u}^n}{\tau} - \Big(1 - \frac{2(s-t)}{\tau} \Big) \Big(\frac{\mathbf{u}^{n+1} - \mathbf{u}^n}{\tau} - \dot{\mathbf{u}}^n \Big) - \dot{\mathbf{u}}(s) \,,
\end{aligned}$$

the term on the right-hand side can be split up as

$$\begin{aligned}
&\frac{1}{2}\big\|\dot{\mathbf{u}}^{n+1}-\dot{\mathbf{u}}(t+\tau)\big\|_{\mathbf{L}_2}^2\\
&=\int_t^{t+\tau}\Big\langle\frac{2}{\tau^2}\big(\mathbf{u}^{n+1}-\mathbf{u}^n-\tau\dot{\mathbf{u}}^n\big)-\ddot{\mathbf{u}}(s),\frac{\mathbf{u}^{n+1}-\mathbf{u}^n}{\tau}-\dot{\mathbf{u}}(s)\Big\rangle_{(\mathbf{H}^1)^*\times\mathbf{H}^1}ds\\
&\quad+\int_t^{t+\tau}\Big(1-\frac{2(s-t)}{\tau}\Big)\Big\langle\ddot{\mathbf{u}}(s)-\frac{2}{\tau^2}\big(\mathbf{u}^{n+1}-\mathbf{u}^n-\tau\dot{\mathbf{u}}^n\big),\tilde{\boldsymbol{\epsilon}}(t,\dot{\mathbf{u}},\tau)\Big\rangle\,ds\,.
\end{aligned}$$

Inserting the definitions of the continuous and discrete contact forces (1.31) and (4.4) into the first term gives (due to the linearity of the external forces)

$$\begin{aligned}
&\frac{1}{2}\big\|\dot{\mathbf{u}}^{n+1}-\dot{\mathbf{u}}(t+\tau)\big\|_{\mathbf{L}_2}^2\\
&=-\int_t^{t+\tau}a\Big(\frac{\mathbf{u}^n+\mathbf{u}^{n+1}}{2}-\mathbf{u}(s),\frac{\mathbf{u}^{n+1}-\mathbf{u}^n}{\tau}-\dot{\mathbf{u}}(s)\Big)\,ds\\
&\quad-\int_t^{t+\tau}b\Big(\frac{\mathbf{u}^{n+1}-\mathbf{u}^n}{\tau}-\dot{\mathbf{u}}(s),\frac{\mathbf{u}^{n+1}-\mathbf{u}^n}{\tau}-\dot{\mathbf{u}}(s)\Big)\,ds\\
&\quad+\int_t^{t+\tau}\Big\langle\mathbf{F}_{\mathrm{con}}(\mathbf{u}^{n+1})-\mathbf{F}_{\mathrm{con}}(\mathbf{u}(s)),\frac{\mathbf{u}^{n+1}-\mathbf{u}^n}{\tau}-\dot{\mathbf{u}}(s)\Big\rangle_{(\mathbf{H}^1)^*\times\mathbf{H}^1}ds\\
&\quad+\int_t^{t+\tau}\Big(1-\frac{2(s-t)}{\tau}\Big)\Big\langle\ddot{\mathbf{u}}(s)-\frac{2}{\tau^2}\big(\mathbf{u}^{n+1}-\mathbf{u}^n-\tau\dot{\mathbf{u}}^n\big),\tilde{\boldsymbol{\epsilon}}(t,\dot{\mathbf{u}},\tau)\Big\rangle\,ds\,.
\end{aligned}\tag{4.16}$$

The first term representing the purely elastic material behavior can be reformulated by the fundamental theorem of calculus (cf. [94, Appendix, Application (25c)]) as

$$\begin{aligned}
&-\int_t^{t+\tau}a\Big(\frac{\mathbf{u}^n+\mathbf{u}^{n+1}}{2}-\mathbf{u}(s),\frac{\mathbf{u}^{n+1}-\mathbf{u}^n}{\tau}-\dot{\mathbf{u}}(s)\Big)\,ds\\
&=-\frac{1}{2}\int_t^{t+\tau}a\Big(\mathbf{u}^{n+1}-\mathbf{u}(t+\tau),\frac{\mathbf{u}^{n+1}-\mathbf{u}^n}{\tau}-\dot{\mathbf{u}}(s)\Big)\,ds\\
&\quad+\int_t^{t+\tau}a\Big(\mathbf{u}(s)-\frac{\mathbf{u}^n+\mathbf{u}(t+\tau)}{2},\frac{\mathbf{u}^{n+1}-\mathbf{u}^n}{\tau}-\dot{\mathbf{u}}(s)\Big)\,ds
\end{aligned}$$

$$= -\frac{1}{2}a\big(\mathbf{u}^{n+1} - \mathbf{u}(t+\tau), \mathbf{u}^{n+1} - \mathbf{u}(t+\tau)\big) + \int_t^{t+\tau} a\Big(\mathbf{u}(s) - \frac{\mathbf{u}(t)+\mathbf{u}(t+\tau)}{2}, \frac{\mathbf{u}^{n+1}-\mathbf{u}^n}{\tau} - \dot{\mathbf{u}}(s)\Big)\, ds\,.$$

The third term containing the contact forces can be written as

$$\begin{aligned}
&\int_t^{t+\tau} \Big\langle \mathbf{F}_{\mathrm{con}}(\mathbf{u}^{n+1}) - \mathbf{F}_{\mathrm{con}}(\mathbf{u}(s)), \frac{\mathbf{u}^{n+1}-\mathbf{u}^n}{\tau} - \dot{\mathbf{u}}(s)\Big\rangle_{(\mathbf{H}^1)^*\times\mathbf{H}^1} ds \\
&= \int_t^{t+\tau} \Big\langle \mathbf{F}_{\mathrm{con}}(\mathbf{u}(t+\tau)) - \mathbf{F}_{\mathrm{con}}(\mathbf{u}(s)), \frac{\mathbf{u}^{n+1}-\mathbf{u}^n}{\tau} - \dot{\mathbf{u}}(s)\Big\rangle_{(\mathbf{H}^1)^*\times\mathbf{H}^1} ds \\
&\quad + \big\langle \mathbf{F}_{\mathrm{con}}(\mathbf{u}^{n+1}) - \mathbf{F}_{\mathrm{con}}(\mathbf{u}(t+\tau)), \mathbf{u}^{n+1} - \mathbf{u}(t+\tau)\big\rangle_{(\mathbf{H}^1)^*\times\mathbf{H}^1}\,.
\end{aligned}$$

Summing up these expressions yields

$$\begin{aligned}
&\frac{1}{2}\|\epsilon(t,\dot{\mathbf{u}},\tau)\|_{\mathbf{L}_2}^2 + \frac{1}{2}\|\epsilon(t,\mathbf{u},\tau)\|_a^2 + \int_t^{t+\tau} \big\|\tilde{\boldsymbol{\epsilon}}(s,\dot{\mathbf{u}},\tau)\big\|_b^2\, ds \\
&- \big\langle \mathbf{F}_{\mathrm{con}}(\mathbf{u}^{n+1}) - \mathbf{F}_{\mathrm{con}}(\mathbf{u}(t+\tau)), \mathbf{u}^{n+1} - \mathbf{u}(t+\tau)\big\rangle_{(\mathbf{H}^1)^*\times\mathbf{H}^1} \\
&= \int_t^{t+\tau} a\Big(\mathbf{u}(s) - \frac{\mathbf{u}(t)+\mathbf{u}(t+\tau)}{2}, \tilde{\boldsymbol{\epsilon}}(s,\dot{\mathbf{u}},\tau)\Big)\, ds \\
&\quad - \int_t^{t+\tau} \langle \mathbf{F}_{\mathrm{con}}(\mathbf{u}(s)) - \mathbf{F}_{\mathrm{con}}(\mathbf{u}(t+\tau)), \tilde{\boldsymbol{\epsilon}}(s,\dot{\mathbf{u}},\tau)\rangle_{(\mathbf{H}^1)^*\times\mathbf{H}^1}\, ds \\
&\quad + \int_t^{t+\tau} \Big(1 - \frac{2(s-t)}{\tau}\Big)\Big\langle \ddot{\mathbf{u}}(s) - \frac{2}{\tau^2}\big(\mathbf{u}^{n+1} - \mathbf{u}^n - \tau\dot{\mathbf{u}}^n\big), \tilde{\boldsymbol{\epsilon}}(t,\dot{\mathbf{u}},\tau)\Big\rangle\, ds\,.
\end{aligned}$$

Due to

$$\int_t^{t+\tau} \Big(1 - \frac{2(s-t)}{\tau}\Big)\, ds = 0\,,$$

the constant term $\frac{2}{\tau^2}(\mathbf{u}^{n+1} - \mathbf{u}^n - \tau\dot{\mathbf{u}}^n)$ in the last line can be replaced by an arbitrary functional in $(\mathbf{H}^1)^*$ that is constant in time. Choosing $\ddot{\mathbf{u}}(t+\tau)$, the last term on the right-hand side can be reformulated as

$$\int_t^{t+\tau} \Big(1 - \frac{2(s-t)}{\tau}\Big) \Big\langle \ddot{\mathbf{u}}(s) - \frac{2}{\tau^2}\big(\mathbf{u}^{n+1} - \mathbf{u}^n - \tau\dot{\mathbf{u}}^n\big), \tilde{\boldsymbol{\epsilon}}(t, \dot{\mathbf{u}}, \tau)\Big\rangle_{(\mathbf{H}^1)^* \times \mathbf{H}^1} \, ds$$
$$= \int_t^{t+\tau} \Big(1 - \frac{2(s-t)}{\tau}\Big) \langle \ddot{\mathbf{u}}(s) - \ddot{\mathbf{u}}(t+\tau), \tilde{\boldsymbol{\epsilon}}(t, \dot{\mathbf{u}}, \tau)\rangle_{(\mathbf{H}^1)^* \times \mathbf{H}^1} \, ds \,.$$

□

Due to the admissibility of the continuous and discrete solutions $\mathbf{u}(t+\tau)$ and $\mathbf{u}^{n+1}$,

$$\big\langle \mathbf{F}_{\mathrm{con}}(\mathbf{u}^{n+1}) - \mathbf{F}_{\mathrm{con}}(\mathbf{u}(t+\tau)), \mathbf{u}^{n+1} - \mathbf{u}(t+\tau)\big\rangle_{(\mathbf{H}^1)^* \times \mathbf{H}^1} \leq 0 \tag{4.17}$$

holds, see (1.31) and (4.5). Hence, in a next step, this term on the left-hand side of equality (4.15) can be omitted. In order to derive consistency error estimates for the contact–implicit and the (improved) contact–stabilized scheme, the inequalities of Korn and Young will be exploited.

Lemma 4.2.3. *Assume that* $\ddot{\mathbf{u}}(\cdot,t)$, $\mathbf{F}_{\mathrm{con}}(\mathbf{u}(\cdot,t)) \in (\mathbf{H}^1)^*$ *for all* $t \in [0,T]$. *Then, for initial values* $\mathbf{u}^n = \mathbf{u}(t)$ *and* $\dot{\mathbf{u}}^n = \dot{\mathbf{u}}(t)$, *the local error* $\bar{\boldsymbol{\Psi}} - \bar{\boldsymbol{\Phi}} = (\boldsymbol{\Psi} - \boldsymbol{\Phi}, \dot{\boldsymbol{\Psi}} - \dot{\boldsymbol{\Phi}})$ *of* (N-CI/CS(+)) *satisfies*

$$\Big(\big\|\bar{\boldsymbol{\Psi}}^{t+\tau,t}\bar{\mathbf{u}}(t) - \bar{\boldsymbol{\Phi}}^{t+\tau,t}\bar{\mathbf{u}}(t)\big\|_E^2 + \int_t^{t+\tau} \|\tilde{\boldsymbol{\epsilon}}(s, \dot{\mathbf{u}}, \tau)\|_b^2 \, ds\Big)^{1/2}$$
$$\leq C\Big[\Big(\int_t^{t+\tau} \Big\|\mathbf{u}(s) - \frac{\mathbf{u}(t) + \mathbf{u}(t+\tau)}{2}\Big\|_{\mathbf{H}^1}^2 ds\Big)^{1/2}$$
$$+ \Big(\int_t^{t+\tau} \|\dot{\mathbf{u}}(s) - \dot{\mathbf{u}}(t)\|_{\mathbf{H}^1}^2 \, ds\Big)^{1/2} + \Big(\int_t^{t+\tau} \Big\|\dot{\mathbf{u}}(s) - \frac{\dot{\mathbf{u}}(t) + \dot{\mathbf{u}}(t+\tau)}{2}\Big\|_{\mathbf{H}^1}^2 ds\Big)^{1/2}$$
$$+ \Big(\int_t^{t+\tau} \|\ddot{\mathbf{u}}(s) - \ddot{\mathbf{u}}(t+\tau)\|_{(\mathbf{H}^1)^*}^2 \, ds\Big)^{1/2} \tag{4.18}$$
$$+ \Big(\int_t^{t+\tau} \|\mathbf{F}_{\mathrm{con}}(\mathbf{u}(s)) - \mathbf{F}_{\mathrm{con}}(\mathbf{u}(t+\tau))\|_{(\mathbf{H}^1)^*}^2 \, ds\Big)^{1/2}\Big] \,.$$

Proof. Omitting the term (4.17) on the left-hand side of (4.15) by positivity and splitting up the last term on the right-hand side leads to

$$
\begin{aligned}
&\big\|\bar{\boldsymbol{\Psi}}^{t+\tau,t}\bar{\mathbf{u}}(t)-\bar{\boldsymbol{\Phi}}^{t+\tau,t}\bar{\mathbf{u}}(t)\big\|_E^2+\int_t^{t+\tau}\|\tilde{\boldsymbol{\epsilon}}(s,\dot{\mathbf{u}},\tau)\|_b^2\,ds\\
&\leq\int_t^{t+\tau}a\Big(\mathbf{u}(s)-\frac{\mathbf{u}(t)+\mathbf{u}(t+\tau)}{2},\tilde{\boldsymbol{\epsilon}}(s,\dot{\mathbf{u}},\tau)\Big)\,ds\\
&\quad-\int_t^{t+\tau}\langle\mathbf{F}_{\mathrm{con}}(\mathbf{u}(s))-\mathbf{F}_{\mathrm{con}}(\mathbf{u}(t+\tau)),\tilde{\boldsymbol{\epsilon}}(s,\dot{\mathbf{u}},\tau)\rangle_{(\mathbf{H}^1)^*\times\mathbf{H}^1}\,ds\\
&\quad+\int_t^{t+\tau}\Big(1-\frac{2(s-t)}{\tau}\Big)\big\langle\ddot{\mathbf{u}}(s)-\ddot{\mathbf{u}}(t+\tau)),\tilde{\boldsymbol{\epsilon}}(s,\dot{\mathbf{u}},\tau)\big\rangle_{(\mathbf{H}^1)^*\times\mathbf{H}^1}\,ds\\
&\quad+\int_t^{t+\tau}\Big(1-\frac{2(s-t)}{\tau}\Big)\big\langle\ddot{\mathbf{u}}(s)-\ddot{\mathbf{u}}(t+\tau)),\dot{\mathbf{u}}(s)-\dot{\mathbf{u}}(t)\big\rangle_{(\mathbf{H}^1)^*\times\mathbf{H}^1}\,ds\,.
\end{aligned}
$$

After using the continuity of the bilinear forms a and b in $\mathbf{H}^1$, cf. (1.22) and (1.23), the inequality of Young is applied to find the estimate

$$
\begin{aligned}
&\Big(\big\|\bar{\boldsymbol{\Psi}}^{t+\tau,t}\bar{\mathbf{u}}(t)-\bar{\boldsymbol{\Phi}}^{t+\tau,t}\bar{\mathbf{u}}(t)\big\|_E^2+\int_t^{t+\tau}\|\tilde{\boldsymbol{\epsilon}}(s,\dot{\mathbf{u}},\tau)\|_b^2\,ds\Big)^{1/2}\\
&\leq C\Big[\Big(\int_t^{t+\tau}\Big\|\mathbf{u}(s)-\frac{\mathbf{u}(t)+\mathbf{u}(t+\tau)}{2}\Big\|_{\mathbf{H}^1}^2\,ds\Big)^{1/2}\\
&\qquad+\Big(\int_t^{t+\tau}\|\mathbf{F}_{\mathrm{con}}(\mathbf{u}(s))-\mathbf{F}_{\mathrm{con}}(\mathbf{u}(t+\tau))\|_{(\mathbf{H}^1)^*}^2\,ds\Big)^{1/2}\\
&\qquad+\Big(\int_t^{t+\tau}\|\ddot{\mathbf{u}}(s)-\ddot{\mathbf{u}}(t+\tau)\|_{(\mathbf{H}^1)^*}^2\,ds\Big)^{1/2}\Big]\cdot\Big(\int_t^{t+\tau}\|\tilde{\boldsymbol{\epsilon}}(s,\dot{\mathbf{u}},\tau)\|_{\mathbf{H}^1}^2\,ds\Big)^{1/2}\\
&\quad+C\Big(\int_t^{t+\tau}\|\ddot{\mathbf{u}}(s)-\ddot{\mathbf{u}}(t+\tau)\|_{(\mathbf{H}^1)^*}^2\,ds\Big)^{1/2}\Big(\int_t^{t+\tau}\|\dot{\mathbf{u}}(s)-\dot{\mathbf{u}}(t)\|_{\mathbf{H}^1}^2\,ds\Big)^{1/2}.
\end{aligned}
\tag{4.19}
$$

Due to the inequalities of Korn (A.1) and Cauchy-Schwarz and Remark 4.1.5, a simple calculation shows that

$$
\begin{aligned}
&\Big(\int_t^{t+\tau} \|\tilde{\boldsymbol{\epsilon}}(s,\dot{\mathbf{u}},\tau)\|_{\mathbf{H}^1}^2\, ds\Big)^{1/2} \\
&\leq C\Big(\int_t^{t+\tau} \|\tilde{\boldsymbol{\epsilon}}(s,\dot{\mathbf{u}},\tau)\|_b^2\, ds + \int_t^{t+\tau} \Big\|\dot{\mathbf{u}}(s) - \frac{\dot{\mathbf{u}}^n + \dot{\mathbf{u}}^{n+1}}{2}\Big\|_{\mathbf{L}_2}^2 ds\Big)^{1/2} \\
&\leq C\Big(\int_t^{t+\tau} \|\tilde{\boldsymbol{\epsilon}}(s,\dot{\mathbf{u}},\tau)\|_b^2\, ds + \frac{\tau}{4}\|\epsilon(t,\dot{\mathbf{u}},\tau)\|_{\mathbf{L}_2}^2\Big)^{1/2} \\
&\quad + C\Big(\int_t^{t+\tau} \Big\|\dot{\mathbf{u}}(s) - \frac{\dot{\mathbf{u}}(t) + \dot{\mathbf{u}}(t+\tau)}{2}\Big\|_{\mathbf{L}_2}^2 ds\Big)^{1/2}.
\end{aligned}
$$

Hence, (4.19) yields an inequality of the type

$$x \leq 2a \cdot x^{1/2} + b^2$$

where $a, b, x \geq 0$. Writing

$$\big(x^{1/2} - a\big)^2 \leq a^2 + b^2\,,$$

gives the inequality

$$\Big(\big\|\bar{\boldsymbol{\Psi}}^{t+\tau,t}\bar{\mathbf{u}}(t) - \bar{\boldsymbol{\Phi}}^{t+\tau,t}\bar{\mathbf{u}}(t)\big\|_E^2 + \int_t^{t+\tau} \|\tilde{\boldsymbol{\epsilon}}(s,\dot{\mathbf{u}},\tau)\|_b^2\, ds\Big)^{1/2} \leq a + \sqrt{a^2+b^2} \leq 2a + b\,.$$

The result of the lemma is obtained due to $cd \leq \frac{1}{2}(c^2 + d^2)$. □

Classical consistency theory. For the sake of comparison, the classical theory will be discussed in the following. There, the continuous solution is assumed to be k-times continuously differentiable with respect to time t. In order to obtain the highest possible consistency order, one would make the assumption that the velocities, the accelerations, and the contact forces satisfy

$$\dot{\mathbf{u}} \in \mathbf{C}^1\big([0,T],\mathbf{H}^1\big)\,, \qquad \ddot{\mathbf{u}} \in \mathbf{C}^1\big([0,T],(\mathbf{H}^1)^*\big)$$

and

$$\mathbf{F}_{\mathrm{con}}(\mathbf{u}) \in \mathbf{C}^1\big([0,T],(\mathbf{H}^1)^*\big)\,.$$

Inserting these regularity assumptions into the right-hand side of (4.18) would yield an error estimate of the kind

$$\|\bar{\boldsymbol{\Psi}} - \bar{\boldsymbol{\Phi}}\|_{\mathcal{E}(t,\tau)} = O\big(\tau^{3/2}\big)\,,$$

i.e., a consistency order 3/2. Upon applying standard techniques (as "Lady Windermere's Fan", [33]), one would lose one order of τ for convergence. Unfortunately, in the presence of contact, the velocities and accelerations are even not continuous. The assumption of boundedness of these quantities leads to an estimate of the form

$$\|\bar{\mathbf{\Psi}} - \bar{\mathbf{\Phi}}\|_{\mathcal{E}(t,\tau)} = O\big(\tau^{1/2}\big)\,, \tag{4.20}$$

i.e., to a consistency order $-1/2$. This, again upon applying standard techniques, would not yield any convergence. That is why a detailed discretization error analysis for the Newmark methods has been missing up to now. Obviously, a more advanced concept is required to treat this complex situation.

Bounded variation. Let $(\mathbf{V}; \|\cdot\|_{\mathbf{V}})$ be a Banach space. The *total variation* of a function $\mathbf{v} : [t_0, t] \to \mathbf{V}$ is defined as

$$\mathrm{TV}(\mathbf{v}, [t_0, t], \mathbf{V}) := \sup\Big\{ \sum_{j=1}^{n} \|\mathbf{v}(t_j) - \mathbf{v}(t_{j-1})\|_{\mathbf{V}} : a = t_0 < t_1 < \ldots < t = b \Big\},$$

i.e., as the supremum of the above differences taken over all partitions of $[t_0, t]$ into finitely many subintervals. As usual, $\mathbf{BV}([t_0, t], \mathbf{V})$ denotes the set of all functions from $[t_0, t]$ into $\mathbf{V}$ that have bounded variation, i.e., for which the property $\mathrm{TV}(\mathbf{v}, [t_0, t], \mathbf{V}) < \infty$ holds. Let $\mathbf{v} : [t_0, t] \to \mathbf{V}$ be a function of bounded variation. Note that $\mathrm{TV}(\mathbf{v}, [t_0, t], \mathbf{V})$ is only a seminorm on the linear space $\mathbf{BV}([t_0, t]; \mathbf{V})$, while the norm

$$\|\mathbf{v}\|_{\mathbf{BV}([t_0,t];\mathbf{V})} := \|\mathbf{v}(a)\|_{\mathbf{V}} + \mathrm{TV}(\mathbf{v}, [t_0, t], \mathbf{V})$$

makes $\mathbf{BV}([t_0, t]; \mathbf{V})$ complete. Moreover, the intriguing property

$$\mathrm{TV}(\mathbf{v}, [t_0, t_1], X) + \mathrm{TV}(\mathbf{v}, [t_1, t], X) = \mathrm{TV}(\mathbf{v}, [t_0, t], X)\,, \quad \text{for } t_0 < t_1 < t \tag{4.21}$$

holds for every function of bounded variation. This feature will become fundamental for the novel convergence theory presented in Chapter 5. Observe that the left- and right-hand limit exists at every $t \in [t_0, t]$. However, a function with bounded variation need not to be continuous. It can be shown that it is only continuous except at countable many points of $[t_0, t]$ (compare, e.g., [84] for these notations and results).

In the following, the considerations are restricted to dynamical contact problems where the following assumption holds.

Assumption 4.2.4.

$$\dot{\mathbf{u}} \in \mathbf{BV}\big([0, T], \mathbf{H}^1\big)\,, \qquad \ddot{\mathbf{u}} \in \mathbf{BV}\big([0, T], \big(\mathbf{H}^1\big)^*\big)$$

Since the displacements $\mathbf{u}(\cdot,t)$, $t\in[0,T]$ are absolutely continuous in $\mathbf{H}^1$, they are especially of bounded variation, i.e., $\mathbf{u}\in\mathbf{BV}([0,T],\mathbf{H}^1)$. By definition (1.31) of the contact forces, Assumption 4.2.4 leads to $\mathbf{F}_{\mathrm{con}}(\mathbf{u})\in\mathbf{BV}([0,T],(\mathbf{H}^1)^*)$. In particular, the velocities $\dot{\mathbf{u}}(\cdot,t)$, the accelerations $\ddot{\mathbf{u}}(\cdot,t)$ and the contact forces $\mathbf{F}_{\mathrm{con}}(\mathbf{u}(\cdot,t))$ have to be defined in $\mathbf{H}^1$ and $(\mathbf{H}^1)^*$, respectively, for every time $t\in[0,T]$. The assumption of bounded variation excludes the case of highly oscillatory functions in time.

In all of the following theorems, the term

$$\begin{aligned}R(\mathbf{u},[t,t+\tau]) := \mathrm{TV}\big(\mathbf{u},[t,t+\tau],\mathbf{H}^1\big)+\mathrm{TV}\big(\dot{\mathbf{u}},[t,t+\tau],\mathbf{H}^1\big)\\ +\mathrm{TV}\big(\ddot{\mathbf{u}},[t,t+\tau],\big(\mathbf{H}^1\big)^*\big)\end{aligned} \tag{4.22}$$

will arise.

Lemma 4.2.5. *Let Assumption* 4.2.4 *hold. Then, for initial values* $\mathbf{u}^n=\mathbf{u}(t)$ *and* $\dot{\mathbf{u}}^n=\dot{\mathbf{u}}(t)$*, the local error* $\bar{\boldsymbol{\Psi}}-\bar{\boldsymbol{\Phi}}=(\boldsymbol{\Psi}-\boldsymbol{\Phi},\dot{\boldsymbol{\Psi}}-\dot{\boldsymbol{\Phi}})$ *of* (N-CI/CS(+)) *satisfies*

$$\Big(\big\|\bar{\boldsymbol{\Psi}}^{t+\tau,t}\bar{\mathbf{u}}(t)-\bar{\boldsymbol{\Phi}}^{t+\tau,t}\bar{\mathbf{u}}(t)\big\|_E^2+\int_t^{t+\tau}\|\tilde{\boldsymbol{\epsilon}}(s,\dot{\mathbf{u}},\tau)\|_b^2\,ds\Big)^{1/2}=R(\mathbf{u},[t,t+\tau])\cdot O\big(\tau^{1/2}\big)\,.$$

Proof. The regularity assumptions on the solution lead to

$$\begin{aligned}&\Big(\big\|\bar{\boldsymbol{\Psi}}^{t+\tau,t}\bar{\mathbf{u}}(t)-\bar{\boldsymbol{\Phi}}^{t+\tau,t}\bar{\mathbf{u}}(t)\big\|_E^2+\int_t^{t+\tau}\|\tilde{\boldsymbol{\epsilon}}(s,\dot{\mathbf{u}},\tau)\|_b^2\,ds\Big)^{1/2}\\
&=\Big(\sup_{s\in[t,t+\tau]}\Big\|\mathbf{u}(s)-\frac{\mathbf{u}(t)+\mathbf{u}(t+\tau)}{2}\Big\|_{\mathbf{H}^1}+\sup_{s\in[t,t+\tau]}\|\dot{\mathbf{u}}(s)-\dot{\mathbf{u}}(t)\|_{\mathbf{H}^1}\\
&\quad+\sup_{s\in[t,t+\tau]}\|\dot{\mathbf{u}}(s)-\dot{\mathbf{u}}(t+\tau)\|_{\mathbf{H}^1}+\sup_{s\in[t,t+\tau]}\|\ddot{\mathbf{u}}(s)-\ddot{\mathbf{u}}(t+\tau)\|_{(\mathbf{H}^1)^*}\\
&\quad+\sup_{s\in[t,t+\tau]}\|\mathbf{F}_{\mathrm{con}}(\mathbf{u}(s))-\mathbf{F}_{\mathrm{con}}(\mathbf{u}(t+\tau))\|_{(\mathbf{H}^1)^*}\Big)\cdot O\big(\tau^{1/2}\big)\\
&=\big(\mathrm{TV}\big(\mathbf{u},[t,t+\tau],\mathbf{H}^1\big)+\mathrm{TV}\big(\dot{\mathbf{u}},[t,t+\tau],\mathbf{H}^1\big)\\
&\quad+\mathrm{TV}\big(\ddot{\mathbf{u}},[t,t+\tau],\big(\mathbf{H}^1\big)^*\big)+\mathrm{TV}\big(\mathbf{F}_{\mathrm{con}}(\mathbf{u}),[t,t+\tau],\big(\mathbf{H}^1\big)^*\big)\big)\cdot O\big(\tau^{1/2}\big)\,.\end{aligned}$$

□

At this point, the consistency error estimate in the lemma above is formulated within the usual kinetic and potential part of the physical energy norm, while the viscoelastic part is slightly modified [53]. In the following theorem, the result will be further improved to an estimate in the proper physical energy norm.

Theorem 4.2.6. *Let Assumption* 4.2.4 *hold. Then, for initial values* $\mathbf{u}^n=\mathbf{u}(t)$ *and* $\dot{\mathbf{u}}^n=\dot{\mathbf{u}}(t)$*, the local error* $\bar{\boldsymbol{\Psi}}-\bar{\boldsymbol{\Phi}}=(\boldsymbol{\Psi}-\boldsymbol{\Phi},\dot{\boldsymbol{\Psi}}-\dot{\boldsymbol{\Phi}})$ *of* (N-CI/CS(+)) *satisfies*

$$\|\bar{\boldsymbol{\Psi}}-\bar{\boldsymbol{\Phi}}\|_{\mathcal{E}(t,\tau)}=R(\mathbf{u},[t,t+\tau])\cdot O\big(\tau^{1/2}\big)\,. \tag{4.23}$$

Proof. In view of an estimate for the physical energy norm of the consistency error, the relation

$$\begin{aligned}\dot{\boldsymbol{\Psi}}^{t+s,t}\bar{\mathbf{u}}(t) - \dot{\boldsymbol{\Phi}}^{t+s,t}\bar{\mathbf{u}}(t) &= -\dot{\mathbf{u}}(t) + \frac{2}{s}\big(\boldsymbol{\Psi}^{t+s,t}\bar{\mathbf{u}}(t) - \mathbf{u}(t)\big) - \dot{\boldsymbol{\Phi}}^{t+s,t}\bar{\mathbf{u}}(t) \\ &= \big(\dot{\boldsymbol{\Phi}}^{t+s,t}\bar{\mathbf{u}}(t) - \dot{\mathbf{u}}(t)\big) + 2\Big(\frac{\boldsymbol{\Psi}^{t+s,t}\bar{\mathbf{u}}(t) - \mathbf{u}(t)}{s} - \dot{\boldsymbol{\Phi}}^{t+s,t}\bar{\mathbf{u}}(t)\Big)\,,\end{aligned}$$

cf. Remark 4.1.5, yields

$$\begin{aligned}&\Big(\int_t^{t+\tau} \big\|\dot{\boldsymbol{\Psi}}^{t+s,t}\bar{\mathbf{u}}(t) - \dot{\boldsymbol{\Phi}}^{t+s,t}\bar{\mathbf{u}}(t)\big\|_b^2\,ds\Big)^{1/2} \\ &\leq \Big(\int_t^{t+\tau} \big\|\dot{\boldsymbol{\Phi}}^{t+s,t}\bar{\mathbf{u}}(t) - \dot{\mathbf{u}}(t)\big\|_b^2\,ds\Big)^{1/2} \\ &\quad + 2\Big(\int_t^{t+\tau} \Big\|\frac{\boldsymbol{\Psi}^{t+s,t}\bar{\mathbf{u}}(t) - \mathbf{u}(t)}{s} - \dot{\boldsymbol{\Phi}}^{t+s,t}\bar{\mathbf{u}}(t)\Big\|_b^2\,ds\Big)^{1/2} \\ &= \Big(\mathrm{TV}\big(\dot{\mathbf{u}}, [t,t+\tau], \mathbf{H}^1\big) + \sup_{s\in[t,t+\tau]}\Big\|\frac{\boldsymbol{\Psi}^{t+s,t}\bar{\mathbf{u}}(t) - \mathbf{u}(t)}{s} - \dot{\boldsymbol{\Phi}}^{t+s,t}\bar{\mathbf{u}}(t)\Big\|_b\Big)\cdot O\big(\tau^{1/2}\big)\,.\end{aligned}$$

Concerning the second term in this estimate, Lemma 4.2.5 leads to

$$\begin{aligned}&\Big\|\frac{\boldsymbol{\Psi}^{t+\tau_0,t}\bar{\mathbf{u}}(t) - \mathbf{u}(t)}{\tau_0} - \dot{\boldsymbol{\Phi}}^{t+\tau_0,t}\bar{\mathbf{u}}(t)\Big\|_b \\ &= \Big(\int_t^{t+\tau_0} \Big\|\frac{\boldsymbol{\Psi}^{t+\tau_0,t}\bar{\mathbf{u}}(t) - \mathbf{u}(t)}{\tau_0} - \dot{\boldsymbol{\Phi}}^{t+\tau_0,t}\bar{\mathbf{u}}(t)\Big\|_b^2\,ds\Big)^{1/2}\cdot\tau_0^{-1/2} \\ &\leq \Big(\int_t^{t+\tau_0} \Big\|\frac{\boldsymbol{\Psi}^{t+\tau_0,t}\bar{\mathbf{u}}(t) - \mathbf{u}(t)}{\tau_0} - \dot{\boldsymbol{\Phi}}^{t+s,t}\bar{\mathbf{u}}(t)\Big\|_b^2\,ds\Big)^{1/2}\cdot\tau_0^{-1/2} \\ &\quad + \Big(\int_t^{t+\tau_0} \big\|\dot{\boldsymbol{\Phi}}^{t+s,t}\bar{\mathbf{u}}(t) - \dot{\boldsymbol{\Phi}}^{t+\tau_0,t}\bar{\mathbf{u}}(t)\big\|_b^2\,ds\Big)^{1/2}\cdot\tau_0^{-1/2} \\ &\leq C\cdot R(\mathbf{u}, [t,t+\tau_0]) + \mathrm{TV}\big(\dot{\mathbf{u}}, [t,t+\tau_0], \mathbf{H}^1\big)\end{aligned}$$

for all $\tau_0 > 0$, and choosing $\tau_0 = s$ for all $s \in [t, t+\tau]$ gives

$$\begin{aligned}
&\Big(\int_t^{t+\tau} \big\| \dot{\boldsymbol{\Psi}}^{t+s,t} \bar{\mathbf{u}}(t) - \dot{\boldsymbol{\Phi}}^{t+s,t} \bar{\mathbf{u}}(t) \big\|_b^2 \, ds \Big)^{1/2} \\
&= \Big(\mathrm{TV}\big(\dot{\mathbf{u}}, [t, t+\tau], \mathbf{H}^1\big) + \sup_{s \in [t,t+\tau]} \big(R(\mathbf{u}, [t, t+s]) + \mathrm{TV}\big(\dot{\mathbf{u}}, [t, t+s], \mathbf{H}^1\big) \big) \Big) \\
&\quad \cdot O\big(\tau^{1/2}\big) \\
&= R(\mathbf{u}, [t, t+\tau]) \cdot O\big(\tau^{1/2}\big) \, .
\end{aligned}$$

The desired result follows from combining this estimate with the one of Lemma 4.2.5. □

Finally, the consistency result for the contact–implicit or the (improved) contact–stabilized Newmark method will be transferred to the classical Newmark method. This algorithm utilizes in every timestep the contact forces from the step before. The following consistency theory is based on the assumption that the contact forces $\mathbf{F}_{\mathrm{con}}(\mathbf{u}^n)$ are identical to the contact forces $\mathbf{F}_{\mathrm{con}}(\mathbf{u}(t))$ of the variational inequality (1.28). This approach is reasonable in view of the novel convergence theory in Chapter 5, but too restrictive for a classical convergence theory. Moreover, the consistency result is not applicable for an adaptive stepsize control of (N-CL) in the way of Chapter 6.

Since the schemes (N-CL) and (N-CI/CS(+)) differ only in the treatment of the contact forces, the proofs above have to be modified only marginally under this assumption.

Theorem 4.2.7. *Let Assumption* 4.2.4 *hold. Then, for* $\mathbf{F}_{\mathrm{con}}(\mathbf{u}^n) - \mathbf{F}_{\mathrm{con}}(\mathbf{u}(t)) = 0$ *in* $(\mathbf{H}^1)^*$ *and initial values* $\mathbf{u}^n = \mathbf{u}(t)$ *and* $\dot{\mathbf{u}}^n = \dot{\mathbf{u}}(t)$*, the local error* $\bar{\boldsymbol{\Psi}} - \bar{\boldsymbol{\Phi}} = (\boldsymbol{\Psi} - \boldsymbol{\Phi}, \dot{\boldsymbol{\Psi}} - \dot{\boldsymbol{\Phi}})$ *of* (N-CL) *satisfies*

$$\|\bar{\boldsymbol{\Psi}} - \bar{\boldsymbol{\Phi}}\|_{\mathcal{E}(t,\tau)} = R(\mathbf{u}, [t, t+\tau]) \cdot O\big(\tau^{1/2}\big) \, . \tag{4.24}$$

Proof. Performing the same calculations as in the proof of Lemma 4.2.1, the contact forces $\mathbf{F}_{\mathrm{con}}(\mathbf{u}^{n+1})$ in expression (4.16) have to be replaced by $\frac{1}{2}(\mathbf{F}_{\mathrm{con}}(\mathbf{u}^n) + \mathbf{F}_{\mathrm{con}}(\mathbf{u}^{n+1}))$. Then,

$$\begin{aligned}
&- \int_t^{t+\tau} \Big\langle \mathbf{F}_{\mathrm{con}}(\mathbf{u}(s)) - \frac{\mathbf{F}_{\mathrm{con}}(\mathbf{u}^n) + \mathbf{F}_{\mathrm{con}}(\mathbf{u}^{n+1})}{2}, \frac{\mathbf{u}^{n+1} - \mathbf{u}^n}{\tau} - \dot{\mathbf{u}}(s) \Big\rangle_{(\mathbf{H}^1)^* \times \mathbf{H}^1} \, ds \\
&= - \int_t^{t+\tau} \Big\langle \mathbf{F}_{\mathrm{con}}(\mathbf{u}(s)) - \frac{\mathbf{F}_{\mathrm{con}}(\mathbf{u}(t)) + \mathbf{F}_{\mathrm{con}}(\mathbf{u}(t+\tau))}{2}, \frac{\mathbf{u}^{n+1} - \mathbf{u}^n}{\tau} - \dot{\mathbf{u}}(s) \Big\rangle_{(\mathbf{H}^1)^* \times \mathbf{H}^1} \, ds \\
&\quad + \frac{1}{2} \big\langle \mathbf{F}_{\mathrm{con}}(\mathbf{u}^{n+1}) - \mathbf{F}_{\mathrm{con}}(\mathbf{u}(t+\tau)), \mathbf{u}^{n+1} - \mathbf{u}(t+\tau) \big\rangle_{(\mathbf{H}^1)^* \times \mathbf{H}^1}
\end{aligned}$$

and the last term on the right-hand side is again non-positive. In analogy to Lemma 4.2.1, this yields

$$
\begin{aligned}
&\Big(\big\|\bar{\boldsymbol{\Psi}}^{t+\tau,t}\bar{\mathbf{u}}(t)-\bar{\boldsymbol{\Phi}}^{t+\tau,t}\bar{\mathbf{u}}(t)\big\|_E^2+\int_t^{t+\tau}\|\tilde{\boldsymbol{\epsilon}}(s,\dot{\mathbf{u}},\tau)\|_b^2\,ds\Big)^{1/2}\\
&-\frac{1}{2}\big\langle\mathbf{F}_{\mathrm{con}}(\mathbf{u}^{n+1})-\mathbf{F}_{\mathrm{con}}(\mathbf{u}(t+\tau)),\mathbf{u}^{n+1}-\mathbf{u}(t+\tau)\big\rangle_{(\mathbf{H}^1)^*\times\mathbf{H}^1}\\
&=\int_t^{t+\tau}a\Big(\mathbf{u}(s)-\frac{\mathbf{u}(t)+\mathbf{u}(t+\tau)}{2},\tilde{\boldsymbol{\epsilon}}(s,\dot{\mathbf{u}},\tau)\Big)\,ds\\
&\quad-\int_t^{t+\tau}\Big\langle\mathbf{F}_{\mathrm{con}}(\mathbf{u}(s))-\frac{\mathbf{F}_{\mathrm{con}}(\mathbf{u}(t))+\mathbf{F}_{\mathrm{con}}(\mathbf{u}(t+\tau))}{2},\tilde{\boldsymbol{\epsilon}}(s,\dot{\mathbf{u}},\tau)\Big\rangle_{(\mathbf{H}^1)^*\times\mathbf{H}^1}\,ds\\
&\quad+\int_t^{t+\tau}\Big(1-\frac{2(s-t)}{\tau}\Big)\langle\ddot{\mathbf{u}}(s)-\ddot{\mathbf{u}}(t+\tau),\tilde{\boldsymbol{\epsilon}}(t,\dot{\mathbf{u}},\tau)\rangle_{(\mathbf{H}^1)^*\times\mathbf{H}^1}\,ds\,.
\end{aligned}
$$

Applying the inequalities of Korn (A.1) and Young again, the corresponding result to Lemma 4.2.3 holds, namely

$$
\begin{aligned}
&\Big(\big\|\bar{\boldsymbol{\Psi}}^{t+\tau,t}\bar{\mathbf{u}}(t)-\bar{\boldsymbol{\Phi}}^{t+\tau,t}\bar{\mathbf{u}}(t)\big\|_E^2+\int_t^{t+\tau}\|\tilde{\boldsymbol{\epsilon}}(s,\dot{\mathbf{u}},\tau)\|_b^2\,ds\Big)^{1/2}\\
&\le C\Big[\Big(\int_t^{t+\tau}\Big\|\mathbf{u}(s)-\frac{\mathbf{u}(t)+\mathbf{u}(t+\tau)}{2}\Big\|_{\mathbf{H}^1}^2\,ds\Big)^{1/2}+\Big(\int_t^{t+\tau}\|\dot{\mathbf{u}}(s)-\dot{\mathbf{u}}(t)\|_{\mathbf{H}^1}^2\,ds\Big)^{1/2}\\
&\quad+\Big(\int_t^{t+\tau}\Big\|\dot{\mathbf{u}}(s)-\frac{\dot{\mathbf{u}}(t)+\dot{\mathbf{u}}(t+\tau)}{2}\Big\|_{\mathbf{H}^1}^2\,ds\Big)^{1/2}+\Big(\int_t^{t+\tau}\|\ddot{\mathbf{u}}(s)-\ddot{\mathbf{u}}(t+\tau)\|_{(\mathbf{H}^1)^*}^2\,ds\Big)^{1/2}\\
&\quad+\Big(\int_t^{t+\tau}\Big\|\mathbf{F}_{\mathrm{con}}(\mathbf{u}(s))-\frac{\mathbf{F}_{\mathrm{con}}(\mathbf{u}(t))+\mathbf{F}_{\mathrm{con}}(\mathbf{u}(t+\tau))}{2}\Big\|_{(\mathbf{H}^1)^*}^2\,ds\Big)^{1/2}\Big]\,.
\end{aligned}
$$

Finally, the total variations can be introduced in the same way as in the proof of Lemma 4.2.5, and the proof of Theorem 4.2.6 gives the estimate of the theorem. □

At first glance, the results above seem to be no progress beyond the mere boundedness condition of the classical consistency theory, see (4.20). In fact, the total variations on the right-hand side of the estimate do not contribute to any additional order in τ. However, due to the telescoping property (4.21), the terms $R(\mathbf{u},[t,t+\tau])$ on the right-hand side sum up to total variations over the whole time interval $[0,T]$. Hence,

global convergence of the improved contact–stabilized Newmark method (which is the algorithm of interest) will be shown in Chapter 5 without losing the order τ as in the classical theory.

In order to analyze the consistency and convergence of the displacements in $\mathbf{L}_2$-norm, a further (weaker) norm will be needed. In the next section, a norm will be presented, which will turn out to be a discrete norm (depending on τ).

4.3. Consistency Error in a Discrete Displacement Norm

In addition to the previous results concerning the local error of Newmark methods in the physical energy norm, here, a consistency result will be given in a discrete norm containing the displacements only.

Notation. For $\mathbf{v} \in \mathbf{H}^1$ and $\tau > 0$, the *discrete displacement norm* is denoted by

$$\|\mathbf{v}\|_\tau^2 := \|\mathbf{v}\|_{\mathbf{L}_2}^2 + \frac{\tau^2}{4}\|\mathbf{v}\|_a^2 + \frac{\tau}{2}\|\mathbf{v}\|_b^2 \,. \tag{4.25}$$

The proofs to follow are less complicated than the ones in Section 4.2, but based on similar principles. Again, the total variation of the continuous solution will show up. First, a result equivalent to the one of Lemma 4.2.1 will be presented, which gives a representation of the error in the considered norm.

Lemma 4.3.1. *Assume that* $\dot{\mathbf{u}}(\cdot,t) \in \mathbf{H}^1$ *and* $\ddot{\mathbf{u}}(\cdot,t)$, $\mathbf{F}_{\mathrm{con}}(\mathbf{u}(\cdot,t)) \in (\mathbf{H}^1)^*$ *for all* $t \in [0,T]$. *Then, for initial values* $\mathbf{u}^n = \mathbf{u}(t)$ *and* $\dot{\mathbf{u}}^n = \dot{\mathbf{u}}(t)$, *the local error of* (N-CI/CS(+)) *satisfies*

$$\begin{aligned}
&\|\boldsymbol{\epsilon}(t,\mathbf{u},\tau)\|_\tau^2 - \frac{\tau^2}{2}\big\langle \mathbf{F}_{\mathrm{con}}(\mathbf{u}^{n+1}) - \mathbf{F}_{\mathrm{con}}(\mathbf{u}(t+\tau)), \mathbf{u}^{n+1} - \mathbf{u}(t+\tau)\big\rangle_{(\mathbf{H}^1)^*\times\mathbf{H}^1} \\
&= -\int_t^{t+\tau}\Big(\int_t^s \langle \ddot{\mathbf{u}}(r) - \ddot{\mathbf{u}}(t+\tau), \boldsymbol{\epsilon}(t,\mathbf{u},\tau)\rangle_{(\mathbf{H}^1)^*\times\mathbf{H}^1}\, dr\Big)\, ds \\
&\quad + \frac{\tau^2}{4}a(\mathbf{u}(t+\tau) - \mathbf{u}(t), \boldsymbol{\epsilon}(t,\mathbf{u},\tau)) - \frac{\tau}{2}\int_t^{t+\tau} b(\dot{\mathbf{u}}(s) - \dot{\mathbf{u}}(t+\tau), \boldsymbol{\epsilon}(t,\mathbf{u},\tau))\, ds \,.
\end{aligned} \tag{4.26}$$

Proof. The consistency error of the positions in the $\mathbf{L}_2$-norm can be written as

$$
\begin{aligned}
&\left\|\mathbf{u}^{n+1} - \mathbf{u}(t+\tau)\right\|_{\mathbf{L}_2}^2 \\
&= \left(\mathbf{u}^n + \tau\dot{\mathbf{u}}^n - \mathbf{u}(t+\tau), \mathbf{u}^{n+1} - \mathbf{u}(t+\tau)\right)_{\mathbf{L}_2} \\
&\quad - \frac{\tau^2}{2} a\Big(\frac{\mathbf{u}^n + \mathbf{u}^{n+1}}{2}, \mathbf{u}^{n+1} - \mathbf{u}(t+\tau)\Big) - \frac{\tau^2}{2} b\Big(\frac{\mathbf{u}^{n+1} - \mathbf{u}^n}{\tau}, \mathbf{u}^{n+1} - \mathbf{u}(t+\tau)\Big) \\
&\quad + \frac{\tau^2}{2}\big\langle \mathbf{F}_{\mathrm{con}}(\mathbf{u}^{n+1}), \mathbf{u}^{n+1} - \mathbf{u}(t+\tau)\big\rangle_{(\mathbf{H}^1)^* \times \mathbf{H}^1} \\
&= \left(\mathbf{u}^n + \tau\dot{\mathbf{u}}^n - \mathbf{u}(t+\tau), \mathbf{u}^{n+1} - \mathbf{u}(t+\tau)\right)_{\mathbf{L}_2} \\
&\quad + \frac{\tau^2}{2}\big\langle \ddot{\mathbf{u}}(t+\tau), \mathbf{u}^{n+1} - \mathbf{u}(t+\tau)\big\rangle_{(\mathbf{H}^1)^* \times \mathbf{H}^1} \\
&\quad - \frac{\tau^2}{2} a\Big(\frac{\mathbf{u}^n + \mathbf{u}^{n+1}}{2} - \mathbf{u}(t+\tau), \mathbf{u}^{n+1} - \mathbf{u}(t+\tau)\Big) \\
&\quad - \frac{\tau^2}{2} b\Big(\frac{\mathbf{u}^{n+1} - \mathbf{u}^n}{\tau} - \dot{\mathbf{u}}(t+\tau), \mathbf{u}^{n+1} - \mathbf{u}(t+\tau)\Big) \\
&\quad + \frac{\tau^2}{2}\big\langle \mathbf{F}_{\mathrm{con}}(\mathbf{u}^{n+1}) - \mathbf{F}_{\mathrm{con}}(\mathbf{u}(t+\tau)), \mathbf{u}^{n+1} - \mathbf{u}(t+\tau)\big\rangle_{(\mathbf{H}^1)^* \times \mathbf{H}^1}
\end{aligned}
$$

which is equivalent to

$$
\begin{aligned}
&\|\boldsymbol{\epsilon}(t,\mathbf{u},\tau)\|_{\mathbf{L}_2}^2 + \frac{\tau^2}{4}\|\boldsymbol{\epsilon}(t,\mathbf{u},\tau)\|_a^2 + \frac{\tau}{2}\|\boldsymbol{\epsilon}(t,\mathbf{u},\tau)\|_b^2 \\
&- \frac{\tau^2}{2}\big\langle \mathbf{F}_{\mathrm{con}}(\mathbf{u}^{n+1}) - \mathbf{F}_{\mathrm{con}}(\mathbf{u}(t+\tau)), \mathbf{u}^{n+1} - \mathbf{u}(t+\tau)\big\rangle_{(\mathbf{H}^1)^* \times \mathbf{H}^1} \\
&= (\mathbf{u}(t) + \tau\dot{\mathbf{u}}(t) - \mathbf{u}(t+\tau), \boldsymbol{\epsilon}(t,\mathbf{u},\tau))_{\mathbf{L}_2} + \frac{\tau^2}{2}\langle \ddot{\mathbf{u}}(t+\tau), \boldsymbol{\epsilon}(t,\mathbf{u},\tau)\rangle_{(\mathbf{H}^1)^* \times \mathbf{H}^1} \\
&\quad - \frac{\tau^2}{4} a(\mathbf{u}(t) - \mathbf{u}(t+\tau), \boldsymbol{\epsilon}(t,\mathbf{u},\tau)) - \frac{\tau^2}{2} b\Big(\frac{\mathbf{u}(t+\tau) - \mathbf{u}(t)}{\tau} - \dot{\mathbf{u}}(t+\tau), \boldsymbol{\epsilon}(t,\mathbf{u},\tau))\Big)\,.
\end{aligned}
$$

Since $\dot{\mathbf{u}} \in \mathbf{W}_2^1(0,T;\mathbf{H}^1,\mathbf{L}_2)$, integration by parts (see, e.g., [93, Proposition 23.23]) can be used to write

$$
\begin{aligned}
&\|\boldsymbol{\epsilon}(t,\mathbf{u},\tau)\|_\tau^2 - \frac{\tau^2}{2}\big\langle \mathbf{F}_{\mathrm{con}}(\mathbf{u}^{n+1}) - \mathbf{F}_{\mathrm{con}}(\mathbf{u}(t+\tau)), \mathbf{u}^{n+1} - \mathbf{u}(t+\tau)\big\rangle_{(\mathbf{H}^1)^* \times \mathbf{H}^1} \\
&= -\int_t^{t+\tau} (\dot{\mathbf{u}}(s) - \dot{\mathbf{u}}(t), \boldsymbol{\epsilon}(t,\mathbf{u},\tau))_{\mathbf{L}_2}\, ds - \int_t^{t+\tau} (s-t)\langle \ddot{\mathbf{u}}(t+\tau), \boldsymbol{\epsilon}(t,\mathbf{u},\tau)\rangle_{(\mathbf{H}^1)^* \times \mathbf{H}^1}\, ds \\
&\quad - \frac{\tau^2}{4} a(\mathbf{u}(t) - \mathbf{u}(t+\tau), \boldsymbol{\epsilon}(t,\mathbf{u},\tau)) - \frac{\tau}{2}\int_t^{t+\tau} b(\dot{\mathbf{u}}(s) - \dot{\mathbf{u}}(t+\tau), \boldsymbol{\epsilon}(t,\mathbf{u},\tau))\, ds
\end{aligned}
$$

$$= -\int_t^{t+\tau} \Big(\int_t^s \langle \ddot{\mathbf{u}}(r) - \ddot{\mathbf{u}}(t+\tau), \boldsymbol{\epsilon}(t,\mathbf{u},\tau) \rangle_{(\mathbf{H}^1)^* \times \mathbf{H}^1} \, dr \Big) \, ds$$

$$- \frac{\tau^2}{4} a(\mathbf{u}(t) - \mathbf{u}(t+\tau), \boldsymbol{\epsilon}(t,\mathbf{u},\tau)) - \frac{\tau}{2} \int_t^{t+\tau} b(\dot{\mathbf{u}}(s) - \dot{\mathbf{u}}(t+\tau), \boldsymbol{\epsilon}(t,\mathbf{u},\tau)) \, ds \,.$$

□

Due to

$$\frac{\tau^2}{2} \big\langle \mathbf{F}_{\mathrm{con}}(\mathbf{u}^{n+1}) - \mathbf{F}_{\mathrm{con}}(\mathbf{u}(t+\tau)), \mathbf{u}^{n+1} - \mathbf{u}(t+\tau) \big\rangle_{(\mathbf{H}^1)^* \times \mathbf{H}^1} \leq 0 \,, \tag{4.27}$$

cf. (1.31) and (4.5), this term on the left-hand side of (4.26) can be omitted again. In order to find a suitable estimate for the right-hand side of the error representation, the same techniques can be used as those in the proof of Lemma 4.2.3.

Lemma 4.3.2. *Assume that* $\dot{\mathbf{u}}(\cdot,t) \in \mathbf{H}^1$ *and* $\ddot{\mathbf{u}}(\cdot,t), \mathbf{F}_{\mathrm{con}}(\mathbf{u}(\cdot,t)) \in (\mathbf{H}^1)^*$ *for all* $t \in [0,T]$. *Then, for initial values* $\mathbf{u}^n = \mathbf{u}(t)$ *and* $\dot{\mathbf{u}}^n = \dot{\mathbf{u}}(t)$, *the local error of* (N-CI/CS(+)) *satisfies*

$$\begin{aligned} \big\| \boldsymbol{\Psi}^{t+\tau,t} \bar{\mathbf{u}}(t) - \boldsymbol{\Phi}^{t+\tau,t} \bar{\mathbf{u}}(t) \big\|_\tau = & \int_t^{t+\tau} \Big(\int_t^s \|\ddot{\mathbf{u}}(r) - \ddot{\mathbf{u}}(t+\tau)\|_{(\mathbf{H}^1)^*} \, dr \Big) \, ds \cdot O\big(\tau^{-1/2}\big) \\ & + \|\mathbf{u}(t) - \mathbf{u}(t+\tau)\|_{\mathbf{H}^1} \cdot O\big(\tau^{3/2}\big) \\ & + \int_t^{t+\tau} \|\dot{\mathbf{u}}(s) - \dot{\mathbf{u}}(t+\tau)\|_{\mathbf{H}^1} \, ds \cdot O\big(\tau^{1/2}\big) \,. \end{aligned} \tag{4.28}$$

Proof. Omitting (4.27) and applying the continuity of the bilinear forms a and b in $\mathbf{H}^1$ to (4.26), cf. (1.22) and (1.23), gives the estimate

$$\begin{aligned} \|\boldsymbol{\epsilon}(t,\mathbf{u},\tau)\|_\tau^2 \leq & \Big(\int_t^{t+\tau} \Big(\int_t^s \|\ddot{\mathbf{u}}(r) - \ddot{\mathbf{u}}(t+\tau)\|_{(\mathbf{H}^1)^*} \, dr \Big) \, ds \Big) \|\boldsymbol{\epsilon}(t,\mathbf{u},\tau)\|_{\mathbf{H}^1} \\ & + \|\mathbf{u}(t) - \mathbf{u}(t+\tau)\|_{\mathbf{H}^1} \|\boldsymbol{\epsilon}(t,\mathbf{u},\tau)\|_{\mathbf{H}^1} \cdot O\big(\tau^2\big) \\ & + \Big(\int_t^{t+\tau} \|\dot{\mathbf{u}}(s) - \dot{\mathbf{u}}(t+\tau)\|_{\mathbf{H}^1} \, ds \Big) \|\boldsymbol{\epsilon}(t,\mathbf{u},\tau)\|_{\mathbf{H}^1} \cdot O(\tau) \,. \end{aligned}$$

After inserting the inequality of Korn (A.1) in the form

$$\|\boldsymbol{\epsilon}(t,\mathbf{u},\tau)\|_{\mathbf{H}^1}^2 \leq C \big(\|\boldsymbol{\epsilon}(t,\mathbf{u},\tau)\|_{\mathbf{L}_2}^2 + \|\boldsymbol{\epsilon}(t,\mathbf{u},\tau)\|_b^2 \big)$$

in this estimate, the whole inequality can be divided by the square root of the left-hand side. This yields the result of the theorem. □

In the presence of contact, the same assumption on the solution of (1.28) is made as in Section 4.2. This leads to an estimate for the consistency error, which uses the total variation of the continuous solution again.

Theorem 4.3.3. *Let Assumption* 4.2.4 *hold. Then, for initial values* $\mathbf{u}^n = \mathbf{u}(t)$ *and* $\dot{\mathbf{u}}^n = \dot{\mathbf{u}}(t)$*, the local error of* (N-CI/CS(+)) *satisfies*

$$\left\| \boldsymbol{\Psi}^{t+\tau,t} \bar{\mathbf{u}}(t) - \boldsymbol{\Phi}^{t+\tau,t} \bar{\mathbf{u}}(t) \right\|_\tau = R(\mathbf{u}, [t, t+\tau]) \cdot O\big(\tau^{3/2}\big) . \tag{4.29}$$

Proof. Due to the regularity assumption, expression (4.28) can be estimated via:

$$\begin{aligned}
&\left\| \boldsymbol{\Psi}^{t+\tau,t} \bar{\mathbf{u}}(t) - \boldsymbol{\Phi}^{t+\tau,t} \bar{\mathbf{u}}(t) \right\|_\tau \\
&= \Big(\sup_{s\in[t,t+\tau]} \|\ddot{\mathbf{u}}(s) - \ddot{\mathbf{u}}(t+\tau)\|_{(\mathbf{H}^1)^*} + \|\mathbf{u}(t) - \mathbf{u}(t+\tau)\|_{\mathbf{H}^1} \\
&\quad + \sup_{s\in[t,t+\tau]} \|\dot{\mathbf{u}}(s) - \dot{\mathbf{u}}(t+\tau)\|_{\mathbf{H}^1} \Big) \cdot O\big(\tau^{3/2}\big) \\
&= \big(\mathrm{TV}\big(\ddot{\mathbf{u}}, [t, t+\tau], \big(\mathbf{H}^1\big)^*\big) + \mathrm{TV}\big(\mathbf{u}, [t, t+\tau], \mathbf{H}^1\big) \\
&\quad + \mathrm{TV}\big(\dot{\mathbf{u}}, [t, t+\tau], \mathbf{H}^1\big) \big) \cdot O\big(\tau^{3/2}\big) .
\end{aligned}$$

□

Again, a corresponding consistency result for the classical Newmark method will be proven, as done in Theorem 4.2.7 for the physical energy norm.

Theorem 4.3.4. *Let Assumption* 4.2.4 *hold. Then, for* $\mathbf{F}_{\mathrm{con}}(\mathbf{u}^n) - \mathbf{F}_{\mathrm{con}}(\mathbf{u}(t)) = 0$ *in* $(\mathbf{H}^1)^*$ *and initial values* $\mathbf{u}^n = \mathbf{u}(t)$ *and* $\dot{\mathbf{u}}^n = \dot{\mathbf{u}}(t)$*, the local error of* (N-CL) *satisfies*

$$\left\| \boldsymbol{\Psi}^{t+\tau,t} \bar{\mathbf{u}}(t) - \boldsymbol{\Phi}^{t+\tau,t} \bar{\mathbf{u}}(t) \right\|_\tau = R(\mathbf{u}, [t, t+\tau]) \cdot O\big(\tau^{3/2}\big) . \tag{4.30}$$

Proof. Following the proof of Lemma 4.3.1 above, $\mathbf{F}_{\mathrm{con}}(\mathbf{u}^{n+1})$ has to be replaced by $\frac{1}{2}(\mathbf{F}_{\mathrm{con}}(\mathbf{u}^n) + \mathbf{F}_{\mathrm{con}}(\mathbf{u}^{n+1}))$, which yields

$$\begin{aligned}
&\|\boldsymbol{\epsilon}(t, \mathbf{u}, \tau)\|_\tau - \frac{\tau^2}{4} \big\langle \mathbf{F}_{\mathrm{con}}(\mathbf{u}^{n+1}) - \mathbf{F}_{\mathrm{con}}(\mathbf{u}(t+\tau)), \mathbf{u}^{n+1} - \mathbf{u}(t+\tau) \big\rangle_{(\mathbf{H}^1)^* \times \mathbf{H}^1} \\
&= - \int_t^{t+\tau} \Big(\int_t^s \langle \ddot{\mathbf{u}}(r) - \ddot{\mathbf{u}}(t+\tau), \boldsymbol{\epsilon}(t, \mathbf{u}, \tau) \rangle_{(\mathbf{H}^1)^* \times \mathbf{H}^1} \, dr \Big) \, ds \\
&\quad - \frac{\tau^2}{4} a(\mathbf{u}(t) - \mathbf{u}(t+\tau), \boldsymbol{\epsilon}(t, \mathbf{u}, \tau)) - \frac{\tau}{2} \int_t^{t+\tau} b(\dot{\mathbf{u}}(s) - \dot{\mathbf{u}}(t+\tau), \boldsymbol{\epsilon}(t, \mathbf{u}, \tau)) \, ds \\
&\quad + \frac{\tau^2}{4} \big\langle \mathbf{F}_{\mathrm{con}}(\mathbf{u}(t)) - \mathbf{F}_{\mathrm{con}}(\mathbf{u}(t+\tau)), \mathbf{u}^{n+1} - \mathbf{u}(t+\tau) \big\rangle_{(\mathbf{H}^1)^* \times \mathbf{H}^1} .
\end{aligned}$$

Compared to Lemma 4.3.2, an additional term including contact forces occurs on the right-hand side. Following the proof of Lemma 4.3.2 leads to

$$\begin{aligned}\left\|\boldsymbol{\Psi}^{t+\tau,t}\bar{\mathbf{u}}(t)-\boldsymbol{\Phi}^{t+\tau,t}\bar{\mathbf{u}}(t)\right\|_{\tau} = &\int_t^{t+\tau}\Big(\int_t^s \|\ddot{\mathbf{u}}(r)-\ddot{\mathbf{u}}(t+\tau)\|_{(\mathbf{H}^1)^*}\,dr\Big)\,ds\cdot O\big(\tau^{-1/2}\big)\\ &+\|\mathbf{u}(t)-\mathbf{u}(t+\tau)\|_{\mathbf{H}^1}\cdot O\big(\tau^{1/2}\big)\\ &+\int_t^{t+\tau}\|\dot{\mathbf{u}}(s)-\dot{\mathbf{u}}(t+\tau)\|_{\mathbf{H}^1}\,ds\cdot O\big(\tau^{3/2}\big)\\ &+\|\mathbf{F}_{\mathrm{con}}(\mathbf{u}(t))-\mathbf{F}_{\mathrm{con}}(\mathbf{u}(t+\tau))\|_{(\mathbf{H}^1)^*}\cdot O\big(\tau^{3/2}\big)\,.\end{aligned}$$

Introducing the total variations as in the proof of Theorem 4.3.3 gives the result of the theorem. □

Finally, the estimate for the displacements measured in a-norm can be improved by means of the inequality of Korn.

Corollary 4.3.5. *Let Assumption* 4.2.4 *hold. Then, for initial values* $\mathbf{u}^n=\mathbf{u}(t)$ *and* $\dot{\mathbf{u}}^n=\dot{\mathbf{u}}(t)$*, the local error of* (N-CI/CS(+)) *satisfies*

$$\left\|\boldsymbol{\Psi}^{t+\tau,t}\bar{\mathbf{u}}(t)-\boldsymbol{\Phi}^{t+\tau,t}\bar{\mathbf{u}}(t)\right\|_a = R(\mathbf{u},[t,t+\tau])\cdot O(\tau)\,. \tag{4.31}$$

For (N-CL)*, the same holds if in addition* $\mathbf{F}_{\mathrm{con}}(\mathbf{u}^n)-\mathbf{F}_{\mathrm{con}}(\mathbf{u}(t))=0$ *in* $(\mathbf{H}^1)^*$*.*

Proof. The inequality of Korn (A.1) yields

$$\begin{aligned}&\left\|\boldsymbol{\Psi}^{t+\tau,t}\bar{\mathbf{u}}(t)-\boldsymbol{\Phi}^{t+\tau,t}\bar{\mathbf{u}}(t)\right\|_{\mathbf{H}^1}\\ &\le C\Big(\left\|\boldsymbol{\Psi}^{t+\tau,t}\bar{\mathbf{u}}(t)-\boldsymbol{\Phi}^{t+\tau,t}\bar{\mathbf{u}}(t)\right\|_{\mathbf{L}_2}^2+\left\|\boldsymbol{\Psi}^{t+\tau,t}\bar{\mathbf{u}}(t)-\boldsymbol{\Phi}^{t+\tau,t}\bar{\mathbf{u}}(t)\right\|_b^2\Big)^{1/2}.\end{aligned}$$

Hence, due to Theorem 4.3.3 and Theorem 4.3.4,

$$\left\|\boldsymbol{\Psi}^{t+\tau,t}\bar{\mathbf{u}}(t)-\boldsymbol{\Phi}^{t+\tau,t}\bar{\mathbf{u}}(t)\right\|_{\mathbf{H}^1} = R(\mathbf{u},[t,t+\tau])\cdot O(\tau)\,.$$

The continuity of the bilinear form a in $\mathbf{H}^1$, cf. (1.22), gives the result of the corollary. □

4.4. Consistency Error for Permanent Active Contact

In the last part of this chapter, the local error behavior of the four Newmark methods under consideration will be studied in the presence of time-constant active contact

boundaries. As noted in Remark 4.2.2, in this case, the schemes are expected to provide an increased consistency order in comparison to the general free boundary problem.

For permanent active contact and under strict complementarity, the variational inequality (1.28) reduces to a linear parabolic equation with additional Dirichlet boundaries that are fixed over time. The smoother the initial and boundary values and the external forces of such a problem, the smoother are the solution and its derivatives in time and space (compare, e.g., [27, Chapter 7.1]). This effect justifies to perform the consistency error analysis of this section under optimal regularity conditions.

As in the case of time-dependent active contact boundaries, the local discretization error of the schemes will be investigated within the physical energy norm first. Afterwards, the corresponding consistency result in the discrete displacement norm will be presented.

Theorem 4.4.1. *Let* $[\mathbf{u}\cdot\boldsymbol{\nu}]_{\boldsymbol{\phi}} = g$ *on* $\Gamma_C \times [t, t+\tau]$. *Furthermore, assume that* $\ddot{\mathbf{u}} \in \mathbf{C}^2([t,t+\tau],\mathbf{L}_2) \cap \mathbf{C}^1([t,t+\tau],\mathbf{H}^1)$. *Then, for initial values* $\mathbf{u}^n = \mathbf{u}(t)$ *and* $\dot{\mathbf{u}}^n = \dot{\mathbf{u}}(t)$, *the local error* $\bar{\boldsymbol{\Psi}} - \bar{\boldsymbol{\Phi}} = (\boldsymbol{\Psi} - \boldsymbol{\Phi}, \dot{\boldsymbol{\Psi}} - \dot{\boldsymbol{\Phi}})$ *of* (N-CI/CS(+)) *satisfies*

$$\|\bar{\boldsymbol{\Psi}} - \bar{\boldsymbol{\Phi}}\|_{\mathcal{E}(t,\tau)} = O\big(\tau^3\big)\,. \tag{4.32}$$

For (N-CL), *the same estimate holds if in addition* $[\mathbf{u}^{n+1}\cdot\boldsymbol{\nu}]_{\boldsymbol{\phi}} = g$ *on* Γ_C *for all* τ.

Proof. In a first step, the scheme (N-CI/CS(+)) is considered. By means of the definitions of both the variational problem (1.31) and algorithm (4.3) and Remark 4.1.5, a short calculation leads to

$$\begin{aligned}
&\frac{1}{2}\|\boldsymbol{\epsilon}(t,\dot{\mathbf{u}},\tau)\|^2_{\mathbf{L}_2} + \frac{1}{2}\|\boldsymbol{\epsilon}(t,\mathbf{u},\tau)\|^2_a + \frac{\tau}{4}\|\boldsymbol{\epsilon}(t,\dot{\mathbf{u}},\tau)\|^2_b \\
&= \frac{1}{2}(\dot{\mathbf{u}}(t) - \dot{\mathbf{u}}(t+\tau), \boldsymbol{\epsilon}(t,\dot{\mathbf{u}},\tau))_{\mathbf{L}_2} \\
&\quad - \frac{\tau}{2}a\Big(\frac{\mathbf{u}(t)+\mathbf{u}^{n+1}}{2}, \boldsymbol{\epsilon}(t,\dot{\mathbf{u}},\tau)\Big) + \frac{1}{2}a(\boldsymbol{\epsilon}(t,\mathbf{u},\tau), \boldsymbol{\epsilon}(t,\mathbf{u},\tau)) \\
&\quad - \frac{\tau}{2}b\Big(\frac{\dot{\mathbf{u}}(t)+\dot{\mathbf{u}}(t+\tau)}{2}, \boldsymbol{\epsilon}(t,\dot{\mathbf{u}},\tau)\Big) + \frac{\tau}{2}\big\langle \mathbf{F}_{\mathrm{con}}(\mathbf{u}^{n+1}), \boldsymbol{\epsilon}(t,\dot{\mathbf{u}},\tau)\big\rangle_{(\mathbf{H}^1)^*\times\mathbf{H}^1} \\
&= \frac{1}{2}\Big(\dot{\mathbf{u}}(t) + \tau\frac{\ddot{\mathbf{u}}(t)+\ddot{\mathbf{u}}(t+\tau)}{2} - \dot{\mathbf{u}}(t+\tau), \boldsymbol{\epsilon}(t,\dot{\mathbf{u}},\tau)\Big)_{\mathbf{L}_2} \\
&\quad + \frac{1}{2}a(\boldsymbol{\epsilon}(t,\mathbf{u},\tau), \boldsymbol{\epsilon}(t,\mathbf{u},\tau) - \frac{\tau}{2}\boldsymbol{\epsilon}(t,\dot{\mathbf{u}},\tau)) \\
&\quad + \frac{\tau}{2}\Big\langle \mathbf{F}_{\mathrm{con}}(\mathbf{u}^{n+1}) - \frac{1}{2}(\mathbf{F}_{\mathrm{con}}(\mathbf{u}(t)) + \mathbf{F}_{\mathrm{con}}(\mathbf{u}(t+\tau))), \boldsymbol{\epsilon}(t,\dot{\mathbf{u}},\tau)\Big\rangle_{(\mathbf{H}^1)^*\times\mathbf{H}^1}\,.
\end{aligned}$$

Using the relation

$$\begin{aligned}\boldsymbol{\epsilon}(t,\mathbf{u},\tau) &= \mathbf{u}^n + \tau\frac{\dot{\mathbf{u}}(t)+\dot{\mathbf{u}}^{n+1}}{2} - \mathbf{u}(t+\tau)\\ &= \frac{\tau}{2}\boldsymbol{\epsilon}(t,\dot{\mathbf{u}},\tau) + \mathbf{u}(t) + \tau\frac{\dot{\mathbf{u}}(t)+\dot{\mathbf{u}}(t+\tau)}{2} - \mathbf{u}(t+\tau)\,,\end{aligned}$$

cf. Remark 4.1.5, the error representation can equivalently be written as

$$\begin{aligned}&\frac{1}{2}\|\boldsymbol{\epsilon}(t,\dot{\mathbf{u}},\tau)\|^2_{\mathbf{L}_2} + \frac{1}{2}\|\boldsymbol{\epsilon}(t,\mathbf{u},\tau)\|^2_a + \frac{\tau}{4}\|\boldsymbol{\epsilon}(t,\dot{\mathbf{u}},\tau)\|^2_b\\ &= \frac{1}{2}\Big(\dot{\mathbf{u}}(t) + \tau\frac{\ddot{\mathbf{u}}(t)+\ddot{\mathbf{u}}(t+\tau)}{2} - \dot{\mathbf{u}}(t+\tau), \boldsymbol{\epsilon}(t,\dot{\mathbf{u}},\tau)\Big)_{\mathbf{L}_2}\\ &\quad + \frac{\tau}{4}a\Big(\mathbf{u}(t) + \tau\frac{\dot{\mathbf{u}}(t)+\dot{\mathbf{u}}(t+\tau)}{2} - \mathbf{u}(t+\tau), \boldsymbol{\epsilon}(t,\dot{\mathbf{u}},\tau)\Big)\\ &\quad + \frac{1}{2}\Big\|\mathbf{u}(t) + \tau\frac{\dot{\mathbf{u}}(t)+\dot{\mathbf{u}}(t+\tau)}{2} - \mathbf{u}(t+\tau)\Big\|^2_a\\ &\quad - \frac{\tau}{2}\Big\langle \mathbf{F}_{\mathrm{con}}(\mathbf{u}^{n+1}) - \frac{1}{2}(\mathbf{F}_{\mathrm{con}}(\mathbf{u}(t)) + \mathbf{F}_{\mathrm{con}}(\mathbf{u}(t+\tau))), \dot{\mathbf{u}}(t)+\dot{\mathbf{u}}(t+\tau)\Big\rangle_{(\mathbf{H}^1)^*\times\mathbf{H}^1}\\ &\quad + \frac{1}{2}\big\langle \mathbf{F}_{\mathrm{con}}(\mathbf{u}^{n+1}) - \mathbf{F}_{\mathrm{con}}(\mathbf{u}(t+\tau)), \mathbf{u}(t+\tau) - \mathbf{u}(t)\big\rangle_{(\mathbf{H}^1)^*\times\mathbf{H}^1}\\ &\quad + \frac{1}{2}\big\langle \mathbf{F}_{\mathrm{con}}(\mathbf{u}^{n+1}) - \mathbf{F}_{\mathrm{con}}(\mathbf{u}(t+\tau)), \mathbf{u}^{n+1} - \mathbf{u}(t+\tau)\big\rangle_{(\mathbf{H}^1)^*\times\mathbf{H}^1}\\ &\quad + \frac{1}{2}\big\langle \mathbf{F}_{\mathrm{con}}(\mathbf{u}^{n+1}) - \mathbf{F}_{\mathrm{con}}(\mathbf{u}(t)), \mathbf{u}^{n+1} - \mathbf{u}(t)\big\rangle_{(\mathbf{H}^1)^*\times\mathbf{H}^1}\,.\end{aligned} \tag{4.33}$$

The last two terms in this expression are less or equal to zero because of the sign of the contact forces, cf. (1.31) and (4.5). Moreover, the assumption $[(\mathbf{u}(t+\tau)-\mathbf{u}(t))\cdot\boldsymbol{\nu}]_{\boldsymbol{\phi}} = 0$ on Γ_C leads to $\mathbf{u}(t+\tau)-\mathbf{u}(t)\in\mathcal{K}$ and $-(\mathbf{u}(t+\tau)-\mathbf{u}(t))\in\mathcal{K}$. Hence,

$$\big\langle \mathbf{F}_{\mathrm{con}}(\mathbf{u}^{n+1}) - \mathbf{F}_{\mathrm{con}}(\mathbf{u}(t+\tau)), \mathbf{u}(t+\tau) - \mathbf{u}(t)\big\rangle_{(\mathbf{H}^1)^*\times\mathbf{H}^1} = 0$$

due to (1.31) and (4.5). In addition, a similar argument yields

$$\begin{aligned}&\Big\langle \mathbf{F}_{\mathrm{con}}(\mathbf{u}^{n+1}) - \frac{1}{2}(\mathbf{F}_{\mathrm{con}}(\mathbf{u}(t)) + \mathbf{F}_{\mathrm{con}}(\mathbf{u}(t+\tau))), \dot{\mathbf{u}}(t)\Big\rangle_{(\mathbf{H}^1)^*\times\mathbf{H}^1}\\ &= \lim_{h\to 0}\Big\langle \mathbf{F}_{\mathrm{con}}(\mathbf{u}^{n+1}) - \frac{1}{2}(\mathbf{F}_{\mathrm{con}}(\mathbf{u}(t)) + \mathbf{F}_{\mathrm{con}}(\mathbf{u}(t+\tau))), \frac{\mathbf{u}(t+h)-\mathbf{u}(t)}{h}\Big\rangle_{(\mathbf{H}^1)^*\times\mathbf{H}^1}\\ &= 0\end{aligned}$$

and

$$\begin{aligned}
&\Big\langle \mathbf{F}_{\mathrm{con}}(\mathbf{u}^{n+1}) - \frac{1}{2}(\mathbf{F}_{\mathrm{con}}(\mathbf{u}(t)) + \mathbf{F}_{\mathrm{con}}(\mathbf{u}(t+\tau))), \dot{\mathbf{u}}(t+\tau) \Big\rangle_{(\mathbf{H}^1)^* \times \mathbf{H}^1} \\
&= \lim_{h \to 0} \Big\langle \mathbf{F}_{\mathrm{con}}(\mathbf{u}^{n+1}) \\
&\qquad -\frac{1}{2}(\mathbf{F}_{\mathrm{con}}(\mathbf{u}(t)) + \mathbf{F}_{\mathrm{con}}(\mathbf{u}(t+\tau))), \frac{\mathbf{u}(t+\tau) - \mathbf{u}(t+\tau-h)}{-h} \Big\rangle_{(\mathbf{H}^1)^* \times \mathbf{H}^1} \\
&= 0\,.
\end{aligned}$$

Summing up these relations leads to

$$\begin{aligned}
&\frac{1}{2}\|\boldsymbol{\epsilon}(t, \dot{\mathbf{u}}, \tau)\|_{\mathbf{L}_2}^2 + \frac{1}{2}\|\boldsymbol{\epsilon}(t, \mathbf{u}, \tau)\|_a^2 + \frac{\tau}{4}\|\boldsymbol{\epsilon}(t, \dot{\mathbf{u}}, \tau)\|_b^2 \\
&\leq \frac{1}{2}\Big(\dot{\mathbf{u}}(t) + \tau\frac{\ddot{\mathbf{u}}(t) + \ddot{\mathbf{u}}(t+\tau)}{2} - \dot{\mathbf{u}}(t+\tau), \boldsymbol{\epsilon}(t, \dot{\mathbf{u}}, \tau)\Big)_{\mathbf{L}_2} \\
&\quad + \frac{\tau}{4} a\Big(\mathbf{u}(t) + \tau\frac{\dot{\mathbf{u}}(t) + \dot{\mathbf{u}}(t+\tau)}{2} - \mathbf{u}(t+\tau), \boldsymbol{\epsilon}(t, \dot{\mathbf{u}}, \tau)\Big) \\
&\quad + \frac{1}{2}\Big\|\mathbf{u}(t) + \tau\frac{\dot{\mathbf{u}}(t) + \dot{\mathbf{u}}(t+\tau)}{2} - \mathbf{u}(t+\tau)\Big\|_a^2,
\end{aligned}$$

which can be further estimated to

$$\begin{aligned}
&\frac{1}{2}\|\boldsymbol{\epsilon}(t, \dot{\mathbf{u}}, \tau)\|_{\mathbf{L}_2}^2 + \frac{1}{2}\|\boldsymbol{\epsilon}(t, \mathbf{u}, \tau)\|_a^2 + \frac{\tau}{4}\|\boldsymbol{\epsilon}(t, \dot{\mathbf{u}}, \tau)\|_b^2 \\
&\leq \frac{1}{2}\Big\|\dot{\mathbf{u}}(t) + \tau\frac{\ddot{\mathbf{u}}(t) + \ddot{\mathbf{u}}(t+\tau)}{2} - \dot{\mathbf{u}}(t+\tau)\Big\|_{\mathbf{L}_2} \|\boldsymbol{\epsilon}(t, \dot{\mathbf{u}}, \tau)\|_{\mathbf{L}_2} \\
&\quad + C\Big(\tau\Big\|\mathbf{u}(t) + \tau\frac{\dot{\mathbf{u}}(t) + \dot{\mathbf{u}}(t+\tau)}{2} - \mathbf{u}(t+\tau)\Big\|_{\mathbf{H}^1} \|\boldsymbol{\epsilon}(t, \dot{\mathbf{u}}, \tau)\|_{\mathbf{H}^1} \\
&\qquad + \Big\|\mathbf{u}(t) + \tau\frac{\dot{\mathbf{u}}(t) + \dot{\mathbf{u}}(t+\tau)}{2} - \mathbf{u}(t+\tau)\Big\|_{\mathbf{H}^1}^2\Big)
\end{aligned}$$

by the continuity of the bilinear form a in $\mathbf{H}^1$, cf. (1.22). Inserting the inequality of Korn (A.1) combined with (1.5) in the form

$$\|\boldsymbol{\epsilon}(t, \dot{\mathbf{u}}, \tau))\|_{\mathbf{H}^1}^2 \leq \frac{1}{c_K}\big(\|\boldsymbol{\epsilon}(t, \dot{\mathbf{u}}, \tau))\|_{\mathbf{L}_2}^2 + \frac{1}{V_0}\|\boldsymbol{\epsilon}(t, \dot{\mathbf{u}}, \tau))\|_b^2\big)$$

into this estimate results in an inequality of the type

$$x \leq 2a \cdot x^{1/2} + b^2$$

with $a, b, x \geq 0$, which is equivalent to

$$\big(x^{1/2} - a\big)^2 \leq a^2 + b^2\,.$$

Thus,

$$x^{1/2} \le a + \sqrt{a^2+b^2} \le 2a + b\,,$$

and this gives the inequality

$$\begin{aligned}
&\Big(\frac{1}{2}\|\boldsymbol{\epsilon}(t,\dot{\mathbf{u}},\tau)\|_{\mathbf{L}_2}^2 + \frac{1}{2}\|\boldsymbol{\epsilon}(t,\mathbf{u},\tau)\|_a^2 + \frac{\tau}{4}\|\boldsymbol{\epsilon}(t,\dot{\mathbf{u}},\tau)\|_b^2\Big)^{1/2}\\
&\le C\Big(\Big\|\dot{\mathbf{u}}(t) + \tau\frac{\ddot{\mathbf{u}}(t)+\ddot{\mathbf{u}}(t+\tau)}{2} - \dot{\mathbf{u}}(t+\tau)\Big\|_{\mathbf{L}_2}\\
&\qquad + \Big\|\mathbf{u}(t) + \tau\frac{\dot{\mathbf{u}}(t)+\dot{\mathbf{u}}(t+\tau)}{2} - \mathbf{u}(t+\tau)\Big\|_{\mathbf{H}^1}\Big)\,.
\end{aligned}$$

Since the trapezoidal rule is of order 2 under the regularity assumptions of the theorem (cf., e.g., [18]),

$$\Big(\frac{1}{2}\|\boldsymbol{\epsilon}(t,\dot{\mathbf{u}},\tau)\|_{\mathbf{L}_2}^2 + \frac{1}{2}\|\boldsymbol{\epsilon}(t,\mathbf{u},\tau)\|_a^2 + \frac{\tau}{4}\|\boldsymbol{\epsilon}(t,\dot{\mathbf{u}},\tau)\|_b^2\Big)^{1/2} = O\big(\tau^3\big)$$

holds. In particular,

$$\|\boldsymbol{\epsilon}(t,\dot{\mathbf{u}},\tau_0)\|_b = O\big(\tau_0^{5/2}\big)$$

for arbitrary $\tau_0 > 0$, and setting $\tau_0 = s$ for $s \in [t, t+\tau]$ leads to

$$\Big(\int_t^{t+\tau} \|\boldsymbol{\epsilon}(t,\dot{\mathbf{u}},s)\|_b^2\,ds\Big)^{1/2} = O\big(\tau^3\big)\,.$$

This yields the result of the theorem for (N-CI/CS(+)).

For (N-CL), definition (2.3) causes a modification of relation (4.33) in the form

$$\begin{aligned}
&\frac{1}{2}\|\boldsymbol{\epsilon}(t,\dot{\mathbf{u}},\tau)\|_{\mathbf{L}_2}^2 + \frac{1}{2}\|\boldsymbol{\epsilon}(t,\mathbf{u},\tau)\|_a^2 + \frac{\tau}{4}\|\boldsymbol{\epsilon}(t,\dot{\mathbf{u}},\tau)\|_b^2\\
&= \frac{1}{2}\Big(\dot{\mathbf{u}}(t) + \tau\frac{\ddot{\mathbf{u}}(t)+\ddot{\mathbf{u}}(t+\tau)}{2} - \dot{\mathbf{u}}(t+\tau), \boldsymbol{\epsilon}(t,\dot{\mathbf{u}},\tau)\Big)_{\mathbf{L}_2}\\
&\quad + \frac{\tau}{4}a\Big(\mathbf{u}(t) + \tau\frac{\dot{\mathbf{u}}(t)+\dot{\mathbf{u}}(t+\tau)}{2} - \mathbf{u}(t+\tau), \boldsymbol{\epsilon}(t,\dot{\mathbf{u}},\tau)\Big)\\
&\quad + \frac{1}{2}\Big\|\mathbf{u}(t) + \tau\frac{\dot{\mathbf{u}}(t)+\dot{\mathbf{u}}(t+\tau)}{2} - \mathbf{u}(t+\tau)\Big\|_a^2\\
&\quad - \frac{\tau}{2}\Big\langle\frac{1}{2}(\mathbf{F}_{\mathrm{con}}(\mathbf{u}^n) + \mathbf{F}_{\mathrm{con}}(\mathbf{u}^{n+1}))\\
&\qquad\quad -\frac{1}{2}(\mathbf{F}_{\mathrm{con}}(\mathbf{u}(t)) + \mathbf{F}_{\mathrm{con}}(\mathbf{u}(t+\tau))), \dot{\mathbf{u}}(t) + \dot{\mathbf{u}}(t+\tau)\Big\rangle_{(\mathbf{H}^1)^*\times\mathbf{H}^1}\\
&\quad + \Big\langle\frac{1}{2}(\mathbf{F}_{\mathrm{con}}(\mathbf{u}^n) + \mathbf{F}_{\mathrm{con}}(\mathbf{u}^{n+1}))\\
&\qquad\quad -\frac{1}{2}(\mathbf{F}_{\mathrm{con}}(\mathbf{u}(t)) + \mathbf{F}_{\mathrm{con}}(\mathbf{u}(t+\tau))), \mathbf{u}^{n+1} - \mathbf{u}(t)\Big\rangle_{(\mathbf{H}^1)^*\times\mathbf{H}^1}\,.
\end{aligned}$$

Following the argumentation already used for (N-CI/CS(+)), the contact terms in this expression are equal to zero since $[(\mathbf{u}^{n+1} - \mathbf{u}(t)) \cdot \boldsymbol{\nu}]_{\boldsymbol{\phi}} = 0$ and $[(\mathbf{u}(t+\tau) - \mathbf{u}(t)) \cdot \boldsymbol{\nu}]_{\boldsymbol{\phi}} = 0$ on Γ_C. Now, the proof can be finished in the same way as for (N-CI/CS(+)). □

The theorem above reveals that the local discretization errors of (N-CL) and (N-CI/CS(+)) are of order 2 in physical energy norm if the active contact boundaries do not vary within the timestep and the solution is sufficiently regular. This is in contrast to the general problem of free contact boundaries, where higher regularity would not entail an increase of the consistency order. In particular, the result incorporates the unconstrained case, in which Newmark schemes are well-known to be of order 2 for ODEs [33].

In a second step, the local discretization error in the presence of permanent active contact is analyzed within the discrete displacement norm. Compared to Theorem 4.4.1, the result is based on weakened regularity assumptions on the solution and its derivatives. Permanent active contact boundaries are explicitly demanded for (N-CL) only, but they are also essential for (N-CI/CS(+)) since they justify the strong regularity assumptions.

Theorem 4.4.2. *Assume that* $\ddot{\mathbf{u}} \in \mathbf{C}^1([t, t+\tau], \mathbf{L}_2) \cap \mathbf{C}([t, t+\tau], \mathbf{H}^1)$. *Then, for initial values* $\mathbf{u}^n = \mathbf{u}(t)$ *and* $\dot{\mathbf{u}}^n = \dot{\mathbf{u}}(t)$, *the local error of* (N-CI/CS(+)) *satisfies*

$$\left\| \boldsymbol{\Psi}^{t+\tau,t} \bar{\mathbf{u}}(t) - \boldsymbol{\Phi}^{t+\tau,t} \bar{\mathbf{u}}(t) \right\|_\tau = O\left(\tau^3\right). \tag{4.34}$$

For (N-CL), *the same estimate holds if in addition* $[(\mathbf{u}^{n+1} - \mathbf{u}(t+\tau)) \cdot \boldsymbol{\nu}]_{\boldsymbol{\phi}} = g$ *on* Γ_C *for all* τ.

Proof. For (N-CI/CS(+)), Lemma 4.3.1 gives

$$\begin{aligned}
&\|\boldsymbol{\epsilon}(t, \mathbf{u}, \tau)\|_\tau^2 \\
&= -\int_t^{t+\tau} \Big(\int_t^s (\ddot{\mathbf{u}}(r) - \ddot{\mathbf{u}}(t+\tau), \boldsymbol{\epsilon}(t, \mathbf{u}, \tau))_{\mathbf{L}_2} \, dr \Big) \, ds \\
&\quad + \frac{\tau^2}{4} a(\mathbf{u}(t+\tau) - \mathbf{u}(t), \boldsymbol{\epsilon}(t, \mathbf{u}, \tau)) - \frac{\tau}{2} \int_t^{t+\tau} b(\dot{\mathbf{u}}(s) - \dot{\mathbf{u}}(t+\tau), \boldsymbol{\epsilon}(t, \mathbf{u}, \tau)) \, ds \\
&\quad + \frac{\tau^2}{2} \big\langle \mathbf{F}_{\mathrm{con}}(\mathbf{u}^{n+1}) - \mathbf{F}_{\mathrm{con}}(\mathbf{u}(t+\tau)), \mathbf{u}^{n+1} - \mathbf{u}(t+\tau) \big\rangle_{(\mathbf{H}^1)^* \times \mathbf{H}^1}
\end{aligned}$$

$$\leq \int_t^{t+\tau} \Big(\int_t^s \|\ddot{\mathbf{u}}(r) - \ddot{\mathbf{u}}(t+\tau)\|_{\mathbf{L}_2} \, dr \Big) \, ds \cdot \|\boldsymbol{\epsilon}(t, \mathbf{u}, \tau)\|_{\mathbf{L}_2}$$

$$+ C \Big(\tau^2 \|\mathbf{u}(t) - \mathbf{u}(t+\tau)\|_{\mathbf{H}^1} + \tau \int_t^{t+\tau} \|\dot{\mathbf{u}}(s) - \dot{\mathbf{u}}(t+\tau)\|_{\mathbf{H}^1} \, ds \Big) \|\boldsymbol{\epsilon}(t, \mathbf{u}, \tau)\|_{\mathbf{H}^1} \,, \tag{4.35}$$

due to the continuity of the bilinear forms a and b in $\mathbf{H}^1$, cf. (1.22) and (1.23), and the sign of the contact forces, cf. (1.31) and (4.5). Inserting the regularity assumptions of the theorem into this expression results in

$$\|\boldsymbol{\epsilon}(t, \mathbf{u}, \tau)\|_\tau^2 \leq C\tau^3 \cdot \big(\|\boldsymbol{\epsilon}(t, \mathbf{u}, \tau)\|_{\mathbf{L}_2} + \|\boldsymbol{\epsilon}(t, \mathbf{u}, \tau))\|_{\mathbf{H}^1} \big) \,.$$

Here, the inequality of Korn (A.1), the estimate (1.5), and the consistency order of the displacements in a-norm (cf. the previous Theorem 4.4.1) lead to

$$\begin{aligned} \|\boldsymbol{\epsilon}(t, \mathbf{u}, \tau))\|_{\mathbf{H}^1} &\leq \frac{1}{c_K^{1/2}} \Big(\|\boldsymbol{\epsilon}(t, \mathbf{u}, \tau))\|_{\mathbf{L}_2}^2 + \frac{1}{E_0} \|\boldsymbol{\epsilon}(t, \mathbf{u}, \tau))\|_a^2 \Big)^{1/2} \\ &= \frac{1}{c_K^{1/2}} \big(\|\boldsymbol{\epsilon}(t, \mathbf{u}, \tau))\|_{\mathbf{L}_2}^2 + O\big(\tau^6\big) \big)^{1/2} \\ &= \frac{1}{c_K^{1/2}} \|\boldsymbol{\epsilon}(t, \mathbf{u}, \tau))\|_{\mathbf{L}_2} + O\big(\tau^3\big) \end{aligned}$$

such that

$$\|\boldsymbol{\epsilon}(t, \mathbf{u}, \tau)\|_\tau^2 = O\big(\tau^3\big) \cdot \|\boldsymbol{\epsilon}(t, \mathbf{u}, \tau)\|_\tau + O\big(\tau^6\big) \,.$$

Finally, the binomial formula yields the desired result (compare, e.g., the proof of Theorem 4.4.1).

For (N-CL), the additional term

$$\frac{\tau^2}{4} \big\langle \mathbf{F}_{\mathrm{con}}(\mathbf{u}^n) - \mathbf{F}_{\mathrm{con}}(\mathbf{u}(t+\tau)), \mathbf{u}^{n+1} - \mathbf{u}(t+\tau) \big\rangle_{(\mathbf{H}^1)^* \times \mathbf{H}^1}$$

occurs on the right-hand side of (4.35). The assumption $[(\mathbf{u}^{n+1} - \mathbf{u}(t+\tau)) \cdot \boldsymbol{\nu}]_{\boldsymbol{\phi}} = 0$ on Γ_C leads to $\pm(\mathbf{u}^{n+1} - \mathbf{u}(t+\tau)) \in \mathcal{K}$. Hence, the whole contact term is equal to zero, see (1.31) and (4.5). Following the proof of the theorem for (N-CI/CS(+)) gives consistency of order 2, too. □

As shown in the theorem above, the consistency error measured in the discrete displacement norm is of the same optimal order 2 as in physical energy norm. This is in contrast to the general case of free contact, where the consistency error in the discrete displacement norm is one order higher than in physical energy norm. The result corresponds to the behavior of Newmark methods in the absence of contact, where both displacements and velocities are of order 2 for ODEs [33].

The optimal consistency order of the improved contact–stabilized Newmark scheme in the case of permanent active contact will become fundamental for the construction of an adaptive timestep control in Chapter 6.

5. Convergence Theory

To date, the question of convergence of Newmark methods for dynamical contact problems has been neglected in engineering and in mathematical literature completely. In the present chapter, the convergence of the improved contact–stabilized Newmark scheme will be analyzed within the method of time layers, both in physical energy norm and in discrete displacement norm.

The conventional approach to this challenge is applying the proof technique for time discretizations of evolution problems by Hairer, Nørsett, and Wanner (also known as "Lady Windermere's Fan", cf. [34]) to the algorithm. The procedure requires results concerning the stability of dynamical contact problems under perturbations of the initial data and consistency of the Newmark method, which have been investigated in Chapter 3 and in Chapter 4. However, the special structure of the consistency error estimate in the presence of contact would not give rise to any convergence of the scheme in this traditional way. Therefore, the proof in this chapter will utilize a second, less popular version of the classical Lady Windermere's Fan instead, which is based on a discrete perturbation result for the time discretization scheme. Here, the telescoping property of the total variations will play a substantial role.

The chapter is organized as follows. In Section 5.1, the focus is on the continuous dependence of the Newmark methods on the initial data in discrete displacement norm and in physical energy norm. This issue will need a discrete stability condition on the contact forces of the algorithm. Afterwards, in Section 5.2, the mathematical insights gained so far will be exploited to prove convergence of the contact–implicit and (improved) contact–stabilized Newmark method in both norms.

5.1. Discrete Perturbation Results

The alternative proof technique of convergence for time discretizations of dynamical contact problems requires information on the continuous dependence of the schemes on the initial data. Within the discrete displacement norm, a perturbation result for the contact–implicit and (improved) contact–stabilized Newmark method in function space can be proven comparatively easy for one timestep. After performing several steps, however, information on the stability behavior of the velocities is required in addition. The proof of a perturbation result in physical energy norm will be based on a stability condition on the contact forces of the algorithm, which is the discrete

analogon to the one introduced in Chapter 3 for dynamical contact problems. The assumption will again be motivated by localizing the discrete contact stresses on small parts of the possible contact boundaries.

5.1.1. A Discrete Perturbation Result in Discrete Displacement Norm

In this section, the stability of the Newmark methods under perturbations of the initial data will be analyzed within the discrete displacement norm. For (N-CI/CS(+)), a discrete perturbation result will be derived. A corresponding estimate for (N-CL) is not valid.

For (N-CI/CS(+)), the following strong relation holds between the initial perturbations and the displacements of the scheme at the end of a timestep.

Lemma 5.1.1. *Let* $\mathbf{u}^{j+1}$ *and* $\tilde{\mathbf{u}}^{j+1}$ *be two solutions of* (N-CI/CS(+)) *with initial values* $\mathbf{u}^j$, $\dot{\mathbf{u}}^j$ *and* $\tilde{\mathbf{u}}^j$, $\dot{\tilde{\mathbf{u}}}^j$, *respectively. Then,*

$$\begin{aligned}
&\big\|\delta\mathbf{u}^{j+1}\big\|_{\mathbf{L}_2}^2 + \frac{\tau_j^2}{4}\big\|\delta\mathbf{u}^{j+1}\big\|_a^2 + \frac{\tau_j}{2}\big\|\delta\mathbf{u}^{j+1}\big\|_b^2 - \tau_j^2\big\langle\delta\mathbf{F}_{\mathrm{con}}(\mathbf{u}^{j+1}),\delta\mathbf{u}^{j+1}\big\rangle_{(\mathbf{H}^1)^*\times\mathbf{H}^1}\\
&+ \big\|\delta\mathbf{u}^{j+1} - \delta\mathbf{u}^j - \tau_j\delta\dot{\mathbf{u}}^j\big\|_{\mathbf{L}_2}^2 + \tau_j^2\Big\|\frac{\delta\mathbf{u}^j + \delta\mathbf{u}^{j+1}}{2}\Big\|_a^2 + \frac{\tau_j^3}{2}\Big\|\frac{\delta\mathbf{u}^{j+1} - \delta\mathbf{u}^j}{\tau_j}\Big\|_b^2 \qquad (5.1)\\
&= \big\|\delta\mathbf{u}^j + \tau_j\delta\dot{\mathbf{u}}^j\big\|_{\mathbf{L}_2}^2 + \frac{\tau_j^2}{4}\big\|\delta\mathbf{u}^j\big\|_a^2 + \frac{\tau_j}{2}\big\|\delta\mathbf{u}^j\big\|_b^2 .
\end{aligned}$$

Proof. Inserting the definition of algorithm (4.3) into the discrete displacement norm of the perturbed solutions leads to

$$\begin{aligned}
&\big\|\delta\mathbf{u}^{j+1}\big\|_{\mathbf{L}_2}^2 + \frac{\tau_j^2}{4}\big\|\delta\mathbf{u}^{j+1}\big\|_a^2 + \frac{\tau_j}{2}\big\|\delta\mathbf{u}^{j+1}\big\|_b^2\\
&- \big\|\delta\mathbf{u}^j + \tau_j\delta\dot{\mathbf{u}}^j\big\|_{\mathbf{L}_2}^2 - \frac{\tau_j^2}{4}\big\|\delta\mathbf{u}^j\big\|_a^2 - \frac{\tau_j}{2}\big\|\delta\mathbf{u}^j\big\|_b^2\\
&= \big(\delta\mathbf{u}^{j+1} - \delta\mathbf{u}^j - \tau_j\delta\dot{\mathbf{u}}^j, \delta\mathbf{u}^{j+1} + \delta\mathbf{u}^j + \tau_j\delta\dot{\mathbf{u}}^j\big)_{\mathbf{L}_2}\\
&\quad + \frac{\tau_j^2}{4}a\big(\delta\mathbf{u}^j + \delta\mathbf{u}^{j+1}, \delta\mathbf{u}^{j+1} - \delta\mathbf{u}^j\big) + \frac{\tau_j}{2}b\big(\delta\mathbf{u}^j + \delta\mathbf{u}^{j+1}, \delta\mathbf{u}^{j+1} - \delta\mathbf{u}^j\big)\\
&= 2\big(\delta\mathbf{u}^{j+1} - \delta\mathbf{u}^j - \tau_j\delta\dot{\mathbf{u}}^j, \delta\mathbf{u}^{j+1}\big)_{\mathbf{L}_2} - \big\|\delta\mathbf{u}^{j+1} - \delta\mathbf{u}^j - \tau_j\delta\dot{\mathbf{u}}^j\big\|_{\mathbf{L}_2}^2\\
&\quad + \tau_j^2 a\Big(\frac{\delta\mathbf{u}^j + \delta\mathbf{u}^{j+1}}{2}, \delta\mathbf{u}^{j+1}\Big) - \tau_j^2\Big\|\frac{\delta\mathbf{u}^j + \delta\mathbf{u}^{j+1}}{2}\Big\|_a^2\\
&\quad + \tau_j^2 b\Big(\frac{\delta\mathbf{u}^{j+1} - \delta\mathbf{u}^j}{\tau_j}, \delta\mathbf{u}^{j+1}\Big) - \frac{\tau_j^3}{2}\Big\|\frac{\delta\mathbf{u}^{j+1} - \delta\mathbf{u}^j}{\tau_j}\Big\|_b^2
\end{aligned}$$

$$= \tau_j^2 \big\langle \delta \mathbf{F}_{\mathrm{con}}(\mathbf{u}^{j+1}), \delta \mathbf{u}^{j+1} \big\rangle_{(\mathbf{H}^1)^* \times \mathbf{H}^1} - \big\| \delta \mathbf{u}^{j+1} - \delta \mathbf{u}^j - \tau_j \delta \dot{\mathbf{u}}^j \big\|_{\mathbf{L}_2}^2 - \tau_j^2 \Big\| \frac{\delta \mathbf{u}^j + \delta \mathbf{u}^{j+1}}{2} \Big\|_a^2 - \frac{\tau_j^3}{2} \Big\| \frac{\delta \mathbf{u}^{j+1} - \delta \mathbf{u}^j}{\tau_j} \Big\|_b^2 .$$

□

The stability result for (N-CI/CS(+)) presented above is valid for arbitrary perturbations of the initial data without any further assumptions. Equation (5.1) shows that, if the initial perturbations in displacements and velocities tend to zero, the perturbations in displacements at the end of a timestep vanish both in $\mathbf{L}_2$-norm and in $\mathbf{H}^1$-norm. In particular, this observation indicates the uniqueness of a discrete solution of (N-CI/CS(+)), compare Chapter 2.

Remark 5.1.2. For the classical Newmark method, Lemma 5.1.1 is not valid due to the same analytical reason that causes energy generation of the scheme in the presence of contact. Performing the calculation in the proof above for (N-CL) yields relation (5.1) up to an additional contact term

$$\tau_j^2 \big\langle \delta \mathbf{F}_{\mathrm{con}}(\mathbf{u}^j), \delta \mathbf{u}^{j+1} \big\rangle_{(\mathbf{H}^1)^* \times \mathbf{H}^1}$$

on the right-hand side. Due to the missing sign or, at least, the lack of an estimate for this quantity, a perturbation result for (N-CL) in discrete displacement norm can only be expected under extra assumptions. For this reason, the investigations of this chapter concentrate on (N-CI/CS(+)).

In view of a convergence proof for (N-CI/CS(+)) in discrete displacement norm, information about the stability of the scheme after performing several timesteps is necessary. For an equidistant mesh of timesteps, the following theorem presents an estimate for a multiple propagation of perturbations in displacements.

Theorem 5.1.3. *Let* $\mathbf{u}^{n+1}$ *and* $\tilde{\mathbf{u}}^{n+1}$ *be two solutions of* (N-CI/CS(+)) *with initial values* $\mathbf{u}^0$, $\dot{\mathbf{u}}^0$ *and* $\tilde{\mathbf{u}}^0$, $\dot{\tilde{\mathbf{u}}}^0$, *respectively. Then,*

$$\big\| \delta \mathbf{u}^{n+1} \big\|_\tau \leq \big\| \delta \mathbf{u}^0 \big\|_\tau + \tau \sum_{j=0}^{n} \big\| \delta \dot{\mathbf{u}}^j \big\|_{\mathbf{L}_2} . \tag{5.2}$$

Proof. Due to the sign of the discrete contact forces, cf. (4.5),

$$\big\langle \delta \mathbf{F}_{\mathrm{con}}(\mathbf{u}^{j+1}), \delta \mathbf{u}^{j+1} \big\rangle_{(\mathbf{H}^1)^* \times \mathbf{H}^1} \leq 0 ,$$

Lemma 5.1.1 yields the estimate

$$\big\| \delta \mathbf{u}^{j+1} \big\|_{\mathbf{L}_2}^2 + \frac{\tau^2}{4} \big\| \delta \mathbf{u}^{j+1} \big\|_a^2 + \frac{\tau}{2} \big\| \delta \mathbf{u}^{j+1} \big\|_b^2 \leq \big\| \delta \mathbf{u}^j + \tau \delta \dot{\mathbf{u}}^j \big\|_{\mathbf{L}_2}^2 + \frac{\tau^2}{4} \big\| \delta \mathbf{u}^j \big\|_a^2 + \frac{\tau}{2} \big\| \delta \mathbf{u}^j \big\|_b^2 .$$

The triangle inequality for norms gives

$$\begin{aligned}&\Big(\big\|\delta\mathbf{u}^{j+1}\big\|_{\mathbf{L}_2}^2+\frac{\tau^2}{4}\big\|\delta\mathbf{u}^{j+1}\big\|_a^2+\frac{\tau}{2}\big\|\delta\mathbf{u}^{j+1}\big\|_b^2\Big)^{1/2}\\&\leq\Big(\big\|\delta\mathbf{u}^{j}\big\|_{\mathbf{L}_2}^2+\frac{\tau^2}{4}\big\|\delta\mathbf{u}^{j}\big\|_a^2+\frac{\tau}{2}\big\|\delta\mathbf{u}^{j}\big\|_b^2\Big)^{1/2}+\tau\big\|\delta\dot{\mathbf{u}}^{j}\big\|_{\mathbf{L}_2}.\end{aligned}$$

Applying this estimate several times leads to

$$\begin{aligned}&\Big(\big\|\delta\mathbf{u}^{n+1}\big\|_{\mathbf{L}_2}^2+\frac{\tau^2}{4}\big\|\delta\mathbf{u}^{n+1}\big\|_a^2+\frac{\tau}{2}\big\|\delta\mathbf{u}^{n+1}\big\|_b^2\Big)^{1/2}\\&\leq\Big(\big\|\delta\mathbf{u}^{0}\big\|_{\mathbf{L}_2}^2+\frac{\tau^2}{4}\big\|\delta\mathbf{u}^{0}\big\|_a^2+\frac{\tau}{2}\big\|\delta\mathbf{u}^{0}\big\|_b^2\Big)^{1/2}+\tau\sum_{j=0}^{n}\big\|\delta\dot{\mathbf{u}}^{j}\big\|_{\mathbf{L}_2},\end{aligned}$$

which is the result of the theorem. □

The presented perturbation result in discrete displacement norm depends on the $\mathbf{L}_2$-norm of the perturbed discrete velocities at every point of the time mesh. This is a typical stability behavior for time discretizations of evolution problems. In consequence, a proof of convergence for (N-CI/CS(+)) in discrete displacement norm additionally requires a discrete perturbation result in physical energy norm.

5.1.2. Discrete Stability Condition

In the following two sections, the challenge is to derive a reliable discrete perturbation result for (N-CI/CS(+)) in physical energy norm. In a first step, a class of discretizations will be characterized that satisfy the necessary continuous dependence on the initial data. To this end, a stability condition on the contact forces of (N-CI/CS(+)) will be imposed, which will turn out to be the discrete analogon to the continuous one in Section 5.1.2. The assumption can be interpreted by means of a localization of the discrete contact forces on certain critical contact boundaries.

A short calculation gives the following lemma concerning the stability of (N-CI/CS(+)) under perturbations of the initial data in physical energy norm. The result corresponds to the one presented in Lemma 3.2.1 for the dynamical contact problem.

Lemma 5.1.4. *Let* $\bar{\mathbf{u}}^{j+1}=(\mathbf{u}^{j+1},\dot{\mathbf{u}}^{j+1})$ *and* $\bar{\tilde{\mathbf{u}}}^{j+1}=(\tilde{\mathbf{u}}^{j+1},\dot{\tilde{\mathbf{u}}}^{j+1})$ *be two solutions of* (N-CI/CS(+)) *with initial values* $\mathbf{u}^0$, $\dot{\mathbf{u}}^0$ *and* $\tilde{\mathbf{u}}^0$, $\dot{\tilde{\mathbf{u}}}^0$, *respectively. Then,*

$$\big\|\delta\bar{\mathbf{u}}^{j+1}\big\|_E^2+\tau_j\Big\|\delta\frac{\mathbf{u}^{j+1}-\mathbf{u}^{j}}{\tau_j}\Big\|_b^2=\big\|\delta\bar{\mathbf{u}}^{j}\big\|_E^2+\tau_j\Big\langle\delta\mathbf{F}_{\mathrm{con}}(\mathbf{u}^{j+1}),\delta\frac{\mathbf{u}^{j+1}-\mathbf{u}^{j}}{\tau_j}\Big\rangle_{(\mathbf{H}^1)^*\times\mathbf{H}^1}$$

and

$$\begin{aligned}&\left\|\delta\bar{\mathbf{u}}^{n+1}\right\|_E^2+\sum_{j=0}^{n}\tau_j\left\|\delta\frac{\mathbf{u}^{j+1}-\mathbf{u}^j}{\tau_j}\right\|_b^2\\&=\left\|\delta\bar{\mathbf{u}}^0\right\|_E^2+\sum_{j=0}^{n}\tau_j\left\langle\delta\mathbf{F}_{\mathrm{con}}(\mathbf{u}^{j+1}),\delta\frac{\mathbf{u}^{j+1}-\mathbf{u}^j}{\tau_j}\right\rangle_{(\mathbf{H}^1)^*\times\mathbf{H}^1}.\end{aligned}\tag{5.3}$$

Proof. Inserting definition (4.3) of the Newmark scheme into the physical energy norm of the perturbed solutions leads to

$$\begin{aligned}&\frac{1}{2}\left\|\delta\dot{\mathbf{u}}^{j+1}\right\|_{\mathbf{L}_2}^2+\frac{1}{2}\left\|\delta\mathbf{u}^{j+1}\right\|_a^2-\frac{1}{2}\left\|\delta\dot{\mathbf{u}}^{j}\right\|_{\mathbf{L}_2}^2-\frac{1}{2}\left\|\delta\mathbf{u}^{j}\right\|_a^2\\&=\frac{1}{2}\left(\delta\dot{\mathbf{u}}^{j+1}-\delta\dot{\mathbf{u}}^{j},\delta\dot{\mathbf{u}}^{j+1}+\delta\dot{\mathbf{u}}^{j}\right)_{\mathbf{L}_2}+\frac{1}{2}a\left(\delta\mathbf{u}^{j+1}+\delta\mathbf{u}^{j},\delta\mathbf{u}^{j+1}-\delta\mathbf{u}^{j}\right)\\&=\left(\delta\dot{\mathbf{u}}^{j+1}-\delta\dot{\mathbf{u}}^{j},\delta\frac{\mathbf{u}^{j+1}-\mathbf{u}^j}{\tau_j}\right)_{\mathbf{L}_2}+\tau_j a\left(\frac{\delta\mathbf{u}^{j+1}+\delta\mathbf{u}^{j}}{2},\frac{\delta\mathbf{u}^{j+1}-\delta\mathbf{u}^{j}}{\tau_j}\right)\\&=-\tau_j\left\|\delta\frac{\mathbf{u}^{j+1}-\mathbf{u}^j}{\tau_j}\right\|_b^2+\tau_j\left\langle\delta\mathbf{F}_{\mathrm{con}}(\mathbf{u}^{j+1}),\delta\frac{\mathbf{u}^{j+1}-\mathbf{u}^j}{\tau_j}\right\rangle_{(\mathbf{H}^1)^*\times\mathbf{H}^1},\end{aligned}$$

where Remark 4.1.5 has been used. Propagating this relation over several timesteps yields the second result of the lemma. □

In the case of time-constant active contact boundaries (and especially in the absence of contact), the Newmark schemes under consideration depend continuously on the initial data in physical energy norm. Though, the general case of time-dependent active contact requires to handle the contact terms on the right-hand side of relation (5.3). For this purpose, viscous material behavior is indispensable since it provides information on the finite differences in displacements at contact boundaries. Nevertheless, a reasonable stability condition on the term including the contact forces is needed, compare the perturbation result for dynamical contact problems in Chapter 3.

The stability condition will be motivated by the intuition that perturbations in the contact forces are effective only on a small part of the possible contact boundaries. Hence, the next aim is to localize the discrete contact stresses on a critical segment of the contact boundaries.

Localization of contact stresses. For simplification, assume that the possible contact boundaries and the bijective mappings between the two possible contact boundaries coincide, i.e., $\Gamma_C=\tilde{\Gamma}_C$ and $\boldsymbol{\phi}=\tilde{\boldsymbol{\phi}}$. This is the special case of interest for the convergence analysis of the Newmark method in Section 5.2.

The *discrete active contact boundaries* of a time discretization can be defined by means of the concept of Sobolev capacity (compare Section 3.3), namely

$$\Gamma_C^{j+1}:=\left\{\mathbf{x}\in\Gamma_C\,\middle|\,\left[\mathbf{u}^{j+1}\cdot\boldsymbol{\nu}\right]_{\boldsymbol{\phi}}=g\right\}\subset\Gamma_C\ \text{q.e.}\tag{5.4}$$

for $j+1 = 0, \ldots, N_\triangle$ and

$$\tilde{\Gamma}_C^{j+1} := \left\{ \mathbf{x} \in \Gamma_C \,\middle|\, \left[\tilde{\mathbf{u}}^{j+1} \cdot \boldsymbol{\nu} \right]_{\boldsymbol{\phi}} = g \right\} \subset \Gamma_C \text{ q.e.} \tag{5.5}$$

for the perturbed solution. For (N-CI/CS(+)), the *critical part of the discrete active contact boundaries* is the set

$$(\Gamma_C^*)^{j+1,j} := (\Gamma_C^*)^{j+1} \cup (\Gamma_C^*)^j \cup (\tilde{\Gamma}_C^*)^{j+1,j} \tag{5.6}$$

for $j+1 = 1, \ldots, N_\triangle$ where

$$\begin{aligned} (\Gamma_C^*)^i :&= \left(\Gamma_C^i \cup \tilde{\Gamma}_C^i\right) \setminus \left(\Gamma_C^i \cap \tilde{\Gamma}_C^i\right) \\ &= \left\{ \mathbf{x} \in \Gamma_C \,\middle|\, \left[\mathbf{u}^i \cdot \boldsymbol{\nu} \right]_{\boldsymbol{\phi}} < g,\ \left[\tilde{\mathbf{u}}^i \cdot \boldsymbol{\nu} \right]_{\boldsymbol{\phi}} = g \text{ or } \left[\mathbf{u}^i \cdot \boldsymbol{\nu} \right]_{\boldsymbol{\phi}} = g,\ \left[\tilde{\mathbf{u}}^i \cdot \boldsymbol{\nu} \right]_{\boldsymbol{\phi}} < g \right\} \text{ q.e.} \end{aligned} \tag{5.7}$$

and

$$\begin{aligned} (\tilde{\Gamma}_C^*)^{i+1,i} := \Big\{ \mathbf{x} \in \Gamma_C \,\Big|\, &\left[\mathbf{u}^j \cdot \boldsymbol{\nu} \right]_{\boldsymbol{\phi}} < g,\ \left[\tilde{\mathbf{u}}^j \cdot \boldsymbol{\nu} \right]_{\boldsymbol{\phi}} < g \text{ and} \\ &\left[\mathbf{u}^{j+1} \cdot \boldsymbol{\nu} \right]_{\boldsymbol{\phi}} = \left[\tilde{\mathbf{u}}^{j+1} \cdot \boldsymbol{\nu} \right]_{\boldsymbol{\phi}} = g \Big\} \text{ q.e.} \end{aligned} \tag{5.8}$$

The first two sets $(\Gamma_C^*)^{j+1}$ and $(\Gamma_C^*)^j$ describe parts of the possible contact boundaries where the discrete solution is in contact and the perturbed one is not, or vice versa. The third component $(\tilde{\Gamma}_C^*)^{j+1,j}$ is a boundary segment where the initial solutions are not in contact, while the final solutions are both in contact. This part of the contact boundaries usually appears in the phase of detecting contact for the first time. By virtue of the discrete perturbation result for (N-CI/CS(+)) in discrete displacement norm, cf. Section 5.1.1, the critical set can be expected to become successively smaller if the initial perturbations tend to zero.

In Appendix B, a trace theorem for the discrete contact stresses is proven under the assumption that $\operatorname{div} \boldsymbol{\sigma}(\mathbf{u}^{j+1}, \dot{\mathbf{u}}^{j+1})$, $\operatorname{div} \boldsymbol{\sigma}(\tilde{\mathbf{u}}^{j+1}, \dot{\tilde{\mathbf{u}}}^{j+1}) \in \mathbf{L}_2(\Omega)$. Using the definitions above, the difference of the contact forces can be written as a functional $\delta\hat{\boldsymbol{\sigma}}^*(\mathbf{u}^{j+1}, \dot{\mathbf{u}}^{j+1}) \in (\mathbf{H}^{1/2})^*((\Gamma_C^*)^{j+1,j})$ acting on the critical contact boundaries only, i.e.,

$$\begin{aligned} &\left\langle \delta\mathbf{F}_{\mathrm{con}}(\mathbf{u}^{j+1}), \delta(\mathbf{u}^{j+1} - \mathbf{u}^j) \right\rangle_{(\mathbf{H}^1)^* \times \mathbf{H}^1} \\ &= \left\langle \delta\hat{\boldsymbol{\sigma}}^*(\mathbf{u}^{j+1}, \dot{\mathbf{u}}^{j+1}), \delta(\mathbf{u}^{j+1} - \mathbf{u}^j) \right\rangle_{(\mathbf{H}^{1/2})^*((\Gamma_C^*)^{j+1,j}) \times \mathbf{H}^{1/2}((\Gamma_C^*)^{j+1,j})} \end{aligned} \tag{5.9}$$

for all $j+1 \in \{1, \ldots, N_\triangle\}$.

The localization of the contact stresses of (N-CI/CS(+)) on critical contact boundaries allows reformulating Lemma 3.2.1 in the following way.

Lemma 5.1.5. *Let* $\bar{\mathbf{u}}^{j+1} = (\mathbf{u}^{j+1}, \dot{\mathbf{u}}^{j+1})$ *and* $\tilde{\bar{\mathbf{u}}}^{j+1} = (\tilde{\mathbf{u}}^{j+1}, \dot{\tilde{\mathbf{u}}}^{j+1})$ *be two solutions of* (N-CI/CS(+)) *with initial values* $\mathbf{u}^0$, $\dot{\mathbf{u}}^0$ *and* $\tilde{\mathbf{u}}^0$, $\dot{\tilde{\mathbf{u}}}^0$, *respectively. Furthermore, assume that* (5.9) *is valid. Then, for all* $n+1 \in \{0, \dots, N_\triangle\}$,

$$\begin{aligned}
&\big\|\delta\bar{\mathbf{u}}^{n+1}\big\|_E^2 + \sum_{j=0}^{n} \tau_j \Big\|\delta\frac{\mathbf{u}^{j+1}-\mathbf{u}^j}{\tau_j}\Big\|_b^2 \\
&= \big\|\delta\bar{\mathbf{u}}^{0}\big\|_E^2 + \sum_{j=0}^{n} \tau_j \Big\langle \delta\hat{\boldsymbol{\sigma}}^*(\mathbf{u}^{j+1}, \dot{\mathbf{u}}^{j+1}), \delta\frac{\mathbf{u}^{j+1}-\mathbf{u}^j}{\tau_j}\Big\rangle_{(\mathbf{H}^{1/2})^*((\Gamma_C^*)^{j+1,j})\times\mathbf{H}^{1/2}((\Gamma_C^*)^{j+1,j})}.
\end{aligned}$$

Remark 5.1.6. For (N-CL), the different contact term

$$\sum_{j=0}^{n} \tau_j \Big\langle \delta\mathbf{F}_{\mathrm{con}}(\mathbf{u}^j) + \delta\mathbf{F}_{\mathrm{con}}(\mathbf{u}^{j+1}), \delta\frac{\mathbf{u}^{j+1}-\mathbf{u}^j}{\tau_j}\Big\rangle_{(\mathbf{H}^1)^*\times\mathbf{H}^1}$$

has to be localized on a critical part of the possible contact boundaries. For sure, this critical set is larger than the one for (N-CI/CS(+)) introduced above. In general, however, these modified critical contact boundaries are not expected to become smaller if the initial perturbations tend to zero. This is due to the missing stability result for (N-CL) in discrete displacement norm, cf. Remark 5.1.2.

In order to motivate a reasonable (localized) stability condition for (N-CI/CS(+)), the special case of quasistatic contact problems will be analyzed in the following.

(N-CI/CS(+)) for quasistatic contact problems. Setting

$$\mathbf{u}^{j+1} - \mathbf{u}^j - \tau\dot{\mathbf{u}}^j = 0$$

in definition (4.3) of (N-CI/CS(+)) yields

$$0 \in \mathbf{F}^{1/2}\big(\mathbf{u}^j, \mathbf{u}^{j+1}\big) + \mathbf{G}\Big(\frac{\mathbf{u}^{j+1}-\mathbf{u}^j}{\tau}\Big) + \partial I_{\mathcal{K}}\big(\mathbf{u}^{j+1}\big). \tag{5.10}$$

The contact forces $\mathbf{F}_{\mathrm{con}}(\mathbf{u}^{j+1}) \in (\mathbf{H}^1)^*$ are given by

$$\begin{aligned}
&\big\langle \mathbf{F}_{\mathrm{con}}(\mathbf{u}^{j+1}), \mathbf{v}\big\rangle_{(\mathbf{H}^1)^*\times\mathbf{H}^1} \qquad (5.11)\\
&:= \big\langle \mathbf{F}^{1/2}(\mathbf{u}^j, \mathbf{u}^{j+1}), \mathbf{v}\big\rangle_{(\mathbf{H}^1)^*\times\mathbf{H}^1} + \Big\langle \mathbf{G}\Big(\frac{\mathbf{u}^{j+1}-\mathbf{u}^j}{\tau}\Big), \mathbf{v}\Big\rangle_{(\mathbf{H}^1)^*\times\mathbf{H}^1}, \qquad \mathbf{v} \in \mathbf{H}^1
\end{aligned}$$

for almost every $t \in [0, T]$.

Let the contact forces be represented by a functional acting on the active contact boundaries only, i.e.,

$$\big\|\mathbf{F}_{\mathrm{con}}(\mathbf{u}^{j+1})\big\|_{(\mathbf{H}^1)^*(\Omega)} = \big\|\delta\hat{\boldsymbol{\sigma}}(\mathbf{u}^{j+1}, \dot{\mathbf{u}}^{j+1})\big\|_{(\mathbf{H}^{1/2})^*(\Gamma_C^{j+1}\cup\tilde{\Gamma}_C^{j+1})},$$

and assume that

$$\Big(\sum_{j=0}^{n}\tau_j\big\|\delta\hat{\boldsymbol{\sigma}}^*(\mathbf{u}^{j+1},\dot{\mathbf{u}}^{j+1})\big\|^2_{(\mathbf{H}^{1/2})^*((\Gamma_C^*)^{j+1,j})}\Big)^{1/2}$$
$$\leq \varepsilon\Big(\sum_{j=0}^{n}\tau_j\big\|\delta\hat{\boldsymbol{\sigma}}(\mathbf{u}^{j+1},\dot{\mathbf{u}}^{j+1})\big\|^2_{(\mathbf{H}^{1/2})^*(\Gamma_C^{j+1}\cup\tilde{\Gamma}_C^{j+1})}\Big)^{1/2}.$$

Then, definition (5.11) of the contact forces and the continuity of the linearly viscoelastic forces, cf. (1.22) and (1.23), lead to

$$\begin{aligned}
&\big\|\delta\hat{\boldsymbol{\sigma}}(\mathbf{u}^{j+1},\dot{\mathbf{u}}^{j+1})\big\|_{(\mathbf{H}^{1/2})^*(\Gamma_C^{j+1}\cup\tilde{\Gamma}_C^{j+1})}\\
&\leq c\Big(\big\|\delta\mathbf{F}^{1/2}(\mathbf{u}^j,\mathbf{u}^{j+1})\big\|_{(\mathbf{H}^1)^*(\Omega)}+\Big\|\delta\mathbf{G}\Big(\frac{\mathbf{u}^{j+1}-\mathbf{u}^j}{\tau}\Big)\Big\|_{(\mathbf{H}^1)^*(\Omega)}\Big)\\
&\leq c\Big(\Big\|\delta\frac{\mathbf{u}^j+\mathbf{u}^{j+1}}{2}\Big\|_{\mathbf{H}^1(\Omega)}+\Big\|\delta\frac{\mathbf{u}^{j+1}-\mathbf{u}^j}{\tau}\Big\|_{\mathbf{H}^1(\Omega)}\Big),
\end{aligned}$$

and

$$\begin{aligned}
&\Big(\sum_{j=0}^{n}\tau_j\big\|\delta\hat{\boldsymbol{\sigma}}^*(\mathbf{u}^{j+1},\dot{\mathbf{u}}^{j+1})\big\|^2_{(\mathbf{H}^{1/2})^*((\Gamma_C^*)^{j+1,j})}\Big)^{1/2}\\
&\leq \varepsilon\, c\Big(\Big(\sum_{j=0}^{n}\tau_j\Big\|\delta\frac{\mathbf{u}^j+\mathbf{u}^{j+1}}{2}\Big\|^2_{\mathbf{H}^1(\Omega)}\Big)^{1/2}+\Big(\sum_{j=0}^{n}\tau_j\Big\|\delta\frac{\mathbf{u}^{j+1}-\mathbf{u}^j}{\tau}\Big\|_{\mathbf{H}^1(\Omega)}\Big)^{1/2}\Big).
\end{aligned}\tag{5.12}$$

As discussed above, for (N-CI/CS(+)), the critical part of the contact boundaries is expected to be only a small segment of the possible contact boundaries for small initial perturbations. This corresponds to the conjecture that the unknown constant ε in the above estimate is also small. Hence, the discretization of a quasistatic contact problem via (N-CI/CS(+)) motivates imposing the following localized stability condition on the discrete contact stresses.

Localized discrete stability condition. Let

$$\begin{aligned}
&\Big(\sum_{j=0}^{n}\tau_j\big\|\delta\hat{\boldsymbol{\sigma}}^*(\mathbf{u}^{j+1},\dot{\mathbf{u}}^{j+1})\big\|^2_{(\mathbf{H}^{1/2})^*((\Gamma_C^*)^{j+1,j})}\Big)^{1/2}\\
&\leq \varepsilon\Big(\kappa\Big(\sum_{j=0}^{n}\tau_j\Big\|\delta\frac{\mathbf{u}^j+\mathbf{u}^{j+1}}{2}\Big\|^2_{\mathbf{H}^1(\Omega)}\Big)^{1/2}+\Big(\sum_{j=0}^{n}\tau_j\Big\|\delta\frac{\mathbf{u}^{j+1}-\mathbf{u}^j}{\tau_j}\Big\|_{\mathbf{H}^1(\Omega)}\Big)^{1/2}\Big)
\end{aligned}\tag{5.13}$$

hold for all $n\in\{0,\dots,N_\triangle-1\}$ with $\varepsilon\geq 0$ sufficiently small and $\kappa\geq 0$.

The localized stability condition should be satisfied if (N-CI/CS(+)) behaves similar to the corresponding discretization of the quasistatic contact problem, which is the case for a small variation in the velocities. The non-localized discrete stability condition reads as follows.

Discrete stability condition. Let

$$\begin{aligned}
&\Big|\sum_{j=0}^{n}\tau_j\Big\langle\delta\mathbf{F}_{\mathrm{con}}(\mathbf{u}^{j+1}),\delta\frac{\mathbf{u}^{j+1}-\mathbf{u}^{j}}{\tau_j}\Big\rangle_{(\mathbf{H}^1)^*\times\mathbf{H}^1}\Big| \\
&\leq\varepsilon\Big(\kappa\Big(\sum_{j=0}^{n}\tau_j\Big\|\delta\frac{\mathbf{u}^{j}+\mathbf{u}^{j+1}}{2}\Big\|_{\mathbf{H}^1}^2\Big)^{1/2}+\Big(\sum_{j=0}^{n}\tau_j\Big\|\delta\frac{\mathbf{u}^{j+1}-\mathbf{u}^{j}}{\tau_j}\Big\|_{\mathbf{H}^1}\Big)^{1/2}\Big) \\
&\quad\cdot\Big(\sum_{j=0}^{n}\tau_j\Big\|\delta\frac{\mathbf{u}^{j+1}-\mathbf{u}^{j}}{\tau_j}\Big\|_{\mathbf{H}^1}^2\Big)^{1/2}
\end{aligned}\tag{5.14}$$

hold for all $n\in\{0,\ldots,N_\triangle-1\}$ with $\varepsilon\geq 0$ sufficiently small and $\kappa\geq 0$.

Both formulations correspond to the (localized) stability conditions (3.8) and (3.18) for the dynamical contact problem, in which the integrals are replaced by sums over the discrete mesh of timesteps. The detailed meaning of the requirement "$\varepsilon\geq 0$ sufficiently small" will be given in the following perturbation theorem for (N-CI/CS(+)) in physical energy norm.

5.1.3. A Discrete Perturbation Result in Physical Energy Norm

In this section, the continuous dependence of (N-CI/CS(+)) on the initial values will be shown in physical energy norm for the class of discretizations satisfying the discrete stability condition (5.14). The discrete perturbation theorem presented below corresponds to Theorem 3.2.2 for dynamical contact problems satisfying the continuous stability condition. For most parts, even the proofs of the stability estimates are similar.

Theorem 5.1.7. *Let* $\bar{\mathbf{u}}^{j+1}=(\mathbf{u}^{j+1},\dot{\mathbf{u}}^{j+1})$ *and* $\bar{\tilde{\mathbf{u}}}^{j+1}=(\tilde{\mathbf{u}}^{j+1},\dot{\tilde{\mathbf{u}}}^{j+1})$ *be two solutions of* (N-CI/CS(+)) *with initial values* $\mathbf{u}^0$, $\dot{\mathbf{u}}^0$ *and* $\tilde{\mathbf{u}}^0$, $\dot{\tilde{\mathbf{u}}}^0$, *respectively. Furthermore, assume the stability condition* (5.14) *with* $\frac{\varepsilon}{V_0\,c_K}<1$ *and* (5.17). *Then, for all* $n+1\in\{0,\ldots,N_\triangle\}$,

$$\big\|\delta\bar{\mathbf{u}}^{n+1}\big\|_E^2+\alpha\sum_{j=0}^{n}\tau_j\Big\|\delta\frac{\mathbf{u}^{j+1}-\mathbf{u}^{j}}{\tau_j}\Big\|_b^2\leq\Big(\big\|\delta\bar{\mathbf{u}}^{0}\big\|_E^2+ct_{n+1}\big\|\delta\mathbf{u}^{0}\big\|_{\mathbf{L}_2}^2\Big)e^{\tilde{\kappa}^2t_{n+1}}\tag{5.15}$$

with $\alpha\in[0,1)$, $c\geq 0$, *and* $\tilde{\kappa}\geq 0$.

Remark 5.1.8. If the Dirichlet boundaries do not vanish, i.e., if $\mathrm{meas}(\Gamma_D)>0$, or if a part of the discrete contact boundaries is active in the whole time interval $[0,T]$,

then the estimate does not depend on the initial perturbation of the displacements in $\mathbf{L}_2$-norm, and

$$\left\|\delta\bar{\mathbf{u}}^{n+1}\right\|_E^2 + \alpha\sum_{j=0}^{n}\tau_j\left\|\delta\frac{\mathbf{u}^{j+1}-\mathbf{u}^j}{\tau_j}\right\|_b^2 \leq \left\|\delta\bar{\mathbf{u}}^0\right\|_E^2 e^{\tilde{\kappa}^2 t_{n+1}}\,. \tag{5.16}$$

Proof. Inserting the stability condition (5.14) into the result of Lemma 5.1.4 yields

$$\begin{aligned}
&\left\|\delta\bar{\mathbf{u}}^{n+1}\right\|_E^2 + \sum_{j=0}^{n}\tau_j\left\|\delta\frac{\mathbf{u}^{j+1}-\mathbf{u}^j}{\tau_j}\right\|_b^2 \\
&\leq \left\|\delta\bar{\mathbf{u}}^0\right\|_E^2 + \left|\sum_{j=0}^{n}\tau_j\left\langle\delta\mathbf{F}_{\mathrm{con}}(\mathbf{u}^{j+1}),\delta\frac{\mathbf{u}^{j+1}-\mathbf{u}^j}{\tau_j}\right\rangle_{(\mathbf{H}^1)^*\times\mathbf{H}^1}\right| \\
&\leq \left\|\delta\bar{\mathbf{u}}^0\right\|_E^2 + \varepsilon\kappa\Big(\sum_{j=0}^{n}\tau_j\left\|\delta\frac{\mathbf{u}^j+\mathbf{u}^{j+1}}{2}\right\|_{\mathbf{H}^1}^2\Big)^{1/2}\Big(\sum_{j=0}^{n}\tau_j\left\|\delta\frac{\mathbf{u}^{j+1}-\mathbf{u}^j}{\tau_j}\right\|_{\mathbf{H}^1}^2\Big)^{1/2} \\
&\quad + \varepsilon\sum_{j=0}^{n}\tau_j\left\|\delta\frac{\mathbf{u}^{j+1}-\mathbf{u}^j}{\tau_j}\right\|_{\mathbf{H}^1}^2.
\end{aligned}$$

The inequality of Young in the form

$$ab \leq \frac{1}{4\,V_0\,c_K\,(1-\alpha)}\,a^2 + V_0\,c_K\,(1-\alpha)\,b^2$$

for an arbitrary parameter $\alpha < 1$ leads to

$$\begin{aligned}
&\left\|\delta\bar{\mathbf{u}}^{n+1}\right\|_E^2 + \sum_{j=0}^{n}\tau_j\left\|\delta\frac{\mathbf{u}^{j+1}-\mathbf{u}^j}{\tau_j}\right\|_b^2 \\
&\leq \left\|\delta\bar{\mathbf{u}}^0\right\|_E^2 + \frac{\varepsilon^2\kappa^2}{4V_0\,c_K\,(1-\alpha)}\sum_{j=0}^{n}\tau_j\left\|\delta\frac{\mathbf{u}^j+\mathbf{u}^{j+1}}{2}\right\|_{\mathbf{H}^1}^2 \\
&\quad + (\varepsilon + V_0\,c_K\,(1-\alpha))\sum_{j=0}^{n}\tau_j\left\|\delta\frac{\mathbf{u}^{j+1}-\mathbf{u}^j}{\tau_j}\right\|_{\mathbf{H}^1}^2.
\end{aligned}$$

Due to the first inequality of Korn (A.1) and the estimate (1.5),

$$\begin{aligned}
&\left\|\delta\bar{\mathbf{u}}^{n+1}\right\|_E^2 + \sum_{j=0}^{n}\tau_j\left\|\delta\frac{\mathbf{u}^{j+1}-\mathbf{u}^j}{\tau_j}\right\|_b^2 \\
&\leq \left\|\delta\bar{\mathbf{u}}^0\right\|_E^2 + \frac{\varepsilon^2\kappa^2}{4\,V_0\,c_K^2\,(1-\alpha)}\sum_{j=0}^{n}\tau_j\Big(\frac{1}{E_0}\left\|\delta\frac{\mathbf{u}^j+\mathbf{u}^{j+1}}{2}\right\|_a^2 + \left\|\delta\frac{\mathbf{u}^j+\mathbf{u}^{j+1}}{2}\right\|_{\mathbf{L}_2}^2\Big) \\
&\quad + \Big(\frac{\varepsilon}{c_K} + V_0(1-\alpha)\Big)\sum_{j=0}^{n}\tau_j\Big(\frac{1}{V_0}\left\|\delta\frac{\mathbf{u}^{j+1}-\mathbf{u}^j}{\tau_j}\right\|_b^2 + \left\|\delta\frac{\mathbf{u}^{j+1}-\mathbf{u}^j}{\tau_j}\right\|_{\mathbf{L}_2}^2\Big),
\end{aligned}$$

and with Remark 4.1.5, the estimate is equivalent to

$$\begin{aligned}
&\left\|\delta\bar{\mathbf{u}}^{n+1}\right\|_E^2 + \tilde{\alpha}\sum_{j=0}^{n}\tau_j\left\|\delta\frac{\mathbf{u}^{j+1}-\mathbf{u}^j}{\tau_j}\right\|_b^2 \\
&\leq \left\|\delta\bar{\mathbf{u}}^0\right\|_E^2 + \frac{c}{2\,E_0}\sum_{j=0}^{n}\tau_j\left\|\delta\frac{\mathbf{u}^j+\mathbf{u}^{j+1}}{2}\right\|_a^2 + \frac{c}{2}\sum_{j=0}^{n}\tau_j\left\|\delta\frac{\mathbf{u}^j+\mathbf{u}^{j+1}}{2}\right\|_{\mathbf{L}_2}^2 \\
&\quad + V_0(1-\tilde{\alpha})\sum_{j=0}^{n}\tau_j\left\|\delta\frac{\dot{\mathbf{u}}^j+\dot{\mathbf{u}}^{j+1}}{2}\right\|_{\mathbf{L}_2}^2,
\end{aligned}$$

where

$$\tilde{\alpha} = \alpha - \frac{\varepsilon}{V_0\,c_K}, \quad c = \frac{\varepsilon^2\kappa^2}{2\,V_0\,c_K^2\,(1-\alpha)}.$$

In order to make sure that the left-hand side of the inequality is non-negative, let $\frac{\varepsilon}{V_0\,c_K} < 1$ and choose $\alpha < 1$ such that $\tilde{\alpha} \geq 0$. Due to the inequality of Young,

$$\begin{aligned}
&\left\|\delta\bar{\mathbf{u}}^{n+1}\right\|_E^2 + \tilde{\alpha}\sum_{j=0}^{n}\tau_j\left\|\delta\frac{\mathbf{u}^{j+1}-\mathbf{u}^j}{\tau_j}\right\|_b^2 \\
&\leq \left\|\delta\bar{\mathbf{u}}^0\right\|_E^2 + \frac{c}{2\,E_0}\sum_{j=0}^{n}\frac{\tau_j}{2}\left(\left\|\delta\mathbf{u}^j\right\|_a^2 + \left\|\mathbf{u}^{j+1}\right\|_a^2\right) + \frac{c}{2}\sum_{j=0}^{n}\frac{\tau_j}{2}\left(\left\|\delta\mathbf{u}^j\right\|_{\mathbf{L}_2}^2 + \left\|\mathbf{u}^{j+1}\right\|_{\mathbf{L}_2}^2\right) \\
&\quad + V_0(1-\tilde{\alpha})\sum_{j=0}^{n}\frac{\tau_j}{2}\left(\left\|\delta\dot{\mathbf{u}}^j\right\|_{\mathbf{L}_2}^2 + \left\|\dot{\mathbf{u}}^{j+1}\right\|_{\mathbf{L}_2}^2\right) \\
&= \left\|\delta\bar{\mathbf{u}}^0\right\|_E^2 + \frac{c}{2\,E_0}\sum_{j=0}^{n+1}\frac{\tau_{j-1}+\tau_j}{2}\left\|\delta\mathbf{u}^j\right\|_a^2 + \frac{c}{2}\sum_{j=0}^{n+1}\frac{\tau_{j-1}+\tau_j}{2}\left\|\delta\mathbf{u}^j\right\|_{\mathbf{L}_2}^2 \\
&\quad + V_0(1-\tilde{\alpha})\sum_{j=0}^{n+1}\frac{\tau_{j-1}+\tau_j}{2}\left\|\delta\dot{\mathbf{u}}^j\right\|_{\mathbf{L}_2}^2
\end{aligned}$$

holds with $\tau_{-1} := 0$ and $\tau_{n+1} := 0$. Using Remark 4.1.5 again, the displacements can be written as

$$\delta\mathbf{u}^j = \delta\mathbf{u}^{j-1} + \tau_{j-1}\delta\frac{\dot{\mathbf{u}}^{j-1}+\dot{\mathbf{u}}^j}{2} = \delta\mathbf{u}^0 + \sum_{i=1}^{j}\tau_{i-1}\delta\frac{\dot{\mathbf{u}}^{i-1}+\dot{\mathbf{u}}^i}{2} = \delta\mathbf{u}^0 + \sum_{i=0}^{j}\frac{\tau_{i-1}+\tau_i}{2}\dot{\mathbf{u}}^i$$

for $\tau_{-1} := 0$ and $\tau_j := 0$, and the inequalities of Young and Cauchy-Schwarz lead to

$$\begin{aligned}
\left\|\delta\mathbf{u}^j\right\|_{\mathbf{L}_2}^2 &\leq \left(\left\|\delta\mathbf{u}^0\right\|_{\mathbf{L}_2} + \sum_{i=0}^{j} \frac{\tau_{i-1}+\tau_i}{2}\left\|\delta\dot{\mathbf{u}}^i\right\|_{\mathbf{L}_2}\right)^2 \\
&\leq 2\Big(\left\|\delta\mathbf{u}^0\right\|_{\mathbf{L}_2}^2 + \Big(\sum_{i=0}^{j} \frac{\tau_{i-1}+\tau_i}{2}\left\|\delta\dot{\mathbf{u}}^i\right\|_{\mathbf{L}_2}\Big)^2\Big) \\
&\leq 2\Big(\left\|\delta\mathbf{u}^0\right\|_{\mathbf{L}_2}^2 + \Big(\sum_{i=0}^{j} \frac{\tau_{i-1}+\tau_i}{2}\Big)\Big(\sum_{i=0}^{j} \frac{\tau_{i-1}+\tau_i}{2}\left\|\delta\dot{\mathbf{u}}^i\right\|_{\mathbf{L}_2}^2\Big)\Big) \\
&\leq 2\Big(\left\|\delta\mathbf{u}^0\right\|_{\mathbf{L}_2}^2 + t_j \sum_{i=0}^{j} \frac{\tau_{i-1}+\tau_i}{2}\left\|\delta\dot{\mathbf{u}}^i\right\|_{\mathbf{L}_2}^2\Big)\,.
\end{aligned}$$

This estimate yields

$$\begin{aligned}
&\left\|\delta\bar{\mathbf{u}}^{n+1}\right\|_E^2 + \tilde{\alpha}\sum_{j=0}^{n}\tau_j\left\|\delta\frac{\mathbf{u}^{j+1}-\mathbf{u}^j}{\tau_j}\right\|_b^2 \\
&\leq \left\|\delta\bar{\mathbf{u}}^0\right\|_E^2 + ct_{n+1}\left\|\delta\mathbf{u}^0\right\|_{\mathbf{L}_2}^2 + \frac{c}{2\,E_0}\sum_{j=0}^{n+1}\frac{\tau_{j-1}+\tau_j}{2}\left\|\delta\mathbf{u}^j\right\|_a^2 \\
&\quad + (ct_{n+1}^2 + V_0(1-\tilde{\alpha}))\sum_{j=0}^{n+1}\frac{\tau_{j-1}+\tau_j}{2}\left\|\delta\dot{\mathbf{u}}^j\right\|_{\mathbf{L}_2}^2 \\
&\leq \left\|\delta\bar{\mathbf{u}}^0\right\|_E^2 + ct_{n+1}\left\|\delta\mathbf{u}^0\right\|_{\mathbf{L}_2}^2 + \tilde{\kappa}^2\sum_{j=0}^{n+1}\frac{\tau_{j-1}+\tau_j}{2}\left\|\delta\bar{\mathbf{u}}^j\right\|_E^2
\end{aligned}$$

with

$$\tilde{\kappa}^2 = \max\Big(\frac{c}{2E_0}, ct_{n+1}^2 + V_0(1-\tilde{\alpha})\Big)\,.$$

Shifting the error components of index $n+1$ on the right-hand side of the inequality to the left-hand side gives

$$\begin{aligned}
&\Big(1-\tilde{\kappa}^2\frac{\tau_n}{2}\Big)\left\|\delta\bar{\mathbf{u}}^{n+1}\right\|_E^2 + \tilde{\alpha}\sum_{j=0}^{n}\tau_j\left\|\delta\frac{\mathbf{u}^{j+1}-\mathbf{u}^j}{\tau_j}\right\|_b^2 \\
&\leq \left\|\delta\bar{\mathbf{u}}^0\right\|_E^2 + ct_{n+1}\left\|\delta\mathbf{u}^0\right\|_{\mathbf{L}_2}^2 + \tilde{\kappa}^2\sum_{j=0}^{n}\frac{\tau_{j-1}+\tau_j}{2}\left\|\delta\bar{\mathbf{u}}^j\right\|_E^2\,.
\end{aligned}$$

Assume that the timesteps τ_j are bounded by $\tau_\triangle$ for all $j = 0, \ldots, N_\triangle - 1$. Now, let ε or $\tau_\triangle$ be such small that the left-hand side of the expression is positive, i.e.,

$$\tilde{\kappa}^2\frac{\tau_\triangle}{2} < 1\,. \tag{5.17}$$

After dividing the whole estimate by $1 - \tilde{\kappa}^2 \frac{\tau_n}{2}$, the discrete Gronwall inequality presented in Appendix A can be applied, which leads to

$$\begin{aligned}
&\left\|\delta\bar{\mathbf{u}}^{n+1}\right\|_E^2 + \left(1 - \tilde{\kappa}^2\frac{\tau_n}{2}\right)^{-1} \tilde{\alpha} \sum_{j=0}^{n} \tau_j \left\|\delta\frac{\mathbf{u}^{j+1} - \mathbf{u}^j}{\tau_j}\right\|_b^2 \\
&\leq \left(\left\|\delta\bar{\mathbf{u}}^0\right\|_E^2 + ct_{n+1}\left\|\delta\mathbf{u}^0\right\|_{\mathbf{L}_2}^2\right) \cdot \left(1 - \tilde{\kappa}^2\frac{\tau_n}{2}\right)^{-1} e^{\left(1-\tilde{\kappa}^2\frac{\tau_n}{2}\right)^{-1}\tilde{\kappa}^2(t_{n+1}-\frac{\tau_n}{2})}.
\end{aligned}$$

By means of

$$1 \leq \left(1 - \tilde{\kappa}^2\frac{\tau_n}{2}\right)^{-1} = 1 + \frac{\tilde{\kappa}^2\frac{\tau_n}{2}}{1 - \tilde{\kappa}^2\frac{\tau_n}{2}} \leq e^{\frac{\tilde{\kappa}^2\frac{\tau_n}{2}}{1-\tilde{\kappa}^2\frac{\tau_n}{2}}},$$

the perturbation result

$$\left\|\delta\bar{\mathbf{u}}^{n+1}\right\|_E^2 + \tilde{\alpha} \sum_{j=0}^{n} \tau_j \left\|\delta\frac{\mathbf{u}^{j+1} - \mathbf{u}^j}{\tau_j}\right\|_b^2 \leq \left(\left\|\delta\bar{\mathbf{u}}^0\right\|_E^2 + ct_{n+1}\left\|\delta\mathbf{u}^0\right\|_{\mathbf{L}_2}^2\right) e^{\left(1-\tilde{\kappa}^2\frac{\tau_\triangle}{2}\right)^{-1}\tilde{\kappa}^2 t_{n+1}}$$

holds. □

5.2. Convergence

The present section is dedicated to the issue of global convergence of the improved contact–stabilized Newmark method both in physical energy norm and in discrete displacement norm. Together with the consistency results of Chapter 4, the discrete perturbation estimates for the Newmark scheme in the previous section ultimately provide the necessary preparations.

The common proof technique of convergence for time discretizations of evolution problems utilizes the classical *"Lady Windermere's Fan"* by Hairer, Nørsett, and Wanner [34] sketched in Figure 5.1. Thereby, the global discretization error $\bar{\mathbf{u}}^{N_\triangle} - \bar{\mathbf{u}}(T)$ of an algorithm is regarded as the sum of the red-marked local errors transported along the exact solution curves. This makes the approach dependent on a perturbation result for the solution of the differential equality. The local errors can be interpreted as consistency errors between the discretization scheme and the continuous problem with different initial values, which are given by the discrete trajectory. For dynamical contact modeled by Signorini's conditions, however, each initial value problem may exhibit high irregularities in the small timestep of interest. In the worst case, the total variations of the solutions and its derivatives do not even tend to zero for decreasing time intervals. Then, the consistency result for Newmark schemes in Chapter 4 yields only order 1/2 for the relevant local errors in physical energy norm. Summing up the local error contributions leads to an estimate for the global error, which is one order below the local one. Hence, the classical theory is

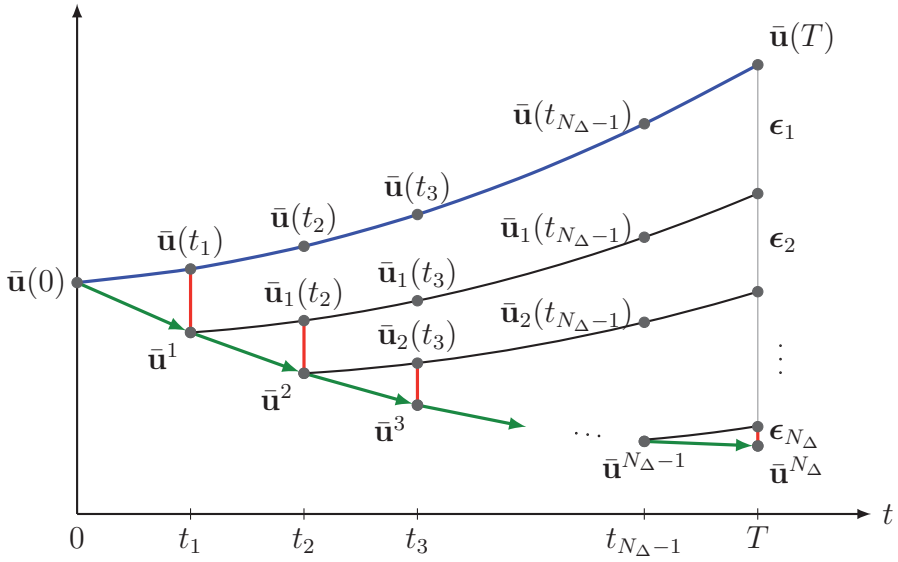

Figure 5.1.: Global error estimation along the discrete trajectory (blue: exact solution, green: numerical solution).

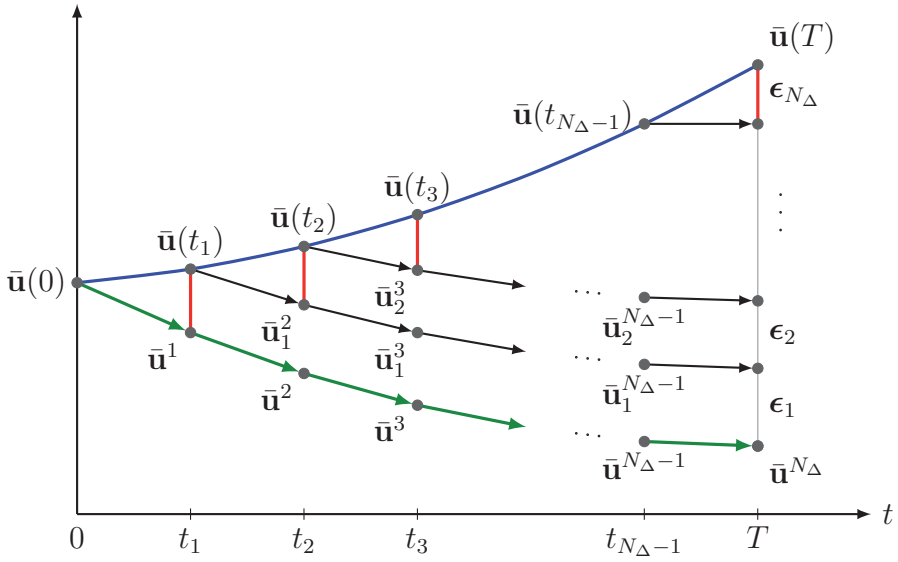

Figure 5.2.: Global error estimation along the exact trajectory (blue: exact solution, green: discrete solution).

not appropriate to prove convergence of the Newmark methods under consideration for dynamical contact.

In contrast, the second version of Lady Windermere's Fan [34] outlined in Figure 5.2 performs the "error transport" along the numerical method. This proof technique requires a perturbation result for the time discretization, which has been analyzed for Newmark schemes in the previous section. The approach estimates the global discretization error against a sum of local errors occurring along the exact trajectory, which are again highlighted in red. The local errors are the consistency errors between the time integration and the original evolution problem at every single timepoint of the mesh. Due to the assumption of bounded variation on the solution of the dynamical contact problem, the local discretization errors of the Newmark methods are of minimal order 1/2 only at countably many timepoints, cf. Chapter 4. These discrete critical timepoints do not alter the global convergence behavior since the local error contributions sum up in a very special way (for a more precise mathematical argumentation see the introduction of Section 5.2.1). In particular, the algorithm can be proven to converge with rate 1/2. In the following two sections, the modified proof technique will be applied to the issue of convergence for the improved contact–stabilized Newmark method in the presence of contact.

The following notations for a global error analysis make use of the continuous and discrete evolution operators $\bar{\mathbf{\Phi}}$ and $\bar{\mathbf{\Psi}}$.

Notations. With respect to a mesh $\triangle$ of adaptive timesteps, the *lattice function*

$$\bar{\mathbf{u}}_{\triangle} := (\mathbf{u}_{\triangle}, \dot{\mathbf{u}}_{\triangle}) : \triangle \longrightarrow \mathbf{H}^1 \times \mathbf{L}_2 \tag{5.18}$$

of a discretization is defined as

$$\mathbf{u}_{\triangle}(t_{n+1}) = \mathbf{\Psi}^{t_{n+1},t_n} \bar{\mathbf{u}}_{\triangle}(t_n)\,, \qquad \dot{\mathbf{u}}_{\triangle}(t_{n+1}) = \dot{\mathbf{\Psi}}^{t_{n+1},t_n} \bar{\mathbf{u}}_{\triangle}(t_n) \tag{5.19}$$

with

$$\mathbf{u}_{\triangle}(t_0) = \mathbf{u}^0\,, \qquad \dot{\mathbf{u}}_{\triangle}(t_0) = \dot{\mathbf{u}}^0\,. \tag{5.20}$$

Let

$$\boldsymbol{\epsilon}_{\triangle}(\bar{\mathbf{u}}, t) = (\boldsymbol{\epsilon}_{\triangle}(\mathbf{u}, t), \boldsymbol{\epsilon}_{\triangle}(\dot{\mathbf{u}}, t)) \tag{5.21}$$

denote the *global error*, where

$$\boldsymbol{\epsilon}_{\triangle}(\mathbf{u}, t) := \mathbf{u}_{\triangle}(t) - \mathbf{u}(t) \tag{5.22}$$

is the *global error in position variables* and

$$\boldsymbol{\epsilon}_{\triangle}(\dot{\mathbf{u}}, t) := \dot{\mathbf{u}}_{\triangle}(t) - \dot{\mathbf{u}}(t) \tag{5.23}$$

is the *global error in velocity variables*. For a mesh of equidistant timesteps, the notations $\bar{\mathbf{u}}_\tau = \big(\mathbf{u}_\tau, \dot{\mathbf{u}}_\tau\big)$ and $\boldsymbol{\epsilon}_\tau(\bar{\mathbf{u}}, t) = \big(\boldsymbol{\epsilon}_\tau(\bar{\mathbf{u}}, t), \boldsymbol{\epsilon}_\tau(\bar{\mathbf{u}}, t)\big)$ are used.

5.2.1. Convergence in Physical Energy Norm

First, the proof technique sketched above will be applied to derive an estimate for the global discretization error of (N-CI/CS(+)) in physical energy norm, which yields convergence of the scheme in the presence of contact.

In order to point out the underlying idea of the novel convergence theory, the approach will be described in more mathematical detail here. As explained above, the global error is estimated against the sum of local discretization errors between the Newmark scheme and the dynamical contact problem via a discrete perturbation estimate, compare Figure 5.2. Due to the consistency result in Chapter 4, these local errors are bounded by the quantity $R(\mathbf{u}, [t, t+\tau])$ multiplied by $\tau^{1/2}$ in physical energy norm. At this point, the telescoping property (4.21) of the total variation is essential. Since the total variations of the solution and its derivatives sum up over the whole time interval, the relation

$$\sum_{i=1}^{N_\triangle} R(\mathbf{u}, [t_{i-1}, t_i]) = R(\mathbf{u}, [0, T])$$

holds. Hence, the global discretization error can be estimated against $R(\mathbf{u}, [0, T])$ multiplied by $\tau^{1/2}$, which gives rise to convergence of (N-CI/CS(+)) with order 1/2. In summary, the novel proof technique primarily takes advantage of the telescoping property of the consistency errors, which ensures that no order is lost for convergence in the presence of contact.

In physical energy norm, the proof of convergence for (N-CI/CS(+)) can be performed in the general case of non-equidistant timesteps. Hence, a bound of the timestep sizes is required, i.e.,

$$\tau_j \leq \tau_\triangle \,, \qquad \text{for all } j = 0, \ldots, N_\triangle - 1 \,. \tag{5.24}$$

The following theorem contains the main convergence result of this chapter.

Theorem 5.2.1. *Let Assumption* 4.2.4 *and Assumption* (5.24) *hold. Furthermore, assume that Theorem 5.1.7 with* $\alpha \in [0, 1)$*, is valid. Then, for initial values* $\mathbf{u}^0 = \mathbf{u}(0)$ *and* $\dot{\mathbf{u}}^0 = \dot{\mathbf{u}}(0)$*, the global error* $\boldsymbol{\epsilon}_\triangle(\bar{\mathbf{u}}, T) = (\boldsymbol{\epsilon}_\triangle(\mathbf{u}, T), \boldsymbol{\epsilon}_\triangle(\dot{\mathbf{u}}, T))$ *of* (N-CI/CS(+)) *satisfies*

$$\Big(\|\boldsymbol{\epsilon}_\triangle(\bar{\mathbf{u}}, T)\|_E^2 + \alpha \sum_{j=1}^{N_\triangle} \tau_{j-1} \Big\| \frac{\boldsymbol{\epsilon}_\triangle(\mathbf{u}, t_j) - \boldsymbol{\epsilon}_\triangle(\mathbf{u}, t_{j-1})}{\tau_{j-1}} \Big\|_b^2 \Big)^{1/2} = O\big(\tau_\triangle^{1/2}\big) \,. \tag{5.25}$$

Proof. Following the notation of Figure 5.2, the global discretization error of (N-CI/CS(+)) measured in physical energy norm is split up via

$$\Big(\|\boldsymbol{\epsilon}_\triangle(\bar{\mathbf{u}},T)\|_E^2+\alpha\sum_{j=1}^{N_\triangle}\tau_{j-1}\Big\|\frac{\boldsymbol{\epsilon}_\triangle(\mathbf{u},t_j)-\boldsymbol{\epsilon}_\triangle(\mathbf{u},t_{j-1})}{\tau_{j-1}}\Big\|_b^2\Big)^{1/2}$$
$$\leq\sum_{i=1}^{N_\triangle}\Big(\|\boldsymbol{\epsilon}_i(\bar{\mathbf{u}},T)\|_E^2+\alpha\sum_{j=i+1}^{N_\triangle}\tau_{j-1}\Big\|\frac{\mathbf{u}_i^j-\mathbf{u}_i^{j-1}}{\tau_{j-1}}-\frac{\mathbf{u}_{i-1}^j-\mathbf{u}_{i-1}^{j-1}}{\tau_{j-1}}\Big\|_b^2\Big)^{1/2}.$$

Here, the discrete perturbation result in physical energy norm, cf. Theorem 5.1.7, leads to the estimate

$$\Big(\|\boldsymbol{\epsilon}_i(\bar{\mathbf{u}},T)\|_E^2+\alpha\sum_{j=i+1}^{N_\triangle}\tau_{j-1}\Big\|\frac{\mathbf{u}_i^j-\mathbf{u}_i^{j-1}}{\tau_{j-1}}-\frac{\mathbf{u}_{i-1}^j-\mathbf{u}_{i-1}^{j-1}}{\tau_{j-1}}\Big\|_b^2\Big)^{1/2}$$
$$\leq\big(\|\boldsymbol{\epsilon}(t_{i-1},\bar{\mathbf{u}},\tau_{i-1})\|_E^2+c(T-t_{i-1})\|\boldsymbol{\epsilon}(t_{i-1},\mathbf{u},\tau_{i-1})\|_{\mathbf{L}_2}^2\big)^{1/2}e^{\frac{\tilde{\kappa}^2}{2}(T-t_{i-1})}$$
$$\leq\big(\|\boldsymbol{\epsilon}(t_{i-1},\bar{\mathbf{u}},\tau_{i-1})\|_E+c^{1/2}T^{1/2}\|\boldsymbol{\epsilon}(t_{i-1},\mathbf{u},\tau_{i-1})\|_{\mathbf{L}_2}\big)e^{\frac{\tilde{\kappa}^2}{2}T},$$

where a norm inequality has been used in the last line. Taking both estimates together, Theorem 4.2.6 and Theorem 4.3.3 concerning the consistency error of (N-CI/CS(+)) yield

$$\Big(\|\boldsymbol{\epsilon}_\triangle(\bar{\mathbf{u}},T)\|_E^2+\alpha\sum_{j=1}^{N_\triangle}\tau_{j-1}\Big\|\frac{\boldsymbol{\epsilon}_\triangle(\mathbf{u},t_j)-\boldsymbol{\epsilon}_\triangle(\mathbf{u},t_{j-1})}{\tau_{j-1}}\Big\|_b^2\Big)^{1/2}$$
$$\leq\sum_{i=1}^{N_\triangle}\Big(\|\boldsymbol{\epsilon}(t_{i-1},\bar{\mathbf{u}},\tau_{i-1})\|_E+c^{1/2}T^{1/2}\|\boldsymbol{\epsilon}(t_{i-1},\mathbf{u},\tau_{i-1})\|_{\mathbf{L}_2}\Big)e^{\frac{\tilde{\kappa}^2}{2}T}$$
$$=\big(O\big(\tau_\triangle^{1/2}\big)+O\big(\tau_\triangle^{3/2}\big)\big)\cdot\sum_{i=1}^{N_\triangle}R(\mathbf{u},[t_{i-1},t_i]).$$

Finally, the telescoping property (4.21) of the total variations gives

$$\Big(\|\boldsymbol{\epsilon}_\triangle(\bar{\mathbf{u}},T)\|_E^2+\alpha\sum_{j=1}^{N_\triangle}\tau_{j-1}\Big\|\frac{\boldsymbol{\epsilon}_\triangle(\mathbf{u},t_j)-\boldsymbol{\epsilon}_\triangle(\mathbf{u},t_{j-1})}{\tau_{j-1}}\Big\|_b^2\Big)^{1/2}$$
$$=\big(O\big(\tau_\triangle^{1/2}\big)+O\big(\tau_\triangle^{3/2}\big)\big)\cdot R(\mathbf{u},[0,T])$$
$$=O\big(\tau_\triangle^{1/2}\big),$$

which is the convergence result of the theorem. □

The result presented above shows that, in physical energy norm, (N-CI/CS(+)) converges with rate 1/2 to a solution of the dynamical contact problem in function

space. In particular, the convergence holds in $\mathbf{L}_2$-norm for the velocities and in a-norm for the displacements. The third term on the left-hand side of (5.25) contains the finite differences in displacements measured in b-norm and summed up over the time interval. This part of the global error estimate represents the viscous error component scaled by an unknown factor α, which is given by the perturbation result in physical energy norm and may be even zero. Hence, the last term does not necessarily provide further information on the convergence of the scheme.

5.2.2. Convergence in Discrete Displacement Norm

Next, the global convergence of (N-CI/CS(+)) will be proven in the discrete displacement norm for an equidistant mesh of timesteps. For this purpose, the same concept will be utilized as in physical energy norm, which is based on the telescoping property of the consistency errors of the algorithm.

Theorem 5.1.3 contains a perturbation result for (N-CI/CS(+)) in discrete displacement norm, which still depends on the stability of the velocities of the scheme. Therefore, the discrete perturbation Theorem 5.1.7 in physical energy norm will be inserted into this result at first.

Lemma 5.2.2. *Let* $\bar{\mathbf{u}}^{j+1} = (\mathbf{u}^{j+1}, \dot{\mathbf{u}}^{j+1})$ *and* $\bar{\tilde{\mathbf{u}}}^{j+1} = (\tilde{\mathbf{u}}^{j+1}, \dot{\tilde{\mathbf{u}}}^{j+1})$ *be two solutions of* (N-CI/CS(+)) *with initial values* $\mathbf{u}^0$, $\dot{\mathbf{u}}^0$ *and* $\tilde{\mathbf{u}}^0$, $\dot{\tilde{\mathbf{u}}}^0$. *Then,*

$$\left\|\delta\mathbf{u}^{n+1}\right\|_\tau \leq \left(1 + c^{1/2}T^{3/2}e^{\frac{\tilde{\kappa}^2}{2}T}\right)\left\|\delta\mathbf{u}^0\right\|_\tau + Te^{\frac{\tilde{\kappa}^2}{2}T}\left\|\delta\bar{\mathbf{u}}^0\right\|_E$$

with $c \geq 0$ *and* $\tilde{\kappa} \geq 0$.

Proof. The discrete perturbation result of Theorem 5.1.7 in physical energy norm leads to

$$\begin{aligned}\left\|\delta\bar{\mathbf{u}}^i\right\|_E &\leq \left(\left\|\delta\bar{\mathbf{u}}^0\right\|_E^2 + ct_i\left\|\delta\mathbf{u}^0\right\|_{\mathbf{L}_2}^2\right)^{1/2} e^{\frac{\tilde{\kappa}^2}{2}t_i} \\ &\leq \left\|\delta\bar{\mathbf{u}}^0\right\|_E + c^{1/2}T^{1/2}\left\|\delta\mathbf{u}^0\right\|_{\mathbf{L}_2} e^{\frac{\tilde{\kappa}^2}{2}T}\end{aligned}$$

for all $i \in \{0, \ldots, n\}$ by means of a simple norm inequality. Inserting this estimate into the perturbation Theorem 5.1.3 in discrete displacement norm yields

$$\begin{aligned}\left\|\delta\mathbf{u}^{n+1}\right\|_\tau &\leq \left\|\delta\mathbf{u}^j\right\|_\tau + \tau\sum_{i=0}^{n}\left\|\delta\bar{\mathbf{u}}^i\right\|_E \\ &\leq \left\|\delta\mathbf{u}^0\right\|_\tau + (n+1)\tau\cdot\left\|\delta\bar{\mathbf{u}}^0\right\|_E e^{\frac{\tilde{\kappa}^2}{2}T} + (n+1)\tau\cdot c^{1/2}T^{1/2}\left\|\delta\mathbf{u}^0\right\|_{\mathbf{L}_2} e^{\frac{\tilde{\kappa}^2}{2}T} \\ &\leq \left(1 + c^{1/2}T^{3/2}e^{\frac{\tilde{\kappa}^2}{2}T}\right)\left\|\delta\mathbf{u}^0\right\|_\tau + Te^{\frac{\tilde{\kappa}^2}{2}T}\left\|\delta\bar{\mathbf{u}}^0\right\|_E.\end{aligned}$$

□

The perturbation result finally allows proving the convergence of (N-CI/CS(+)) in discrete displacement norm.

Theorem 5.2.3. *Let Assumption* 4.2.4 *hold, and assume that Theorem 5.1.7 is valid. Then, for initial values* $\mathbf{u}^0 = \mathbf{u}(0)$ *and* $\dot{\mathbf{u}}^0 = \dot{\mathbf{u}}(0)$*, the global error of* (N-CI/CS(+)) *satisfies*

$$\|\boldsymbol{\epsilon}_\tau(\mathbf{u}, T)\|_\tau = O\big(\tau^{1/2}\big)\,. \tag{5.26}$$

Proof. Following the same approach as in the proof of Theorem 5.2.1, the global discretization error of (N-CI/CS(+)) in discrete displacement norm is split up via

$$\|\boldsymbol{\epsilon}_\tau(\mathbf{u}, T)\|_\tau \leq \sum_{i=1}^{N} \|\boldsymbol{\epsilon}_i(\mathbf{u}, T)\|_\tau$$

using the notations of Figure 5.2. Applying the discrete perturbation Lemma 5.2.2 in discrete displacement norm on every single error component yields

$$\|\boldsymbol{\epsilon}_\tau(\mathbf{u}, T)\|_\tau \leq \sum_{i=1}^{N} \Big(\big(1 + c^{1/2} T^{3/2} e^{\frac{\tilde{\kappa}^2}{2} T}\big) \|\epsilon(t_{i-1}, \mathbf{u}, \tau)\|_\tau + T e^{\frac{\tilde{\kappa}^2}{2} T} \|\epsilon(t_{i-1}, \bar{\mathbf{u}}, \tau)\|_E \Big)\,.$$

The estimates for the consistency error in physical energy norm and discrete displacement norm, cf. Theorem 4.2.6 and Theorem 4.3.3, lead to

$$\|\boldsymbol{\epsilon}_\tau(\mathbf{u}, T)\|_\tau = \big(O\big(\tau^{3/2}\big) + O\big(\tau^{1/2}\big)\big) \cdot \sum_{i=1}^{N} R(\mathbf{u}, [t_{i-1}, t_i])\,.$$

By means of the telescoping property (4.21) of the total variations

$$\|\boldsymbol{\epsilon}_\tau(\mathbf{u}, T)\|_\tau = \big(O\big(\tau^{3/2}\big) + O\big(\tau^{1/2}\big)\big) \cdot R(\mathbf{u}, [0, T]) = O\big(\tau^{1/2}\big)\,,$$

which is the desired estimate for the global discretization error. □

The convergence of (N-CI/CS(+)) turns out to have identical order in discrete displacement norm and in physical energy norm. This is due to the evolutionary structure of dynamical contact problems, which causes a dependence of the global discretization error in displacements on the error in velocities. Actually, the convergence order of displacements measured in $\mathbf{L}_2$-norm is in principle restricted by the order of the velocities in $\mathbf{L}_2$-norm, which is usually lower.

The presented result shows global convergence of the displacements in $\mathbf{L}_2$-norm with rate 1/2. The discrete displacement norm does not contribute to any convergence of the displacements in a-norm or b-norm due to the scaling of these error contributions with timestep size. By means of Korn's inequality, the estimates for the global error in displacements measured in $\mathbf{L}_2$-norm and a-norm can be combined to find convergence of the displacements in $\mathbf{H}^1$-norm with identical order 1/2. The following corollary summarizes the insight on the global convergence of (N-CI/CS(+)) in displacements and velocities gained in this chapter.

Corollary 5.2.4. *Let Assumption* 4.2.4 *hold, and assume that Theorem 5.1.7 is valid. Then, for initial values* $\mathbf{u}^0 = \mathbf{u}(0)$ *and* $\dot{\mathbf{u}}^0 = \dot{\mathbf{u}}(0)$*, the global error of* (N-CI/CS(+)) *satisfies*

$$\|\boldsymbol{\epsilon}_\tau(\dot{\mathbf{u}}, t)\|_{\mathbf{L}_2} = O\big(\tau^{1/2}\big) \tag{5.27}$$

and

$$\|\boldsymbol{\epsilon}_\tau(\mathbf{u}, t)\|_{\mathbf{H}^1} = O\big(\tau^{1/2}\big)\,. \tag{5.28}$$

Proof. The first estimate follows directly from Theorem 5.2.1. For the second estimate, Korn's inequality (A.1) is applied to find

$$\|\boldsymbol{\epsilon}_\tau(\mathbf{u}, t)\|_{\mathbf{H}^1} \leq C\big(\|\boldsymbol{\epsilon}_\tau(\mathbf{u}, t)\|_{\mathbf{L}_2}^2 + \|\boldsymbol{\epsilon}_\tau(\mathbf{u}, t)\|_a^2\big)^{1/2} = O\big(\tau^{1/2}\big)\,,$$

where Theorem 5.2.1 and Theorem 5.2.3 have been used. □

6. Adaptive Timestep Control

In view of dynamical contact problems appearing in real life applications as, e.g., the motion of a human knee, an adaptive timestep control is of crucial importance in order to increase the efficiency of the time integration. Phases of active contact and, especially, moments when the two bodies get into or leave contact necessitate a much higher temporal resolution than phases without any active contact. The aim of this chapter is to work out such a device for the improved contact–stabilized Newmark method [52].

The construction of an adaptive timestep control requires a realistic estimation of the local discretization error (cf., e.g., the textbook [18]). For this purpose, the physical energy norm will be exploited due to the perturbation result in the presence of contact derived in Chapter 3. In order to construct a comparative scheme of higher-order accuracy measured in this norm, extrapolation techniques will be extended. This approach demands the existence of an asymptotic error expansion of the local discretization error. In Section 6.1, an asymptotic error expansion of the improved contact–stabilized Newmark method will be analyzed theoretically as well as numerically. In Section 6.2, a problem-adapted error estimator and a suitable timestep selection (called ContacX[1]) will be suggested, which also cover the presence of contact. These techniques are based on the consistency order of the improved contact–stabilized Newmark method as analyzed in Chapter 4. Finally, the actually achieved global discretization error of the adaptive timestep control will be estimated in Section 6.3.

As proven in Section 4.1, the (improved) contact–stabilized Newmark method coincides with the contact–implicit Newmark scheme by Kane et al. [46] in function space. Since this thesis uses the method of time layers, the numerical analysis in this chapter covers all three Newmark methods simultaneously. Nevertheless, the considerations are restricted to the improved contact–stabilized Newmark method due to its nice numerical features, compare Chapter 2.

6.1. Towards an Asymptotic Error Expansion

The main challenge for an adaptive timestep control is the construction of a suitable error estimator. Usually, the numerical integrator of interest is compared to a

[1] by convention, 'X' stands for extrapolation.

second, higher-order discrete evolution. The construction of such a scheme can be performed by means of extrapolation techniques, which are based on an asymptotic error expansion. The scope of this section is to analyze the existence of such an error representation for the improved contact–stabilized Newmark method.

6.1.1. Conical Derivative

An asymptotic error expansion of the improved contact–stabilized Newmark method requires well-posedness results of (N-CS+) with respect to perturbations of the initial data. Here, known results concerning the sensitivity of the scheme from [73] are recalled.

In [73], an important result has been given that concerns the directional differentiability of the solution $\mathbf{u} = \mathbf{u}(\mathbf{f}) \in \mathcal{K}$ of an elliptic variational inequality

$$a(\mathbf{u}, \mathbf{v} - \mathbf{u}) \geq \langle \mathbf{f}, \mathbf{v} - \mathbf{u} \rangle_{\mathbf{V}^* \times \mathbf{V}}\,, \qquad \forall\, \mathbf{v} \in \mathcal{K}$$

on a Hilbert space $\mathbf{V}$. The convex set $\mathcal{K}$ is of the form $\mathcal{K} = \{\mathbf{w} \in \mathbf{V} \,|\, \mathbf{w} \leq \mathbf{g} \text{ a.e.}\}$ with $\mathbf{g}$ continuous, $a(\cdot,\cdot)$ has to fulfill usual ellipticity and continuity assumptions, and $\mathbf{f} \in \mathbf{V}^*$. Then, the mapping $\mathbf{f} \longrightarrow \mathbf{u}(\mathbf{f})$ has a conical derivative $\mathbf{Du}(\mathbf{f})(\cdot)$ on $\mathbf{V}^*$, and $\mathbf{Du}(\mathbf{f})(\mathbf{w}) \in \tilde{\mathcal{K}}^{\mathbf{u}}$ is the solution of the variational inequality

$$a(\mathbf{Du}(\mathbf{f})(\mathbf{w}), \mathbf{v} - \mathbf{Du}(\mathbf{f})(\mathbf{w})) \geq \langle \mathbf{w}, \mathbf{v} - \mathbf{Du}(\mathbf{f})(\mathbf{w}) \rangle_{\mathbf{V}^* \times \mathbf{V}}\,, \qquad \forall\, \mathbf{v} \in \tilde{\mathcal{K}}^{\mathbf{u}}$$

with a modified admissible set

$$\tilde{\mathcal{K}}^{\mathbf{u}} = \{\mathbf{w} \in \mathbf{V} \,|\, \mathbf{w} \leq 0 \text{ if } \mathbf{u} = \mathbf{g},\ a(\mathbf{u}, \mathbf{w}) = \langle \mathbf{f}, \mathbf{w} \rangle_{\mathbf{V}^* \times \mathbf{V}}\}\,.$$

The transfer of this insight to (N-CS+) yields the following sensitivity result.

Theorem 6.1.1 ([73]). *The discrete evolution operator possesses a* conical derivative $\bar{\mathbf{D}}\boldsymbol{\Psi}^{t+\tau,t} := \left(\mathbf{D}\boldsymbol{\Psi}^{t+\tau,t}, \dot{\mathbf{D}}\boldsymbol{\Psi}^{t+\tau,t}\right)$*, i.e.,*

$$\boldsymbol{\Psi}^{t+\tau,t}(\bar{\mathbf{u}} + h\bar{\mathbf{w}}) = \boldsymbol{\Psi}^{t+\tau,t}\bar{\mathbf{u}} + h\mathbf{D}\boldsymbol{\Psi}^{t+\tau,t}\bar{\mathbf{u}}(\bar{\mathbf{w}}) + \boldsymbol{\theta}(h, \bar{\mathbf{w}})$$

and

$$\dot{\boldsymbol{\Psi}}^{t+\tau,t}(\bar{\mathbf{u}} + h\bar{\mathbf{w}}) = \dot{\boldsymbol{\Psi}}^{t+\tau,t}\bar{\mathbf{u}} + h\dot{\mathbf{D}}\boldsymbol{\Psi}^{t+\tau,t}\bar{\mathbf{u}}(\bar{\mathbf{w}}) + \frac{2}{\tau}\boldsymbol{\theta}(h, \bar{\mathbf{w}})$$

where

$$\lim_{h \to 0} \|\boldsymbol{\theta}(h, \bar{\mathbf{w}})\|_{\mathbf{H}^1}/h = 0$$

for all $h > 0$ and $\bar{\mathbf{u}} = (\mathbf{u}, \dot{\mathbf{u}})\,, \bar{\mathbf{w}} = (\mathbf{w}, \dot{\mathbf{w}}) \in \mathbf{H}^1 \times \mathbf{L}_2$. The conical derivative is given as the solution of

$$
\begin{aligned}
0 &\in \mathbf{w}_{\mathrm{pred}} - (\mathbf{w} + \tau\dot{\mathbf{w}}) + \partial I_{\tilde{\mathcal{K}}^{\mathbf{D}\boldsymbol{\Psi}^{t+\tau,t}\bar{\mathbf{u}}}}(\mathbf{w}_{\mathrm{pred}}) \\
0 &\in \mathbf{D}\boldsymbol{\Psi}^{t+\tau,t}\bar{\mathbf{u}}(\bar{\mathbf{w}}) - \mathbf{w}_{\mathrm{pred}} + \frac{1}{2}\tau^2\Big(\mathbf{F}\Big(\tfrac{\mathbf{w}+\mathbf{D}\boldsymbol{\Psi}^{t+\tau,t}\bar{\mathbf{u}}(\bar{\mathbf{w}})}{2}\Big) + \mathbf{G}\Big(\tfrac{\mathbf{D}\boldsymbol{\Psi}^{t+\tau,t}\bar{\mathbf{u}}(\bar{\mathbf{w}})-\mathbf{w}}{\tau}\Big) \\
&\qquad + \partial I_{\tilde{\mathcal{K}}^{\mathbf{D}\boldsymbol{\Psi}^{t+\tau,t}\bar{\mathbf{u}}}}\big(\mathbf{D}\boldsymbol{\Psi}^{t+\tau,t}\bar{\mathbf{v}}(\bar{\mathbf{w}})\big)\Big) \qquad (6.1) \\
\dot{\mathbf{D}}\boldsymbol{\Psi}^{t+\tau,t}\bar{\mathbf{u}}(\bar{\mathbf{w}}) &= \dot{\mathbf{w}} - \tau\Big(\mathbf{F}\Big(\tfrac{\mathbf{w}+\mathbf{D}\boldsymbol{\Psi}^{t+\tau,t}\bar{\mathbf{u}}(\bar{\mathbf{w}})}{2}\Big) + \mathbf{G}\Big(\tfrac{\mathbf{D}\boldsymbol{\Psi}^{t+\tau,t}\bar{\mathbf{u}}(\bar{\mathbf{w}})-\mathbf{w}}{\tau}\Big) \\
&\qquad - \mathbf{F}_{\mathrm{con}}\big(\mathbf{D}\boldsymbol{\Psi}^{t+\tau,t}\bar{\mathbf{u}}(\bar{\mathbf{w}})\big)\Big)
\end{aligned}
$$

with contact forces

$$
\begin{aligned}
&\frac{\tau^2}{2}\big\langle \mathbf{F}_{\mathrm{con}}\big(\mathbf{D}\boldsymbol{\Psi}^{t+\tau,t}\bar{\mathbf{u}}(\bar{\mathbf{w}})\big), \mathbf{v}\big\rangle \qquad (6.2) \\
&= \Big\langle \mathbf{D}\boldsymbol{\Psi}^{t+\tau,t}\bar{\mathbf{u}}(\bar{\mathbf{w}}) - \mathbf{w}_{\mathrm{pred}} + \frac{1}{2}\tau^2\Big(\mathbf{F}\Big(\tfrac{\mathbf{w}+\mathbf{D}\boldsymbol{\Psi}^{t+\tau,t}\bar{\mathbf{u}}(\bar{\mathbf{w}})}{2}\Big) + \mathbf{G}\Big(\tfrac{\mathbf{D}\boldsymbol{\Psi}^{t+\tau,t}\bar{\mathbf{u}}(\bar{\mathbf{w}})-\mathbf{w}}{\tau}\Big)\Big), \mathbf{v}\Big\rangle
\end{aligned}
$$

for $\mathbf{v} \in \mathbf{H}^1$ *and*

$$
\tilde{\mathcal{K}}^{\mathbf{D}\boldsymbol{\Psi}^{t+\tau,t}\bar{\mathbf{u}}} = \big\{ \mathbf{w} \in \mathbf{H}^1_D \,\big|\, [\mathbf{w}\cdot\boldsymbol{\nu}]_{\boldsymbol{\phi}} \le 0 \text{ if } \big[\boldsymbol{\Psi}^{t+\tau,t}\bar{\mathbf{u}}\cdot\boldsymbol{\nu}\big]_{\boldsymbol{\phi}} = g,\ \big\langle \mathbf{F}_{\mathrm{con}}\big(\boldsymbol{\Psi}^{t+\tau,t}\bar{\mathbf{u}}\big), \mathbf{w}\big\rangle = 0 \big\}. \qquad (6.3)
$$

The conical derivative is defined via the Newmark scheme (N-CS+) on a modified admissible set $\tilde{\mathcal{K}}^{\mathbf{D}\boldsymbol{\Psi}^{t+\tau,t}\bar{\mathbf{u}}}$. Strict complementarity implies that $[\mathbf{D}\boldsymbol{\Psi}^{t+\tau,t}\bar{\mathbf{u}}(\bar{\mathbf{w}})\cdot\boldsymbol{\nu}]_{\boldsymbol{\phi}} = 0$ on those parts of the possible contact boundaries where $[\boldsymbol{\Psi}^{t+\tau,t}\bar{\mathbf{u}}\cdot\boldsymbol{\nu}]_{\boldsymbol{\phi}} = g$. Then, the variational inclusion in the second line of the scheme reduces to a minimization problem with time-dependent Dirichlet boundaries. The theorem does not give any information about the sensitivity of (N-CS+) in the special case of interest where h coincides with the parameter τ.

Remark 6.1.2. A simple calculation shows that

$$
\dot{\mathbf{D}}\boldsymbol{\Psi}^{t+\tau,t}\bar{\mathbf{u}}(\bar{\mathbf{w}}) = \dot{\mathbf{w}} + \frac{2}{\tau}\big(\mathbf{D}\boldsymbol{\Psi}^{t+\tau,t}\bar{\mathbf{u}}(\bar{\mathbf{w}}) - \mathbf{w}_{\mathrm{pred}}\big).
$$

As proven in Lemma 4.1.1, the predictor $\mathbf{w}_{\mathrm{pred}}$ resulting from a $\mathbf{L}_2$-projection converges to $\mathbf{w} + \tau\dot{\mathbf{w}}$ if the spatial discretization parameter h tends to zero. Hence, the relation

$$
\dot{\mathbf{D}}\boldsymbol{\Psi}^{t+\tau,t}\bar{\mathbf{u}}(\bar{\mathbf{w}}) = -\dot{\mathbf{w}} + \frac{2}{\tau}\big(\mathbf{D}\boldsymbol{\Psi}^{t+\tau,t}\bar{\mathbf{u}}(\bar{\mathbf{w}}) - \mathbf{w}\big)
$$

holds in function space.

A central role for the construction of an adaptive timestep control is played by the choice of norm in which the approximation error of the scheme is measured.

The existing perturbation and consistency results for (N-CS+) suggest to use the full physical energy norm $\|\cdot\|_{\mathcal{E}}$. In the absence of contact, the Newmark scheme has pointwise consistency order 2 in positions as well as velocities. Hence, due to the integral over time, the viscoelastic part of the physical energy norm is of higher order than the kinetic and potential parts. In view of an adaptive timestep control, the viscoelastic part is neglected, and only the reduced physical energy norm $\|\cdot\|_E$ is used.

6.1.2. Extension of Extrapolation Techniques

For ordinary differential equations, a proof technique for an asymptotic error expansion can be found in [32]. Here, this approach will be extended to dynamical contact problems.

Consider a discrete evolution

$$\bar{\boldsymbol{\Psi}}_*^{t+\tau,t} := \big(\boldsymbol{\Psi}_*^{t+\tau,t}, \dot{\boldsymbol{\Psi}}_*^{t+\tau,t}\big) : \mathbf{H}^1 \times \mathbf{L}_2 \longrightarrow \mathbf{H}^1 \times \mathbf{L}_2 \tag{6.4}$$

which is defined via the formulas

$$\begin{aligned} \boldsymbol{\Psi}_*^{t+\tau,t}\bar{\mathbf{u}}(t) &:= \boldsymbol{\Psi}^{t+\tau,t}\big(\bar{\mathbf{u}}(t) + \bar{\mathbf{e}}(t)\tau^p\big) - \mathbf{e}(t+\tau)\tau^p \\ \dot{\boldsymbol{\Psi}}_*^{t+\tau,t}\bar{\mathbf{u}}(t) &:= \dot{\boldsymbol{\Psi}}^{t+\tau,t}\big(\bar{\mathbf{u}}(t) + \bar{\mathbf{e}}(t)\tau^p\big) - \boldsymbol{\epsilon}(t+\tau)\tau^p\,. \end{aligned} \tag{6.5}$$

For fixed initial time t_0, the functions

$$\bar{\mathbf{e}} := (\mathbf{e}, \boldsymbol{\epsilon}) : [t_0, T] \longrightarrow \mathbf{H}^1 \times \mathbf{L}_2 \tag{6.6}$$

should have initial values equal to zero, i.e.,

$$\mathbf{e}(t_0) = 0\,, \quad \boldsymbol{\epsilon}(t_0) = 0\,. \tag{6.7}$$

These functions will be specified in Section 6.1.3. For constant stepsize τ, the lattice function

$$\bar{\mathbf{u}}_\tau^* = \big(\mathbf{u}_\tau^*, \dot{\mathbf{u}}_\tau^*\big) : \triangle_\tau \longrightarrow \mathbf{H}^1 \times \mathbf{L}_2 \tag{6.8}$$

of the new evolution correlates with the one of (N-CS+) in the following way.

Lemma 6.1.3. *For $t \in \triangle_\tau$, the lattice functions $(\mathbf{u}_\tau^*, \dot{\mathbf{u}}_\tau^*)$ and $(\mathbf{u}_\tau, \dot{\mathbf{u}}_\tau)$ satisfy the relations*

$$\begin{aligned} \mathbf{u}_\tau(t) - \mathbf{u}(t) - \mathbf{e}(t)\tau^p &= \mathbf{u}_\tau^*(t) - \mathbf{u}(t) \\ \dot{\mathbf{u}}_\tau(t) - \dot{\mathbf{u}}(t) - \boldsymbol{\epsilon}(t)\tau^p &= \dot{\mathbf{u}}_\tau^*(t) - \dot{\mathbf{u}}(t)\,. \end{aligned}$$

Proof. Definition (6.5) with initial values (6.7) yields

$$\begin{aligned} \bar{\mathbf{u}}_\tau^*(t_0+\tau) &= \bar{\boldsymbol{\Psi}}_*^{t_0+\tau,t_0}\bar{\mathbf{u}}(t_0) \\ &= \bar{\boldsymbol{\Psi}}^{t_0+\tau,t_0}\big(\bar{\mathbf{u}}(t_0) + \bar{\mathbf{e}}(t_0)\tau^p\big) - \bar{\mathbf{e}}(t_0+\tau)\tau^p \\ &= \bar{\mathbf{u}}_\tau(t_0+\tau) - \bar{\mathbf{e}}(t_0+\tau)\tau^p \\ &= \bar{\boldsymbol{\Psi}}^{t_0+\tau,t_0}\bar{\mathbf{u}}(t_0) - \bar{\mathbf{e}}(t_0+\tau)\tau^p\,. \end{aligned}$$

An induction leads to

$$\begin{aligned}\bar{\mathbf{u}}_\tau^*(t) &= \bar{\boldsymbol{\Psi}}_*^{t,t-\tau}\bar{\mathbf{u}}_\tau^*(t-\tau)\\ &= \bar{\boldsymbol{\Psi}}^{t,t-\tau}\big(\bar{\mathbf{u}}_\tau^*(t-\tau)+\bar{\mathbf{e}}(t-\tau)\tau^p\big)-\bar{\mathbf{e}}(t)\tau^p\\ &= \bar{\mathbf{u}}_\tau(t)-\bar{\mathbf{e}}(t)\tau^p\\ &= \bar{\boldsymbol{\Psi}}^{t,t-\tau}\bar{\mathbf{u}}_\tau(t-\tau)-\bar{\mathbf{e}}(t)\tau^p\end{aligned}$$

which gives the desired relation. □

The lemma yields an asymptotic error expansion of order p for (N-CS+) if the approximation error $\bar{\mathbf{u}}_\tau^*-\bar{\mathbf{u}}$ of the new scheme is of order $o(\tau^p)$. In order to gain more information on this quantity, the error of the scheme after performing two timesteps with stepsize $\tau/2$ is considered for simplicity. The global error of a numerical integration is based on the continuous dependence of the scheme on the initial data. In the general case of non-vanishing Dirichlet boundaries, the discrete perturbation result for (N-CI/CS(+)) in Section 5.1.3 contains the initial perturbation of the displacements in $\mathbf{L}_2$-norm in addition to the physical energy norm. In order to handle with this term, let

$$\|\boldsymbol{\Psi}-\boldsymbol{\Phi}\|_{\mathbf{L}_2} = \|\bar{\boldsymbol{\Psi}}-\bar{\boldsymbol{\Phi}}\|_E\cdot O\big(\tau^{-1}\big) \qquad \text{for } \tau\to 0\,. \tag{6.9}$$

This assumption is more than reasonable since the consistency error of (N-CS+) is expected to be even of one order higher in $\mathbf{L}_2$-norm than in physical energy norm, cf. Chapter 4. Now, an estimate for the approximation error of the new scheme $(\boldsymbol{\Psi}_*, \dot{\boldsymbol{\Psi}}_*)$ can be proven.

Theorem 6.1.4. *Assume that Theorem 5.1.7 and Assumption* (6.9) *are valid. Then,*

$$\begin{aligned}&\Big\|\bar{\mathbf{u}}_{\frac{\tau}{2}}^*(t+\tau)-\bar{\mathbf{u}}(t+\tau)\Big\|_E\\ &\le C\cdot\Big\|\Big(\bar{\boldsymbol{\Psi}}_*^{t+\frac{\tau}{2},t}-\bar{\boldsymbol{\Phi}}^{t+\frac{\tau}{2},t}\Big)\bar{\mathbf{u}}(t)\Big\|_E+\Big\|\Big(\bar{\boldsymbol{\Psi}}_*^{t+\tau,t+\frac{\tau}{2}}-\bar{\boldsymbol{\Phi}}^{t+\tau,t+\frac{\tau}{2}}\Big)\bar{\mathbf{u}}\Big(t+\frac{\tau}{2}\Big)\Big\|_E\,.\end{aligned} \tag{6.10}$$

Proof. The error of a numerical scheme after performing two timesteps can be divided into the consistency error of the second step and the propagation of the consistency error of the first step, i.e.,

$$\begin{aligned}&\bar{\mathbf{u}}_{\frac{\tau}{2}}^*(t+\tau)-\bar{\mathbf{u}}(t+\tau)\\ &= \bar{\boldsymbol{\Psi}}_*^{t+\tau,t+\frac{\tau}{2}}\bar{\boldsymbol{\Psi}}_*^{t+\frac{\tau}{2},t}\bar{\mathbf{u}}(t)-\bar{\boldsymbol{\Phi}}^{t+\tau,t+\frac{\tau}{2}}\bar{\boldsymbol{\Phi}}^{t+\frac{\tau}{2},t}\bar{\mathbf{u}}(t)\\ &= \bar{\boldsymbol{\Psi}}_*^{t+\tau,t+\frac{\tau}{2}}\bar{\boldsymbol{\Psi}}_*^{t+\frac{\tau}{2},t}\bar{\mathbf{u}}(t)-\bar{\boldsymbol{\Psi}}_*^{t+\tau,t+\frac{\tau}{2}}\bar{\boldsymbol{\Phi}}^{t+\frac{\tau}{2},t}\bar{\mathbf{u}}(t)+\Big(\bar{\boldsymbol{\Psi}}_*^{t+\tau,t+\frac{\tau}{2}}-\bar{\boldsymbol{\Phi}}^{t+\tau,t+\frac{\tau}{2}}\Big)\bar{\mathbf{u}}\Big(t+\frac{\tau}{2}\Big)\,.\end{aligned}$$

Due to definitions (6.5)–(6.7) and Theorem 5.1.7, the propagated consistency error satisfies

$$\begin{aligned}
&\left\| \bar{\boldsymbol{\Psi}}_*^{t+\tau,t+\frac{\tau}{2}} \bar{\boldsymbol{\Psi}}_*^{t+\frac{\tau}{2},t} \bar{\mathbf{u}}(t) - \bar{\boldsymbol{\Psi}}_*^{t+\tau,t+\frac{\tau}{2}} \bar{\boldsymbol{\Phi}}^{t+\frac{\tau}{2},t} \bar{\mathbf{u}}(t) \right\|_E \\
&= \left\| \bar{\boldsymbol{\Psi}}^{t+\tau,t+\frac{\tau}{2}} \bar{\boldsymbol{\Psi}}^{t+\frac{\tau}{2},t} \bar{\mathbf{u}}(t) - \bar{\boldsymbol{\Psi}}^{t+\tau,t+\frac{\tau}{2}} \Big(\bar{\boldsymbol{\Phi}}^{t+\frac{\tau}{2},t} \bar{\mathbf{u}}(t) + \bar{\mathbf{e}}\Big(t+\frac{\tau}{2}\Big)\Big(\frac{\tau}{2}\Big)^p \Big) \right\|_E \\
&\leq \Big(\left\| \bar{\boldsymbol{\Psi}}^{t+\frac{\tau}{2},t} \bar{\mathbf{u}}(t) - \Big(\bar{\boldsymbol{\Phi}}^{t+\frac{\tau}{2},t} \bar{\mathbf{u}}(t) + \bar{\mathbf{e}}\Big(t+\frac{\tau}{2}\Big)\Big(\frac{\tau}{2}\Big)^p \Big) \right\|_E \\
&\quad + c\tau \left\| \boldsymbol{\Psi}^{t+\frac{\tau}{2},t} \bar{\mathbf{u}}(t) - \Big(\boldsymbol{\Phi}^{t+\frac{\tau}{2},t} \bar{\mathbf{u}}(t) + \bar{\mathbf{e}}\Big(t+\frac{\tau}{2}\Big)\Big(\frac{\tau}{2}\Big)^p \Big) \right\|_{\mathbf{L}_2} \Big) \cdot e^{\tilde{\kappa}^2 \tau} \\
&= C \cdot \left\| \bar{\boldsymbol{\Psi}}^{t+\frac{\tau}{2},t} \bar{\mathbf{u}}(t) - \Big(\bar{\boldsymbol{\Phi}}^{t+\frac{\tau}{2},t} \bar{\mathbf{u}}(t) + \bar{\mathbf{e}}\Big(t+\frac{\tau}{2}\Big)\Big(\frac{\tau}{2}\Big)^p \Big) \right\|_E \\
&= C \cdot \left\| \Big(\bar{\boldsymbol{\Psi}}_*^{t+\frac{\tau}{2},t} - \bar{\boldsymbol{\Phi}}^{t+\frac{\tau}{2},t} \Big) \bar{\mathbf{u}}(t) \right\|_E
\end{aligned}$$

with a constant $C > 0$ independent of τ. This gives the estimate of the theorem. □

In view of an asymptotic error expansion of (N-CS+), the results of Lemma 6.1.3 and Theorem 6.1.4 have to be combined. This yields that the functions $(\mathbf{e}, \boldsymbol{\epsilon})$ have to be constructed such that

$$\frac{\left\| \bar{\boldsymbol{\Psi}}_*^{t+\tau,t} - \bar{\boldsymbol{\Phi}}^{t+\tau,t} \right\|_E}{\left\| \bar{\boldsymbol{\Psi}}^{t+\tau,t} - \bar{\boldsymbol{\Phi}}^{t+\tau,t} \right\|_E} \longrightarrow 0 \quad \text{for } \tau \to 0\,, \tag{6.11}$$

i.e., the consistency error of $(\boldsymbol{\Psi}_*, \dot{\boldsymbol{\Psi}}_*)$ in energy norm should be of higher order than the one of (N-CS+) for arbitrary initial times.

6.1.3. Construction of a Higher-Order Scheme

The task of this section is to find a definition for the functions $(\mathbf{e}, \boldsymbol{\epsilon})$ such that the initial values (6.7) and condition (6.11) on the consistency error of the new scheme are fulfilled. For this purpose, information about the pointwise error behavior of (N-CS+) are needed. While such information is given in the absence of contact, up to now, the only consistency result for (N-CS+) in the presence of contact is given in energy norm (cf. Theorem 4.2.7). Hence, the following analysis of an asymptotic error expansion of (N-CS+) is laid on a very general basis.

Assumption 6.1.5. Let the consistency error of (N-CS+) be of the form

$$\begin{aligned}
\boldsymbol{\Psi}^{t+\tau,t} \bar{\mathbf{u}} - \boldsymbol{\Phi}^{t+\tau,t} \bar{\mathbf{u}} &= \mathbf{m}(t) \cdot \tau^{p+1} + \mathbf{r}(t,\tau) \cdot \tau^p \\
\dot{\boldsymbol{\Psi}}^{t+\tau,t} \bar{\mathbf{u}} - \dot{\boldsymbol{\Phi}}^{t+\tau,t} \bar{\mathbf{u}} &= \int_t^{t+\tau} \boldsymbol{\mu}(s)\, ds \cdot \tau^p + \boldsymbol{\rho}(t,\tau) \cdot \tau^p
\end{aligned}$$

with $\mathbf{m} \in \mathbf{C}([0,T], \mathbf{H}^1)$ and $\dot{\mathbf{m}}, \boldsymbol{\mu} \in \mathbf{W}_2^1(0,T; \mathbf{H}^1, \mathbf{L}_2)$. The quantities $\mathbf{r}(t,\tau)$ and $\boldsymbol{\rho}(t,\tau)$ are not further specified at this moment, but they will be discussed in Section 6.1.4.

In the following, the abbreviation $\bar{\mathbf{m}} := (\mathbf{m}, \boldsymbol{\mu})$ is often used. Please note that the second line of Assumption 6.1.5 is not the derivative of the first one due to the definition of the discrete evolution operator. The integral term in the consistency error of the velocities is related to the viscoelastic part of the physical energy norm. In the classical approach, a pointwise Taylor expansion of the consistency error of the scheme would be expected. This is included in the ansatz if

$$\int_t^{t+\tau} \boldsymbol{\mu}(s)\, ds = \boldsymbol{\mu}(t) \cdot \tau + o(\tau)$$

and

$$|\mathbf{r}(t,\tau)| = o(\tau)\,, \quad |\boldsymbol{\rho}(t,\tau)| = o(\tau)\,.$$

For a perturbation of the initial values of (N-CS+),

$$\begin{aligned} \boldsymbol{\Psi}^{t+\tau,t}\big(\bar{\mathbf{u}} + \bar{\mathbf{e}}\tau^p\big) - \boldsymbol{\Psi}^{t+\tau,t}\bar{\mathbf{u}} &= \big(\mathbf{D}\boldsymbol{\Psi}^{t+\tau,t}\bar{\mathbf{u}}(\bar{\mathbf{e}}) + \mathbf{p}(t,\tau)\big) \cdot \tau^p \\ \dot{\boldsymbol{\Psi}}^{t+\tau,t}\big(\bar{\mathbf{u}} + \bar{\mathbf{e}}\tau^p\big) - \dot{\boldsymbol{\Psi}}^{t+\tau,t}\bar{\mathbf{u}} &= \big(\dot{\mathbf{D}}\boldsymbol{\Psi}^{t+\tau,t}\bar{\mathbf{u}}(\bar{\mathbf{e}}) + \boldsymbol{\pi}(t,\tau)\big) \cdot \tau^p \end{aligned} \tag{6.12}$$

is written where $(\mathbf{D}\boldsymbol{\Psi}^{t+\tau,t}\bar{\mathbf{u}}(\bar{\mathbf{e}}), \dot{\mathbf{D}}\boldsymbol{\Psi}^{t+\tau,t}\bar{\mathbf{u}}(\bar{\mathbf{e}}))$ denotes the conical derivative of the scheme introduced in Section 6.1.1. A short calculation shows that $\boldsymbol{\pi}(t,\tau) = \frac{2}{\tau}\mathbf{p}(t,\tau)$, and the notation $\bar{\mathbf{p}} := (\mathbf{p}, \boldsymbol{\pi})$ is often used. The quantities $\mathbf{p}(t,\tau)$ and $\boldsymbol{\pi}(t,\tau)$ are expected to be of order $o(\tau)$. In the case of time-constant Dirichlet boundaries, the variational problem is linear and $|\bar{\mathbf{p}}(t,\tau)| = 0$.

On the basis of these notations, a formula for the consistency error of the new evolution $(\boldsymbol{\Psi}_*, \dot{\boldsymbol{\Psi}}_*)$ can be presented.

Lemma 6.1.6. *Let Assumption* 6.1.5 *hold. Then, the consistency error* $(\boldsymbol{\Psi}_* - \boldsymbol{\Phi}, \dot{\boldsymbol{\Psi}}_* - \dot{\boldsymbol{\Phi}})$ *satisfies*

$$\begin{aligned} \boldsymbol{\Psi}_*^{t+\tau,t}\bar{\mathbf{u}}(t) - \boldsymbol{\Phi}^{t+\tau,t}\bar{\mathbf{u}}(t) &= \big(\mathbf{D}\boldsymbol{\Psi}^{t+\tau,t}\bar{\mathbf{u}}(t)(\bar{\mathbf{e}}(t)) - \mathbf{e}(t+\tau) + \tau\mathbf{m}(t)\big) \cdot \tau^p \\ &\quad + (\mathbf{r}(t,\tau) + \mathbf{p}(t,\tau)) \cdot \tau^p \\ \dot{\boldsymbol{\Psi}}_*^{t+\tau,t}\bar{\mathbf{u}}(t) - \dot{\boldsymbol{\Phi}}^{t+\tau,t}\bar{\mathbf{u}}(t) &= \Big(\dot{\mathbf{D}}\boldsymbol{\Psi}^{t+\tau,t}\bar{\mathbf{u}}(t)(\bar{\mathbf{e}}(t)) - \boldsymbol{\epsilon}(t+\tau) + \int_t^{t+\tau} \boldsymbol{\mu}(s)\, ds\Big) \cdot \tau^p \\ &\quad + (\boldsymbol{\rho}(t,\tau) + \boldsymbol{\pi}(t,\tau)) \cdot \tau^p\,. \end{aligned}$$

Proof. Inserting definition (6.5) into the consistency error yields

$$\bar{\boldsymbol{\Psi}}_*^{t+\tau,t}\bar{\mathbf{u}}(t) - \bar{\boldsymbol{\Phi}}^{t+\tau,t}\bar{\mathbf{u}}(t) = \bar{\boldsymbol{\Psi}}^{t+\tau,t}\big(\bar{\mathbf{u}}(t) + \bar{\mathbf{e}}(t)\tau^p\big) - \bar{\mathbf{e}}(t+\tau)\tau^p - \bar{\boldsymbol{\Phi}}^{t+\tau,t}\bar{\mathbf{u}}(t)\,.$$

Assumption 6.1.5 on the consistency error of (N-CS+) gives

$$\begin{aligned} \bar{\boldsymbol{\Psi}}_*^{t+\tau,t}\bar{\mathbf{u}}(t) - \bar{\boldsymbol{\Phi}}^{t+\tau,t}\bar{\mathbf{u}}(t) &= \bar{\boldsymbol{\Psi}}^{t+\tau,t}\big(\bar{\mathbf{u}}(t) + \bar{\mathbf{e}}(t)\tau^p\big) - \bar{\boldsymbol{\Psi}}^{t+\tau,t}\bar{\mathbf{u}}(t) - \bar{\mathbf{e}}(t+\tau) \cdot \tau^p \\ &\quad + \bar{\mathbf{m}}(t) \cdot \tau^{p+1} + \bar{\mathbf{r}}(t,\tau) \cdot \tau^p\,. \end{aligned}$$

Using (6.12) leads to

$$\bar{\boldsymbol{\Psi}}_*^{t+\tau,t}\bar{\mathbf{u}}(t) - \bar{\boldsymbol{\Phi}}^{t+\tau,t}\bar{\mathbf{u}}(t) = \big(\bar{\mathbf{D}}\boldsymbol{\Psi}^{t+\tau,t}\bar{\mathbf{u}}(t)(\bar{\mathbf{e}}(t)) - \bar{\mathbf{e}}(t+\tau) + \tau\bar{\mathbf{m}}(t)\big)\cdot\tau^p + (\bar{\mathbf{r}}(t,\tau) + \bar{\mathbf{p}}(t,\tau))\cdot\tau^p\,.$$

□

The aim is to define the functions $(\mathbf{e},\boldsymbol{\epsilon})$ such that the terms of order $p+1$ in the consistency error of $(\boldsymbol{\Psi}_*,\dot{\boldsymbol{\Psi}}_*)$ vanish and the scheme is of higher order $o(\tau^{p+1})$. This leads to the following definition of the functions $(\mathbf{e},\boldsymbol{\epsilon})$.

Variational problem for $(\mathbf{e},\boldsymbol{\epsilon})$. For almost every $t\in[t_0,T]$, find $\mathbf{e}(\cdot,t)\in\tilde{\mathcal{K}}^{\mathbf{u}(t)}$ with $\mathbf{e}\in\mathbf{C}\big([t_0,T],\mathbf{H}^1\big)$ and $\dot{\mathbf{e}}\in\mathbf{W}_2^1(t_0,T;\mathbf{H}^1,\mathbf{L}_2)$ such that for all $\mathbf{v}(t)\in\tilde{\mathcal{K}}^{\mathbf{u}(t)}$

$$\langle\ddot{\mathbf{e}} - \boldsymbol{\mu} - \dot{\mathbf{m}} + \mathbf{F}(\mathbf{e}) + \mathbf{G}(\dot{\mathbf{e}}-\mathbf{m}), \mathbf{v}-\mathbf{e}\rangle_{(\mathbf{H}^1)^*\times\mathbf{H}^1} \geq 0 \tag{6.13}$$

and

$$\mathbf{e}(t_0) = 0\,,\quad \dot{\mathbf{e}}(t_0) = \mathbf{m}(t_0) \tag{6.14}$$

where

$$\tilde{\mathcal{K}}^{\mathbf{u}(t)} = \big\{\mathbf{w}\in\mathbf{H}_D^1 \,\big|\, [\mathbf{w}\cdot\boldsymbol{\nu}]_{\boldsymbol{\phi}}\leq 0 \text{ if } [\mathbf{u}(t)\cdot\boldsymbol{\nu}]_{\boldsymbol{\phi}} = g,\ \langle\mathbf{F}_{\mathrm{con}}(\mathbf{u}(t)),\mathbf{w}\rangle_{(\mathbf{H}^1)^*\times\mathbf{H}^1} = 0\big\}\,. \tag{6.15}$$

Further, set

$$\boldsymbol{\epsilon}(t) = \dot{\mathbf{e}}(t) - \mathbf{m}(t)\,,\qquad \forall\, t\in[t_0,T] \tag{6.16}$$

such that the initial values (6.7) are fulfilled. The contact forces $\mathbf{F}_{\mathrm{con}}(\mathbf{e})\in(\mathbf{H}^1)^*$ are given by

$$\langle\mathbf{F}_{\mathrm{con}}(\mathbf{e}),\mathbf{v}\rangle_{(\mathbf{H}^1)^*\times\mathbf{H}^1} := \langle\ddot{\mathbf{e}}-\boldsymbol{\mu}-\dot{\mathbf{m}}+\mathbf{F}(\mathbf{e})+\mathbf{G}(\dot{\mathbf{e}}-\mathbf{m}),\mathbf{v}\rangle_{(\mathbf{H}^1)^*\times\mathbf{H}^1}\,,\qquad \mathbf{v}\in\mathbf{H}^1\,. \tag{6.17}$$

In the case of strict complementarity, this is a parabolic equality with Dirichlet boundaries that are varying in time. These boundaries correspond to the active contact boundaries of the solution of the original variational inequality (1.28). Hence, let $\mathbf{e}$ and its derivatives be of bounded variation in the same sense.

Assumption 6.1.7. Let the solution of (6.13) satisfy

$$\dot{\mathbf{e}}\in\mathbf{BV}\big([t,t+\tau],\mathbf{H}^1\big)\,,\qquad \ddot{\mathbf{e}}\in\mathbf{BV}\big([t,t+\tau],(\mathbf{H}^1)^*\big)\,.$$

This leads to an estimate for the consistency error of the new evolution $(\boldsymbol{\Psi}_*,\dot{\boldsymbol{\Psi}}_*)$.

Lemma 6.1.8. *Let Assumptions* 6.1.5 *and* 6.1.7 *hold. Then, the consistency error* $\bar{\boldsymbol{\Psi}}_* - \bar{\boldsymbol{\Phi}} = (\boldsymbol{\Psi}_* - \boldsymbol{\Phi}, \dot{\boldsymbol{\Psi}}_* - \dot{\boldsymbol{\Phi}})$ *satisfies*

$$\begin{aligned}
&\Big(\big\| \bar{\boldsymbol{\Psi}}_*^{t+\tau,t} \bar{\mathbf{u}}(t) - \bar{\boldsymbol{\Phi}}^{t+\tau,t} \bar{\mathbf{u}}(t) - (\bar{\mathbf{r}}(t,\tau) + \bar{\mathbf{p}}(t,\tau)) \cdot \tau^p \big\|_E^2 \\
&\quad + \frac{\tau}{4} \Big\| \dot{\mathbf{D}} \boldsymbol{\Psi}^{t+\tau,t} \bar{\mathbf{u}}(t)(\bar{\mathbf{e}}(t)) - \boldsymbol{\epsilon}(t+\tau) + \int_t^{t+\tau} \boldsymbol{\mu}(s)\, ds \Big\|_b^2 \cdot \tau^{2p} \Big)^{1/2} \\
&\leq \Big(\frac{1}{2} \Big| \Big\langle \mathbf{F}_{\mathrm{con}}\big(\mathbf{D}\boldsymbol{\Psi}^{t+\tau,t} \bar{\mathbf{u}}(t)(\bar{\mathbf{e}}(t))\big) - \mathbf{F}_{\mathrm{con}}(\mathbf{e}(t)), \\
&\qquad\qquad \dot{\mathbf{D}} \boldsymbol{\Psi}^{t+\tau,t} \bar{\mathbf{u}}(t)(\bar{\mathbf{e}}(t)) - \boldsymbol{\epsilon}(t+\tau) + \int_t^{t+\tau} \boldsymbol{\mu}(s)\, ds \Big\rangle_{(\mathbf{H}^1)^* \times \mathbf{H}^1} \Big| \Big)^{1/2} \cdot \tau^{p+1/2} \\
&\quad + R(\mathbf{e}, [t, t+\tau]) \cdot O\big(\tau^{p+1/2}\big) + o\big(\tau^{p+1}\big)
\end{aligned} \tag{6.18}$$

with $R(\mathbf{e}, [t, t+\tau])$ *defined in* (4.22).

Remark 6.1.9. Due to the definition of the modified admissible sets (6.3) and (6.15), the first term on the right-hand side of (6.18) can be written as a linear functional on the part of the possible contact boundaries where $\boldsymbol{\Psi}^{t+\tau,t} \bar{\mathbf{u}}(t)$ and $\mathbf{u}(t)$ are actually in contact. Moreover, $\dot{\mathbf{D}} \boldsymbol{\Psi}^{t+\tau,t} \bar{\mathbf{u}}(t)(\bar{\mathbf{e}}(t)) - \boldsymbol{\epsilon}(t+\tau)$ is zero on the part of the contact boundaries where the active sets of $\boldsymbol{\Psi}^{t+\tau,t} \bar{\mathbf{u}}(t)$ and $\mathbf{u}(t+\tau)$ are unchanged and coincide with those of $\mathbf{u}(t)$. This is the same part of the contact boundaries on which $\int_t^{t+\tau} \boldsymbol{\mu}(s)\, ds$ can be assumed to be zero by its definition as the consistency error of (N-CS+). Hence, the contact term in the estimate (6.18) is only effective on a small part of the possible contact boundaries, namely where the active sets vary in time. For most initial times t, this part tends to a set of measure zero as $\tau \to 0$. This effect corresponds to the consistency theory for permanent active contact in Section 4.4, and will also become visible in the numerical examples of Section 6.1.4 and Section 7.1.

In Appendix B, a localization of contact stresses on a critical part of the possible contact boundaries has in detail been worked out for the interpretation of the stability condition in Chapter 3. A similar argumentation would not yield further insight here. Hence, the matter is rested by this heuristic discussion. Instead, a rough estimate for the contact term on the right-hand side of (6.18) is used in the main theorem.

Proof. By means of Lemma 6.1.6, the physical energy norm of the consistency error is of the form

$$\begin{aligned}
&\big\| \bar{\boldsymbol{\Psi}}_*^{t+\tau,t} \bar{\mathbf{u}}(t) - \bar{\boldsymbol{\Phi}}^{t+\tau,t} \bar{\mathbf{u}}(t) - (\bar{\mathbf{r}}(t,\tau) + \bar{\mathbf{p}}(t,\tau)) \cdot \tau^p \big\|_E^2 \\
&= \Big(\frac{1}{2} \Big\| \dot{\mathbf{D}} \boldsymbol{\Psi}^{t+\tau,t} \bar{\mathbf{u}}(t)(\bar{\mathbf{e}}(t)) - \boldsymbol{\epsilon}(t+\tau) + \int_t^{t+\tau} \boldsymbol{\mu}(s)\, ds \Big\|_{\mathbf{L}_2}^2 \\
&\qquad + \frac{1}{2} \big\| \mathbf{D}\boldsymbol{\Psi}^{t+\tau,t} \bar{\mathbf{u}}(t)(\bar{\mathbf{e}}(t)) - \mathbf{e}(t+\tau) + \tau \mathbf{m}(t) \big\|_a^2 \Big) \cdot \tau^{2p}\,.
\end{aligned} \tag{6.19}$$

The aim is to insert the defining equations for $\mathbf{e}$ and $\boldsymbol{\epsilon}$ into this estimate. For ease of presentation, the abbreviation

$$\mathbf{v} := \dot{\mathbf{D}}\boldsymbol{\Psi}^{t+\tau,t}\bar{\mathbf{u}}(t)(\bar{\mathbf{e}}(t)) - \boldsymbol{\epsilon}(t+\tau) + \int_t^{t+\tau} \boldsymbol{\mu}(s)\,ds$$

is used in the following. Since $\dot{\mathbf{e}}, \dot{\mathbf{m}} \in \mathbf{L}_2(t, t+\tau; \mathbf{H}^1)$, integration by parts is applicable. Using Remark 6.1.2 and relation (6.16), the term in a-seminorm can be written as

$$\begin{aligned}
&\mathbf{D}\boldsymbol{\Psi}^{t+\tau,t}\bar{\mathbf{u}}(t)(\bar{\mathbf{e}}(t)) - \mathbf{e}(t+\tau) + \tau\mathbf{m}(t) \\
&= \frac{\tau}{2}\big(\dot{\mathbf{D}}\boldsymbol{\Psi}^{t+\tau,t}\bar{\mathbf{u}}(t)(\bar{\mathbf{e}}(t)) + \boldsymbol{\epsilon}(t)\big) - \int_t^{t+\tau} \dot{\mathbf{e}}(s)\,ds + \tau\mathbf{m}(t) \\
&= \frac{\tau}{2}\mathbf{v} + \int_t^{t+\tau} \frac{\boldsymbol{\epsilon}(t+\tau) + \boldsymbol{\epsilon}(t)}{2} - \dot{\mathbf{e}}(s)\,ds + \tau\mathbf{m}(t) - \frac{\tau}{2}\int_t^{t+\tau} \boldsymbol{\mu}(s)\,ds \\
&= \frac{\tau}{2}\mathbf{v} + \frac{1}{2}\int_t^{t+\tau} (\dot{\mathbf{e}}(t+\tau) - \dot{\mathbf{e}}(s)) + (\dot{\mathbf{e}}(t) - \dot{\mathbf{e}}(s))\,ds \\
&\quad - \frac{1}{2}\int_t^{t+\tau} \Big(\int_t^{t+\tau} \dot{\mathbf{m}}(\eta) + \boldsymbol{\mu}(s)\,d\eta\Big)\,ds\,.
\end{aligned}$$

Due to the inequality of Young and the absolute continuity of the integral (see, e.g., [94, Appendix, Application (20)]),

$$\|\mathbf{v}\|_{\mathbf{L}_1(t,t+\tau;\mathbf{V})} := \int_t^{t+\tau} \|\mathbf{v}(s)\|_{\mathbf{V}}\,ds \le \|\mathbf{v}\|_{\mathbf{L}_2(t,t+\tau;\mathbf{V})} \cdot \tau^{1/2} = o\big(\tau^{1/2}\big) \tag{6.20}$$

for every fixed $\mathbf{v} \in \mathbf{L}_2(t, t+\tau_0; \mathbf{V})$ and for all $\tau \le \tau_0$. Applying this result to $\dot{\mathbf{m}}, \boldsymbol{\mu} \in \mathbf{L}_2(t, t+\tau; \mathbf{H}^1)$, the inequality of Korn (A.1) allows proving the estimate

$$\begin{aligned}
&\big\|\mathbf{D}\boldsymbol{\Psi}^{t+\tau,t}\bar{\mathbf{u}}(t)(\bar{\mathbf{e}}(t)) - \mathbf{e}(t+\tau) + \tau\mathbf{m}(t)\big\|_a \\
&\le \frac{\tau}{2}\|\mathbf{v}\|_a + \frac{1}{2}\int_t^{t+\tau} \big(\|\dot{\mathbf{e}}(t+\tau) - \dot{\mathbf{e}}(s)\|_{\mathbf{H}^1} + \|\dot{\mathbf{e}}(t) - \dot{\mathbf{e}}(s)\|_{\mathbf{H}^1}\big)\,ds \\
&\quad + \frac{\tau}{2}\big(\|\dot{\mathbf{m}}\|_{\mathbf{L}_1(t,t+\tau;\mathbf{H}^1)} + \|\boldsymbol{\mu}\|_{\mathbf{L}_1(t,t+\tau;\mathbf{H}^1)}\big) \\
&= \frac{\tau}{2}\|\mathbf{v}\|_a + \mathrm{TV}\big(\dot{\mathbf{e}}, [t, t+\tau], \mathbf{H}^1\big) \cdot O(\tau) + o\big(\tau^{3/2}\big)\,.
\end{aligned} \tag{6.21}$$

Since $\boldsymbol{\epsilon} = \dot{\mathbf{e}} - \mathbf{m} \in \mathbf{W}_2^1(t, t+\tau; \mathbf{H}^1, \mathbf{L}_2)$, integration by parts (see, e.g., [93, Proposition 23.23]) and definition (6.16) yield

$$
\begin{aligned}
&\Big\| \dot{\mathbf{D}}\boldsymbol{\Psi}^{t+\tau,t}\bar{\mathbf{u}}(t)(\bar{\mathbf{e}}(t)) - \boldsymbol{\epsilon}(t+\tau) + \int_t^{t+\tau} \boldsymbol{\mu}(s)\,ds \Big\|_{\mathbf{L}_2}^2 = \|\mathbf{v}\|_{\mathbf{L}_2}^2 \\
&= \Big\langle \dot{\mathbf{D}}\boldsymbol{\Psi}^{t+\tau,t}\bar{\mathbf{u}}(t)(\bar{\mathbf{e}}(t)) - \boldsymbol{\epsilon}(t) - \int_t^{t+\tau} \dot{\boldsymbol{\epsilon}}(s) - \boldsymbol{\mu}(s)\,ds, \mathbf{v} \Big\rangle_{(\mathbf{H}^1)^* \times \mathbf{H}^1} \\
&= \Big\langle \dot{\mathbf{D}}\boldsymbol{\Psi}^{t+\tau,t}\bar{\mathbf{u}}(t)(\bar{\mathbf{e}}(t)) - \boldsymbol{\epsilon}(t) - \int_t^{t+\tau} \ddot{\mathbf{e}}(s) - \dot{\mathbf{m}}(s) - \boldsymbol{\mu}(s)\,ds, \mathbf{v} \Big\rangle_{(\mathbf{H}^1)^* \times \mathbf{H}^1} \\
&= \big\langle \dot{\mathbf{D}}\boldsymbol{\Psi}^{t+\tau,t}\bar{\mathbf{u}}(t)(\bar{\mathbf{e}}(t)) - \boldsymbol{\epsilon}(t) - \tau(\ddot{\mathbf{e}}(t) - \dot{\mathbf{m}}(t) - \boldsymbol{\mu}(t)), \mathbf{v} \big\rangle_{(\mathbf{H}^1)^* \times \mathbf{H}^1} \\
&\quad - \Big\langle \int_t^{t+\tau} \ddot{\mathbf{e}}(s) - \ddot{\mathbf{e}}(t)\,ds, \mathbf{v} \Big\rangle_{(\mathbf{H}^1)^* \times \mathbf{H}^1} - \Big\langle \int_t^{t+\tau} \Big(\int_t^s \dddot{\mathbf{m}}(\eta)\,d\eta \Big)\,ds, \mathbf{v} \Big\rangle_{(\mathbf{H}^1)^* \times \mathbf{H}^1} \\
&\le \big| \big\langle \dot{\mathbf{D}}\boldsymbol{\Psi}^{t+\tau,t}\bar{\mathbf{u}}(t)(\bar{\mathbf{e}}(t)) - \boldsymbol{\epsilon}(t) - \tau(\ddot{\mathbf{e}}(t) - \dot{\mathbf{m}}(t) - \boldsymbol{\mu}(t)), \mathbf{v} \big\rangle_{(\mathbf{H}^1)^* \times \mathbf{H}^1} \big| \\
&\quad + \Big(\int_t^{t+\tau} \|\ddot{\mathbf{e}}(s) - \ddot{\mathbf{e}}(t)\|_{(\mathbf{H}^1)^*}\,ds \Big) \|\mathbf{v}\|_{\mathbf{H}^1} + \tau \|\dddot{\mathbf{m}}\|_{\mathbf{L}_1(t,t+\tau;(\mathbf{H}^1)^*)} \|\mathbf{v}\|_{\mathbf{H}^1} \\
&= \big| \big\langle \dot{\mathbf{D}}\boldsymbol{\Psi}^{t+\tau,t}\bar{\mathbf{u}}(t)(\bar{\mathbf{e}}(t)) - \boldsymbol{\epsilon}(t) - \tau(\ddot{\mathbf{e}}(t) - \dot{\mathbf{m}}(t) - \boldsymbol{\mu}(t)), \mathbf{v} \big\rangle_{(\mathbf{H}^1)^* \times \mathbf{H}^1} \big| \\
&\quad + \mathrm{TV}\big(\ddot{\mathbf{e}}, [t, t+\tau], \mathbf{H}^1\big) \|\mathbf{v}\|_{\mathbf{H}^1} \cdot O(\tau) + \|\mathbf{v}\|_{\mathbf{H}^1} \cdot o\big(\tau^{3/2}\big)
\end{aligned}
$$

for the squared $\mathbf{L}_2$-norm. Now, the numerical scheme (6.1), the variational inequality (6.13), and definition (6.16) are inserted into the first term on the right-hand side of this estimate. Then, Remark 6.1.2 and integration by parts lead to

$$
\begin{aligned}
&\big\langle \dot{\mathbf{D}}\boldsymbol{\Psi}^{t+\tau,t}\bar{\mathbf{u}}(t)(\bar{\mathbf{e}}(t)) - \boldsymbol{\epsilon}(t) - \tau(\ddot{\mathbf{e}}(t) - \dot{\mathbf{m}}(t) - \boldsymbol{\mu}(t)), \mathbf{v} \big\rangle_{(\mathbf{H}^1)^* \times \mathbf{H}^1} \\
&= -\frac{\tau^2}{4} \big\langle \mathbf{F}\big(\dot{\mathbf{D}}\boldsymbol{\Psi}^{t+\tau,t}\bar{\mathbf{u}}(t)(\bar{\mathbf{e}}(t)) + \boldsymbol{\epsilon}(t) \big), \mathbf{v} \big\rangle - \frac{\tau}{2} \big\langle \mathbf{G}\big(\dot{\mathbf{D}}\boldsymbol{\Psi}^{t+\tau,t}\bar{\mathbf{u}}(t)(\bar{\mathbf{e}}(t)) - \boldsymbol{\epsilon}(t) \big), \mathbf{v} \big\rangle \\
&\quad + \tau \big\langle \mathbf{F}_{\mathrm{con}}\big(\mathbf{D}\boldsymbol{\Psi}^{t+\tau,t}\bar{\mathbf{u}}(t)(\bar{\mathbf{e}}(t)) \big) - \mathbf{F}_{\mathrm{con}}(\mathbf{e}(t)), \mathbf{v} \big\rangle_{(\mathbf{H}^1)^* \times \mathbf{H}^1} \\
&= -\frac{\tau^2}{4} \|\mathbf{v}\|_a^2 - \frac{\tau^2}{4} a(\boldsymbol{\epsilon}(t) + \boldsymbol{\epsilon}(t+\tau), \mathbf{v}) + \frac{\tau^2}{4} a\Big(\int_t^{t+\tau} \boldsymbol{\mu}(s)\,ds, \mathbf{v} \Big) \\
&\quad - \frac{\tau}{2} \|\mathbf{v}\|_b^2 - \frac{\tau}{2} b(\boldsymbol{\epsilon}(t+\tau) - \boldsymbol{\epsilon}(t), \mathbf{v}) + \frac{\tau}{2} b\Big(\int_t^{t+\tau} \boldsymbol{\mu}(s)\,ds, \mathbf{v} \Big) \\
&\quad + \tau \big\langle \mathbf{F}_{\mathrm{con}}\big(\mathbf{D}\boldsymbol{\Psi}^{t+\tau,t}\bar{\mathbf{u}}(t)(\bar{\mathbf{e}}(t)) \big) - \mathbf{F}_{\mathrm{con}}(\mathbf{e}(t)), \mathbf{v} \big\rangle_{(\mathbf{H}^1)^* \times \mathbf{H}^1} \\
&= -\frac{\tau^2}{4} \|\mathbf{v}\|_a^2 - \frac{\tau^2}{4} a(\dot{\mathbf{e}}(t) + \dot{\mathbf{e}}(t+\tau), \mathbf{v}) + \frac{\tau^2}{4} a\Big(\mathbf{m}(t) + \mathbf{m}(t+\tau) + \int_t^{t+\tau} \boldsymbol{\mu}(s)\,ds, \mathbf{v} \Big) \\
&\quad - \frac{\tau}{2} \|\mathbf{v}\|_b^2 + \frac{\tau}{2} b(\dot{\mathbf{e}}(t+\tau) - \dot{\mathbf{e}}(t), \mathbf{v}) + \frac{\tau}{2} b\Big(\int_t^{t+\tau} \dot{\mathbf{m}}(s) + \boldsymbol{\mu}(s)\,ds, \mathbf{v} \Big) \\
&\quad + \tau \big\langle \mathbf{F}_{\mathrm{con}}\big(\mathbf{D}\boldsymbol{\Psi}^{t+\tau,t}\bar{\mathbf{u}}(t)(\bar{\mathbf{e}}(t)) \big) - \mathbf{F}_{\mathrm{con}}(\mathbf{e}(t)), \mathbf{v} \big\rangle_{(\mathbf{H}^1)^* \times \mathbf{H}^1} .
\end{aligned}
$$

Due to estimate (6.20) and the inequality of Korn (A.1),

$$\begin{aligned}
&\Big\|\dot{\mathbf{D}}\boldsymbol{\Psi}^{t+\tau,t}\bar{\mathbf{u}}(t)(\bar{\mathbf{e}}(t)) - \boldsymbol{\epsilon}(t+\tau) + \int_t^{t+\tau} \boldsymbol{\mu}(s)\,ds\Big\|_{\mathbf{L}_2}^2 + \frac{\tau}{2}\|\mathbf{v}\|_b^2 \\
&\leq -\frac{\tau^2}{4}\|\mathbf{v}\|_a^2 + \frac{\tau^2}{4}\big(\|\dot{\mathbf{e}}(t)\|_{\mathbf{H}^1} + \|\dot{\mathbf{e}}(t+\tau)\|_{\mathbf{H}^1}\big)\|\mathbf{v}\|_{\mathbf{H}^1} \\
&\quad + \frac{\tau^2}{4}\big(\|\mathbf{m}(t)\|_{\mathbf{H}^1} + \|\mathbf{m}(t+\tau)\|_{\mathbf{H}^1} + \|\boldsymbol{\mu}\|_{\mathbf{L}_1(t,t+\tau;\mathbf{H}^1)}\big)\|\mathbf{v}\|_{\mathbf{H}^1} \\
&\quad + \frac{\tau}{2}\|\dot{\mathbf{e}}(t+\tau) - \dot{\mathbf{e}}(t)\|_{\mathbf{H}^1}\|\mathbf{v}\|_{\mathbf{H}^1} + \frac{\tau}{2}\big(\|\dot{\mathbf{m}}\|_{\mathbf{L}_1(t,t+\tau;\mathbf{H}^1)} + \|\boldsymbol{\mu}\|_{\mathbf{L}_1(t,t+\tau;\mathbf{H}^1)}\big)\|\mathbf{v}\|_{\mathbf{H}^1} \\
&\quad + \tau\big|\big\langle \mathbf{F}_{\mathrm{con}}\big(\mathbf{D}\boldsymbol{\Psi}^{t+\tau,t}\bar{\mathbf{u}}(t)(\bar{\mathbf{e}}(t))\big) - \mathbf{F}_{\mathrm{con}}(\mathbf{e}(t)), \mathbf{v}\big\rangle_{(\mathbf{H}^1)^*\times\mathbf{H}^1}\big| \\
&\quad + \big(\mathrm{TV}\big(\ddot{\mathbf{e}}, [t,t+\tau], \mathbf{H}^1\big) + o\big(\tau^{1/2}\big)\big)\|\mathbf{v}\|_{\mathbf{H}^1}\cdot O(\tau) \\
&= -\frac{\tau^2}{4}\|\mathbf{v}\|_a^2 + \tau\big|\big\langle \mathbf{F}_{\mathrm{con}}\big(\mathbf{D}\boldsymbol{\Psi}^{t+\tau,t}\bar{\mathbf{u}}(t)(\bar{\mathbf{e}}(t))\big) - \mathbf{F}_{\mathrm{con}}(\mathbf{e}(t)), \mathbf{v}\big\rangle_{(\mathbf{H}^1)^*\times\mathbf{H}^1}\big| \\
&\quad + \big(\mathrm{TV}\big(\dot{\mathbf{e}}, [t,t+\tau], \mathbf{H}^1\big) + \mathrm{TV}\big(\ddot{\mathbf{e}}, [t,t+\tau], \mathbf{H}^1\big) + o\big(\tau^{1/2}\big)\big)\|\mathbf{v}\|_{\mathbf{H}^1}\cdot O(\tau)
\end{aligned}$$

holds. Adding the square of (6.21), the inequality of Young leads to

$$\begin{aligned}
&\frac{1}{2}\Big\|\dot{\mathbf{D}}\boldsymbol{\Psi}^{t+\tau,t}\bar{\mathbf{u}}(t)(\bar{\mathbf{e}}(t)) - \boldsymbol{\epsilon}(t+\tau) + \int_t^{t+\tau} \boldsymbol{\mu}(s)\,ds\Big\|_{\mathbf{L}_2}^2 \\
&+ \frac{1}{2}\big\|\mathbf{D}\boldsymbol{\Psi}^{t+\tau,t}\bar{\mathbf{u}}(t)(\bar{\mathbf{e}}(t)) - \mathbf{e}(t+\tau) + \tau\mathbf{m}(t)\big\|_a^2 + \frac{\tau}{4}\|\mathbf{v}\|_b^2 \\
&= \frac{\tau}{2}\big|\big\langle \mathbf{F}_{\mathrm{con}}\big(\mathbf{D}\boldsymbol{\Psi}^{t+\tau,t}\bar{\mathbf{u}}(t)(\bar{\mathbf{e}}(t))\big) - \mathbf{F}_{\mathrm{con}}(\mathbf{e}(t)), \mathbf{v}\big\rangle_{(\mathbf{H}^1)^*\times\mathbf{H}^1}\big| \\
&\quad + \big(R(\mathbf{e},[t,t+\tau])\cdot O(\tau) + o\big(\tau^{3/2}\big)\big)^2 + \big(R(\mathbf{e},[t,t+\tau]) + o\big(\tau^{1/2}\big)\big)\|\mathbf{v}\|_{\mathbf{H}^1}\cdot O(\tau)\,.
\end{aligned}$$

This is an estimate of the type

$$x^2 + \frac{\tau}{4}\|\mathbf{v}\|_b^2 \leq a^2 + b\|\mathbf{v}\|_{\mathbf{H}^1}\cdot\tau$$

with $a, b > 0$, and $x^2\cdot\tau^{2p}$ is the right-hand side of (6.19). The inequality of Korn (A.1) yields

$$\|\mathbf{v}\|_{\mathbf{H}^1} \leq \frac{1}{c_K}\big(\|\mathbf{v}\|_{\mathbf{L}_2}^2 + \|\mathbf{v}\|_b^2\big)^{1/2} \leq \frac{2}{c_K}\Big(x^2 + \frac{\tau}{4}\|\mathbf{v}\|_b^2\Big)^{1/2}\cdot\tau^{-1/2}$$

for τ sufficiently small. Hence,

$$x^2 + \frac{\tau}{4}\|\mathbf{v}\|_b^2 \leq a^2 + \frac{2b}{c_K}\Big(x^2 + \frac{\tau}{4}\|\mathbf{v}\|_b^2\Big)^{1/2}\cdot\tau^{1/2}\,,$$

and by means of the binomial formula, this is equivalent to

$$\Big(\Big(x^2 + \frac{\tau}{4}\|\mathbf{v}\|_b^2\Big)^{1/2} - \frac{b}{c_K}\cdot\tau^{1/2}\Big)^2 \leq a^2 + \frac{b^2}{c_K^2}\cdot\tau\,.$$

Finally,

$$\Big(x^2 + \frac{\tau}{4}\|\mathbf{v}\|_b^2\Big)^{1/2} \leq a + b \cdot O\big(\tau^{1/2}\big)\,,$$

and (6.19) gives the result of the lemma. □

With these rather lengthy preparations, the central theorem of this chapter can be proven now.

Theorem 6.1.10. *Let Assumptions* 6.1.5 *and* 6.1.7 *hold. Then, the consistency error* $\bar{\boldsymbol{\Psi}}_* - \bar{\boldsymbol{\Phi}} = (\boldsymbol{\Psi}_* - \boldsymbol{\Phi}, \dot{\boldsymbol{\Psi}}_* - \dot{\boldsymbol{\Phi}})$ *satisfies*

$$\begin{aligned}
&\big\|\bar{\boldsymbol{\Psi}}_*^{t+\tau,t}\bar{\mathbf{u}}(t) - \bar{\boldsymbol{\Phi}}^{t+\tau,t}\bar{\mathbf{u}}(t) - (\bar{\mathbf{r}}(t,\tau) + \bar{\mathbf{p}}(t,\tau)) \cdot \tau^p\big\|_E \\
&= \Big(\big\|\mathbf{F}_{\mathrm{con}}\big(\mathbf{D}\boldsymbol{\Psi}^{t+\tau,t}\bar{\mathbf{u}}(t)(\bar{\mathbf{e}}(t))\big) - \mathbf{F}_{\mathrm{con}}(\mathbf{e}(t))\big\|_{(\mathbf{H}^1)^*} + R(\mathbf{e},[t,t+\tau])\Big) \cdot O\big(\tau^{p+1/2}\big) \\
&\quad + o\big(\tau^{p+1}\big) \qquad (6.22)
\end{aligned}$$

with $R(\mathbf{e},[t,t+\tau])$ *defined in* (4.22).

Proof. With $\mathbf{v} := \dot{\mathbf{D}}\boldsymbol{\Psi}^{t+\tau,t}\bar{\mathbf{u}}(t)(\bar{\mathbf{e}}(t)) - \boldsymbol{\epsilon}(t+\tau) + \int_t^{t+\tau}\boldsymbol{\mu}(s)\,ds$, Lemma 6.1.8 yields

$$\begin{aligned}
&\Big(\big\|\bar{\boldsymbol{\Psi}}_*^{t+\tau,t}\bar{\mathbf{u}}(t) - \bar{\boldsymbol{\Phi}}^{t+\tau,t}\bar{\mathbf{u}}(t) - (\bar{\mathbf{r}}(t,\tau) + \bar{\mathbf{p}}(t,\tau)) \cdot \tau^p\big\|_E^2 + \frac{\tau}{4}\|\mathbf{v}\|_b^2 \cdot \tau^{2p}\Big)^{1/2} \\
&\leq \Big(\frac{1}{2}\big\|\mathbf{F}_{\mathrm{con}}\big(\mathbf{D}\boldsymbol{\Psi}^{t+\tau,t}\bar{\mathbf{u}}(t)(\bar{\mathbf{e}}(t))\big) - \mathbf{F}_{\mathrm{con}}(\mathbf{e}(t))\big\|_{(\mathbf{H}^1)^*}\Big)^{1/2}\|\mathbf{v}\|_{\mathbf{H}^1}^{1/2} \cdot \tau^{p+1/2} \\
&\quad + R\big(\mathbf{e},[t,t+\tau]\big) \cdot O\big(\tau^{p+1/2}\big) + o\big(\tau^{p+1}\big)\,.
\end{aligned}$$

This is an estimate of the form

$$\Big(x^2 + \frac{\tau}{4}\|\mathbf{v}\|_b^2 \cdot \tau^{2p}\Big)^{1/2} \leq a + b^{1/2}\|\mathbf{v}\|_{\mathbf{H}^1}^{1/2} \cdot \tau^{p+1/2}$$

with $a, b, x > 0$. The inequality of Young leads to

$$\Big(x^2 + \frac{\tau}{4}\|\mathbf{v}\|_b^2 \cdot \tau^{2p}\Big)^{1/2} \leq a + \alpha b \cdot \tau^{p+1/2} + \frac{1}{\alpha}\|\mathbf{v}\|_{\mathbf{H}^1} \cdot \tau^{p+1/2}$$

with $\alpha > 0$, and due to the inequality of Korn (A.1)

$$\|\mathbf{v}\|_{\mathbf{H}^1} \cdot \tau^{p+1/2} \leq \frac{1}{c_K}\big(\|\mathbf{v}\|_{\mathbf{L}_2}^2 + \|\mathbf{v}\|_b^2\big)^{1/2} \cdot \tau^{p+1/2} \leq \frac{2}{c_K}\Big(x^2 + \frac{\tau}{4}\|\mathbf{v}\|_b^2 \cdot \tau^{2p}\Big)^{1/2}$$

holds for τ sufficiently small. Choosing $\alpha = 4/c_K$, the estimate above can be reformulated as

$$\frac{1}{2}\Big(x^2 + \frac{\tau}{4}\|\mathbf{v}\|_b^2 \cdot \tau^{2p}\Big)^{1/2} \leq a + \frac{4b}{c_K} \cdot \tau^{p+1/2}$$

such that

$$x = O\big(a + b \cdot \tau^{p+1/2}\big)\,.$$

□

6.1.4. Discussion of Consistency Order

The purpose in the previous section was to construct the discrete evolution operator $(\boldsymbol{\Psi}_*, \dot{\boldsymbol{\Psi}}_*)$ such that the resulting scheme is of higher consistency order in energy norm than (N-CS+), compare condition (6.11). In order to analyze the actual order of the scheme, the result of Theorem 6.1.10 will be discussed in detail.

First of all, the error estimate (6.22) contains the remainder term $\bar{\mathbf{r}}(t, \tau)$ of Assumption 6.1.5 on the consistency error of (N-CS+), which strongly depends on the choice of the order p. The consistency result 4.2.7 in energy norm does not give any information about the local behavior of the error in space. In order to gain some insight into this problem, a numerical study concerning the spatial distribution of the consistency error of (N-CS+) has been performed.

Numerical Experiment. As an illustrative test problem, the Hertzian contact in 2D from Section 2.5 with further five refinements within the circle around the bottom of the semicircle has been selected. The elastic and viscous material parameters can be found in Table 6.1.

parameter	value
Young's modulus	10
Poisson ratio	0.4
shear viscosity	10
bulk viscosity	10

Table 6.1.: Material specifications.

In order to get an approximation of the exact solution of the variational problem, (N-CS+) is performed with an extremely high timestep resolution. The difference between this fine reference solution and one large step of (N-CS+) acts as an indicator for the consistency error of the scheme.

Figure 6.1 shows the time evolution of the estimated consistency error of (N-CS+) in velocities as the timestep τ tends to zero. The domain where the error has a significant value shrinks for decreasing timesteps. For small τ, the error is concentrated near those parts of the contact boundary where the active set changes. Moreover, the error seems to consist of two different parts, a regular one in the interior of the domain and a second one at the changing active contact boundary. This effect corresponds to the theoretical analysis of the consistency error as discussed in Section 4.4 and Remark 6.1.9 and will become important for the timestep control in Section 6.2.

The observations above lead to the following conjecture on the local behavior of the consistency error. Due to the viscous material behavior, the irregularity of the problem from the changing active contact boundaries is smoothened in the interior

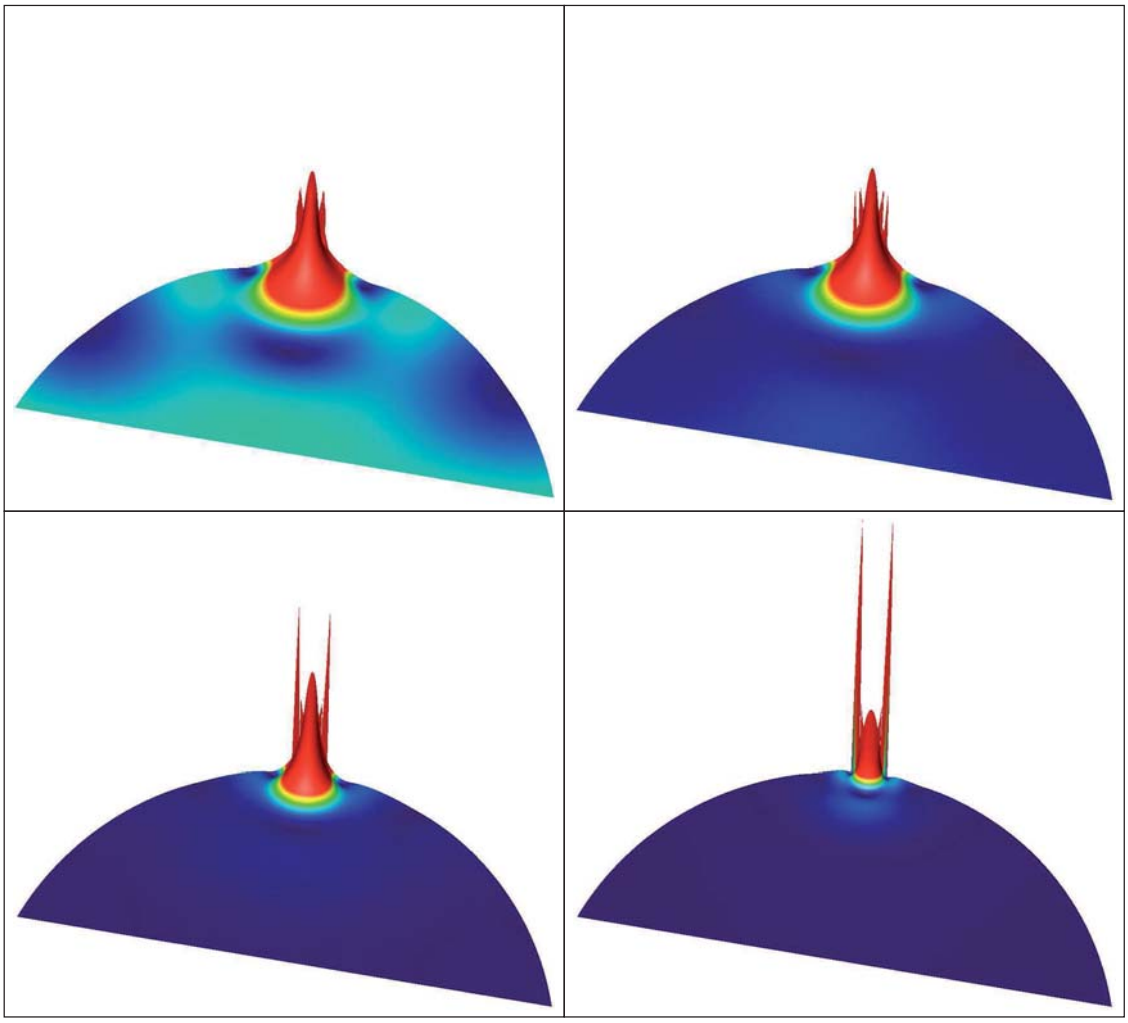

Figure 6.1.: Estimated spatial distribution of the temporal consistency error of (N-CS+) in velocities for $\tau \to 0$ (4 snapshots). The error consists of two parts: a regular one in the interior of the domain and a second one with large values near the changing active contact boundary.

of the domain. If a suitable subdomain $\tilde{\Omega}$ of Ω is picked with positive minimal distance to the contact boundaries, maximal order of consistency $p = 2$ should be found on $\tilde{\Omega}$, eventually for small τ. However, the range of τ for which the asymptotic behavior becomes visible most likely depends on the choice of $\tilde{\Omega}$. Exhausting Ω by a sequence of sets $\tilde{\Omega}_k \subset \tilde{\Omega}_{k+1} \subset \ldots$ leads to maximal order of consistency on each of these sets, but a lower total order of consistency on the whole domain Ω.

The local behavior of the consistency error (and the sensitivity) of (N-CS+) is reflected in the assumption

$$\|\bar{\mathbf{r}}(t,\tau)+\bar{\mathbf{p}}(t,\tau)\|_{E(\tilde{\Omega})}\cdot\tau^2=o\big(\tau^3\big)$$

where the reduced physical energy norm with respect to the subdomain $\tilde{\Omega}$ is denoted by $\|\cdot\|_{E(\tilde{\Omega})}$. Applying the lower triangle inequality on the result of Theorem 6.1.10 with $p=2$, the consistency error estimate

$$\begin{aligned}
&\big\|\bar{\boldsymbol{\Psi}}_*^{t+\tau,t}\bar{\mathbf{u}}(t)-\bar{\boldsymbol{\Phi}}^{t+\tau,t}\bar{\mathbf{u}}(t)\big\|_{E(\tilde{\Omega})}\\
&\leq\Big(\big\|\mathbf{F}_{\mathrm{con}}\big(\mathbf{D}\boldsymbol{\Psi}^{t+\tau,t}\bar{\mathbf{u}}(t)(\bar{\mathbf{e}}(t))\big)-\mathbf{F}_{\mathrm{con}}(\mathbf{e}(t))\big\|_{(\mathbf{H}^1(\Omega))^*}+R(\mathbf{e},[t,t+\tau])\Big)\cdot O\big(\tau^{5/2}\big)\\
&\quad+\|(\bar{\mathbf{r}}(t,\tau)+\bar{\mathbf{p}}(t,\tau))\|_{E(\tilde{\Omega})}\cdot\tau^2+o\big(\tau^3\big)\\
&=\Big(\big\|\mathbf{F}_{\mathrm{con}}\big(\mathbf{D}\boldsymbol{\Psi}^{t+\tau,t}\bar{\mathbf{u}}(t)(\bar{\mathbf{e}}(t))\big)-\mathbf{F}_{\mathrm{con}}(\mathbf{e}(t))\big\|_{(\mathbf{H}^1(\Omega))^*}+R(\mathbf{e},[t,t+\tau])\Big)\cdot O\big(\tau^{5/2}\big)\\
&\quad+o\big(\tau^3\big)
\end{aligned}$$

holds on $\tilde{\Omega}$. The discussion in Remark 6.1.9 has provided that the difference of the contact forces $\mathbf{F}_{\mathrm{con}}(\mathbf{D}\boldsymbol{\Psi}^{t+\tau,t}\bar{\mathbf{u}}(t)(\bar{\mathbf{e}}(t)))$ and $\mathbf{F}_{\mathrm{con}}(\mathbf{e}(t))$ only act on a small part of the possible contact boundaries, which is expected to tend to zero for most times t as $\tau\to 0$. However, for ease of presentation, this behavior has been neglected by applying an $(\mathbf{H}^1(\Omega))^*$-norm estimate. This norm depends on the behavior of the differences $\mathbf{D}\boldsymbol{\Psi}^{t+\tau,t}\bar{\mathbf{u}}(t)(\bar{\mathbf{e}}(t))-\mathbf{e}(t)$ and $\dot{\mathbf{D}}\boldsymbol{\Psi}^{t+\tau,t}\bar{\mathbf{u}}(t)(\bar{\mathbf{e}}(t))-\boldsymbol{\epsilon}(t)$, which tend to zero in $\mathbf{H}^1$ and in $\mathbf{L}_2$, respectively. For most times t, even an $\mathbf{H}^1$-convergence to zero of order τ may be expected, and the assumption

$$\big\|\mathbf{F}_{\mathrm{con}}\big(\mathbf{D}\boldsymbol{\Psi}^{t+\tau,t}\bar{\mathbf{u}}(t)(\bar{\mathbf{e}}(t))\big)-\mathbf{F}_{\mathrm{con}}(\mathbf{e}(t))\big\|_{(\mathbf{H}^1(\Omega))^*}=O(\tau)$$

is reasonable. The quantity $R(\mathbf{e},[t,t+\tau])$ corresponds to the right-hand side of the consistency result 4.2.7, which contains $R(\mathbf{u},[t,t+\tau])$ in turn. Since $\bar{\mathbf{e}}$ and $\bar{\mathbf{u}}$ are defined via variational inequalities with coinciding active contact boundaries, $R(\mathbf{e},[t,t+\tau])$ is expected to originate from a quantity that has a similar local behavior as the consistency error of (N-CS+). However, since $R(\mathbf{e},[t,t+\tau])$ refers to the whole domain Ω, the considerations are restricted to

$$R(\mathbf{e},[t,t+\tau])=O(\tau)\,,$$

which again is a reasonable assumption, at least for most times t. Then,

$$\big\|\bar{\boldsymbol{\Psi}}_*^{t+\tau,t}\bar{\mathbf{u}}(t)-\bar{\boldsymbol{\Phi}}^{t+\tau,t}\bar{\mathbf{u}}(t)\big\|_{E(\tilde{\Omega})}=o\big(\tau^3\big)\,,\tag{6.23}$$

and the scheme $(\boldsymbol{\Psi}_*,\dot{\boldsymbol{\Psi}}_*)$ is of higher consistency order on $\tilde{\Omega}$ than (N-CS+). In summary, an asymptotic error expansion of (N-CS+) with order $p=2$ is expected that is visible on a subdomain in the interior.

6.2. Timestep Control

In this section, the aim is to develop a strategy for choosing the size of timesteps for the improved contact–stabilized Newmark method adaptively. This variant of (N-CS+) will be called ContacX further on.

Ideally, an adaptive timestep control guarantees that the global discretization error of the approximation is below a prescribed tolerance. However, global errors are difficult to control since they consist of the actual consistency error as well as the propagation of all errors that arise during time integration. Following the standard approach, the intention is to control the actual consistency error in the reduced physical energy norm such that

$$\|\bar{\boldsymbol{\Psi}} - \bar{\boldsymbol{\Phi}}\|_E \leq \mathrm{TOL} \tag{6.24}$$

where TOL is a *local tolerance* defined by the user. The idea behind is that smaller consistency errors lead to a decrease of the global error, which will be analyzed in Section 6.3. Since the local error cannot be determined exactly, a computable estimate

$$\left[\|\bar{\boldsymbol{\Psi}} - \bar{\boldsymbol{\Phi}}\|_E\right] \approx \|\bar{\boldsymbol{\Psi}} - \bar{\boldsymbol{\Phi}}\|_E \tag{6.25}$$

is needed with the implementable condition

$$\left[\|\bar{\boldsymbol{\Psi}} - \bar{\boldsymbol{\Phi}}\|_E\right] \leq \mathrm{TOL}\,. \tag{6.26}$$

The construction of a problem-adapted *error estimator* is the main challenge in the establishment of an adaptive timestep control. Let $\bar{\hat{\boldsymbol{\Psi}}} = \left(\hat{\boldsymbol{\Psi}}, \dot{\hat{\boldsymbol{\Psi}}}\right)$ be a second discrete evolution that is of higher accuracy than (N-CS+) for sufficiently small timesteps. Then, the difference between the two numerical solutions

$$\left[\|\bar{\boldsymbol{\Psi}} - \bar{\boldsymbol{\Phi}}\|_E\right] := \|\bar{\boldsymbol{\Psi}} - \bar{\hat{\boldsymbol{\Psi}}}\|_E \tag{6.27}$$

is an error estimator. If the more accurate time integration scheme is even of higher consistency order than (N-CS+), then the error estimator is asymptotically exact (for more details see, e.g., [18]).

In order to develop a comparative scheme of higher order, the intention is to employ extrapolation techniques, which require an asymptotic error expansion of (N-CS+). As seen in the foregoing Section 6.1, the classical theory can not directly be applied to dynamical contact problems due to the missing regularity at time-dependent contact boundaries. In order to ensure a reliable timestep control, the classical error estimator and timestep selection have to be adapted in the presence of contact.

6.2.1. Error Estimator in the Absence of Contact

In the absence of contact, (N-CS+) has pointwise optimal consistency order $p = 2$ both in displacements and in velocities. Furthermore, the consistency error has a pointwise Taylor expansion due to the linearity of the problem. Hence, the results of Section 6.1 yield the existence of an asymptotic error expansion of the Newmark method.

$$\begin{array}{lll} \bar{\boldsymbol{u}}_\tau = & \bar{\boldsymbol{u}}_{11} & \searrow \\ \bar{\boldsymbol{u}}_{\frac{\tau}{2}} = & \bar{\boldsymbol{u}}_{21} & \longrightarrow \ \bar{\boldsymbol{u}}_{22} \end{array}$$

Figure 6.2.: Extrapolation table in the absence of contact, compare Figure 6.3.

In order to construct a scheme of higher order, a one-step extrapolation method is applied, see Figure 6.2. A second numerical solution with half timestep $\tau/2$ is computed, and then, the asymptotic error expansions

$$\begin{aligned} \bar{\mathbf{u}}_{11}(t+\tau) &= \bar{\mathbf{u}}(t+\tau) + \bar{\mathbf{e}}(t+\tau)\tau^2 + o\big(\tau^3\big) \\ \bar{\mathbf{u}}_{21}(t+\tau) &= \bar{\mathbf{u}}(t+\tau) + \bar{\mathbf{e}}(t+\tau)\Big(\frac{\tau}{2}\Big)^2 + o\big(\tau^3\big) \end{aligned} \tag{6.28}$$

of (N-CS+) are considered. The extrapolated method

$$\bar{\mathbf{u}}_{22}(t+\tau) := \frac{1}{1-2^2}\big(\bar{\mathbf{u}}_{11}(t+\tau) - 2^2\bar{\mathbf{u}}_{21}(t+\tau)\big) \tag{6.29}$$

is of higher consistency order in energy norm than (N-CS+) since

$$\begin{aligned} &\|\bar{\mathbf{u}}_{22}(t+\tau) - \bar{\mathbf{u}}(t+\tau)\|_E \\ &\leq \frac{1}{2^2-1}\big\|\bar{\mathbf{u}}_{11}(t+\tau) - \bar{\mathbf{u}}(t+\tau) - \bar{\mathbf{e}}(t+\tau)\tau^2\big\|_E \\ &\quad + \frac{2^2}{2^2-1}\Big\|\bar{\mathbf{u}}_{21}(t+\tau) - \bar{\mathbf{u}}(t+\tau) - \bar{\mathbf{e}}(t+\tau)\Big(\frac{\tau}{2}\Big)^2\Big\|_E \\ &= o\big(\tau^3\big)\,. \end{aligned}$$

The *subdiagonal* error estimator

$$\big[\|\bar{\mathbf{u}}_{21}(t+\tau) - \bar{\mathbf{u}}(t+\tau)\|_E\big] := \|\bar{\mathbf{u}}_{21}(t+\tau) - \bar{\mathbf{u}}_{22}(t+\tau)\|_E \tag{6.30}$$

is chosen since the computation should be continued with the higher-order solution $\bar{\mathbf{u}}_{21}(t+\tau)$. The extrapolated solution $\bar{\mathbf{u}}_{22}(t+\tau)$ is not practical due to the missing energy dissipativity of the scheme. The choice of a subdiagonal error estimator avoids that condition (6.24) is over satisfied (see, e.g., [18]).

6.2.2. Error Estimator in the Presence of Contact

If active contact boundaries are found in a time interval, the discussion on the existence of an asymptotic error expansion of (N-CS+) in Section 6.1 has to be taken into account.

Due to the theoretical insight in Section 4.4 or Remark 6.1.9 and the numerical observations in Section 6.1.4, the consistency error seems to consist of two different parts. The first one acts on points in the interior of the domain and is assumed to be of optimal order $p = 2$. The second one becomes extremely large at points near changing active contact boundaries. The extrapolated solution (6.29) is of higher consistency order than (N-CS+) only at points that have already reached the asymptotic phase $p = 2$. Hence, the classical error estimator (6.30) is only applicable on a subdomain. If this subdomain grows as the timestep tends to zero, the estimator becomes more and more accurate for small τ. However, the classical approach underestimates the remainder terms in the asymptotic error expansion near the critical changing contact boundaries.

In order to control the additional contribution to the consistency error in the presence of contact, a quantity $\bar{\mathbf{X}} = (\mathbf{X}, \dot{\mathbf{X}})$ is added to the model for the approximation error. The term including $\bar{\mathbf{X}}$ may be of worst possible order $p = 1/2$ as shown by the consistency result 4.2.7 up to sets of measure zero. The quantity should have a significant value at points near those parts of the active contact boundaries that vary within the timestep. In the limit $\tau \to 0$, the domain where the quantity vanishes should increase.

Again, two numerical solutions with timesteps τ and $\tau/2$ are computed, and the ansatz

$$\begin{aligned} \bar{\mathbf{u}}_{11}(t+\tau) &\approx \bar{\mathbf{u}}(t+\tau) + \bar{\mathbf{e}}(t+\tau)\tau^2 + \bar{\mathbf{X}}(t+\tau)\tau^{1/2} \\ \bar{\mathbf{u}}_{21}(t+\tau) &\approx \bar{\mathbf{u}}(t+\tau) + \bar{\mathbf{e}}(t+\tau)\Big(\frac{\tau}{2}\Big)^2 + \bar{\mathbf{X}}(t+\tau)\Big(\frac{\tau}{2}\Big)^{1/2} \end{aligned} \tag{6.31}$$

for the approximation error is made. Within this model, the extrapolated solution $\bar{\mathbf{u}}_{22}(t+\tau)$ from (6.29) satisfies

$$\bar{\mathbf{u}}_{22}(t+\tau) \approx \bar{\mathbf{u}}(t+\tau) + \frac{1 - 2^{2-1/2}}{1 - 2^2}\bar{\mathbf{X}}(t+\tau)\tau^{1/2}\,.$$

In order to handle the low order term in this formula, the extrapolation table is extended by a third solution with timestep $\tau/3$, see Figure 6.3. This approximation satisfies

$$\bar{\mathbf{u}}_{31}(t+\tau) \approx \bar{\mathbf{u}}(t+\tau) + \bar{\mathbf{e}}(t+\tau)\Big(\frac{\tau}{3}\Big)^2 + \bar{\mathbf{X}}(t+\tau)\Big(\frac{\tau}{3}\Big)^{1/2}, \tag{6.32}$$

and the extrapolated solution

$$\bar{\mathbf{u}}_{32}(t+\tau) := \frac{1}{2^2 - 3^2}\big(2^2\bar{\mathbf{u}}_{21}(t+\tau) - 3^2\bar{\mathbf{u}}_{31}(t+\tau)\big) \tag{6.33}$$

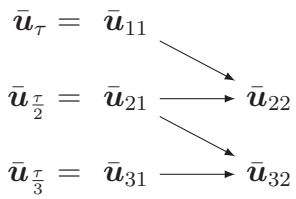

Figure 6.3.: Extrapolation table in the presence of contact, compare Figure 6.2.

yields

$$\bar{\mathbf{u}}_{32}(t+\tau) \approx \bar{\mathbf{u}}(t+\tau) + \frac{2^{2-1/2} - 3^{2-1/2}}{2^2 - 3^2} \bar{\mathbf{X}}(t+\tau)\tau^{1/2} .$$

In a next step, both extrapolation schemes are combined via

$$\bar{\hat{\mathbf{u}}}(t+\tau) := \frac{1}{\alpha - \beta}\big(\alpha \bar{\mathbf{u}}_{22}(t+\tau) - \beta \bar{\mathbf{u}}_{32}(t+\tau)\big) \tag{6.34}$$

with

$$\alpha = \frac{2^{2-1/2} - 3^{2-1/2}}{2^2 - 3^2} , \quad \beta = \frac{1 - 2^{2-1/2}}{1 - 2^2} \tag{6.35}$$

such that

$$\bar{\hat{\mathbf{u}}}(t+\tau) \approx \bar{\mathbf{u}}(t+\tau) .$$

As before, the computation is proceeded with the finest solution $\bar{\mathbf{u}}_{31}(t+\tau)$. Hence, the subdiagonal error estimator

$$\big[\|\bar{\mathbf{u}}_{31}(t+\tau) - \bar{\mathbf{u}}(t+\tau)\|_E\big] := \big\|\bar{\mathbf{u}}_{31}(t+\tau) - \bar{\hat{\mathbf{u}}}(t+\tau)\big\|_E \tag{6.36}$$

is taken. Due to

$$\begin{aligned} &\big[\|\bar{\mathbf{u}}_{31}(t+\tau) - \bar{\mathbf{u}}(t+\tau)\|_E\big] \\ &\approx \left\|\bar{\mathbf{u}}_{31}(t+\tau) - \bar{\mathbf{u}}_{32}(t+\tau) - \frac{2^{2-1/2} - 3^{2-1/2}}{2^2 - 3^2} \bar{\mathbf{X}}(t+\tau)\tau^{1/2}\right\|_E , \end{aligned}$$

the constructed error estimator consists of two parts. The first one corresponds to the classical estimator (6.30) with timestep $\tau/3$. The second one is proportional to the quantity $\bar{\mathbf{X}}(t+\tau)$ in the asymptotic error expansion and mainly acts near the changing contact boundaries. Hence, the error estimator takes into account the special structure of the consistency error of (N-CS+) as shown by the theoretical investigations in Section 4.4 or Remark 6.1.9 and the numerical experiment in Section 6.1.4.

6.2.3. Combined Timestep Strategy

The construction of an adaptive timestep control requires a suggestion for the new timestep from the actual information. Usually, this timestep is given by the optimal timestep τ^* for the actual step, which is characterized by

$$\|\bar{\mathbf{u}}_{21}(t+\tau^*) - \bar{\mathbf{u}}(t+\tau^*)\|_E \approx \rho \cdot \mathrm{TOL}\,, \tag{6.37}$$

or

$$\|\bar{\mathbf{u}}_{31}(t+\tau^*) - \bar{\mathbf{u}}(t+\tau^*)\|_E \approx \rho \cdot \mathrm{TOL} \tag{6.38}$$

with a *safety factor* $\rho < 1$.

No contact. In the absence of contact, $\bar{\mathbf{e}}(t+\tau) \approx \bar{\dot{\mathbf{e}}}(t) \cdot \tau$ is taken. Inserting this approximation into the asymptotic error expansion (6.28) of (N-CS+) yields

$$\bar{\mathbf{u}}_{21}(t+\tau) - \bar{\mathbf{u}}(t+\tau) \approx \bar{\dot{\mathbf{e}}}(t)\tau \cdot \Big(\frac{\tau}{2}\Big)^2$$

for all τ up to terms of higher order. This leads to

$$\bar{\mathbf{u}}_{21}(t+\tau^*) - \bar{\mathbf{u}}(t+\tau^*) \approx (\bar{\mathbf{u}}_{21}(t+\tau) - \bar{\mathbf{u}}(t+\tau)) \cdot \Big(\frac{\tau^*}{\tau}\Big)^3 .$$

Taking the energy norm of this approximation and inserting condition (6.37), the optimal timestep τ^* can be predicted by the classical timestep formula

$$\tau^* = \sqrt[3]{\frac{\rho \cdot \mathrm{TOL}}{\|\bar{\mathbf{u}}_{21}(t+\tau) - \bar{\mathbf{u}}_{22}(t+\tau)\|_E}} \cdot \tau\,. \tag{6.39}$$

Contact. In the presence of contact, ansatz (6.32) for the discretization error of (N-CS+) and assumption $\bar{\mathbf{e}}(t+\tau) \approx \bar{\dot{\mathbf{e}}}(t) \cdot \tau$ yield

$$\bar{\mathbf{u}}_{31}(t+\tau^*) - \bar{\mathbf{u}}(t+\tau^*) \approx \bar{\mathbf{e}}(t+\tau)\Big(\frac{\tau}{3}\Big)^2\Big(\frac{\tau^*}{\tau}\Big)^3 + \bar{\mathbf{X}}(t+\tau^*)\Big(\frac{\tau^*}{3}\Big)^{1/2}.$$

In order to make sure that $\tau^* < \tau$ if $\|\bar{\mathbf{u}}_{31}(t+\tau) - \bar{\hat{\mathbf{u}}}(t+\tau)\|_E > \rho \cdot \mathrm{TOL}$, the relation

$$\bar{\mathbf{u}}_{31}(t+\tau) - \bar{\hat{\mathbf{u}}}(t+\tau) \approx \bar{\mathbf{e}}(t+\tau)\Big(\frac{\tau}{3}\Big)^2 + \bar{\mathbf{X}}(t+\tau)\Big(\frac{\tau}{3}\Big)^{1/2}$$

and the triangle inequality are used to find that

$$\begin{aligned}
&\|\bar{\mathbf{u}}_{31}(t+\tau^*) - \bar{\mathbf{u}}(t+\tau^*)\|_E \\
&\gtrsim \big\|\bar{\mathbf{u}}_{31}(t+\tau) - \bar{\hat{\mathbf{u}}}(t+\tau)\big\|_E \cdot \Big(\frac{\tau^*}{\tau}\Big)^3 \\
&\quad + \Big|\|\bar{\mathbf{X}}(t+\tau^*)\|_E\Big(\frac{\tau^*}{3}\Big)^{1/2} - \|\bar{\mathbf{X}}(t+\tau)\|_E\Big(\frac{\tau}{3}\Big)^{1/2}\Big(\frac{\tau^*}{\tau}\Big)^3\Big|\,.
\end{aligned}$$

Due to condition (6.38), the optimal timestep should fulfill

$$\begin{aligned}\rho \cdot \mathrm{TOL} = \big\|\bar{\mathbf{u}}_{31}(t+\tau) - \bar{\hat{\mathbf{u}}}(t+\tau)\big\|_E \cdot \Big(\frac{\tau^*}{\tau}\Big)^3 \\ + \Big|\|\bar{\mathbf{X}}(t+\tau^*)\|_E \Big(\frac{\tau^*}{3}\Big)^{1/2} - \|\bar{\mathbf{X}}(t+\tau)\|_E \Big(\frac{\tau}{3}\Big)^{1/2}\Big(\frac{\tau^*}{\tau}\Big)^3\Big|\,.\end{aligned} \tag{6.40}$$

The quantity $\bar{\mathbf{X}}(t+\tau^*)$ does not necessarily tend to zero as $\tau \to 0$. Thus, the careful assumption $\|\bar{\mathbf{X}}(t+\tau^*)\|_E = \|\bar{\mathbf{X}}(t+\tau)\|_E$ is taken, and the optimal timestep τ^* is determined by

$$\begin{aligned}&\big\|\bar{\mathbf{u}}_{31}(t+\tau) - \bar{\hat{\mathbf{u}}}(t+\tau)\big\|_E \Big(\frac{\tau^*}{\tau}\Big)^3 + \|\bar{\mathbf{X}}(t+\tau)\|_E \Big(\frac{\tau}{3}\Big)^{1/2}\Big|\Big(\frac{\tau^*}{\tau}\Big)^{1/2} - \Big(\frac{\tau^*}{\tau}\Big)^3\Big| \\ &= \rho \cdot \mathrm{TOL}\,.\end{aligned} \tag{6.41}$$

Subtracting the first equation of the approximations (6.31) from the second one and (6.32) from the second equation of (6.31) yields

$$\begin{aligned}\bar{\mathbf{u}}_{11}(t+\tau) - \bar{\mathbf{u}}_{21}(t+\tau) &\approx \bar{\mathbf{e}}(t+\tau)\Big(1 - \frac{1}{2^2}\Big)\tau^2 + \bar{\mathbf{X}}(t+\tau)\Big(1 - \frac{1}{2^{1/2}}\Big)\tau^{1/2} \\ \bar{\mathbf{u}}_{21}(t+\tau) - \bar{\mathbf{u}}_{31}(t+\tau) &\approx \bar{\mathbf{e}}(t+\tau)\Big(\frac{1}{2^2} - \frac{1}{3^2}\Big)\tau^2 + \bar{\mathbf{X}}(t+\tau)\Big(\frac{1}{2^{1/2}} - \frac{1}{3^{1/2}}\Big)\tau^{1/2}\,.\end{aligned}$$

By taking suitable differences of these approximations and using definitions (6.29) and (6.33), the unknown quantity $\bar{\mathbf{X}}(t+\tau)$ may be estimated via

$$\begin{aligned}&\bar{\mathbf{X}}(t+\tau)\frac{\delta-\gamma}{\delta}\frac{1-\frac{1}{2^{1/2}}}{1-\frac{1}{2^2}}\tau^{1/2} \\ &\approx \frac{1}{1-\frac{1}{2^2}}(\bar{\mathbf{u}}_{11}(t+\tau) - \bar{\mathbf{u}}_{21}(t+\tau)) - \frac{1}{\frac{1}{2^2}-\frac{1}{3^2}}(\bar{\mathbf{u}}_{21}(t+\tau) - \bar{\mathbf{u}}_{31}(t+\tau)) \\ &= 2^2(\bar{\mathbf{u}}_{21}(t+\tau) - \bar{\mathbf{u}}_{22}(t+\tau)) - 3^2(\bar{\mathbf{u}}_{31}(t+\tau) - \bar{\mathbf{u}}_{32}(t+\tau))\end{aligned} \tag{6.42}$$

with

$$\gamma = \Big(\frac{1}{2^{1/2}} - \frac{1}{3^{1/2}}\Big)\Big(1 - \frac{1}{2^2}\Big)\,, \quad \delta = \Big(\frac{1}{2^2} - \frac{1}{3^2}\Big)\Big(1 - \frac{1}{2^{1/2}}\Big)\,.$$

The next stepsize proposal is gained from (6.41) by computing τ^* as the root of a scalar function. For $\tau^* = \tau$, the left-hand side of (6.41) is larger than the right-hand side due to $\|\bar{\mathbf{u}}_{31}(t+\tau) - \bar{\hat{\mathbf{u}}}(t+\tau)\|_E \geq \mathrm{TOL}$. In the limit $\tau^* \to 0$, the left-hand side is zero, and less than the positive right-hand side. Hence, the corresponding scalar function has at least one root since all terms are continuous in τ^*

In the case of vanishing $\bar{\mathbf{X}}(t+\tau)$, the defining equation (6.41) reduces to the classical stepsize formula (6.39).

Switch between no contact and contact. A certain difficulty in timestep selection arises if a switch between contact and no contact occurs in a timestep. In this case, the quantity $\bar{\mathbf{X}}$ is very large at the timepoint when the two bodies are in contact, but zero in the absence of contact. In order to ensure an efficient timestep selection, a suitable assumption on the behavior of this quantity in time is needed.

For this aim, the current timestep is divided into phases of no contact, contact, and a switch between no contact and contact. The approximations with stepsize $\tau/2$ and $\tau/3$ give the information in which part of the interval the switch occurs, cf. Figure 6.4.

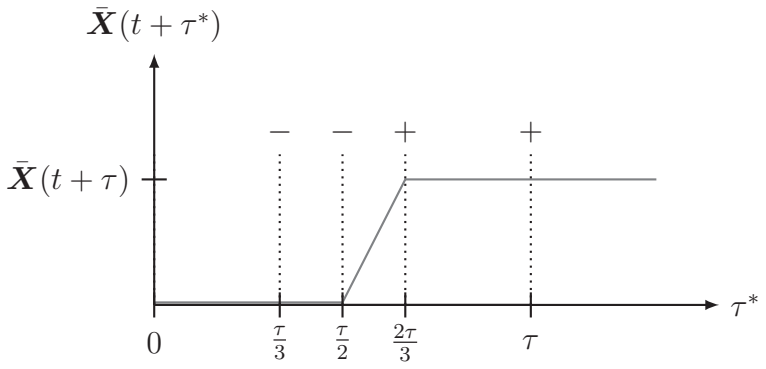

Figure 6.4.: Model assumption on $\bar{\mathbf{X}}(t+\tau)$ ('+' and '–' indicate whether contact occurs or not).

If the stepsize τ^* touches an interval where no contact occurs,

$$\bar{\mathbf{X}}(t+\tau^*) = 0 \tag{6.43}$$

is taken, and within an interval with contact, the assumption

$$\bar{\mathbf{X}}(t+\tau^*) = \bar{\mathbf{X}}(t+\tau) \tag{6.44}$$

is made. For a subinterval $[t_j, t_{j+1}]$ with a switch between no contact and contact, a linear interpolation is used such that

$$\bar{\mathbf{X}}(t+\tau^*) = \Big(\frac{t+\tau}{t_{j+1}-t_j} - \frac{t+t_j}{t_{j+1}-t_j}\Big) \cdot \bar{\mathbf{X}}(t+\tau)\,. \tag{6.45}$$

If no contact has been found in an accepted timestep, the controller accesses to the last rejected step with active contact boundaries. The optimal stepsize τ^* is given by (6.40) as the root of a scalar function.

6.3. Global Discretization Error

In the previous section, an adaptive variant of the improved contact–stabilized Newmark method has been suggested that keeps the local discretization error in the reduced physical energy norm below a user-defined tolerance. However, controlling the *global discretization error* of the scheme is of interest originally. In this last section, the focus is on the actually achieved accuracy by the adaptive timestep control ContacX at the end of the time integration. The notations used in the following are introduced in Section 5.2.

The global discretization error $\boldsymbol{\epsilon}_\triangle(\bar{\mathbf{u}}, T)$ at final time T can be considered as the propagation of all local discretization errors occurring during time integration. Decomposing the global error as sketched in Figure 5.1 gives access to those consistency errors that are bounded by the adaptive timestep control, namely

$$\|\boldsymbol{\epsilon}(t_j, \bar{\mathbf{u}}, \tau_j)\|_E \approx \left[\|\boldsymbol{\epsilon}(t_j, \bar{\mathbf{u}}, \tau_j)\|_E\right] \approx \mathrm{TOL}\,, \qquad \text{for all } j = 1, \ldots, N_\triangle \tag{6.46}$$

due to (6.25) and (6.26). Estimating the propagation of these local errors requires the application of the perturbation result for the dynamical contact problem in Chapter 3. This is in contrast to the approach applied for the convergence theory in Chapter 5, which is based on a discrete perturbation theorem (compare Figure 5.2).

In the case of vanishing Dirichlet boundaries, the perturbation result in physical energy norm contains the initial perturbation of the displacements in $\mathbf{L}_2$-norm. This norm is not controlled by the adaptive timestep control. However, since the consistency order of Newmark methods is expected to be higher in physical energy norm than in $\mathbf{L}_2$-norm, cf. Chapter 4, the assumption

$$\|\boldsymbol{\epsilon}(t_j, \mathbf{u}, \tau_j)\|_{\mathbf{L}_2} = \|\boldsymbol{\epsilon}(t_j, \bar{\mathbf{u}}, \tau_j)\|_E \cdot o(1) \qquad \text{for } \tau_j \to 0\,, \text{ for all } j = 1, \ldots, N_\triangle \tag{6.47}$$

is reasonable (compare Assumption (6.9)). Furthermore, let the adaptive timesteps be bounded as in Assumption (5.24).

The following theorem gives a heuristic bound for the global discretization error of ContacX, which only depends on the user-defined local tolerance TOL and the number of performed timesteps $N_\triangle$.

Theorem 6.3.1. *Assume that Theorem 3.2.2 with $\alpha \in [0, 1)$ and Assumptions* (5.24)*,* (6.46)*, and* (6.47) *are valid. Then, the global error of* (N-CI/CS+) *satisfies*

$$\left(\|\boldsymbol{\epsilon}_\triangle(\bar{\mathbf{u}}, T)\|_E^2 + \alpha \sum_{j=1}^{N_\triangle} \tau_{j-1} \left\| \frac{\boldsymbol{\epsilon}_\triangle(\mathbf{u}, t_j) - \boldsymbol{\epsilon}_\triangle(\mathbf{u}, t_{j-1})}{\tau_{j-1}} \right\|_b^2 \right)^{1/2} \lesssim \mathrm{TOL} \cdot N_\triangle \tag{6.48}$$

in the limit $\tau_\triangle \to 0$. In particular,

$$\|\boldsymbol{\epsilon}_\triangle(\bar{\mathbf{u}}, T)\|_E \lesssim \mathrm{TOL} \cdot N_\triangle\,. \tag{6.49}$$

Proof. Referring to Figure 5.1, the global discretization error in physical energy norm can be decomposed via

$$\begin{aligned}
&\Big(\|\boldsymbol{\epsilon}_\triangle(\bar{\mathbf{u}},T)\|_E^2+\alpha\sum_{j=1}^{N_\triangle}\tau_{j-1}\Big\|\frac{\boldsymbol{\epsilon}_\triangle(\mathbf{u},t_j)-\boldsymbol{\epsilon}_\triangle(\mathbf{u},t_{j-1})}{\tau_{j-1}}\Big\|_b^2\Big)^{1/2}\\
&\leq\sum_{i=1}^{N_\triangle}\Big(\|\boldsymbol{\epsilon}_i(\bar{\mathbf{u}},T)\|_E^2+\alpha\sum_{j=i+1}^{N_\triangle}\tau_{j-1}\Big\|\frac{\mathbf{u}_i(t_j)-\mathbf{u}_i(t_{j-1})}{\tau_{j-1}}-\frac{\mathbf{u}_{i-1}(t_j)-\mathbf{u}_{i-1}(t_{j-1})}{\tau_{j-1}}\Big\|_b^2\Big)^{1/2}.
\end{aligned}$$

Here, the error contributions $\boldsymbol{\epsilon}_i(\bar{\mathbf{u}},T)$ denote the propagation of the local discretization errors $\boldsymbol{\epsilon}(t_{i-1},\bar{\mathbf{u}},\tau_{i-1})$ by the variational inequality (1.28) of the dynamical contact problem. Applying perturbation theorem 3.2.2 on every single error component yields the estimate

$$\begin{aligned}
&\Big(\|\boldsymbol{\epsilon}_\triangle(\bar{\mathbf{u}},T)\|\|_E^2+\alpha\sum_{j=1}^{N_\triangle}\tau_{j-1}\Big\|\frac{\boldsymbol{\epsilon}_\triangle(\mathbf{u},t_j)-\boldsymbol{\epsilon}_\triangle(\mathbf{u},t_{j-1})}{\tau_{j-1}}\Big\|_b^2\Big)^{1/2}\\
&\leq\sum_{i=1}^{N_\triangle}\big(\|\boldsymbol{\epsilon}(t_{i-1},\bar{\mathbf{u}},\tau_{i-1})\|_E+c(T-t_{i-1})\|\boldsymbol{\epsilon}(t_{i-1},\bar{\mathbf{u}},\tau_{i-1})\|_{\mathbf{L}_2}\big)\cdot e^{\tilde{\kappa}^2(T-t_{i-1})}
\end{aligned}$$

with constants $c,\tilde{\kappa}>0$ independent of the adaptive timesteps. Now, the local error control (6.46) as well as assumption (6.47) can be inserted into this expression. This leads to the approximate bound

$$\begin{aligned}
&\Big(\|\boldsymbol{\epsilon}_\triangle(\bar{\mathbf{u}},T)\|_E^2+\alpha\sum_{j=1}^{N_\triangle}\tau_{j-1}\Big\|\frac{\boldsymbol{\epsilon}_\triangle(\mathbf{u},t_j)-\boldsymbol{\epsilon}_\triangle(\mathbf{u},t_{j-1})}{\tau_{j-1}}\Big\|_b^2\Big)^{1/2}\\
&\lesssim\sum_{i=1}^{N_\triangle}(\mathrm{TOL}+\mathrm{TOL}\cdot o(1))\cdot e^{\tilde{\kappa}^2(T-t_{i-1})}\\
&=\mathrm{TOL}\cdot(1+o(1))\cdot\sum_{i=1}^{N_\triangle}\cdot e^{\tilde{\kappa}^2(T-t_{i-1})}
\end{aligned}$$

for the global error. Reordering the sum and inserting the upper bound (5.24) of the adaptive timesteps gives

$$\begin{aligned}
&\Big(\|\boldsymbol{\epsilon}_\triangle(\bar{\mathbf{u}},T)\|_E^2+\alpha\sum_{j=1}^{N_\triangle}\tau_{j-1}\Big\|\frac{\boldsymbol{\epsilon}_\triangle(\mathbf{u},t_j)-\boldsymbol{\epsilon}_\triangle(\mathbf{u},t_{j-1})}{\tau_{j-1}}\Big\|_b^2\Big)^{1/2}\\
&\lesssim\mathrm{TOL}\cdot\sum_{k=0}^{N_\triangle-1}e^{\tilde{\kappa}^2t_k}
\end{aligned}$$

$$\leq \mathrm{TOL} \cdot \sum_{k=0}^{N_\triangle - 1} e^{\tilde{\kappa}^2 k \tau_\triangle}$$
$$= \mathrm{TOL} \cdot \frac{\left(e^{\tilde{\kappa}^2 \tau_\triangle}\right)^{N_\triangle} - 1}{\tilde{\kappa}^2 \tau_\triangle},$$

where the closed expression for geometrical series has been used in the last step. Finally, taking the limit $\tau_\triangle \to 0$ yields the result of the theorem. □

The theorem presented above gives a rough guide for assessing the influence of the prescribed local tolerance TOL on the global discretization error measured in physical energy norm. The first term provides information about the actually achieved error in displacements and velocities measured in a-norm and $\mathbf{L}_2$-norm, respectively. The additional sum of the finite differences in displacements in b-norm over the time interval is scaled by a factor α from the perturbation result, which may be equal to zero. Hence, this part of the error estimate does not necessarily yield further information.

The question how the number $N_\triangle$ of required timesteps depends on the tolerance is still open. In general, a reduction of the tolerance increases the number of timesteps, and the achieved global error is not proportional to the tolerance. In order to gain more insight into this problem, the dependence of the number of timesteps on the tolerance will be investigated in the first numerical example of Chapter 7. The numerics will show that the number of timesteps grows much slower than the prescribed tolerance decreases. Hence, the actually achieved global discretization error of ContacX is expected to tend to zero.

7. Numerical Results

In the last chapter of this thesis, two numerical examples will conclude the theoretical establishment of the adaptive timestep control ContacX for the improved contact–stabilized Newmark method. The main purpose is to demonstrate the practical performance of the adaptive integrator for the simulation of dynamical contact problems. Moreover, numerical findings will illustrate the close connection with the theoretical insight of the previous chapters.

First, the 2D Hertzian contact of Section 2.5 is chosen as a simple test problem. The characteristic quantities of the adaptive control, as the history of timesteps and the number of accepted and rejected timesteps, will be presented. In view of the theoretical analysis of the global discretization error achieved by ContacX in Section 6.3, a numerical study on the relation between the number of timesteps and the prescribed tolerance will be given. Furthermore, the behavior of the estimated quantity $\bar{\mathbf{X}}$ will be investigated in time and space with regard to its motivation in Chapter 6.

Next, a much more complex 3D application problem will be exhibited as a real-world example for an adaptive numerical integration via ContacX: the simulation of the motion of a human knee including bones and cartilage. Again, the adaptively chosen timesteps beyond contact and the number of timesteps, rejected and accepted, will be discussed. At the end, the time evolution of computed stresses and energies in the knee joint will be illustrated.

The implementation of ContacX is done within the same software environment as the numerical example in Section 2.5. As suggested in Chapter 6, the proposal of the adaptive controller for the next timestep is obtained from the scalar equations (6.40) or (6.41). Therefore, the open source code zeroin is utilized, which returns an estimate for the root of a scalar function within a given range with prescribed accuracy.

7.1. Hertzian Contact Problem

In this section, a Hertzian contact problem in 2D will be treated as a first illustrative example (Example 1) for the suggested adaptive numerical integrator ContacX. The configuration of the test problem is identical with the one in Section 2.5, though the material parameters are chosen as in Table 7.1. The parameters for the adaptive timestep control are given in Table 7.2, where E(0) denotes the initial energy of the system.

parameter	value
Young's modulus	10
Poisson ratio	0.4
shear viscosity	10^{-3}
bulk viscosity	10^{-3}

Table 7.1.: Example 1: Material specifications.

parameter	value
tolerance TOL	$10^{-4} \cdot \mathrm{E}(0)$
safety factor ρ	0.9
initial timestep	10^{-2}
maximal timestep	1
maximal growth factor for timesteps	10

Table 7.2.: Example 1: Specifications for adaptive timestep control.

Figure 7.1 shows the size of the adaptively chosen timesteps. When the semicircle is entering the phase of contact, the controller reduces the timesteps significantly. Then, the timesteps increase moderately up to the moment when the body removes from the plate. At this moment, depending on the desired time tolerance, the controller reduces the timesteps again. However, this reduction is much less distinctive than in the moment when the body gets into touch with the plate for the first time. This is due to the higher regularity of dynamical contact problems when contact is lost compared to the timepoint when contact is found initially. In the absence of contact, the growth in timesteps is considerable.

The numerical integration has carried out 48 timesteps, while only 3 of them have been rejected. Figure 7.2 shows that the repeats only occur when the semicircle gets into contact with the plate for the first time.

Table 7.3 contains the number of accepted and rejected timesteps for different tolerances and refinement levels of the spatial grid. For small tolerances, the adaptive timestep control requires a sufficiently high resolution of the grid near the changing active contact boundaries in order to avoid effects of spatial discretization.

In Theorem 6.3.1, an estimate for the achieved global discretization error of ContacX has been presented, which refers to the number of performed timesteps $N_{\triangle}$ and the user-defined tolerance TOL. However, the dependence of the number of timesteps on the tolerance is still an open problem. In Figure 7.3, the product of the number of accepted timesteps and the prescribed tolerance is plotted against the tolerance for different grid refinements (with values taken from Table 7.3). For this test problem, the product of timesteps and tolerance becomes smaller and smaller

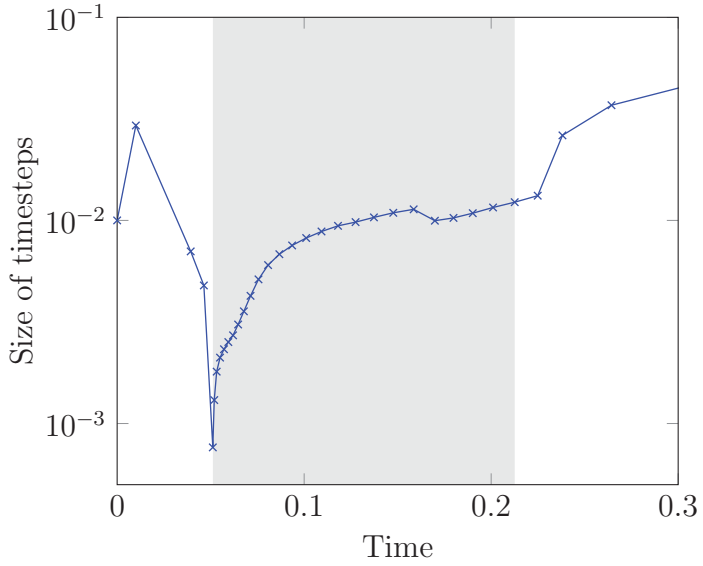

Figure 7.1.: Example 1: Timestep history beyond contact (grey: phase of contact).

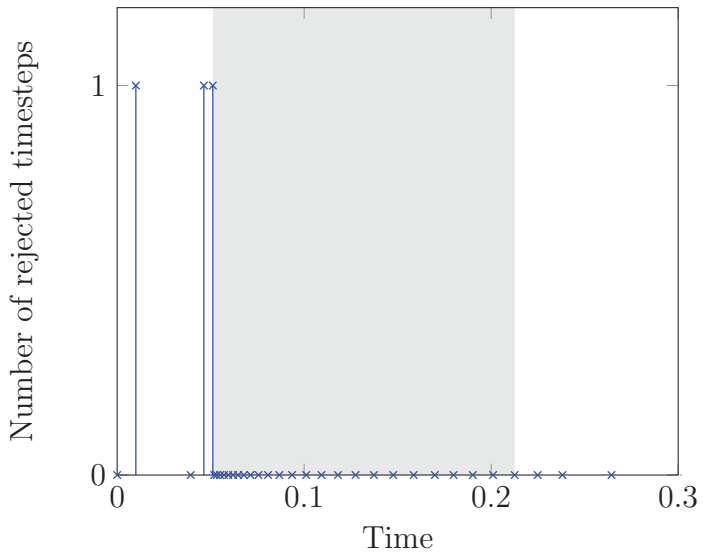

Figure 7.2.: Example 1: Time evolution of the number of rejected timesteps (grey: phase of contact).

j (nodes) / TOL	$10^{-3} \cdot \mathrm{E}(0)$	$10^{-4} \cdot \mathrm{E}(0)$	$10^{-5} \cdot \mathrm{E}(0)$
5 (1617)	17 (2)	45 (3)	144 (24)
6 (2759)	17 (2)	47 (3)	142 (18)
7 (7288)	18 (2)	48 (3)	133 (11)
8 (25054)	18 (2)	49 (3)	132 (8)
9 (95375)	18 (2)	51 (3)	143 (9)

Table 7.3.: Example 1: Total number of timesteps (number of rejected timesteps) depending on tolerance TOL and refinement level j of the grid (or number of nodes).

as the tolerance decreases. Combining this numerical observation with the result of Theorem 6.3.1 leads to the conjecture that the adaptive numerical integrator ContacX converges if the user-defined tolerance or the maximal timestep tends to zero. As expected for algorithms designed in function space, the behavior observed in Figure 7.3 is independent of the spatial mesh.

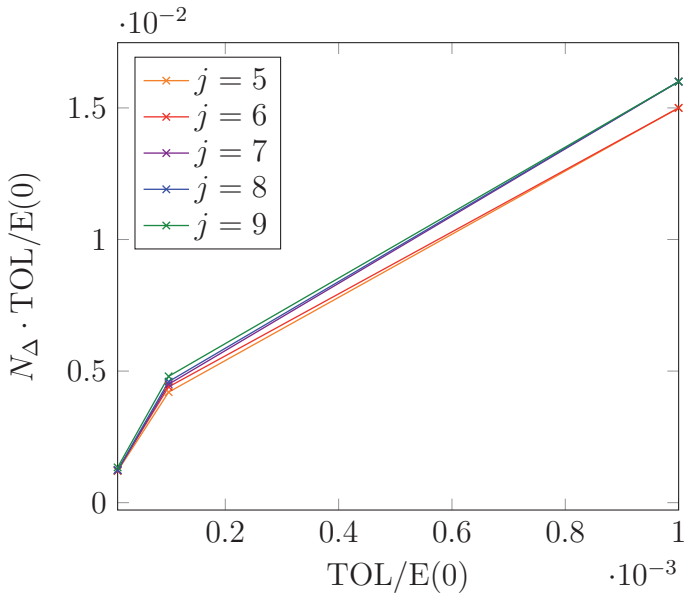

Figure 7.3.: Example 1: Product of the number of accepted timesteps $N_\triangle$ and the tolerance TOL vs. TOL for different refinement levels j of the grid.

Figure 7.4 shows the time evolution of the (reduced) physical energy norm of the quantity $\bar{\mathbf{X}}$ introduced in Section 6.2. The norm of $\bar{\mathbf{X}}$ becomes extremely large at the timepoint when the semicircle gets into contact with the plate for the first time. In Figure 7.5, the spatial distribution of $\dot{\mathbf{X}}$ can be found for a fixed timepoint in

the beginning of the contact phase. As expected, the quantity is located near those parts of the possible contact boundaries where the active contact set changes.

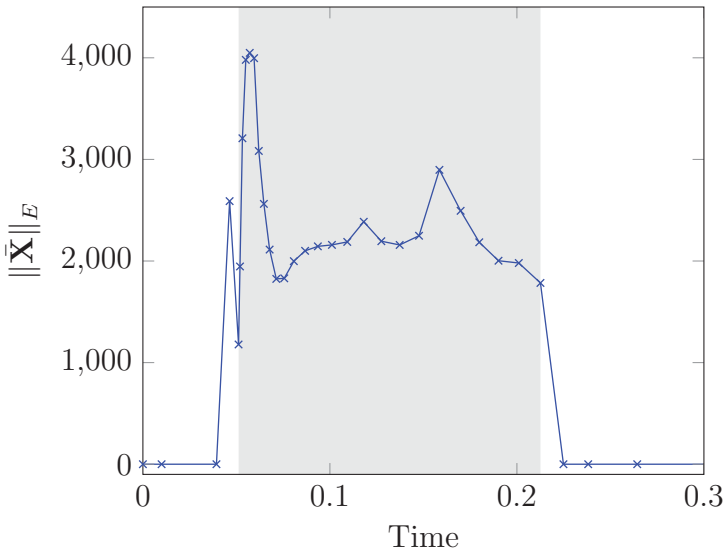

Figure 7.4.: Example 1: Time evolution of $\|\bar{\mathbf{X}}\|_E$ (grey: phase of contact).

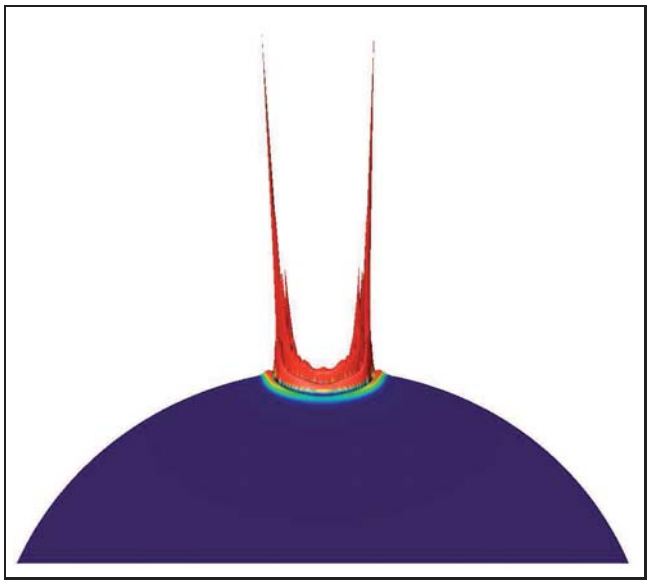

Figure 7.5.: Example 1: Estimated spatial distribution of $\dot{\mathbf{X}}(t+\tau)|_{t=0.0524}$.

7.2. Motion of the Human Knee

As an example for a real life problem, in this section, the adaptive timestep controller ContacX will be utilized to integrate the motion of a human knee (Example 2). The computational results will have qualitative relevance only.

The numerical simulation is carried out for a prototype of a knee joint, which incorporates the femur and the tibia bone covered by articular cartilage. As indicated in the introductory part of this thesis, the two bones are modeled with an isotropic, homogeneous, and linear elastic material, while the layering cartilage is modeled as a linear viscoelastic tissue. For human bones, many experimental results concerning material parameters have been published, but the range of values spreads widely. The values used for the two bones in the following simulation are taken from [15] as an average of different measurements and can be found in Table 7.4. Unfortunately, retrieving realistic parameters for articulating cartilage is much more

parameter	value
Young's modulus	17 GPa
Poisson ratio	0.3

Table 7.4.: Example 2: Material specifications of bone.

difficult. The size of the values for elasticity given in Table 7.5 have been chosen on the basis of [21, 91]. Viscous material parameters for cartilage could not be found in literature, and the values for viscosity in Table 7.5 are only a rough estimation.

parameter	value
Young's modulus	10 MPa
Poisson ratio	0.4
shear viscosity	10 MPa
bulk viscosity	10 MPa

Table 7.5.: Example 2: Material specifications of cartilage.

As in the PhD thesis of Sander [82], the geometry of the two bones was selected as the left distal femur and proximal tibia from the Visible Human data set [4]. By image segmentation and using the grid generator of Amira [1], a computational model of the bones was constructed, which consists of two tetrahedral grids with 378 and 306 vertices for tibia and femur, and 1328 and 1044 elements, respectively. In a second step, the grids were refined further two times. Beyond that, a certain additional distance between femur and tibia was set in order to accomplish a suitable dynamical simulation. On the parts of femur and tibia that are usually covered by articular cartilage, a thin layer of prisms was fixed with a thickness of 1.5 mm [91]. The computational grid consisting of femur, tibia, and covering cartilage is shown

in Figure 7.6. At initial time, the two components of the knee joint are moving in vertical direction towards each other with velocity $\dot{\mathbf{u}}_0 = \pm(0, 0, 0.1)\,\mathrm{m/s}$.

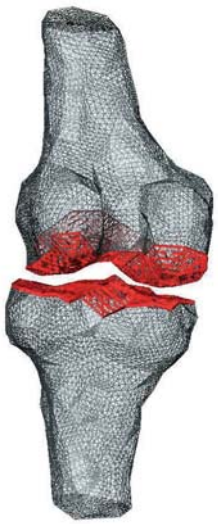

Figure 7.6.: Example 2: Initial configuration.

Details concerning mortar and nonmortar contact boundaries and the contact mapping in between can be found in [82]. The coupling of elastic bones and viscoelastic cartilage is performed by means of mortar element methods, see the bachelor thesis [92].

The parameters for the adaptive timestep control are given in Table 7.6.

parameter	value
tolerance TOL	$10^{-5} \cdot \mathrm{E}(0)$
safety factor ρ	0.9
initial timestep	$10^{-2}\,\mathrm{s}$
maximal timestep	$10^{-1}\,\mathrm{s}$
maximal growth factor for timesteps	10

Table 7.6.: Example 2: Specifications for adaptive timestep control.

Figure 7.7 shows the history of adaptive timesteps as they have been chosen by the controller for the integration of the movement of the knee. As already observed for the simple Hertzian contact in Section 7.1, the timesteps decrease significantly when the two bones covered by cartilage are getting into contact initially. During the phase of contact, the timesteps increase, but they are reduced slightly when the two bones or, more precisely, the covering cartilage loose contact. In the absence of contact, the timesteps grow considerably again.

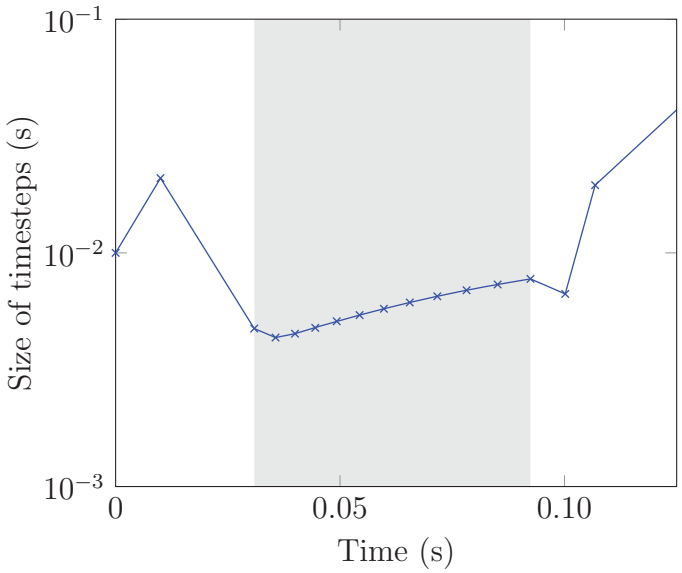

Figure 7.7.: Example 2: Timestep history beyond contact (grey: phase of contact).

The adaptive numerical integration of the motion of the knee model via ContacX requires 17 timesteps in total. Thereof, only 2 timesteps have been rejected just before active contact between the articular cartilage has been detected for the first time.

The thesis will be finished by a presentation of some computational results on the dynamics of the knee joint. Figure 7.8 illustrates the distribution of the stresses occurring in femur, tibia, and articulating cartilage at various single timepoints. The stresses arise at the contact interfaces for the first time and then, are spreading wavelike over the whole bones as time proceeds.

In Figures 7.9–7.12, the energy of the system is plotted during the considered time interval. As predicted in Chapter 2, the total energy is preserved in the absence of contact and dissipative in the presence of contact. The progression of potential and kinetic energy in time oppose each other: the potential energy is maximal in the presence of contact and minimal in the absence of contact, while the kinetic energy is minimal at contact and maximal without. Viscous energy is lost during the phase of active contact mostly.

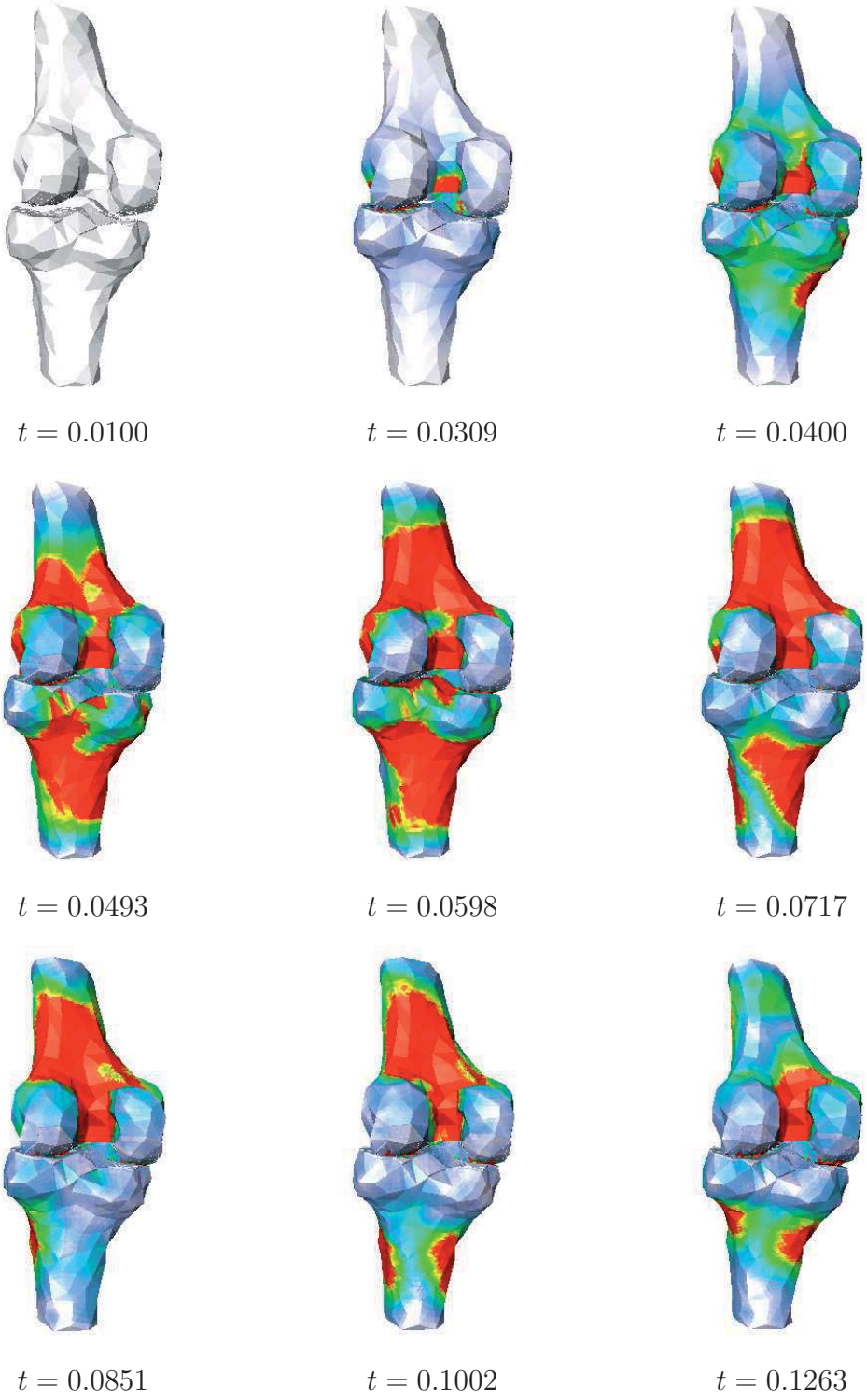

$t = 0.0100$ $t = 0.0309$ $t = 0.0400$

$t = 0.0493$ $t = 0.0598$ $t = 0.0717$

$t = 0.0851$ $t = 0.1002$ $t = 0.1263$

Figure 7.8.: Example 2: Time evolution of the spatial distribution of stresses.

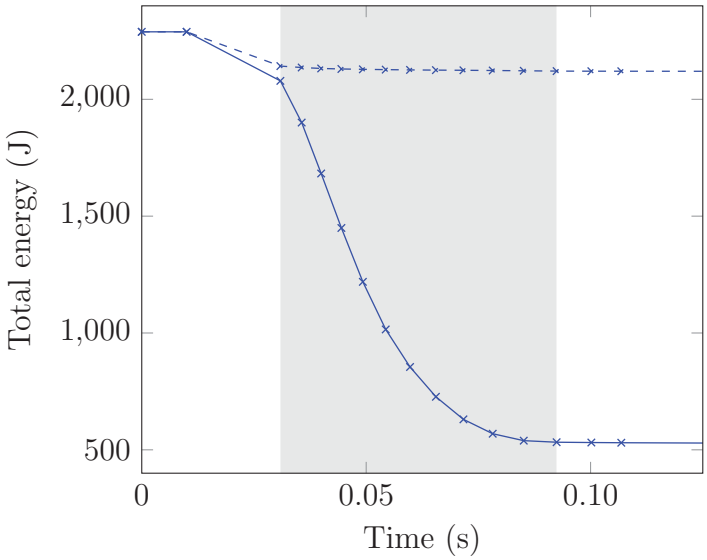

Figure 7.9.: Example 2: Total energy (grey: phase of contact) including and excluding viscous energy (dashed and solid).

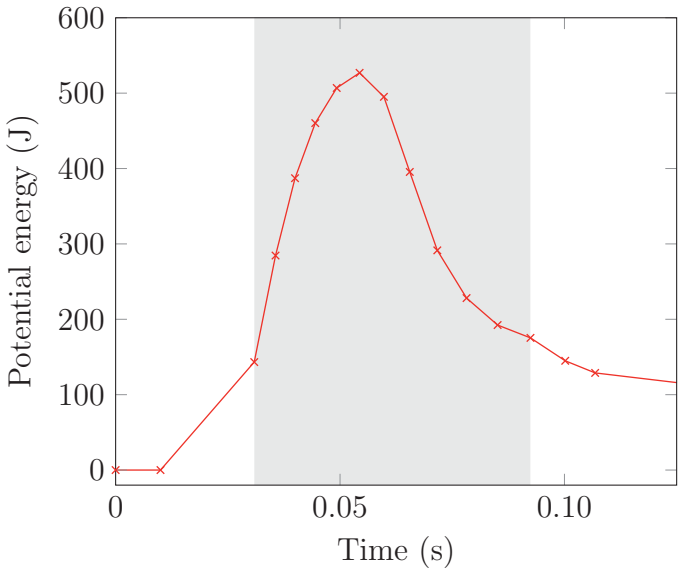

Figure 7.10.: Example 2: Potential energy (grey: phase of contact).

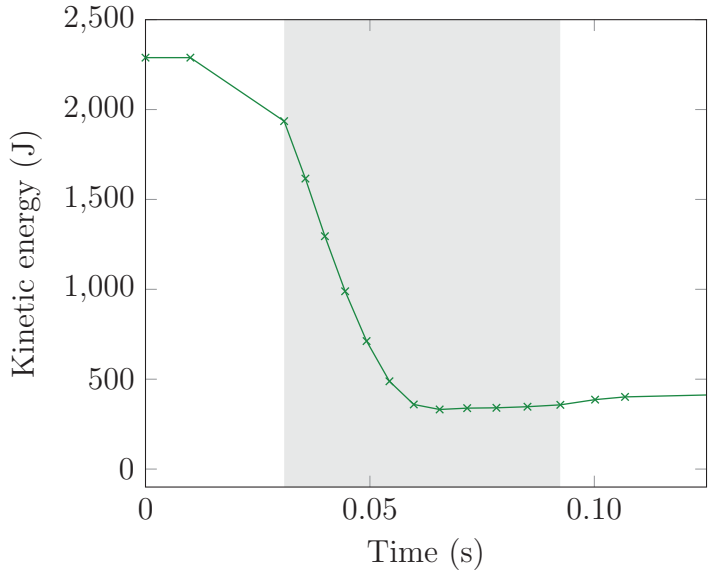

Figure 7.11.: Example 2: Kinetic energy (grey: phase of contact).

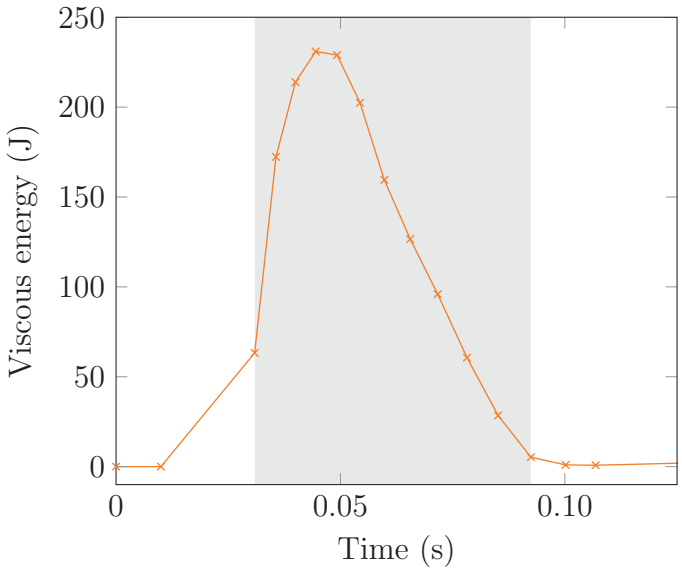

Figure 7.12.: Example 2: Viscous energy (grey: phase of contact).

Conclusion

In this thesis, an adaptive numerical integrator for dynamical contact problems (ContacX) has been presented. The solver is based on a contact–stabilized Newmark method, for which an automatic timestep control has been constructed within the time layer approach.

The theoretical foundation has been laid on the derivation of consistency and perturbation results. Viscous material behavior and the choice of a problem-adapted norm was found to be important. In fact, these findings even led to a novel convergence theory for the Newmark scheme in function space. The essential idea is to integrate over discontinuities appearing only at a few timepoints in the presence of contact. As it turned out, the requirement of bounded variation of the solution is absolutely crucial. A refinement of the numerical analysis needs supplementary knowledge about uniqueness, regularity, and well-posedness of the dynamical contact problem.

In a first attempt towards an adaptive timestep control, non-standard extrapolation techniques accounting for the special structure of the problem at dynamical contact have been worked out. For this purpose, a theoretical investigation of an asymptotic error expansion has been performed, which has been supported by numerical experiments. An illustrative example has shown a detailed agreement between the theoretical estimates and the numerical observations. Moreover, the code ContacX has been demonstrated to be reliable, robust, and efficient for practical applications.

On the basis of ContacX, a fast and accurate simulation of human motion with regard to computational surgery planning comes into reach.

A. Inequalities

Korn's inequalities. On Ω, the inequality of Korn

$$c_K \, \|\mathbf{v}\|^2_{\mathbf{H}^1} \leq \|\mathbf{v}\|^2_{\mathbf{L}_2} + \|\boldsymbol{\varepsilon}(\mathbf{v})\|^2_{\mathbf{L}_2} \,, \qquad \forall\, \mathbf{v} \in \mathbf{H}^1 \tag{A.1}$$

holds, where $c_K > 0$ is a constant depending only on Ω and Γ_D. Under the additional assumption that $\Gamma_D \subset \partial\Omega$ is connected with $\mathrm{meas}(\Gamma_D) > 0$, the inequality reduces to

$$c_K \, \|\mathbf{v}\|^2_{\mathbf{H}^1} \leq \|\boldsymbol{\varepsilon}(\mathbf{v})\|^2_{\mathbf{L}_2} \,, \qquad \forall\, \mathbf{v} \in \mathbf{H}^1_{\mathbf{D}} \,. \tag{A.2}$$

Proofs of Korn's inequalities can be found, for instance, in [75, 77].

Gronwall's inequality. Let δ, λ be two mappings from an interval $[0, T]$ into $[0, \infty)$. Assume that δ is continuous, λ is integrable, $C \geq 0$, and

$$\delta(t) \leq C + \int_0^t \lambda(s)\delta(s)\, ds \,, \qquad \forall\, t \in [0, T] \,.$$

Then,

$$\delta(t) \leq C \exp\Big(\int_0^t \lambda(s)\, ds \Big) \,, \qquad \forall\, t \in [0, T] \,.$$

A proof of this generalized version of the inequality of Gronwall is presented, e.g., in [84, Section 30.8].

Discrete Gronwall's inequality. Let (a_n), (b_n) be two nonnegative sequences. Assume that $\rho \geq 0$ and

$$a_n \leq \rho + \sum_{j=0}^{n-1} b_j a_j \,, \qquad n = 0, 1, \ldots .$$

Then,

$$a_n \leq \rho \exp\Big(\sum_{j=0}^{n-1} b_j \Big) \,, \qquad n = 0, 1, \ldots .$$

For this discrete version of Gronwall's inequality see, e.g., [18, Exercise 7.7].

B. Interpretation of Contact Stresses

In Chapter 3 and Chapter 5, stability conditions have been derived for which a perturbation result for dynamical contact problems and the improved contact–stabilized Newmark method hold in physical energy norm. The necessary assumptions on the contact stresses have been motivated by the formulation and interpretation of localized versions of the conditions. In this part of the appendix, the underlying localization of the contact forces on active and critical contact boundaries will be justified by means of an abstract trace theorem.

B.1. An Abstract Trace Theorem

In the following, a generalized trace theorem will be proven, which provides the basis for characterizing contact forces as functionals acting on the active contact boundaries only. Similar but less general formulations of this theorem can be found, e.g., in [7, 49].

Theorem B.1.1. *Let* $\mathbf{U}$, $\mathbf{V}$, $\mathbf{W}$ *be Banach spaces. Assume that* $\mathbf{A} : \mathbf{U} \to \mathbf{V}^*$ *is linear and continuous and* $\boldsymbol{\gamma} : \mathbf{V} \to \mathbf{W}$ *linear, continuous, and surjective. If*

$$\langle \mathbf{A}\mathbf{u}, \mathbf{v} \rangle_{\mathbf{V}^* \times \mathbf{V}} = 0 \,, \quad \forall\, \mathbf{u} \in \mathbf{U} \,, \qquad \forall\, \mathbf{v} \in \ker \boldsymbol{\gamma} \,, \tag{B.1}$$

then there exists a linear and continuous operator $\boldsymbol{\pi} : \mathbf{U} \to \mathbf{W}^*$ *satisfying*

$$\langle \mathbf{A}\mathbf{u}, \mathbf{v} \rangle_{\mathbf{V}^* \times \mathbf{V}} = \langle \boldsymbol{\pi}\mathbf{u}, \boldsymbol{\gamma}\mathbf{v} \rangle_{\mathbf{W}^* \times \mathbf{W}} \,, \quad \forall\, \mathbf{u} \in \mathbf{U} \,, \qquad \forall\, \mathbf{v} \in \mathbf{V} \,. \tag{B.2}$$

Proof. Due to the continuity of $\boldsymbol{\gamma}$, the kernel $\ker \boldsymbol{\gamma}$ is a closed subspace of the Banach space $\mathbf{V}$ [81, Theorem 1.18], and the factor space $\mathbf{V}/\ker \boldsymbol{\gamma}$ is a Banach space again [81, Theorem 1.41]. Hence, the linear, continuous, and surjective mapping $\boldsymbol{\gamma}$ induces the bijective mapping

$$\boldsymbol{\gamma}_0 : \mathbf{V}/\ker \boldsymbol{\gamma} \longrightarrow \operatorname{ran} \boldsymbol{\gamma} = \mathbf{W} \,,$$

which is linear and continuous [81, Chapter 1, Exercise 9]. By Banach's open mapping principle [81, Theorem 2.12], the inverse operator

$$\boldsymbol{\gamma}_0^{-1} : \mathbf{W} \longrightarrow \mathbf{V}/\ker \boldsymbol{\gamma}$$

of the mapping is continuous (and linear). In turn, the inverse has a uniquely determined linear and continuous dual operator

$$(\boldsymbol{\gamma}_0^{-1})^* : (\mathbf{V}/\ker\boldsymbol{\gamma})^* \longrightarrow \mathbf{W}^* ,$$

see [81, Theorem 4.10]. Assumption (B.1) directly yields that the range of $\mathbf{A}$ is a subset of the annihilator of the kernel of $\boldsymbol{\gamma}$, i.e., $\operatorname{ran}\mathbf{A} \subset (\ker\boldsymbol{\gamma})^\perp$. Because of $(\ker\boldsymbol{\gamma})^\perp = (\mathbf{V}/\ker\boldsymbol{\gamma})^*$ [81, Theorem 4.9], it even holds $\mathbf{Au} \subset (\mathbf{V}/\ker\boldsymbol{\gamma})^*$ for all $\mathbf{u} \in \mathbf{U}$. Hence, the linear and continuous operator

$$\boldsymbol{\pi} := (\boldsymbol{\gamma}_0^{-1})^*\mathbf{A} : \mathbf{U} \supset \mathbf{U} \longrightarrow \mathbf{W}^*$$

is well-defined. A simple calculation shows that

$$\langle \boldsymbol{\gamma}^*\boldsymbol{\pi}\mathbf{u}, \mathbf{v}\rangle_{\mathbf{W}^*\times\mathbf{W}} = \left\langle \left(\boldsymbol{\gamma}_0^{-1}\boldsymbol{\gamma}\right)^*\mathbf{Au}, \mathbf{v}\right\rangle_{\mathbf{W}^*\times\mathbf{W}} = \left\langle \mathbf{Au}, \boldsymbol{\gamma}_0^{-1}\boldsymbol{\gamma}\mathbf{v}\right\rangle_{\mathbf{V}^*\times bba\mathbf{V}} .$$

Now, write $\mathbf{v} \in \mathbf{V}$ as a sum of an element of $\ker\boldsymbol{\gamma}$ and a representative of the equivalence class $\boldsymbol{\gamma}_0^{-1}\boldsymbol{\gamma}\mathbf{v} \in (\mathbf{V}/\ker\boldsymbol{\gamma})$. Then, the relation

$$\left\langle \mathbf{Au}, \boldsymbol{\gamma}_0^{-1}\boldsymbol{\gamma}\mathbf{v}\right\rangle_{\mathbf{V}^*\times\mathbf{V}} = \langle \mathbf{Au}, \mathbf{v}\rangle_{\mathbf{V}^*\times\mathbf{V}} , \qquad \forall\, \mathbf{u} \in \mathbf{U} ,\ \forall\, \mathbf{v} \in \mathbf{V}$$

holds due to $\operatorname{ran}\mathbf{A} \subset (\ker\boldsymbol{\gamma})^\perp$. This gives the desired trace theorem. □

B.2. Localization on Active Contact Boundaries

In a first step, the abstract trace theorem will be applied to derive a characterization of the contact forces of the continuous problem as functionals acting on the active contact boundaries. The underlying definition of the active contact boundaries $\boldsymbol{\Gamma}_C(t)$ of a solution $\mathbf{u}$ of (1.28), for almost every t, is based on the concept of Sobolev capacity, compare Section 3.3.

Theorem B.2.1. *For $T > 0$, let $\boldsymbol{\gamma}_C : \mathbf{L}_2(0,T;\mathbf{H}^1_D(\Omega)) \to \mathbf{L}_2(0,T;\mathbf{H}^{1/2}(\Gamma_C(t)))$ denote a linear, continuous, and surjective trace operator. Further, define $\mathbf{U}_D$ as the closure of*

$$\mathbf{D} = \left\{ \mathbf{v} \in \mathbf{C}^\infty([0,T]\times\bar{\Omega})) \,\middle|\, \hat{\boldsymbol{\sigma}}(\mathbf{v},\dot{\mathbf{v}}) = \mathbf{0} \text{ on } \Gamma_C \setminus \Gamma_C(t)\times[0,T] \right\}$$

with respect to the canonical norm on

$$\mathbf{U} = \left\{ \mathbf{v} \in \mathbf{L}_2(0,T;\mathbf{H}^1(\Omega)) \,\middle|\, \begin{array}{l} \dot{\mathbf{v}} \in \mathbf{L}_2(0,T;\mathbf{H}^1(\Omega)), \\ \operatorname{div}\boldsymbol{\sigma}(\mathbf{v},\dot{\mathbf{v}}) \in \mathbf{L}_2(0,T;\mathbf{L}_2(\Omega)), \\ \hat{\boldsymbol{\sigma}}(\mathbf{v},\dot{\mathbf{v}}) \in \mathbf{L}_2(0,T;\mathbf{L}_2(\Gamma_N)) \end{array} \right\} .$$

If $\mathbf{u}$ *is a solution of the variational problem* (1.28) *with* $\mathbf{u} \in \mathbf{U}_D$*, then*

$$\int_0^T \langle \mathbf{F}_{\mathrm{con}}(\mathbf{u}(t)), \mathbf{v}(t) \rangle_{(\mathbf{H}^1(\Omega))^* \times \mathbf{H}^1(\Omega)} \, dt = \langle \boldsymbol{\pi}(\mathbf{u}), \boldsymbol{\gamma}_C \mathbf{v} \rangle \,, \qquad \forall\, \mathbf{v} \in \mathbf{L}_2(0,T;\mathbf{H}^1_D(\Omega)) \tag{B.3}$$

with a continuous operator $\boldsymbol{\pi} : \mathbf{U}_D \to \mathbf{L}_2(0,T;(\mathbf{H}^{1/2})^*(\Gamma_C(t)))$*.*

Proof. First of all, the trace operator $\boldsymbol{\gamma}_C$ can be taken as the composition of the classical trace operator $\boldsymbol{\gamma} : \mathbf{L}_2(0,T;\mathbf{H}^1(\Omega)) \to \mathbf{L}_2(0,T;\mathbf{H}^{1/2}(\Gamma))$ with the restriction operator from $\mathbf{L}_2(0,T;\mathbf{H}^{1/2}(\Gamma))$ to $\mathbf{L}_2(0,T;\mathbf{H}^{1/2}(\Gamma_C(t)))$. By definition, this mapping is linear, continuous, and surjective.

For $T > 0$, define the linear operator $\mathbf{A} : \mathbf{U}_D \supset \mathbf{D} \to \mathbf{L}_2(0,T;(\mathbf{H}^1)^*(\Omega))$ as

$$\begin{aligned}\langle \mathbf{A}\mathbf{u}, \mathbf{v} \rangle := \int_0^T a(\mathbf{u}(t), \mathbf{v}(t)) + b(\dot{\mathbf{u}}(t), \mathbf{v}(t)) \, dt - \int_0^T \Big(\int_{\Gamma_N} \hat{\boldsymbol{\sigma}}(\mathbf{u}(t), \dot{\mathbf{u}}(t)) \cdot \mathbf{v}(t) \Big) \, dt \\ + \int_0^T \Big(\int_\Omega \operatorname{div} \boldsymbol{\sigma}(\mathbf{u}(t), \dot{\mathbf{u}}(t)) \cdot \mathbf{v}(t) \, d\mathbf{x} \Big) \, dt \,, \qquad \mathbf{v} \in \mathbf{L}_2(0,T;\mathbf{H}^1_D(\Omega))\end{aligned}$$

for $\mathbf{u} \in \mathbf{D}$. This mapping is continuous in $\mathbf{L}_2(0,T;(\mathbf{H}^1)^*(\Omega))$ due to

$$\begin{aligned}&|\langle \mathbf{A}\mathbf{u}, \mathbf{v} \rangle| \\ &\le C \big(\|\mathbf{u}\|_{\mathbf{L}_2(0,T;\mathbf{H}^1(\Omega))} + \|\dot{\mathbf{u}}\|_{\mathbf{L}_2(0,T;\mathbf{H}^1(\Omega))} + \|\hat{\boldsymbol{\sigma}}(\mathbf{u}, \dot{\mathbf{u}})\|_{\mathbf{L}_2(0,T;\mathbf{L}_2(\Gamma_N))} \big) \|\mathbf{v}\|_{\mathbf{L}_2(0,T;\mathbf{H}^1(\Omega))} \\ &\quad + \| \operatorname{div} \hat{\boldsymbol{\sigma}}(\mathbf{u}, \dot{\mathbf{u}})\|_{\mathbf{L}_2(0,T;\mathbf{L}_2(\Omega))} \|\mathbf{v}\|_{\mathbf{L}_2(0,T;\mathbf{L}_2(\Omega))} \,.\end{aligned}$$

A classical integration by parts in space leads to

$$\langle \mathbf{A}\mathbf{u}, \mathbf{v} \rangle = \int_0^T \Big(\int_{\Gamma_C(t)} \hat{\boldsymbol{\sigma}}(\mathbf{u}(t), \dot{\mathbf{u}}(t)) \cdot \mathbf{v}(t) \, d\mathbf{a} \Big) \, dt \,.$$

Since

$$\ker \boldsymbol{\gamma}_C = \big\{ \mathbf{v} \in \mathbf{L}_2(0,T;\mathbf{H}^1_D(\Omega)) \,\big|\, \boldsymbol{\gamma}_C(\mathbf{v}) = 0 \text{ a.e. on } \Gamma_C(t) \text{ for a.e. } t \in [0,T] \big\} \,,$$

it holds

$$\langle \mathbf{A}\mathbf{u}, \mathbf{v} \rangle = 0, \quad \forall\, \mathbf{u} \in \mathbf{D} \,, \qquad \forall\, \mathbf{v} \in \ker \boldsymbol{\gamma}_C \,.$$

By means of $\mathbf{U}_D = \bar{\mathbf{D}}^{\|\cdot\|_{\mathbf{U}}}$, the linear and continuous operator $\mathbf{A}$ can be extended to $\mathbf{U}_D$ [93, Proposition 18.29], and a classical density argument leads to

$$\langle \mathbf{A}\mathbf{u}, \mathbf{v} \rangle = 0 \,, \quad \forall\, \mathbf{u} \in \mathbf{U}_D \,, \qquad \forall\, \mathbf{v} \in \ker \boldsymbol{\gamma}_C \,.$$

Now, the trace theorem B.1.1 gives the existence of a linear and continuous operator $\boldsymbol{\pi} : \mathbf{U}_D \to \mathbf{L}_2(0,T;(\mathbf{H}^{1/2})^*(\Gamma_C(t)))$ such that

$$\langle \mathbf{A}\mathbf{u}, \mathbf{v} \rangle = \langle \boldsymbol{\pi}(\mathbf{u}), \boldsymbol{\gamma}_C \mathbf{v} \rangle \,, \qquad \forall\, \mathbf{u} \in \mathbf{U}_D \,,\ \forall\, \mathbf{v} \in \mathbf{L}_2(0,T;\mathbf{H}^1_D(\Omega)) \,.$$

If $\mathbf{u}$ is a weak solution of the variational problem (1.28) and $\mathbf{u} \in \mathbf{D} \subset \mathbf{U}_D$, then $\mathbf{u}$ satisfies the strong problem formulation as well, and

$$\langle \mathbf{A}\mathbf{u}, \mathbf{v} \rangle = \int_0^T \langle \mathbf{F}_{\mathrm{con}}(\mathbf{u}(t)), \mathbf{v}(t) \rangle \, dt \,, \quad \forall\, \mathbf{v} \in \mathbf{L}_2(0,T;\mathbf{H}^1_D(\Omega)) \,.$$

By a density argument, this relation can be extended to all solutions $\mathbf{u} \in \mathbf{U}_D$, which yields the result of the theorem. □

The theorem above shows that the contact forces of a solution $\mathbf{u}$ of (1.28) can be localized on the active contact boundaries under additional regularity assumptions on the dynamical contact problem. The most important one is the condition $\operatorname{div} \boldsymbol{\sigma}(\mathbf{u}, \dot{\mathbf{u}}) \in \mathbf{L}_2(0,T;\mathbf{L}_2(\Omega))$, which is necessary in order to perform integration by parts in space within the proof above. However, it is not clear up to now if dynamical contact problems provide this regularity in general.

B.3. Localization on Critical Contact Boundaries

In a second step, the abstract trace theorem B.2.1 will be applied in order to prove the representation (3.16) of the contact forces of the continuous problem, which has motivated the introduction of the (localized) stability condition for dynamical contact problems in Chapter 3.

In the following, the possible contact boundaries and the bijective mappings between the two possible contact boundaries are assumed to be identical. The definition of the critical part $\Gamma_C^*(t)$ of the active contact boundaries for a solution $\mathbf{u}$ of (1.28) and its perturbation $\tilde{\mathbf{u}}$, for almost every t, has been given in Section 3.3. The assumptions and notations allow presenting the central theorem of this appendix.

Theorem B.3.1. *For $T > 0$, let $\boldsymbol{\gamma}_C^* : \mathbf{V}_C \to \mathbf{L}_2(0,T;\mathbf{H}^{1/2}(\Gamma_C^*(t)))$ denote a linear, continuous, and surjective trace operator, where*

$$\mathbf{V}_C = \big\{ \mathbf{v} \in \mathbf{C}^\infty([0,T] \times \bar{\Omega})) \,\big|\, [\mathbf{v} \cdot \boldsymbol{\nu}]_{\boldsymbol{\phi}} = 0 \text{ a.e. on } \Gamma_C(t) \cap \tilde{\Gamma}_C(t) \text{ for a.e. } t \in [0,T] \big\} \,.$$

Further, define $\mathbf{U}_D$ as the closure of

$$\mathbf{D} = \big\{ \mathbf{v} \in \mathbf{L}_2(0,T;\mathbf{C}^\infty(\bar{\Omega})) \,\big|\, \dot{\mathbf{v}} \in \mathbf{L}_2(0,T;\mathbf{C}^\infty(\bar{\Omega})), \; \hat{\boldsymbol{\sigma}}(\mathbf{v}, \dot{\mathbf{v}}) = \mathbf{0} \text{ on } \Gamma_C \setminus (\Gamma_C(t) \cup \tilde{\Gamma}_C(t)) \times [0,T] \big\}$$

with respect to the canonical norm on

$$\mathbf{U} = \big\{ \mathbf{v} \in \mathbf{L}_2(0,T;\mathbf{H}^1(\Omega)) \,\big|\, \dot{\mathbf{v}} \in \mathbf{L}_2(0,T;\mathbf{H}^1(\Omega)), \; \operatorname{div} \boldsymbol{\sigma}(\mathbf{v}, \dot{\mathbf{v}}) \in \mathbf{L}_2(0,T;\mathbf{L}_2(\Omega)), \; \hat{\boldsymbol{\sigma}}(\mathbf{v}, \dot{\mathbf{v}}) \in \mathbf{L}_2(0,T;\mathbf{L}_2(\Gamma_N)) \big\} \,.$$

If $\mathbf{u}$ *and* $\tilde{\mathbf{u}}$ *are solutions of the variational problem* (1.28) *with* $\mathbf{u}, \tilde{\mathbf{u}} \in \mathbf{U}_D$*, then*

$$\int_0^T \big\langle \mathbf{F}_{\mathrm{con}}(\mathbf{u}) - \mathbf{F}_{\mathrm{con}}(\tilde{\mathbf{u}}), \dot{\mathbf{u}}(t)) - \dot{\tilde{\mathbf{u}}}(t) \big\rangle \, dt = \big\langle \boldsymbol{\pi}(\mathbf{u}) - \boldsymbol{\pi}(\tilde{\mathbf{u}}), \boldsymbol{\gamma}_C^*(\dot{\mathbf{u}}(t) - \dot{\tilde{\mathbf{u}}}(t)) \big\rangle \quad \text{(B.4)}$$

with a continuous operator $\boldsymbol{\pi} : \mathbf{U}_D \to \mathbf{L}_2(0,T;(\mathbf{H}^{1/2})^*(\Gamma_C^*(t)))$.

Proof. First, a trace operator from $\mathbf{V}_C$ to the set

$$\big\{ \mathbf{v} \in \mathbf{L}_2(0,T;\mathbf{H}^{1/2}(\Gamma)) \,\big|\, [\mathbf{v} \cdot \boldsymbol{\nu}]_{\boldsymbol{\phi}} = 0 \text{ a.e. on } \Gamma_C(t) \cap \tilde{\Gamma}_C(t) \text{ for a.e. } t \in [0,T] \big\}$$

is chosen and concatenated with the canonical restriction to $\mathbf{L}_2(0,T;\mathbf{H}^{1/2}(\Gamma_C^*(t)))$. This yields the existence of the linear, continuous, and surjective operator $\boldsymbol{\gamma}_C^*$.

The linear and continuous operator $\mathbf{A} : \mathbf{U}_D \supset \mathbf{D} \to \mathbf{V}_C^*$ is defined as

$$\begin{aligned} \langle \mathbf{A}\mathbf{u}, \mathbf{v} \rangle := & \int_0^T a(\mathbf{u}(t), \mathbf{v}(t)) + b(\dot{\mathbf{u}}(t), \mathbf{v}(t)) \, dt - \int_0^T \Big(\int_{\Gamma_N} \hat{\boldsymbol{\sigma}}(\mathbf{u}(t), \dot{\mathbf{u}}(t)) \cdot \mathbf{v}(t) \, d\mathbf{a} \Big) \, dt \\ & + \int_0^T \Big(\int_\Omega \operatorname{div} \boldsymbol{\sigma}(\mathbf{u}(t), \dot{\mathbf{u}}(t)) \cdot \mathbf{v}(t) \, d\mathbf{x} \Big) \, dt \,, \qquad \mathbf{v} \in \mathbf{V}_C \end{aligned}$$

for $\mathbf{u} \in \mathbf{D}$, and integration by parts in space leads to

$$\langle \mathbf{A}\mathbf{u}, \mathbf{v} \rangle = \int_0^T \Big(\int_{\Gamma_C(t) \cup \tilde{\Gamma}_C(t)} \hat{\boldsymbol{\sigma}}(\mathbf{u}(t), \dot{\mathbf{u}}(t)) \cdot \mathbf{v}(t) \, d\mathbf{a} \Big) \, dt \,.$$

Due to $\ker \boldsymbol{\gamma}_C^* = \{ \mathbf{v} \in \mathbf{L}_2(0,T;\mathbf{H}_D^1(\Omega)) \,|\, \mathbf{v} = 0 \text{ on } \Gamma_C(t) \cup \tilde{\Gamma}_C(t) \}$, it holds

$$\langle \mathbf{A}\mathbf{u}, \mathbf{v} \rangle = 0, \quad \forall \, \mathbf{u} \in \mathbf{D} \,, \qquad \forall \, \mathbf{v} \in \ker \boldsymbol{\gamma}_C^* \,.$$

Since $\mathbf{D}$ is dense in $\mathbf{U}_D$, the linear and continuous operator $\mathbf{A}$ can be extended to $\mathbf{U}_D$ [93, Proposition 18.29], and a classical density argument leads to

$$\langle \mathbf{A}\mathbf{u}, \mathbf{v} \rangle = 0 \,, \quad \forall \, \mathbf{u} \in \mathbf{U}_D \,, \qquad \forall \, \mathbf{v} \in \ker \boldsymbol{\gamma}_C^* \,.$$

Now, the trace theorem B.1.1 yields the existence of a continuous operator $\boldsymbol{\pi} : \mathbf{U}_D \to \mathbf{L}_2(0,T;(\mathbf{H}^{1/2})^*(\Gamma_C^*(t)))$ satisfying

$$\langle \mathbf{A}\mathbf{u}, \mathbf{v} \rangle = \langle \boldsymbol{\pi}(\mathbf{u}), \boldsymbol{\gamma}_C^* \mathbf{v} \rangle \,, \qquad \forall \, \mathbf{u} \in \mathbf{U}_D \,, \, \forall \, \mathbf{v} \in \mathbf{V}_C \,.$$

If $\mathbf{u} \in \mathbf{D} \subset \mathbf{U}_D$ and solution of the variational problem (1.28), then

$$\langle \mathbf{A}\mathbf{u}, \mathbf{v} \rangle = \int_0^T \langle \mathbf{F}_{\mathrm{con}}(\mathbf{u}(t)), \mathbf{v}(t) \rangle \, dt \,, \qquad \forall \, \mathbf{v} \in \mathbf{V}_C \,,$$

and the same is valid for the perturbed solution $\tilde{\mathbf{u}} \in \mathbf{D} \subset \mathbf{U}_D$. Thus,

$$\int_0^T \langle \mathbf{F}_{\mathrm{con}}(\mathbf{u}) - \mathbf{F}_{\mathrm{con}}(\tilde{\mathbf{u}}), \mathbf{v} \rangle \, dt = \langle \mathbf{A}\mathbf{u} - \mathbf{A}\tilde{\mathbf{u}}, \mathbf{v} \rangle = \langle \boldsymbol{\pi}(\mathbf{u}) - \boldsymbol{\pi}(\tilde{\mathbf{u}}), \boldsymbol{\gamma}_C^* \mathbf{v} \rangle \,, \qquad \forall\, \mathbf{v} \in \mathbf{V}_C \,.$$

By the generalized main theorem of calculus (compare, e.g., [93, Problem 23.5]), the time derivative $\dot{\mathbf{u}}(t)$ exists in the classical sense for almost every $t \in [0,T]$ and coincides with the generalized derivative in $\mathbf{L}_2(0,T;\mathbf{H}^1(\Omega))$. For t such that $\dot{\mathbf{u}}(t)$ exists and condition (1.28) holds,

$$\begin{aligned} [\dot{\mathbf{u}}(t) \cdot \boldsymbol{\nu}]_{\boldsymbol{\phi}} &= \lim_{h \to 0} \frac{[\mathbf{u}(t+h) \cdot \boldsymbol{\nu}]_{\boldsymbol{\phi}} - [\mathbf{u}(t) \cdot \boldsymbol{\nu}]_{\boldsymbol{\phi}}}{h} \\ &= \lim_{h \to 0} \frac{[\mathbf{u}(t+h) \cdot \boldsymbol{\nu}]_{\boldsymbol{\phi}} - g}{h} \\ &= \begin{cases} \geq 0 & \text{if } h > 0 \\ \leq 0 & \text{if } h < 0 \end{cases} \end{aligned}$$

on $\Gamma_C(t)$ and hence, $[\dot{\mathbf{u}}(t) \cdot \boldsymbol{\nu}]_{\boldsymbol{\phi}} = 0$. The same argumentation leads to $[\dot{\tilde{\mathbf{u}}}(t) \cdot \boldsymbol{\nu}]_{\boldsymbol{\phi}} = 0$ on $\tilde{\Gamma}_C(t)$ for almost every $t \geq 0$. This yields that $\dot{\mathbf{u}}, \dot{\tilde{\mathbf{u}}} \in \mathbf{V}_C$, which directly gives the result of the theorem. □

B.4. Interpretation of Discrete Contact Stresses

The last section of this appendix is dedicated to the localization of the contact stresses of the contact–implicit and (improved) contact–stabilized Newmark method on certain critical contact boundaries.

For stationary Signorini problems, the dual interpretation of contact forces as functionals on the active contact boundaries is well-known, cf. [49, Chapter 5] or [58, Chapter 2]. For this reason, the derivation of this result on the basis of Green's Theorem will not be presented here. Instead, the contact forces of (N-CI/CS(+)) will be directly localized on the critical contact boundaries $(\Gamma_C^*)^{j+1,j}$ introduced in Section 5.1.2.

Denote by Γ_C^{j+1} and $\tilde{\Gamma}_C^{j+1}$ the active contact boundaries of a discrete solution $\mathbf{u}^{j+1}$ and a perturbed solution $\tilde{\mathbf{u}}^{j+1}$, respectively. Moreover, assume again that the possible contact boundaries and the bijective mappings between the two possible contact boundaries coincide, i.e., $\Gamma_C = \tilde{\Gamma}_C$ and $\boldsymbol{\phi} = \tilde{\boldsymbol{\phi}}$.

Theorem B.4.1. *For $j+1 \in \{1, \ldots, N_\triangle\}$, let $(\boldsymbol{\gamma}_C^*)^{j+1,j} : \mathbf{V}_C^{j+1,j} \to \mathbf{H}^{1/2}((\Gamma_C^*)^{j+1,j})$ denote a linear, continuous, and surjective trace operator, where*

$$\mathbf{V}_C^{j+1,j} = \left\{ \mathbf{v} \in \mathbf{H}_D^1(\Omega) \,\middle|\, [\mathbf{v} \cdot \boldsymbol{\nu}]_{\boldsymbol{\phi}} = 0 \text{ a.e. on } (\Gamma_C^{j+1} \cup \tilde{\Gamma}_C^{j+1}) \setminus (\Gamma_C^*)^{j+1,j} \right\}.$$

Further, define $\mathbf{U}_D^{j+1}$ *as the closure of*

$$\mathbf{D}^{j+1} = \left\{ \bar{\mathbf{v}} \in \mathbf{C}^\infty(\bar{\Omega}) \,\middle|\, \hat{\boldsymbol{\sigma}}(\mathbf{v}, \dot{\mathbf{v}}) = \mathbf{0} \text{ on } \Gamma_C \setminus (\Gamma_C^{j+1} \cup \tilde{\Gamma}_C^{j+1}) \right\}$$

with respect to the canonical norm on

$$\mathbf{U}^{j+1} = \left\{ \bar{\mathbf{v}} \in \mathbf{H}^1(\Omega) \,\middle|\, \operatorname{div} \boldsymbol{\sigma}(\mathbf{v}, \dot{\mathbf{v}}) \in \mathbf{L}_2(\Omega),\ \hat{\boldsymbol{\sigma}}(\mathbf{v}, \dot{\mathbf{v}}) \in \mathbf{L}_2(\Gamma_N) \right\}.$$

If $\mathbf{u}^{j+1}$ *and* $\tilde{\mathbf{u}}^{j+1}$ *are discrete solutions of* (N-CI/CS(+)) *with* $\mathbf{u}^{j+1}, \tilde{\mathbf{u}}^{j+1} \in \mathbf{U}_D^{j+1}$, *then*

$$\begin{aligned} &\left\langle \mathbf{F}_{\mathrm{con}}(\mathbf{u}^{j+1}) - \mathbf{F}_{\mathrm{con}}(\tilde{\mathbf{u}}^{j+1}), (\mathbf{u}^{j+1} - \tilde{\mathbf{u}}^{j+1}) - (\mathbf{u}^j - \tilde{\mathbf{u}}^j) \right\rangle \\ &= \left\langle \boldsymbol{\pi}^{j+1,j}(\mathbf{u}^{j+1}) - \boldsymbol{\pi}^{j+1,j}(\tilde{\mathbf{u}}^{j+1}), (\boldsymbol{\gamma}_C^*)^{j+1,j}((\mathbf{u}^{j+1} - \tilde{\mathbf{u}}^{j+1}) - (\mathbf{u}^j - \tilde{\mathbf{u}}^j)) \right\rangle \end{aligned} \tag{B.5}$$

with a continuous operator $\boldsymbol{\pi}^{j+1,j} : \mathbf{U}_D^{j+1} \to (\mathbf{H}^{1/2})^*((\Gamma_C^*)^{j+1,j})$.

Proof. The linear, continuous, and surjective trace operator $(\boldsymbol{\gamma}_C^*)^{j+1,j}$ can be chosen as the trace operator from $\mathbf{V}_C^{j+1,j}$ to the set

$$\left\{ \mathbf{v} \in \mathbf{H}^{1/2}(\Gamma) \,\middle|\, [\mathbf{v} \cdot \boldsymbol{\nu}]_{\boldsymbol{\phi}} = 0 \text{ a.e. on } (\Gamma_C^*)^{j+1,j} \setminus \Gamma_C^{j+1} \cap \tilde{\Gamma}_C^{j+1} \right\}$$

concatenated with the canonical restriction to $\mathbf{H}^{1/2}((\Gamma_C^*)^{j+1,j})$.

Define the linear operator $\mathbf{A} : \mathbf{U}_D^{j+1} \supset \mathbf{D}^{j+1} \to (V_C^{j+1,j})^*$ as

$$\begin{aligned} \langle \mathbf{A}\bar{\mathbf{u}}^{j+1}, \mathbf{v} \rangle := a(\mathbf{u}^{j+1}, \mathbf{v}) + b(\dot{\mathbf{u}}^{j+1}, \mathbf{v}) - \int_{\Gamma_N} \hat{\boldsymbol{\sigma}}(\mathbf{u}^{j+1}, \dot{\mathbf{u}}^{j+1}) \cdot \mathbf{v}\, d\mathbf{a} \\ + \int_\Omega \operatorname{div} \boldsymbol{\sigma}(\mathbf{u}^{j+1}, \dot{\mathbf{u}}^{j+1}) \cdot \mathbf{v}\, d\mathbf{x}\,, \quad \mathbf{v} \in \mathbf{V}_C^{j+1,j} \end{aligned}$$

for $\mathbf{u}^{j+1} \in \mathbf{D}^{j+1}$. This mapping is continuous in $(\mathbf{H}^1)^*(\Omega)$ since

$$\begin{aligned} \left| \langle \mathbf{A}\bar{\mathbf{u}}^{j+1}, \mathbf{v} \rangle \right| \leq & C\big(\|\mathbf{u}^{j+1}\|_{\mathbf{H}^1(\Omega)} + \|\dot{\mathbf{u}}^{j+1}\|_{\mathbf{H}^1(\Omega)} + \|\hat{\boldsymbol{\sigma}}(\mathbf{u}^{j+1}, \dot{\mathbf{u}}^{j+1})\|_{\mathbf{L}_2(\Gamma_N)} \big) \|\mathbf{v}\|_{\mathbf{H}^1(\Omega)} \\ & + \| \operatorname{div} \hat{\boldsymbol{\sigma}}(\mathbf{u}^{j+1}, \dot{\mathbf{u}}^{j+1})\|_{\mathbf{L}_2(\Omega)} \|\mathbf{v}\|_{\mathbf{L}_2(\Omega)}\,. \end{aligned}$$

Integration by parts in space leads to

$$\langle \mathbf{A}\bar{\mathbf{u}}^{j+1}, \mathbf{v} \rangle = \int_{\Gamma_C^{j+1} \cup \tilde{\Gamma}_C^{j+1}} \hat{\boldsymbol{\sigma}}(\mathbf{u}^{j+1}, \dot{\mathbf{u}}^{j+1}) \cdot \mathbf{v}\, d\mathbf{a}\,.$$

By means of $\ker(\boldsymbol{\gamma}_C^*)^{j+1,j} = \{\mathbf{v} \in \mathbf{H}_D^1(\Omega) \,|\, \mathbf{v} = 0 \text{ on } \Gamma_C^{j+1} \cup \tilde{\Gamma}_C^{j+1}\}$,

$$\langle \mathbf{A}\bar{\mathbf{u}}^{j+1}, \mathbf{v} \rangle = 0\,, \qquad \forall\, \mathbf{u}^{j+1} \in \mathbf{D}^{j+1}\,,\ \forall\, \mathbf{v} \in \ker(\boldsymbol{\gamma}_C^*)^{j+1,j}$$

holds. Since $\mathbf{D}^{j+1}$ is dense in $\mathbf{U}_D^{j+1}$, the linear and continuous operator $\mathbf{A}$ can be extended to $\mathbf{U}_D^{j+1}$ [93, Proposition 18.29], and a classical density argument leads to

$$\langle \mathbf{A}\bar{\mathbf{u}}^{j+1}, \mathbf{v} \rangle = 0\,, \qquad \forall\, \mathbf{u}^{j+1} \in \mathbf{U}_D^{j+1}\,,\ \forall\, \mathbf{v} \in \ker(\boldsymbol{\gamma}_C^*)^{j+1,j}\,.$$

The trace theorem B.1.1 yields the existence of a continuous operator $\boldsymbol{\pi}^{j+1,j} : \mathbf{U}_D^{j+1} \to (\mathbf{H}^{1/2})^*((\Gamma_C^*)^{j+1,j})$ that satisfies

$$\langle \mathbf{A}\bar{\mathbf{u}}^{j+1}, \mathbf{v}\rangle = \left\langle \boldsymbol{\pi}^{j+1,j}(\mathbf{u}^{j+1}), (\boldsymbol{\gamma}_C^*)^{j+1,j}\mathbf{v}\right\rangle, \qquad \forall\, \mathbf{u}^{j+1} \in \mathbf{U}_D^{j+1}\,,\ \forall\, \mathbf{v} \in \mathbf{V}_C^{j+1,j}\,.$$

For a solution $\mathbf{u} \in \mathbf{D}^{j+1} \subset \mathbf{U}_D^{j+1}$ of (N-CI/CS(+)),

$$\begin{aligned}
&\langle \mathbf{A}\bar{\mathbf{u}}^{j+1}, \mathbf{v}\rangle \\
&= \langle \mathbf{F}(\mathbf{u}^{j+1}), \mathbf{v}\rangle + \langle \mathbf{G}(\dot{\mathbf{u}}^{j+1}), \mathbf{v}\rangle - \langle \mathbf{f}, \mathbf{v}\rangle + \int_\Omega \operatorname{div} \boldsymbol{\sigma}(\mathbf{u}^{j+1}, \dot{\mathbf{u}}^{j+1}) \cdot \mathbf{v}\, d\mathbf{x} \\
&= -\frac{2}{\tau_j^2}\big(\mathbf{u}^{j+1} - \mathbf{u}^j - \tau_j \dot{\mathbf{u}}^j, \mathbf{v}\big) - \left\langle \mathbf{F}(\mathbf{u}^j), \mathbf{v}\right\rangle - \left\langle \mathbf{G}(\dot{\mathbf{u}}^j), \mathbf{v}\right\rangle + \left\langle \mathbf{F}_{\mathrm{con}}(\mathbf{u}^{j+1}), \mathbf{v}\right\rangle \\
&\quad - \langle \mathbf{f}, \mathbf{v}\rangle + \int_\Omega \operatorname{div} \boldsymbol{\sigma}(\mathbf{u}^{j+1}, \dot{\mathbf{u}}^{j+1}) \cdot \mathbf{v}\, d\mathbf{x} \\
&= \left\langle \mathbf{F}_{\mathrm{con}}(\mathbf{u}^{j+1}), \mathbf{v}\right\rangle
\end{aligned}$$

for all $\mathbf{v} \in \mathbf{V}_C^{j+1,j}$, and the same is valid for the perturbed solution $\tilde{\mathbf{u}}^{j+1} \in \mathbf{D}^{j+1} \subset \mathbf{U}_D^{j+1}$. Hence,

$$\begin{aligned}
&\left\langle \mathbf{F}_{\mathrm{con}}(\mathbf{u}^{j+1}) - \mathbf{F}_{\mathrm{con}}(\tilde{\mathbf{u}}^{j+1}), \mathbf{v}\right\rangle \\
&= \langle \mathbf{A}\bar{\mathbf{u}}^{j+1} - \mathbf{A}\tilde{\bar{\mathbf{u}}}^{j+1}, \mathbf{v}\rangle \\
&= \left\langle \boldsymbol{\pi}^{j+1,j}(\mathbf{u}^{j+1}) - \boldsymbol{\pi}^{j+1,j}(\tilde{\mathbf{u}}^{j+1}), (\boldsymbol{\gamma}_C^*)^{j+1,j}\mathbf{v}\right\rangle, \quad \forall\, \mathbf{v} \in \mathbf{V}_C^{j+1,j}\,.
\end{aligned}$$

The difference of the perturbations in displacements at the beginning and at the end of a timestep satisfies $(\mathbf{u}^{j+1} - \tilde{\mathbf{u}}^{j+1}) - (\mathbf{u}^j - \tilde{\mathbf{u}}^j) \in \mathbf{V}_C^{j+1,j}$, since

$$\begin{aligned}
&(\Gamma_C^{j+1} \cup \tilde{\Gamma}_C^{j+1}) \setminus (\Gamma_C^*)^{j+1,j} \\
&= (\Gamma_C^{j+1} \cup \tilde{\Gamma}_C^{j+1}) \setminus (\Gamma_C^*)^{j+1} \cap (\Gamma_C^{j+1} \cup \tilde{\Gamma}_C^{j+1}) \setminus ((\Gamma_C^*)^j \cup (\tilde{\Gamma}_C^*)^{j+1,j}) \\
&= (\Gamma_C^{j+1} \cap \tilde{\Gamma}_C^{j+1}) \cap (\Gamma_C^{j+1} \cup \tilde{\Gamma}_C^{j+1}) \setminus ((\Gamma_C^*)^j \cup (\tilde{\Gamma}_C^*)^{j+1,j}) \\
&= (\Gamma_C^{j+1} \cap \tilde{\Gamma}_C^{j+1}) \setminus ((\Gamma_C^*)^j \cup (\tilde{\Gamma}_C^*)^{j+1,j}) \\
&= \Gamma_C^{j+1} \cap \tilde{\Gamma}_C^{j+1} \cap \Gamma_C^j \cap \tilde{\Gamma}_C^j\,.
\end{aligned}$$

This leads to the result of the theorem. □

List of Symbols

Acronyms

$(\text{N-CL})_h$ classical Newmark method

$(\text{N-CI})_h$ contact–implicit Newmark method

$(\text{N-CS})_h$ contact–stabilized Newmark method

$(\text{N-CS+})_h$ improved contact–stabilized Newmark method

(N-CL) classical Newmark method in function space

(N-CI/CS(+)) contact–implicit and (improved) contact–stabilized Newmark method in function space

ContacX adaptive improved contact–stabilized Newmark method

General Notations

Ω reference configuration

Γ, Γ_D, Γ_N, Γ_C boundary of Ω, Dirichlet-, Neumann-, and contact boundaries

$\mathbf{u}$ displacements

$\bar{\mathbf{\Phi}}$ evolution operator of continuous solution

$\mathcal{K}$ admissible set

$I_{\mathcal{K}}$ characteristic functional of $\mathcal{K}$

$\boldsymbol{\phi}$ contact mapping

$\boldsymbol{\nu}_{\boldsymbol{\phi}}$ normal vector

$[\mathbf{u} \cdot \boldsymbol{\nu}]_{\boldsymbol{\phi}}$ relative displacement of $\mathbf{u}$ in direction of $\boldsymbol{\nu}_{\boldsymbol{\phi}}$

g gap function

$\boldsymbol{\varepsilon}$ strain tensor

$\boldsymbol{\sigma}$, $\hat{\boldsymbol{\sigma}}$ stress tensor and boundary stresses

$\mathbf{E}$, $\mathbf{V}$ elasticity and viscosity tensor

E_0, V_0 constant for positive definite elasticity and viscosity tensor

a, b bilinearform of elastic and viscous forces

$\mathbf{F}$, $\mathbf{G}$ functional of elastic and viscous forces

f_{ext} external forces

$\mathbf{F}_{\text{con}}$ contact forces

$\boldsymbol{\mathcal{L}}$ linear momentum

$\mathcal{E}$, $\mathcal{E}_{\text{kin}}$, $\mathcal{E}_{\text{pot}}$, $\mathcal{E}_{\text{visco}}$ total, kinetic, elastic, and viscous energy

$\bar{\mathbf{v}}$ function $\mathbf{v}$ and its first derivative $\dot{\mathbf{v}}$

$\delta\mathbf{v}$ perturbation of $\mathbf{v}$

Numerics

Ω_h polyhedral reference configuration

τ, h timestep and maximal spatial diameter

$N_\triangle$ number of discrete timepoints

$\bar{\mathbf{u}}^n$,$\bar{\mathbf{u}}_h^n$ approximations of $\bar{\mathbf{u}}(t_n)$

$\mathbf{u}_{\text{pred}}^n$, $\mathbf{u}_{h,\text{pred}}^n$ predictor for approximations of $\mathbf{u}(t_n)$

$\bar{\boldsymbol{\Psi}}$ evolution operator of discrete solution

$\bar{\mathbf{u}}_\triangle$,$\bar{\mathbf{u}}_\tau$ lattice function

$\mathcal{K}_h$ discrete admissible set

$\mathbf{S}_h$ finite element space

$\mathbf{F}^\lambda(\mathbf{u},\mathbf{v})$ weighting of $\mathbf{F}(\mathbf{u})$ and $\mathbf{F}(\mathbf{v})$

$\boldsymbol{\epsilon}(t,\bar{\mathbf{u}},\tau)$ local error

$\boldsymbol{\epsilon}_{\triangle}(\mathbf{u},t), \boldsymbol{\epsilon}_{\tau}(\bar{\mathbf{u}},t)$ global error

$[\mathbf{v}]$ estimation of $\mathbf{v}$

TOL tolerance

$\bar{\mathbf{X}}$ non-standard quantity in asymptotic error expansion

Function Spaces and Norms

$\mathbf{L}_2$ Lebesgue space

$\mathbf{H}^1$, $\mathbf{H}^1_D$ Sobolev space and Sobolev space with Dirichlet values

$\mathbf{H}^{1/2}$ space of traces

$\mathbf{C}([t_0,t],\mathbf{V})$ set of continuous functions $\mathbf{v} : [t_0,t] \to \mathbf{V}$

$\mathbf{C}^k([t_0,t],\mathbf{V})$ set of k-times continuously differentiable functions $\mathbf{v} : [t_0,t] \to \mathbf{V}$

$\mathbf{L}_2(t_0,t;\mathbf{V})$ set of square-integrable functions $\mathbf{v} : [t_0,t] \to \mathbf{V}$

$\mathbf{W}^1_2(t_0,t;\mathbf{H}^1,\mathbf{L}_2)$ set of all functions $\mathbf{v} \in \mathbf{L}_2(t_0,t;\mathbf{H}^1)$ with $\dot{\mathbf{v}} \in \mathbf{L}_2(t_0,t;(\mathbf{H}^1)^*)$

$\|\cdot\|_{\mathbf{V}}$, $(\cdot,\cdot)_{\mathbf{V}}$ norm and scalar product on $\mathbf{V}$

$\mathbf{V}^*$, $\langle\cdot,\cdot\rangle_{\mathbf{V}^*\times\mathbf{V}}$ dual space of $\mathbf{V}$ and dual pairing

$\|\cdot\|_a$, $\|\cdot\|_b$ seminorms from bilinearforms a and b

$\|\cdot\|_{\mathcal{E}(t,\tau)}$, $\|\cdot\|_E$ physical energy norm and reduced physical energy norm

$\|\cdot\|_\tau$ discrete displacement norm

$\mathrm{TV}(\mathbf{v},[t_0,t],\mathbf{V})$ total variation of a function $\mathbf{v} : [t_0,t] \to \mathbf{V}$

$\mathbf{BV}([t_0,t],\mathbf{V})$ set of all functions $\mathbf{v} : [t_0,t] \to \mathbf{V}$ with bounded variation

$R(\mathbf{u},[t,t+\tau])$ sum of total variations of $\mathbf{u}$

c_K constant in Korn's inequality

Bibliography

[1] AMIRA. http://www.amira.com.

[2] DUNE – distributed and unified numerics environment. http://www.dune-project.org/.

[3] UG. http://atlas.gcsc.uni-frankfurt.de/~ug/index.html.

[4] The visible human project. http://www.nlm.nih.gov/research/visible/visible_human.html.

[5] R. A. Adams and J. J. F. Fournier. *Sobolev Spaces*, volume 140 of *Pure and Applied Mathematics*. Elsevier, Oxford Amsterdam, 2nd edition, 2003.

[6] J. Ahn and D. E. Stewart. Dynamic frictionless contact in linear viscoelasticity. *IMA J. Numer. Anal.*, 29(1):43–71, 2009.

[7] J.-P. Aubin. *Applied Functional Analysis*. Pure and Applied Mathematics: A Wiley-Interscience Series of Texts, Monographs and Tracts. John Wiley & Sons, New York, 2nd edition, 2000.

[8] P. Boieri, F. Gastaldi, and D. Kinderlehrer. Existence, uniqueness, and regularity results for the two-body contact problem. *Appl. Math. Optim.*, 15(1):251–277, 1987.

[9] F. Bornemann. An adaptive multilevel approach to parabolic equations I. General theory and 1d-implementation. *IMPACT Comput. Sci. Engrg.*, 2(4):279–317, 1990.

[10] F. Bornemann. *An Adaptive Multilevel Approach for Parabolic Equations in Two Space Dimensions*. PhD thesis, Freie Universität Berlin, 1991. published as TR 91-07 at Zuse-Institut Berlin, http://opus.kobv.de/zib/volltexte/1991/482/.

[11] A. E. Chapman. *Biomechanical Analysis of Fundamental Human Movements*. Human Kinetics, Champaign, 2008.

[12] P. G. Ciarlet. *Mathematical Elasticity. Volume I: Three-Dimensional Elasticity*, volume 20 of *Studies in Mathematics & Its Applications*. Elsevier Science, Amsterdam, 1988.

[13] M. Cocou. Existence of solutions of a dynamic Signorini's problem with nonlocal friction in viscoelasticity. *Z. Angew. Math. Phys.*, 53(6):1099–1109, 2002.

[14] M. Cocou and J. M. Ricaud. Analysis of a class of implicit evolution inequalities associated to viscoelastic dynamic contact problems with friction. *Internat. J. Engrg. Sci.*, 38(14):1535–1552, 2000.

[15] J. D. Currey. *Bones: Structure and Mechanics*. Princeton University Press, Princeton, 2002.

[16] B. M. F. de Veubeke. *A Course in Elasticity*, volume 29 of *Applied Mathematical Sciences*. Springer-Verlag, New York Heildelberg Berlin, 1979.

[17] P. Deuflhard. Differential equations in technology and medicine: Computational concepts, adaptive algorithms, and virtual labs. In *Computational Mathematics Driven by Industrial Problems*, volume 1739 of *Lecture Notes in Mathematics*, pages 69–125. Springer-Verlag, Berlin Heidelberg New York, 2000.

[18] P. Deuflhard and F. Bornemann. *Scientific Computing with Ordinary Differential Equations*, volume 42 of *Texts in Applied Mathematics*. Springer-Verlag, Berlin Heidelberg New York, 2002.

[19] P. Deuflhard, R. Krause, and S. Ertel. A contact-stabilized Newmark method for dynamical contact problems. *Internat. J. Numer. Methods Engrg.*, 73(9):1274–1290, 2007.

[20] P. Deuflhard and M. Weiser. *Numerische Mathematik 3: Adaptive Lösung partieller Differentialgleichungen*. de Gruyter Lehrbuch. Walter de Gruyter, Berlin, 2011.

[21] T. L. Haut Donahue, M. L. Hull, M. M. Rashid, and C. R. Jacobs. A finite element model of the human knee joint for the study of tibio-femoral contact. *J. Biomech. Eng.*, 124(3):273–280, 2002.

[22] D. Doyen, A. Ern, and S. Piperno. Time–integration schemes for the finite element dynamic Signorini problem. *SIAM J. Sci. Comput.*, 33(1):223–249, 2011.

[23] G. Duvaut and J. L. Lions. *Inequalities in Mechanics and Physics*. Springer-Verlag, Berlin Heidelberg New York, 1976.

[24] C. Eck. *Existenz und Regularität der Lösungen für Kontaktprobleme mit Reibung*. PhD thesis, Universität Stuttgart, 1996.

[25] C. Eck, J. Jarušek, and M. Krebeč. *Unilateral Contact Problems: Variational Methods and Existence Theorems*, volume 270 of *Pure and Applied Mathematics*. Taylor & Francis Group, Boca Raton, 2005.

[26] I. Ekeland and R. Temam. *Convex Analysis and Variational Problems*. Number 28 in Classics in Applied Mathematics. Society for Industrial and Applied Mathematics, Amsterdam New York, 1987.

[27] L. D. Evans. *Partial Differential Equations*. Number 19 in Graduate Studies in Mathematics. American Mathematical Society, Providence, 2nd edition, 2010.

[28] R. P. Feynman, R. B. Leighton, and M. Sands. *The Feynman Lectures on Physics, Volume 1. The Definitive Edition*. Addison-Wesley, Reading, 2nd edition, 2005.

[29] C. Gräser and R. Kornhuber. Multigrid methods for obstacle problems. *J. Comp. Math.*, 27(1):1–44, 2009.

[30] Y. M. Haddad. *Viscoelasticity of Engineering Materials*. Chapman & Hall, London, 1995.

[31] C. Hager, S. Hüeber, and B. Wohlmuth. A stable energy conserving approach for frictional contact problems based on quadrature formulas. *Internat. J. Numer. Methods Engrg.*, 73(2):205–225, 2008.

[32] E. Hairer and C. Lubich. Asymptotic expansions of the global error of fixed-stepsize methods. *Numer. Math.*, 45(3):345–360, 1982.

[33] E. Hairer, C. Lubich, and G. Wanner. *Geometric Numerical Integration. Structure–Preserving Algorithms for Ordinary Differential Equations*. Number 31 in Computational Mathematics. Springer-Verlag, Berlin Heidelberg New York, 2nd edition, 2006.

[34] E. Hairer, S. P. Nørsett, and G. Wanner. *Solving Ordinary Differential Equations I. Nonstiff Problems.* Springer-Verlag, Berlin Heidelberg New York, 1987.

[35] W. Han and M. Sofonea. *Quasistatic Contact Problems in Viscoelasticity and Viscoplasticity*. AMS/IP Studies in Advanced Mathematics. American Mathematical Society, Providence, 2002.

[36] J. Haslinger and I. Hlaváček. Contact between elastic bodies I. Continuous problems. *Apl. Mat.*, 25(5):324–347, 1980.

[37] W. C. Hayes and L. F. Mockros. Viscoelastic properties of human articular cartilage. *J. Appl. Physiol.*, 31(4):562–568, 1971.

[38] J. Heinonen, T. Kilpelainen, and O. Martio. *Nonlinear Potential Theory of Degenerate Elliptic Equations*. Oxford University Press, New York, 1993.

[39] H. Hertz. Über die Berührung fester elastischer Körper. *J. Reine Angew. Math.*, 92:156–171, 1881.

[40] H. M. Hilber, T. J. R. Hughes, and R. L. Taylor. Improved numerical dissipation for time integration algorithms in structural dynamics. *Earthquake Engineering and Structural Dynamics*, 51(3):283–292, 1977.

[41] T. J. R. Hughes. *The Finite Element Method. Linear Static and Dynamic Finite Element Analysis*. Prentice-Hall, Englewood Cliffs, 2003.

[42] J. Jarušek. Dynamical contact problems for bodies with a singular memory. *Boll. Un. Mat. Ital. A*, 9(3):581–592, 1995.

[43] J. Jarušek. Dynamical contact problems with given friction for viscoelastic bodies. *Czechoslovak Math. J.*, 46(3):475–487, 1996.

[44] J. Jarušek. Remark to dynamic contact problems for bodies with a singular memory. *Comment. Math. Univ. Carolin.*, 39(3):545–550, 1998.

[45] J. Jarušek and C. Eck. Dynamical contact problems with small Coulomb friction for viscoelastic bodies. Existence of solutions. *Math. Models Methods Appl. Sci.*, 9(1):11–34, 1999.

[46] C. Kane, E. A. Repetto, M. Ortiz, and J. E. Marsden. Finite element analysis of nonsmooth contact. *Comput. Methods Appl. Mech. Engrg.*, 180(1-2):1–26, 1999.

[47] H. B. Khenous, P. Laborde, and Y. Renard. On the discretization of contact problems in elastodynamics. *Lecture Notes in Appl. Comp. Mech.*, 27:31–38, 2006.

[48] H. B. Khenous, P. Laborde, and Y. Renard. Mass redistribution method for finite element contact problems in elastodynamics. *Eur. J. Mech., A/Solids*, 27(5):918–932, 2008.

[49] N. Kikuchi and J. T. Oden. *Contact Problems in Elasticity*. SIAM Studies in Applied Mathematics. Society for Industrial and Applied Mathematics, Philadelphia, 1988.

[50] C. Klapproth, P. Deuflhard, and A. Schiela. A perturbation result for dynamical contact problems. Preprint, Zuse-Institut Berlin, 2008. ZR 08-27. `http://opus.kobv.de/zib/volltexte/2008/1113/`.

[51] C. Klapproth, P. Deuflhard, and A. Schiela. A perturbation result for dynamical contact problems. *Numer. Math. Theor. Meth. Appl.*, 2(3):237–257, 2009.

[52] C. Klapproth, A. Schiela, and P. Deuflhard. Adaptive timestep control for the contact-stabilized Newmark method. Preprint, Zuse-Institut Berlin, 2010. ZR 10-09. `http://opus.kobv.de/zib/volltexte/2010/1232/`. accepted for publication in Numer. Math.

[53] C. Klapproth, A. Schiela, and P. Deuflhard. Consistency results on Newmark methods for dynamical contact problems. *Numer. Math.*, 116(1):65–94, 2010.

[54] A. Klarbring, A. Mikelič, and M. Shillor. Frictional contact problems with normal compliance. *Internat. J. Engrg. Sci.*, 26(80):811–832, 1988.

[55] R. Kornhuber. *Adaptive Monotone Multigrid Methods for Nonlinear Variational Problems*. B. G. Teubner, Stuttgart, 1997.

[56] R. Kornhuber and R. Krause. Adaptive multigrid methods for Signorini's problem in linear elasticity. *Comput. Vis. Sci.*, 4(1):9–20, 2001.

[57] R. Kornhuber, R. Krause, O. Sander, P. Deuflhard, and S. Ertel. A monotone multigrid solver for two body contact problems in biomechanics. *Comput. Vis. Sci.*, 11(1):3–15, 2008.

[58] R. Krause. *Monotone Multigrid Methods for Signorini's Problem with Friction*. PhD thesis, Freie Universität Berlin, 2000. `http://www.diss.fu-berlin.de/2001/240/indexe.html`.

[59] R. Krause and M. Walloth. Presentation and comparison of selected algorithms for dynamic contact based on the Newmark scheme. Technical report, Institute of Computational Science, University of Lugano, 2009. ICS Preprint 2009-08.

[60] K. L. Kuttler. Dynamic friction contact problems for general normal and frictional laws. *Nonlinear Anal.*, 28(3):559–575, 1997.

[61] K. L. Kuttler and M. Shillor. Set-valued pseudomonotone maps and degenerate evolution inclusions. *Commun. Contemp. Math.*, 1(1):87–123, 1999.

[62] K. L. Kuttler and M. Shillor. Dynamic contact with Signorini's condition and slip rate dependent friction. *Electron. J. Differential Equations*, 83:1–21, 2004.

[63] K. L. Kuttler and M. Shillor. Regularity of solutions to a dynamic frictionless contact problem with normal compliance. *Nonlinear Anal.*, 59(7):1063–1075, 2004.

[64] J. Lang. *Adaptive Multilevel Solution of Nonlinear Parabolic PDE Systems: Theory, Algorithm, and Applications*, volume 16 of *Lecture Notes in Computational Science and Engineering*. Springer-Verlag, Berlin Heidelberg New York, 2000.

[65] T. A. Laursen. *Computational Contact and Impact Mechanics. Fundamentals of Modeling Interfacial Phenomena in Nonlinear Finite Element Analysis*. Springer-Verlag, Berlin Heidelberg New York, 2003.

[66] T. A. Laursen and V. Chawla. Design of energy conserving algorithms for frictionless dynamic contact problems. *Internat. J. Numer. Methods Engrg.*, 40(5):863–886, 1997.

[67] T. A. Laursen and G. R. Love. Improved implicit integrators for transient impact problems – geometric admissibility within the conserving framework. *Internat. J. Numer. Methods Engrg.*, 53(2):245–274, 2002.

[68] G. Lebeau and M. Schatzman. A wave problem in a half-space with a unilateral constraint at the boundary. *J. Differential Equations*, 53(3):309–361, 1984.

[69] J. L. Lions and E. Magenes. *Non-Homogeneous Boundary Value Problems and Applications*. Springer-Verlag, Berlin Heidelberg New York, 1973.

[70] J. Marsden and M. West. Discrete mechanics and variational integrators. *Acta Numer.*, 10(5):357–514, 2001.

[71] J. E. Marsden and T. J. R. Hughes. *Mathematical Foundations of Elasticity*. Prentice-Hall, Englewood Cliffs, 1994.

[72] J. A. C. Martins and J. T. Oden. Existence and uniqueness results for dynamic contact problems with nonlinear normal friction and interface laws. *Nonlinear Anal.*, 11(3):407–428, 1987.

[73] F. Mignot. Contrôle dans les inequations variationelles elliptiques. *J. Funct. Anal.*, 22(2):130–185, 1976.

[74] S. Migòrski and A. Ochal. A unified approach to dynamic contact problems in viscoelasticity. *J. Elasticity*, 83(3):247–265, 2006.

[75] J. Nečas and I. Hlaváček. *Mathematical Theory of Elastic and Elasto-Plastic Bodies: An Introduction.* Elsevier Science, Amsterdam, 1981.

[76] N. M. Newmark. A method of computation for structural dynamics. *J. Engrg. Mech. Div., ASCE*, pages 67–94, 1959.

[77] J. A. Nitsche. On Korn's second inequality. *RAIRO Anal. Numér.*, 15:237–248, 1981.

[78] M. Nordin and V. H. Frankel. *Basic Biomechanics of the Musculoskeletal System*. Lippincott Williams & Wilkins, Baltimore Philadelphia, 3rd edition, 2001.

[79] P. D. Panagiotopoulos. *Inequality Problems in Mechanics and Applications: Convex and Nonconvex Energy Functions*. Birkhäuser, Boston Basel Stuttgart, 1985.

[80] E. Rothe. Zweidimensionale parabolische Randwertaufgabe als Grenzfall eindimensionaler Randwertaufgaben. *Math. Ann.*, 102(1):650–670, 1930.

[81] W. Rudin. *Functional Analysis*. International Series in Pure & Applied Mathematics. McGraw-Hill, 2nd edition, 1991.

[82] O. Sander. *Multidimensional Coupling in a Human Knee Model*. PhD thesis, Freie Universität Berlin, 2008. `http://www.diss.fu-berlin.de/diss/receive/FUDISS_thesis_000000006010`.

[83] M. Schatzman. A hyperbolic problem of second order with unilateral constraints: the vibrating string with a concave obstacle. *J. Math. Anal. Appl.*, 73(1):138–191, 1980.

[84] E. Schechter. *Handbook of Analysis and Its Foundations*. Academic Press, San Diego, 1997.

[85] A. Signorini. Sopra alcune questioni di elastostatic. *Atti Soc. Ital. per il Progresso delle Scienze*, 1933.

[86] J. C. Simo and N. Tarnow. The discrete energy-momentum method. conserving algorithms for nonlinear elastodynamics. *Z. Angew. Math. Phys.*, 43(5):757–792, 1992.

[87] J. M. Solberg and P. Papadopoulos. A finite element method for contact/impact. *Finite Elem. Anal. Des.*, 30(4):297–311, 1998.

[88] R. L. Taylor and P. Papadopoulos. On a finite element method for dynamic contact/impact problems. *Internat. J. Numer. Methods Engrg.*, 36(12):2123–2140, 1993.

[89] B. Wohlmuth. A mortar finite element method using dual spaces for the Lagrange multiplier. *SIAM J. Numer. Anal.*, 38(3):989–1012, 2000.

[90] B. Wohlmuth and R. Krause. Monotone methods on nonmatching grids for nonlinear contact problems. *SIAM J. Sci. Comput.*, 25(1):324–347, 2003.

[91] J. Yao, A. D. Salo, J. Lee, and A. L. Lerner. Sensitivity of tibio-menisco-femoral joint contact behavior to variations in knee kinematics. *J. Biomech. Eng.*, 41(2), 2008.

[92] J. W. Youett. An introduction to mortar techniques with applications in biomechanics. Bachelor's thesis, Freie Universität Berlin, 2009.

[93] E. Zeidler. *Nonlinear Functional Analysis and Applications II/A: Linear Monotone Operators*. Springer-Verlag, Berlin Heidelberg New York, 1986.

[94] E. Zeidler. *Nonlinear Functional Analysis and Applications II/B: Nonlinear Monotone Operators*. Springer-Verlag, Berlin Heidelberg New York, 1986.

[95] E. Zeidler. *Nonlinear Functional Analysis and Applications I: Fixed-Point Theorems*. Springer-Verlag, Berlin Heidelberg New York, 3rd edition, 1990.

Danksagung

Mein größter Dank gilt Prof. Peter Deuflhard. Sein reicher Erfahrungsschatz auf dem Gebiet der numerischen Mathematik und seine klare Vision von virtueller Medizin haben wesentlich zum Erfolg dieses spannenden und zugleich anspruchsvollen Forschungsprojektes beigetragen. Herzlich danken möchte ich Prof. Deuflhard für sein kontinuierliches Interesse an meiner Arbeit, seine Unterstützung und Förderung und – ganz besonders – für sein großes Vertrauen in mich und meine Fähigkeiten.

Dr. Anton Schiela danke ich für viele interessante Diskussionen, aus denen sich wertvolle Ideen entwickelt haben. Durch seine Kritik, seine Hinweise und nicht zuletzt durch seine Beharrlichkeit wurde die Arbeit deutlich verbessert. Desweiteren danke ich Dr. Martin Weiser für anregende Gespräche, die mir zu einem tieferen Verständnis der Thematik verholfen haben. Für die Entwicklung und Betreuung des Software-Paketes DUNE und des Kontaktlösers gilt mein besonderer Dank Jun.-Prof. Oliver Sander. Jonathan Youett aus der Arbeitsgruppe von Prof. Ralf Kornhuber danke ich für die Implementierung der Kopplung unterschiedlicher Materialien in die Algorithmen. Außerdem bedanke ich mich bei Prof. Rolf Krause und Mirjam Walloth für die gute Zusammenarbeit gerade in der Anfangsphase dieser Arbeit.

Die vorliegende Dissertation wurde durch das DFG-Forschungszentrum MATHEON in Berlin gefördert. Diese Umgebung hat mir die optimale Möglichkeit geboten, numerische Analysis und Algorithmendesign mit meinem Interesse an medizinischen Anwendungen zu verbinden. Sowohl das MATHEON als auch das Zuse-Institut Berlin haben mir dafür exzellente Arbeitsbedingungen zur Verfügung gestellt – auch hierfür vielen Dank.

Zu guter Letzt möchte ich mich von Herzen bei meinen Eltern, meiner Schwester und meinem Mann bedanken, die mich in den vergangenen Jahren uneingeschränkt unterstützt und immer wieder ermutigt haben.

Zusammenfassung

Die vorliegende Dissertation ist der schnellen und stabilen numerischen Lösung von dynamischen Kontaktproblemen gewidmet, wie sie beispielsweise bei der Modellierung und Simulation des menschlichen Ganges auftreten. Adaptivität bietet hier die Möglichkeit effektive Algorithmen zu konstruieren, die mit vertretbarem Rechenaufwand eine vorgegebene Genauigkeit erreichen.

Der Fokus der Dissertation liegt auf dynamischem Kontakt zwischen zwei viskoelastischen Körpern, der durch die Signorini-Bedingung modelliert wird. Dies führt auf nichtglatte und nichtlineare Variationsungleichungen, für die bisher lediglich die Existenz einer Lösung nachgewiesen ist, während Eindeutigkeit und stetige Abhängigkeit von den Anfangsdaten nach wie vor ungelöste Probleme darstellen. Für die numerische Zeitintegration bietet sich das kontaktstabilisierte Newmarkverfahren von Deuflhard et al. an, das im Gegensatz zu den meisten anderen Diskretisierungen sowohl energiedissipativ als auch frei von numerischen Instabilitäten ist.

Im Rahmen dieser Arbeit wird zunächst das kontaktstabilisierte Newmarkverfahren unter dem Aspekt einer diskreten Persistenzbedingung weiter entwickelt. Ziel ist es dann, für diesen Algorithmus eine adaptive Steuerung der Zeitschrittweite zu konstruieren. Als erster notwendiger Schritt wird hierzu die "physikalische Energienorm" im Funktionenraum eingeführt, in der ein Störungsresultat für eine Klasse von dynamischen Kontaktproblemen hergeleitet werden kann. Im zweiten Schritt werden in dieser Norm neuartige Konsistenzresultate für unterschiedliche Newmarkverfahren bewiesen. Mit Hilfe einer Modifikation der Beweistechnik "Lady Windermere's Fan" läss t sich dann die Konvergenz des verbesserten kontaktstabilisierten Newmarkverfahrens im Rahmen der Zeitschichtenmethode nachweisen. Hierfür ist zusätzlich die Untersuchung von Störungsresultaten für die diskrete Evolution notwendig. Die adaptive Steuerung der Zeitschrittweiten erfordert schließlich die Konstruktion eines Verfahrens höherer Ordnung, um daraus einen Schätzer für den Konsistenzfehler zu erhalten. Hierfür werden speziell angepasste Extrapolationsmethoden entwickelt, die auf einer modifizierten asymptotischen Entwicklung des Fehlers basieren.

Abschließend wird die adaptive Variante des verbesserten kontaktstabilisierten Newmarkverfahren an verschiedenen Beispielen getestet. Dabei zeigt sich eine deutliche Übereinstimmung von theoretischen Erkenntnissen und numerischen Experimenten. Sowohl für ein einfaches Testproblem als auch für die Simulation der Bewegung des menschlichen Knies verhält sich der Algorithmus sehr stabil und effizient.

Lebenslauf

Corinna Klapproth

geboren am 21. April 1982 in Detmold

1992 – 2001	Stadtgymnasium Detmold Abschluss mit der Allgemeinen Hochschulreife
10/2001 – 09/2006	Studium der Mathematik mit Nebenfach Physik, Westfälische Wilhelms-Universität Münster Abschluss mit Diplom
10/2003 – 09/2006	Studentische Hilfskraft mit Lehraufgaben am Fachbereich Mathematik und Informatik der Westfälischen Wilhelms-Universität Münster
seit 10/2006	Wissenschaftliche Mitarbeiterin am Zuse-Institut Berlin (ZIB) Bereich Numerische Mathematik, Abteilung Numerische Analysis und Modellierung, Arbeitsgruppe Virtuelle Medizin